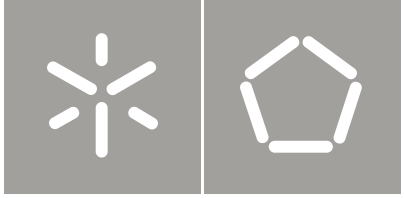

Universidade do Minho
Escola de Engenharia

SAPIENZA - University of Rome
School of Engineering

Claudio Maruccio

Numerical Analysis of FRP Strengthened Masonry Structures

Tese de Doutoramento
Engenharia Civil

Trabalho efectuado sob a orientação do
Professor Doutor Daniel V. Oliveira
Universidade do Minho

Co-Orientadores:
Professor Doutor Paulo B. Lourenço
Universidade do Minho

Professor Doutor Giorgio Monti
Universitá di Roma La Sapienza

Dezembro de 2010

December 2010

DISSERTAZIONE PRESENTATA PER IL CONSEGUIMENTO DEL TITOLO
DI DOTTORE DI RICERCA IN INGEGNERIA DELLE STRUTTURE

NUMERICAL ANALYSIS OF FRP STRENGTHENED MASONRY STRUCTURES

Claudio Maruccio

Rome, December 2010

Dottorato di Ricerca in Ingegneria delle Strutture
Università di Roma "La Sapienza" (Italia) e Università del Minho (Portogallo)
XXIII Ciclo

Il coordinatore del Dottorato
Prof. Giuseppe Rega

Supervisors:

Prof. Daniel Oliveira (Assistant Professor, University of Minho)
Prof. Paulo Lourenço (Full Professor, University of Minho)
Prof. Giorgio Monti (Full Professor, University of Rome - La Sapienza)

To Alessandra

For ever in our heart

"We will never cease from exploration. And the end of all our exploring will be to arrive where we began and to know the place for the first time" T. S. Eliot

PREFACE AND ACKNOWLEDGEMENTS

In this thesis, numerical approaches to model FRP strengthened masonry structures are discussed. The primary contributions are the development of a material model for the analysis of the FRP-masonry interface and of a suitable finite element for analysis of masonry buildings under seismic actions. The micro-modeling strategy is used to validate the macro-modeling approach and the results are compared to experimental tests on small scale walls and large scale prototypes of buildings. This new element is extremely effective for the seismic analysis of masonry buildings because it drastically reduces the number of degrees of freedom of the FEM model. The work reported in this thesis was possible thanks to the scholarship made available by the FCT (Portuguese Science and Technology Foundation) and was developed during the first part at the University of Minho (Department of Civil Engineering) in Guimaraes, Portugal, and in the second part at the University of Rome (Department of Structural Engineering and Geotechnics) in Italy. This research work could not be possible without the guidance of Dr. Daniel V. Oliveira and the supervision of Prof. Paulo B. Lourenço at the University of Minho and Prof. Giorgio Monti and Prof. Domenico Liberatore at the University of Rome. They are all very well acknowledged for strong encouraging, deep understanding and very fruitful discussions. I would like to record my thanks to Dr. Laura De Lorenzis from the University of Salento, for making the first contacts leading to my stay at University of Minho, since the time I was working for my Master's Degree. I am also very grateful to several doctoral students for much support and the good time we have had together: Konrad, Rajendra, Gihad and Ismael in particular at the "Division of Masonry Structures" in Portugal, Vincenzo, Andrea and Marco at the "Department of Structural Engineering and Geotechnics" in Rome. I would like to specially thank Chen Zhi Xiong for much help and support during the development of a finite element for masonry in the Opensees framework, without our strong cooperation several results could not be achieved. Moreover, special thanks go to my family: my mother and my father, they taught me love, support, and understanding, and my brother, he taught me passion and love for science, strict and creative approach, without forgetting all my Italian friends: their company made my best days and years. Furthermore, I cannot forget Tommaso, my uncle, who introduced me to engineering and taught me a pragmatic approach to analyze phenomena around us. Special thanks to Rossana for her love and understanding. Finally to the memory of those relatives whose life will remain in my mind for ever, specially to my dearest grandfather Giuseppe and my cousin Alessandra whose young death kept a big hole in my heart. To her this thesis is dedicated.

Summary

Masonry structures have always been used since the dawn of construction, and nowadays, due to aging, material degradation, settlements, and structural alterations, members often need strengthening to re-establish their performance. In this frame, fiber-reinforced polymer (FRP) composites in the form of bonded laminates applied to the external surface can be a viable strengthening solution provided that they comply with the cultural value of the building. Despite research efforts in the last years, for the seismic analysis of strengthened masonry system, reliable numerical models, endowed with accuracy, high efficiency and good convergence properties, are still lacking. In this thesis, numerical approaches to model FRP strengthened masonry structures are discussed and in the first part, a material model suitable for micro-modeling of the FRP-masonry interfacial behavior implemented in the Diana FEM program with a user-subroutine is presented. This micro-modeling approach based on interface elements within the framework provided from the theory of multi-surface plasticity is then used to assess the global behavior of a different type of finite element that was implemented in the OpenSees framework. This new element is extremely effective for the seismic analysis of masonry buildings because it drastically reduces the number of degrees of freedom (DOF) of the FEM model. Each panel in the structure can be modeled by using a single "MultiFan" element based on a simplification of the material behavior and the stress field within the panel. The approach proposed is validated through comparison with the results obtained according the simplified model proposed in the recent Italian Code DM2008 modified and extended to include the effect of FRP pier retrofits. Numerical results are validated by comparison with experimental results from tests performed at the University of Pavia, Italy, and the Georgia Institute of Technology, USA and the usefulness of the proposed approaches for solving engineering problems is demonstrated. In particular, macro-modeling shows a satisfactory degree of accuracy at the global level, and, at the same time, is efficient enough, from the computational point of view, to analyze complex assemblages of masonry buildings, including cyclic loads effects and FRP strengthening.

Resumo

As estruturas de alvenaria têm sido usadas desde sempre na construção, mas o seu envelhecimento, a degradação material, os assentamentos e as alterações estruturais têm levado à necessidade do seu reforço para garantir um desempenho adequado. Neste contexto, o uso de materiais compósitos com matriz polimérica (FRP) aplicados externamente no reforço de estruturas pode ser uma solução viável, desde que respeite o valor cultural da construção. Apesar dos esforços de pesquisa dos últimos anos, a análise sísmica de estruturas de alvenaria reforçadas com FRP ainda carece de modelos numéricos precisos e mais eficientes.

Nesta tese são estudadas ferramentas numéricas para representar o reforço com FRP em estruturas de alvenaria. Na primeira parte apresenta-se um modelo material adequado à micro-modelação do comportamento da interface FRP-alvenaria, desenvolvido e implementado no programa de elementos finitos Diana. A micro-modelação, baseada em elementos de interface onde a teoria da plasticidade é aplicada a multi-superfícies de cedência, foi posteriormente usada para avaliar o comportamento global de um outro tipo de elemento, implementado no programa OpenSees. Este novo elemento é adequado à análise sísmica de edifícios em alvenaria pois reduz o número de graus de liberdade do modelo estrutural.

A abordagem proposta nesta tese é validada através da comparação com os resultados obtidos de acordo com os modelos propostos no recente código italiano DM2008, modificado e ampliado para incluir o efeito do reforço com FRP. Os resultados numéricos são validados por comparação com os resultados experimentais realizados na Universidade de Pavia (Itália) e no Instituto de Tecnologia da Geórgia (EUA). De uma forma geral, obteve-se uma boa comparação entre os resultados experimentais e numéricos a nível global e, ao mesmo tempo, eficiência do ponto de vista computacional, para analisar a complexidade do conjunto em alvenaria, incluindo os efeitos cíclicos de cargas e reforço com FRP.

Sommario

In questi ultimi anni, la necessità di sviluppare ed implementare in codici di calcolo modelli numerici affidabili per l'analisi del comportamento di strutture in muratura sta assumendo sempre più rilevanza scientifica in particolare alla luce di eventi tragici come il recente terremoto dell'Aquila. Contemporaneamente, tra le varie tipologie di rinforzo strutturale, i materiali compositi fibro-rinforzati (FRP) hanno mostrato di essere una soluzione valida per il ripristino di edifici in muratura esistenti. In questa tesi, partendo da una attenta analisi dello stato dell'arte, differenti approcci numerici per la modellazione di strutture in muratura rinforzate con i materiali compositi sono impiegati allo scopo di individuare e poi implementare in codici di calcolo agli elementi finiti (Diana ed OpenSees) dei modelli costitutivi adatti per la valutazione della sicurezza strutturale di singoli elementi (muri e archi) o edifici in presenza di FRP. Sulla base dei risultati prodotti da una recente campagna sperimentale, si è sviluppato un modello costitutivo in grado di descrivere il comportamento meccanico dell'interfaccia muratura-FRP. La formulazione matematica si fonda sulla teoria incrementale della plasticità dove la relazione tensioni-deformazioni è definita attraverso una matrice di rigidezza tangente del materiale che a sua volta è funzione della forma delle superfici di snervamento e delle leggi di incrudimento adottate. L'introduzione in un modello costitutivo esistente di una legge di hardening/softening multi-lineare si è rivelata efficace nel cogliere la natura complessa del comportamento dell'interfaccia FRP-muratura come evidenziato dalle simulazioni di test di aderenza effettuati su substrati sia piani che curvi. La corretta calibrazione del modello ha poi consentito di riprodurre con buona approssimazione il comportamento di archi in muratura rinforzati con FRP all'intradosso ed estradosso. L'approccio basato sulla micromodellazione è poi impiegato per la validazione di un nuovo elemento finito in grado di descrivere il comportamento degli edifici in muratura con tecniche di macromodellazione. Il nuovo macroelemento è basato su una schematizzazione a ventaglio dello stato tensionale al suo interno e sull'introduzione di cerniere plastiche sulle facce estreme superiore ed inferiore in grado attraverso tecniche di condensazione di introdurre differenti criteri di collasso sia a taglio che a flessione anche in presenza di eventuali rinforzi in materiale composito. Le cerniere plastiche introdotte consentono di identificare il comportamento strutturale di pannelli murari sia in presenza di carichi monotonici che ciclici. In fine, vengono presentati alcuni confronti tra i risultati numerici ottenuti con la discretizzazione a macroelementi ed i risultati sperimentali su edifici in muratura ottenuti presso i laboratori dell'Università di Pavia (Italia) e del Georgia Institute of Technology (Stati Uniti). I due prototipi analizzati sono considerati due validi benchmark per quanto riguarda edifici soggetti a carichi ciclici, il primo in assenza di materiali di rinforzo, il secondo in presenza di FRP per prevenire meccanismi di crisi a flessione e taglio.

CONTENTS

1 Introduction

Considering that almost the half of all construction market goes into renovation and restoration and that much of the world's architectural heritage consists of historic buildings in masonry, the field of masonry research deserves greater attention than it usually received in the past. Moreover, in addition to their historical and cultural values, such monuments often have also important social and economical values. As an example, the partial collapse of the vaults in the Basilica of St. Francis in Assisi during the 1997 earthquake in Italy, caused the destruction of irreplaceable and priceless frescos by Giotto and Cimabue of the early 14^{th} century. Even more tragically, four people lost their lives when the masonry vaulting collapsed (Croci 1998 and 2001). Thus, though many existing masonry structures have survived for centuries, there is an acute need for new tools to analyze the stability and the safety of such structures (Block 2005; Block 2009; De Jong, De Lorenzis et al. 2008). The master builders of the Middle Ages were able to use geometrical rules, developed through centuries of trial and error, to build structural elements. In those days, there was no knowledge of material properties or allowable stresses. Nevertheless, many of these architectural marvels are still standing in a state of equilibrium (Huerta 2001; Romano and Ochsendorf 2010). For all these reasons, modeling and analysis of masonry constructions is receiving more and more attention in the wide field of conservation and restoration and a main point is which type of analysis should be used.

Key aspects to be considered are (Lourenço $2006_{a,b}$):

- geometry data is missing;
- information about the inner core of the structural elements is unknown ;
- characterization of the mechanical properties of the materials is difficult;
- large variability of mechanical properties;
- construction sequence is unknown;
- existing damage in the structure is unknown;

In this framework, before performing an advanced numerical analysis, it is important to understand that further resources are required to understand the mechanical behavior of masonry, which include non destructive in-situ testing, adequate experimental tests and

development of reliable numerical tools. Significant contributions have occurred recently in the cited research fields.

Moreover, the quality of any intervention has to be based on modern principles that include aspects like: retractability, reversibility, unobtrusiveness, minimum repair and respect by the original conception, safety of the construction, durability and compatibility of the materials, balance between costs and available financial resources. In this framework, fiber-reinforced polymers (FRP) can be a good option for strengthening masonry buildings**.**

1.1 Motivation

In recent years, the importance of rational methods of analysis for masonry structures has been recognized. Masonry structures have always been used since the dawn of construction, and nowadays, due to aging, material degradation, settlements, and structural alterations, usually some members need strengthening to re-establish their performance. In this framework, FRP composites in the form of bonded laminates applied to the external surface of masonry can be a viable solution provided that they comply with the cultural value of the building. Despite research efforts in the last years, for the seismic analysis of strengthened masonry systems, reliable numerical models, endowed with accuracy, high efficiency and good convergence properties, are still lacking.

1.2 Objectives of this study

The primary objectives of this thesis are the development of a material model for the analysis of the FRP-masonry interface and of a suitable finite element for analysis of strengthened masonry buildings under seismic actions. The micro-modeling strategy is used to validate the macro-modeling approach and the results are compared to experimental tests of small scale walls and large scale prototypes of buildings. The material model proposed and implemented in the finite element program Diana 8 as a user subroutine is very useful to model the FRP-masonry interface: both for planar and curved substrates and allows to obtain the global full shear force-displacement path and also to simulate the stress distribution at the interface. The MultiFan element proposed is instead extremely effective for the seismic analysis of masonry buildings and has been implemented in the Object-Oriented Nonlinear Dynamic Analysis program OpenSees. Then the Zero-Length Spring has been added to the MultiFan element

system to model shear and bending failure and the cyclic behavior has been included. The MultiFan element developed is used to analyze the building prototypes experimented at the Department of Structural Mechanics of the University of Pavia and at the Georgia Institute of Technology. Finally, satisfactory accuracy at the global level is shown when complex assemblages are analyzed in 3D even in the case of cyclic loads or when strengthening techniques are considered.

1.3 Outline of contents

In this thesis, numerical approaches to model FRP strengthened masonry structures are discussed. In particular in the second chapter a general description of the techniques available in earthquake engineering for the analysis of masonry buildings is provided. The different approaches are detailed and the nonlinear procedures suitable for this study are introduced. A brief description of the advanced numerical techniques that are the starting point of the research work is detailed: in particular the finite element formulation of the continuum mechanics equations and the theory of multi-surface plasticity. Based on this theoretical framework and recent experimental results, in chapter three a material model for the analysis of the FRP-masonry interface is developed starting from an existing constitutive model developed at the University of Delft and Minho by Lourenço 1996, suitable to analyze masonry structures. The material model is then used to analyze curved masonry structures with and without strengthening. A case study is represented from an arch bridge structure with and without strengthening analyzed using both linear and nonlinear analysis showing the advantages and drawbacks of each technique. The micro-modeling approach used in chapter three represents the starting point to assess the behavior in chapter four of a new finite element to analyze with a macro-modeling approach masonry buildings under seismic actions. The new finite element is used to reproduce experimental results on small scale walls under both monotonic and cyclic loads, even in presence of strengthening. In chapter five, the numerical approaches developed in this thesis in chapter four are validated by comparison to experimental results to demonstrate advantages of the proposed approaches for solving engineering problems. Applications considered are the tests performed at the University of Pavia, Italy, and the Georgia Institute of Technology, USA on small prototypes of two floors masonry buildings. The results obtained with the new finite element proposed are furthermore validated

through comparison with the results obtained according the simplified model proposed in the recent Italian Code DM2008 modified and extended to include the effect of FRP pier retrofits.

2 Masonry buildings and earthquake engineering

2.1 Introduction

Only recently the scientific community has begun to show interest in developing sophisticated numerical tools for masonry as an opposition to the prevailing tradition of rules-of-thumb and empirical formulae. The difficulties in adopting existing numerical tools from more advanced research fields, namely the mechanics of concrete or composite materials, were hindered by the particular characteristics of masonry. Masonry is a composite material that consists of units and mortar joints. A detailed analysis of masonry, denoted micro-modeling, must therefore include a representation of units, mortar and the unit/mortar interface. This approach is suited for small structural elements with particular interest in strongly heterogeneous states of stress and strain. The primary aim of micro-modeling is to closely represent masonry from the knowledge of the properties of each constituent and the interface. The necessary experimental data must be obtained from laboratory tests and small masonry samples. Several researchers developed reasonably simple models to describe the masonry behavior but only recently gradual softening behavior and all failure mechanisms: namely tensile, shear and compressive failure, have been fully included (Lourenço and Rots 1997). In large and practice-oriented analysis, the knowledge of the interaction between units and mortar is, generally, negligible for the global structural behavior. In these cases, different approaches can be used, denoted as macro-modeling. One option is to regard the material as an anisotropic composite and a relation is established between average masonry strains and average masonry stresses. This is clearly a phenomenological approach, with material parameters to be obtained in masonry tests of sufficiently large size under homogeneous states of stress. This approach allows to reproduce an orthotropic material with different tensile and compressive strengths along the material axes as well as different inelastic behavior for each material axis (Lourenço, Rots et al. 1998; Lourenço 2000; Zucchini and Lourenço 2002, 2004, 2009; Luciano and Sacco 1997, 1998). A second option extremely effective for the seismic analysis of masonry buildings is to model each panel in the structure by using a single element based on a simplification of both the material behavior and the stress field within the panel. This approach drastically reduces the number of degrees of freedom (DOF) of the FEM model and the computational time (Braga, Liberatore et al. 1998).
Together with advances in the developments of suitable material models for masonry, the current engineering practice for the seismic analysis of masonry buildings is moving away from simplified linear-elastic methods of analysis, and towards a more

complex nonlinear-inelastic techniques. These procedures focus on the nonlinear behavior of the structural response and employ methods not previously emphasized in seismic codes. Up to now, in the design of buildings, the seismic effects and the effects of the other actions included in the seismic design situation, may be determined on the basis of four different methods: linear static procedures, mode superposition procedures, nonlinear static (pushover) procedures, nonlinear dynamic (time history) procedures (Norme tecniche per le costruzioni, 2008). Limit analysis is often not sufficient for a full structural analysis under seismic loads, but it can be profitably used in order to obtain a simple and fast estimation of collapse loads (Cavicchi and Gambarotta 2005, 2006, 2007; Gilbert, Casapulla et al. 2006; Gilbert and Melbourne 1994).

Nonlinear analyses should be properly substantiated with respect to the seismic input, the constitutive model used, the method of interpreting the results of the analysis and the requirements to be met. The mathematical model used for elastic analysis shall be extended to include the strength of structural elements and their post-elastic behavior. As a minimum, bilinear force – deformation envelopes (elasto-plastic springs) should be used at the element level. In masonry buildings, the elastic stiffness relation should correspond to cracked sections and zero post-yield stiffness may be assumed. If strength degradation is expected, e.g. for masonry walls or for brittle elements, it has to be included in the envelope. Unless otherwise specified, element properties should be based on mean values of the properties of the materials. Gravity loads shall be applied to appropriate elements of the mathematical model and the seismic action shall be applied in both positive and negative directions while the maximum seismic effects are used (Norme tecniche per le costruzioni, 2008).

Furthermore, due to the great difficulty in the formulation of robust numerical algorithms representing satisfactorily the inelastic behavior very often micro- and macro-analyses of masonry structures are limited to the structural pre-peak regime. However, the importance of computations beyond the limit load is clear, in order to evaluate residual load and to assess the structural safety.

Summarizing, key aspects to assess the global behavior of masonry buildings are:

- The failure mode observed (in plane and out of plane behavior)
- The mechanical behavior of the material (micro-modeling, macro-modeling and macro-element)
- The structural modeling strategies used (finite element method, simplified spring models, limit analysis)
- The method of analysis considered (linear, modal, nonlinear-static, nonlinear-dynamic)

Fig. 2.1 provides a schematic representation of these aspects.

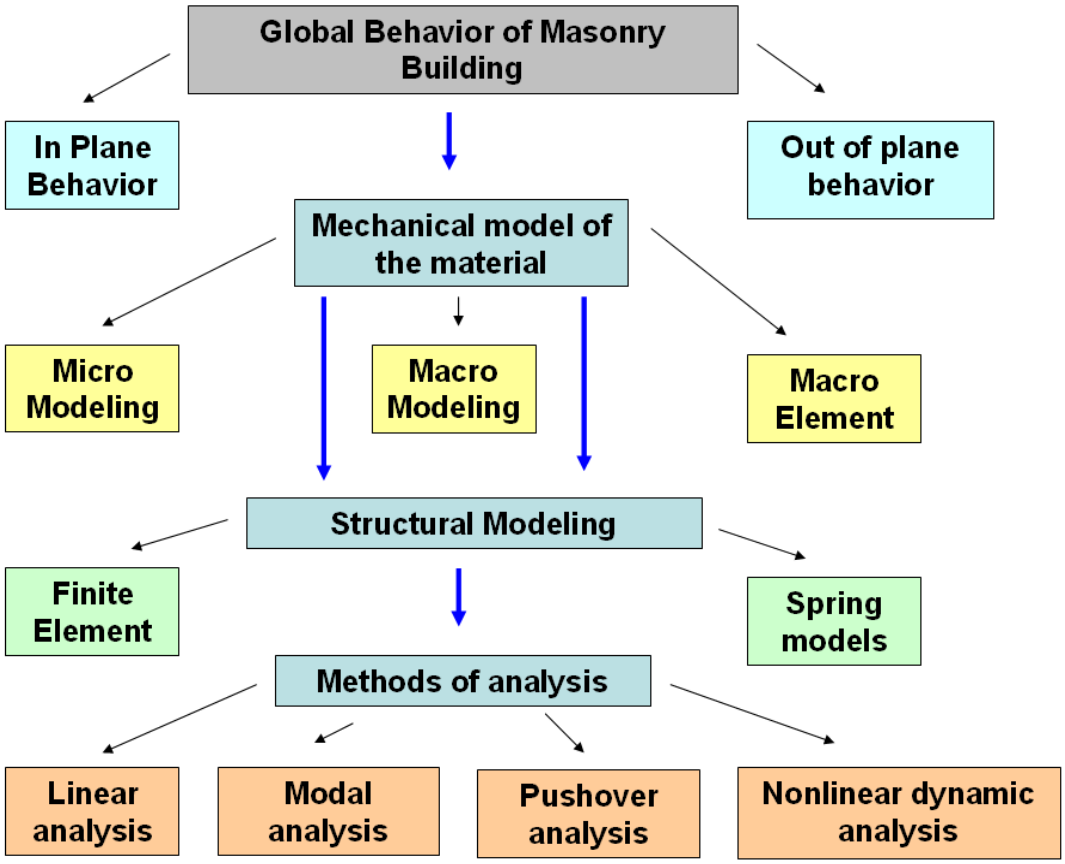

Fig. 2.1 Key aspects that affect the structural analysis of masonry buildings

2.2 The Aquila earthquake: In plane and out of plane failure

On 6th April 2009 an earthquake of magnitude 6.3 occurred in L'Aquila city, Italy. In the city center and surrounding villages many masonry and reinforced concrete (RC) buildings were heavily damaged or collapsed. After the earthquake, the inspection carried out in the region provided relevant results concerning the quality of the materials, method of construction and the performance of the structures. The region has many masonry buildings in historical centers. The main structural materials are unreinforced masonry (URM) composed of rubble stone, brick, and hollow clay tile. Masonry units suffered the worst damage. Wood flooring systems and corrugated steel roofs are common in URM buildings. Moreover, unconfined gable walls, excessive wall thicknesses without connection with each other are among the most common deficiencies of poorly constructed masonry structures. These walls caused an increase in earthquake loads. The quality of the materials and the construction were not in accordance with the standards. On the other hand, several modern, non-ductile concrete

frame buildings have collapsed. Poor concrete quality and poor reinforcement detailing caused damage in reinforced concrete structures. Furthermore, many structural deficiencies such as non-ductile detailing, strong beams-weak columns were commonly observed.

This short description (see from Fig. 2.2 to Fig. 2.16) shows examples of the typical damages suffered by masonry buildings during the Aquila earthquake. In particular the pictures refer to the historical centre of Paganica and they represent an extract of a wider photographic documentation taken by the team (that the author had the chance to join) of the Department of Structural Engineering and Geotechnics of the University of Rome, which went to Paganica in the periods between 27th July and 4th August 2009 in the framework of the ReLUIS activities of evaluating the structural conditions of the buildings damaged by the main seismic event (co-ordinated by Prof. Giorgio Monti).

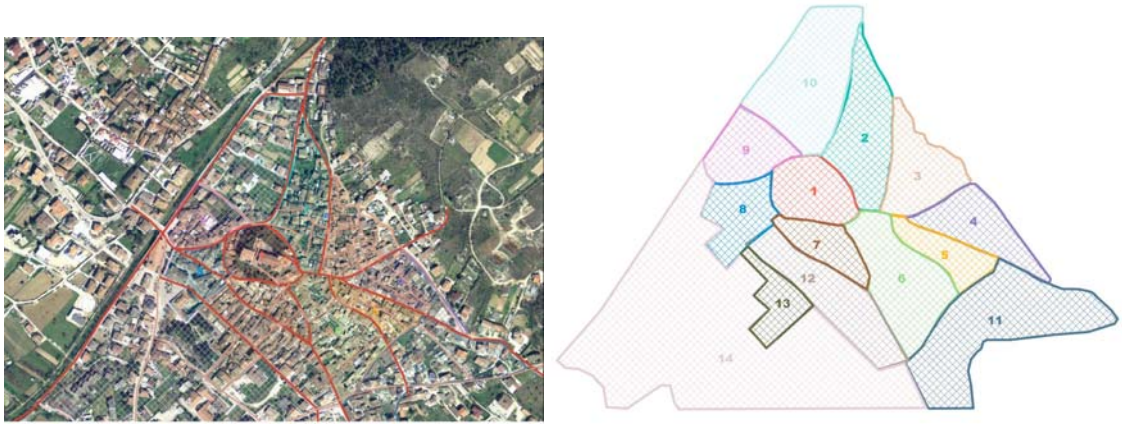

Fig. 2.2 Historical centre of Paganica (main area of investigation)

Fig. 2.3 Structural survey in the historical center of Paganica – General view

Out of plane failure mechanisms and in-plane damages to masonry walls are reported, as representation of the structural behavior of different masonry buildings typologies. For this purpose, also some undamaged buildings are shown.

Fig. 2.4 Historical centre of Paganica – Lower view.

Fig. 2.5 Building located in the historical centre of Paganica. Out of plane behavior: overturning mechanism of the facade wall detached from orthogonal walls.

Fig. 2.6 Several wood frames and iron ties, placed after Aquila's earthquake, avoided out of the plane global failure of external walls, which resulted very damaged in their own plane. The cracks in the masonry walls demonstrate the strong engagement of these structural elements in the global response.

Fig. 2.7 Ancient masonry of a building located in the historical centre of Paganica. Out of plane behavior: separation between two orthogonal masonry walls due to poor arrangement of the stones.

Fig. 2.8 Facade of a building located in the historical centre of Paganica. Out of plane behavior: flexural mechanism of facade wall. Note the inefficient connection of the wall to the roof, while iron ties avoided global overturning of the bottom part.

Fig. 2.9 Facade of a building located in the historical centre of Paganica. Out of plane behavior: flexural mechanism of facade wall. Note the inefficient connection of the wall to the roof, while the absence of iron ties made possible global overturning

Fig. 2.10 Row of buildings located in the historical centre of Paganica. Out of plane behavior: collapse mechanism of the upper zone of the walls (left part). Note the poor quality of masonry, without efficient transversal connection elements, and the roof structure not well anchored to the wall. Iron ties avoided global overturning.

Fig. 2.11 Building located in the historical centre of Paganica. Out of plane behavior: collapse of the central zone of a wall determined by the horizontal action due to earthquake. The strengthened walls, a fair connection with the roof structure and iron ties avoided global overturning.

Fig. 2.12 Building located in the historical centre of Paganica. In plane behavior: several iron ties, placed in correspondence of orthogonal walls at each storey, avoided the out of the plane collapse. Diagonal cracks, in both spandrels and piers, demonstrate the engagement of the wall in its own plane.

Fig. 2.13 Building located in the historical centre of Paganica. In plane behavior: the iron ties at floor level allowed the formation of diagonal struts in the masonry piers.

Fig. 2.14 Building located in the historical centre of Paganica. Global failure due to the poor quality of the masonry material. In plane and out of plane failure modes are visible. Presence of out of plane instability with expulsion of the corner between perpendicular walls.

Fig. 2.15 Buildings located in the historical centre of Paganica. Good behavior of masonry buildings in presence of ancient iron ties: only some negligible diagonal cracks are visible on the spandrels.

Fig. 2.16 Aggregates and complex buildings in the historical centre of Paganica. Damages due to different heights of adjacent buildings.

In the following, a summary of the construction errors found during the inspection is provided. Masonry structures mainly suffered out-of-plane failures. Many of these masonry buildings were constructed as rubble stone masonry in rural areas. Materials and construction techniques of these stone masonry buildings did not provide earthquake resistance to the buildings. Considering the construction techniques of these buildings, the most important defects are: lack of interlocking elements between external and internal units of the wall section and lack of connection between crossing walls, the floors were too thick and this increased the weight of the structure and therefore resulted in higher earthquake forces. The joining of rubble stones with mud and lack of interlocking walls caused damage of these buildings under the effect of the earthquake loads. Almost all the walls of the masonry buildings were not appropriate to carry the earthquake loads and in joining the corners of the masonry buildings many mistakes were made. The interlocking walls were not connected properly, while the percentage of the doors and windows was relatively high. The placement of the windows near the corners resulted in damages and due to lack of proper connection between the walls and roof in the roof level the structural response was different and damages were observed. From this inspection, it is possible to summarize that in the cities under similar earthquake risk, necessary precautions must be taken into consideration to avoid similar disasters in the future because the potential for damage of masonry buildings is high. For these kinds of buildings new retrofitting methodology

must be proposed, which will not influence the functionality and will not disturb normal usage by the inhabitants. Finally, it is stressed as through the adoption of suitable measures, the out-plane failure can be prevented and in-plane is then of concern (Valluzzi, Binda et al. 2002; Valluzzi 2007).

2.3 Materials and mechanical models

2.3.1 Masonry

The mechanical behavior of masonry has generally these salient features: a very low tensile strength, and stresses typically only a fraction of the crushing capacity of the stone. The first property is so important that it has determined the shape of existing masonry constructions (Heyman 1982 and 2007).

Common idealizations of the masonry behavior used for the analysis of existing masonry constructions are elastic behavior (with or without redistribution), plastic behavior and nonlinear behavior. Moreover limit analysis provides also a stable theoretical framework (Ochsendorf 2002, Orduna and Lourenço 2003 and 2005, Milani, Lourenço et al. $2006_{a,b}$).

To apply limit analysis to masonry, three main assumptions were initially proposed (Heyman 1995):

- masonry has no tensile strength;
- masonry can resist infinite compression;
- no sliding will occur within the masonry.

Collapse mechanism analysis (limit or plastic analysis) is very useful for engineering purposes also to analyze complicated 3D-structural systems. For traditional masonry constructions, such as the buildings in historical centers, the method can be readily applicable to analysis and strengthening. For more complex and unique monumental structures, this method is still of interest to calculate strengthening, once the relevant collapse mechanisms are identified and the structural behavior is understood resorting to a nonlinear analysis.

In particular, in this study the finite element method is used to simulate the structural behavior. A mathematical description of the material behavior, which yields the relation between the stress and strain tensor in a material point of the body, is necessary for this purpose. This mathematical description is commonly named a constitutive model. Constitutive models will be developed in chapter three and four in a plasticity framework according to a phenomenological approach in which the observed mechanisms are represented in such a fashion that simulations are in reasonable agreement with experiments. It is not realistic to try to formulate constitutive models

which fully incorporate all the interacting mechanisms of a specific material because any constitutive model or theory is a simplified representation of reality. It is believed that more insight can be gained by tracing the entire response of a structure than by modeling it with a highly sophisticated material model or theory which does not result in a converged solution close to the failure load (Lourenço 2007$_{a,b}$).

In particular the use of FRP material led to new and important modeling problems (Brencich and Gambarotta 2005; Grande, Milani et al. 2008), despite several material modeling strategies were developed in the last years aiming to reproduce the structural behavior of both un-strengthened and FRP-strengthened masonry structures (Grande, Imbimbo et al. 2011; Marfia and Sacco 2001). If micromechanical and multiscale models (Trovalusci and Masiani 2003 and 2005; Gambarotta and Lagomarsino 1997$_a$; Alfano and Sacco 2006; Pina and Lourenço 2006; Sacco and Toti 2010; Massart, Peerlings et al. 2007) could be more suitable for reinforced structures, as they allow to evaluate the local stresses, responsible of the FRP decohesion, development of macro elements is necessary for the analysis of real constructions, for the assessment of the safety level of existing structures and for the design of FRP-strengthening. Many improvements can be introduced (different constitutive laws, 3D-behaviour, debonding of FRP, etc.). When micromechanical models are used, units and the mortar joints are characterized by different constitutive laws, the structural analysis is performed considering each constituent of the masonry material, the mortar joints are modeled as interfaces and bricks characterized by a linear or nonlinear response (Oliveira and Lourenço 2004). The structural analyses are characterized by great computational effort, but can be successfully adopted for reproducing laboratory tests (Senthivel and Lourenço 2009). Since in the finite element model, the unit blocks and the mortar beds are discretized, this results in a high number of nodal unknowns.

Macro mechanical models are based on phenomenological constitutive laws for the masonry, derived performing tests on masonry, without distinguishing the blocks and the mortar behavior. They are unable to describe in detail some micro-mechanisms occurring in the damage evolution of masonry but are very effective from a computational point of view for the structural analyses. In most of the cases they are no-tension models. (Luciano and Sacco 1998$_{a,b}$; Addessi, Marfia et al. 2002; Addessi, Sacco et al. 2010; Gambarotta and Lagomarsino 1997$_b$; Sacco 2009;).

Macro elements are simplified macro models for the masonry elements able to simulate the behavior of masonry structures proposed as an alternative to sophisticated models. The use of macro models for the nonlinear analysis of masonry structures is encouraged by several guidelines (FEMA 356, Eurocode 8, Italian Seismic Code) since macro models are characterized by few parameters and a reduced computational effort

regarding the modeling and the structural analysis phases. Nonlinear finite elements, detailed structural analyses, sophisticated models require the determination of too many material parameters, which are often not easy to evaluate and softening models could lead to mesh sensitivity. All these problems can be by-passed with the latter approach. Macro elements allow to extend the frame approach valid for reinforce concrete structures to masonry. This is possible using frame elements both for piers and spandrels and nonlinearities distributed along the elements (Tomazevic 1978; D'Asdia and Viskovic 1994; Braga, Liberatore et al. 1990 and 1996; Magenes 2000; Roca 2006). With the POR method proposed by Tomazevic 1978, the failure takes place only in the piers (elasto-plastic spring) due to the limited shear strength, with the equivalent frame model proposed by Magenes and co-authors 2000 and implemented in the ANDILWall software, spandrels and piers are modeled as elastic beam elements, their intersections as rigid parts and non-linearity is concentrated in some well-defined cross-sections inside the elastic elements. The MultiFan approach proposed by Braga and Liberatore 1990, is based on special strut-and-tie schemes, representing the combination of the compression or tension stress fields which are mobilized in the masonry shear-walls. Finally with the macro model proposed by Brencich and Lagomarsino 1997 and implemented in the TREMURI software, masonry elements are represented as the assembly of three substructures, the axial and bending compliance is concentrated at the extremities, while the shear deformability is presented in the central part. Fig. 2.17 provides a schematic representation of the available strategies to define the constitutive material model of masonry components and structures. The blue box identifies the strategies considered also in this thesis.

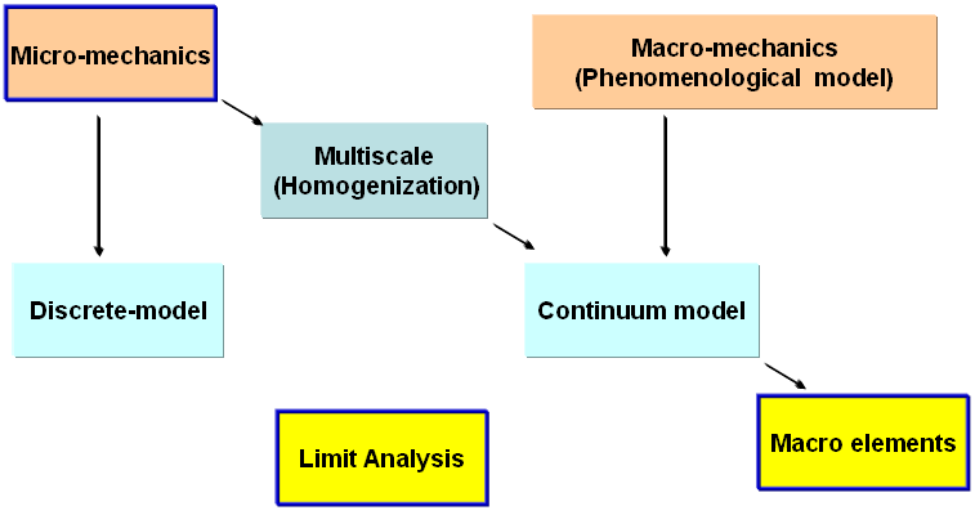

Fig. 2.17 Numerical strategies to model the mechanical behavior of the masonry material

2.3.2 Composite materials (FRP)

Due to the significant level of investment that developed countries have placed in their public and private infrastructure, and the aging of this infrastructure, rehabilitation and strengthening of existing structures has become a research focus. With the advent of FRP new strengthening approaches have become available using external bonding technologies. The advantages of using FRP for reinforcement, renovation, restoration, or retrofitting structures arise from its high mechanical strength, resistance to chemical agents, impermeability to water and reversibility.

This strengthening method has shown significant advantages compared to traditional methods, mainly due to the outstanding mechanical properties of the composite materials, their light weight and the simple application to structural members. Their special properties, in the last years, allowed applying FRP on many different types of structures: Fig. 2.18 shows FRP applications respectively on timber (a), concrete (b) and masonry (c) structures.

Fig. 2.18 FRP applications to structures: (a) Timber; (b) Reinforced concrete; (c) Masonry

FRP materials were developed from aeronautic and mechanical industry where strength is required, together with durability and lightweight. Tab. 2.1 shows a comparison between various types of FRP and metals. The table refers to one-directional fabrics.

Tab. 2.1: Summary of properties for material comparison

Material	Density (Kg/m^3)	Elastic modulus (GPa)	Tensile strength (MPa)
CFRP	1.5	210	2500
GFRP	2	70	1500
AFRP	1.4	77	1750
Steel	7.8	200-210	500-2000
Aluminum	2.8	75	500
Titanium	4.5	110	1200

Due to the aforementioned properties of FRP materials, restoration of historical heritage with such materials has become an attractive solution, besides remaining doubts on compatibility and durability of the bond. Moreover, several experimental investigations have revealed the occurrence of new, often brittle, failure modes due to debonding at the interface between the FRP and the substrate material.

Careful considerations must be taken into account when materials having different mechanical properties are combined to work together, specifically in the context of strengthening of existing structures. In addition to the complexity of masonry itself, the contribution of the FRP and the stress transfer mechanisms must be considered. Among the different types of FRP, Fig. 2.19, Glass FRP (GFRP) seems to be the most suitable material to be used for strengthening of masonry structures. In fact, it is more reasonable to combine materials with closer mechanical properties, especially stiffness. Strengthening of masonry structures with GFRP composites appears an attractive and wise option (Triantafillou 1998$_{a,b}$; Tumialan 2001; Turco, Secondin et al. 2006; Valluzzi, Tinazzi et al. 2002 and 2005; Valluzzi Valdemarca et al. 2001) . Although GFRP does not present mechanical properties as high as carbon FRP (CFRP), its application can effectively lead to a higher increase in strength due to a better compatibility with the masonry substrate and hence to delayed debonding.

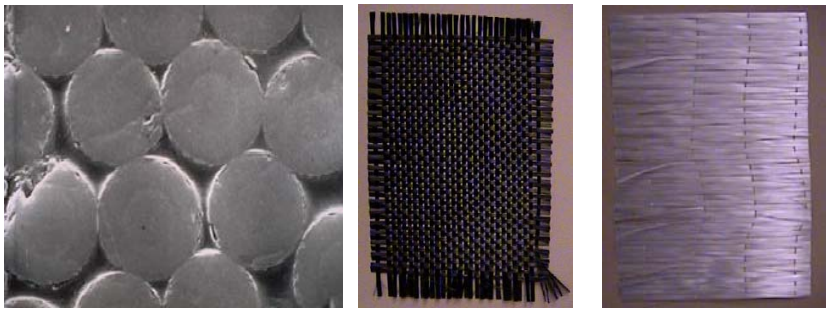

(a) (b) (c)

Fig. 2.19 (a) cross section of FRP laminate; (b) CFRP strip; (c) GFRP strip

The strengthening of masonry structures with GFRP materials necessarily requires a clear understanding of the structural behavior of the strengthened structure. In addition, masonry joints represent the weakest element of masonry and notably affect the overall structural response. The GFRP to masonry interfacial behavior clearly represents a key aspect which must be fully characterized (Oliveira, Basilio et al. 2011). Hence, experimental tests allow a comprehensive insight into this issue giving the possibility

to calibrate constitutive models, and hence to accomplish a deep understanding of the interfacial behavior (Oliveira, Basilio et al. 2010; Cancelliere, Imbimbo et al. 2010).

2.4 Structural modeling and finite element method

As previously mentioned, an important objective in the present study is to obtain robust numerical tools, capable of predicting the behavior of the structure from the linear elastic stage until complete loss of strength. Only then, it is possible to control the serviceability limit state, to fully understand the failure mechanism and assess the safety of the structure under earthquake actions.

This section contains an introduction to linear and nonlinear finite elements and solution procedures. For a detailed description of the finite element method the reader is referred to text books (Zienkiewicz, Taylor et al. 2005; Bathe 1996). Furthermore, the algorithmic aspects of the theory of single and multi-surface plasticity are reviewed in modern concepts. A comprehensive description of the plasticity theory can be found in several books about plasticity (e.g. Hill 1950 and 1998; Chen and Han 1988).

First of all, it is observed that linear elastic finite element models have been widely used for analyzing existing masonry constructions but usually, the act of preparing a finite element model is very time consuming. Given the effort and costs involved in the preparation, the additional time requirements to carry out a nonlinear static analysis are only marginal and the benefits for understanding the behavior of the structure are considerably high (Lourenço 2001). In particular, linear elastic analysis requires the elastic properties of the materials and maximum allowable stresses resulting in information on the deformational behavior and stress distribution of the structure. Limit analysis instead requires the strength of the materials, resulting in information on the failure mechanism of the structure. Finally, nonlinear analysis requires the elastic properties, the strength of the materials and additional inelastic information (the stress-strain diagrams) resulting in information on the deformational behavior, stress distribution and on the failure mechanism of the structure. It is important to observe that the "safety factors" associated with a linear elastic analysis (the so called maximum allowable stress) and with a static limit analysis (the so-called geometric safety factor) cannot be compared with the remaining safety factors, meaning that different methods of analysis lead to different safety factors and different completeness of results.

2.4.1 Continuum mechanics equations

The starting point is the equilibrium equation: (or strong form of the differential equation):

$$\sigma_{ij,j} + b_i = 0 \tag{2.1}$$

Where σ_{ij} is the generic stress component, and b_i indicates a body force per unit volume. If this equation is multiplied by a weighting function δa that fulfils the condition to be zero at the essential boundary conditions, the following equation results:

$$(\sigma_{ij,j} + b_i)\delta a_i = 0 \tag{2.2}$$

and integrating over the volume yields:

$$\int_V (\sigma_{ij,j} + b_i)\delta a_i \, dV = 0 = \int_V \sigma_{ij,j}\delta a_i \, dV + \int_V b_i \delta a_i \, dV \tag{2.3}$$

When the left term is integrated by parts it is possible to obtain:

$$\int_V \sigma_{ij,j}\delta a_i \, dV = \int_V (\sigma_{ij,j}\delta a_i)_j \, dV - \int_V \sigma_{ij,j}\delta a_{i,j} \, dV \tag{2.4}$$

Now, for the right term it is possible to write:

$$\frac{\sigma_{ij}\delta a_{i,j}}{2} = \frac{\sigma_{ji}\delta a_{i,j}}{2} \qquad \text{(due to the symmetry of the stress tensor)} \tag{2.5}$$

or switching the indices:

$$\frac{\sigma_{ij}\delta a_{i,j}}{2} = \frac{\sigma_{ij}\delta a_{j,i}}{2} \tag{2.6}$$

therefore this leads to:

$$\sigma_{ij}\delta a_{i,j} = \frac{1}{2}\sigma_{ij}(\delta a_{i,j} + \delta a_{j,i}) \tag{2.7}$$

and using the strain-displacement relation:

$$\sigma_{ij} a_{i,j} = \frac{1}{2}\sigma_{ij}\delta\varepsilon_{ij} \tag{2.8}$$

substituting this gives:

$$\int_V \sigma_{ij,j}\delta a_i \, dV = \int_V (\sigma_{ij}\delta a_i)_j \, dV - \int_V \sigma_{ij}\delta\varepsilon_{i,j} \, dV \tag{2.9}$$

Employing the divergence theorem for the second term of eq. 2.9, it is possible to convert the volume integral to a surface integral obtaining:

$$\int_V \sigma_{ij,j}\delta a_i \, dV = \int_{\partial V} \sigma_{ij}\delta a_i n_j \, dS - \int_V \sigma_{ij}\delta\varepsilon_{i,j} \, dV \tag{2.10}$$

Finally, using the relationship between surface traction and stress: $p_i = \sigma_{ij} n_j$ in eq. 2.10, this yields:

$$\int_V \sigma_{ij,j} \delta a_i \, dV = \int_{\partial V} p_i \delta a_i \, dS - \int_V \sigma_{ij} \delta \varepsilon_{i,j} \, dV \tag{2.11}$$

and substituting eq. 2.11 in eq. 2.3 leads to:

$$\int_V \sigma_{ij} \delta \varepsilon_{ij} \, dV = \int_{\partial V} p_i \delta a_i \, dS + \int_V b_i \delta a_i \, dV \tag{2.12}$$

This is the weak form of the differential equation governing the problems of continuum mechanics. Along with the essential boundary conditions, it describes any problem (linear and nonlinear). The previous equation is also widely called: principle of virtual work, where the left-hand side represents the internal work, while the right-hand side corresponds to external force plus body force work. This formulation provides the basis of the next finite element approximation, in fact now the statement of the problem can be defined in this way: given the external surface force *p* and the body force ρg where ρg replaces *b* in eq. 2.12, obtain *a* that satisfies the following condition:

$$\int_V \sigma\,(a)\,\varepsilon\,(\delta a)\,dV = \int_{\delta V} \delta a \times p \, dS + \int_V \rho\, \delta a \times g \, dV \quad \forall\, \delta a \in V \tag{2.13}$$

where σ is the stress field vector, ε is the strain field vector, a is the displacement field vector, V is the volume of the body, and ∂V is the boundary of the body.

In the finite element method, the region V is divided into elements with finite magnitude and can be expressed as:

$$V = \sum_e V_e \tag{2.14}$$

and therefore the integration can be discretized as:

$$\int_V dV = \sum_e \int_{V_e} dV \quad \text{and} \quad \int_{\delta V} dS = \sum_e \int_{\delta V_e} dS \tag{2.15}$$

where the subscript *e* stays for each element. Hence eq. 2.13 becomes:

$$\sum_e \left[\int_{V_e} \sigma\,(a)\,\varepsilon\,(\delta a)\,dV - \int_{\delta V_e} \delta a \times p \, dS - \int_{V_e} \rho\, \delta a \times g \, dV \right] = 0 \quad \forall \delta a \in V \tag{2.16}$$

2.4.2 Linear elastic behavior

In finite element computations based on the displacement method the structure is subdivided into elements (step 1), each with its own material properties and for which

relations between the nodal forces and the nodal displacements can be defined. The assembly of elements (step 2) with the consideration of external loads and boundary conditions provides a system of equations describing the equilibrium of structure (step 3), which has to be solved to obtain the nodal displacements of the structure. From these displacements, it is possible to obtain strains and stresses in the integration points (step 4):

Step N. ❶	1_a) Discretization of the displacement field $\{a\}$ 1_b) Calculation of the stiffness matrix of each element	$\{a(x,y,z)\} = [N]\{a_i\}$ $\left[K_l^{(e)}\right] = \int_{V_e} [B]^T [D][B] dV_e$
Step N. ❷	2_a) Transformation from local (l) to global (g) system 2_b) Assembling of the global stiffness matrix starting from local stiffness matrix	$\{a_l\} = [L]\{a_g\}$ $[K_g] = \left[\sum_{e=1}^{m} K_{ij}^{(e)}\right]$
Step N. ❸	Adding loading conditions and boundary conditions	$\begin{Bmatrix} R \\ F \end{Bmatrix} = \begin{bmatrix} K_{11} & K_{12} \\ K_{12}^T & K_{22} \end{bmatrix} \begin{Bmatrix} v \\ x \end{Bmatrix}$
Step N. ❹	Mathematical solution of the algebraic system	$[K_{22}]^{-1}(\{F\} - [K_{12}^T]\{v\}) = \{x\}$ $\{\sigma_l^{(e)}\} = [S_l^{(e)}]\{a_l^{(e)}\}$

The equilibrium condition introduced in eq. 2.12 can be written as:

$$L_V^E = L_V^I \Rightarrow \left\{\delta a_i^{(e)}\right\}^T \left\{R^e\right\} = \left\{\delta a_i^{(e)}\right\}^T \left(\int_V [B]^T \{\sigma\} dV - \int_V [N]^T \{b\} dV\right) \tag{2.17}$$

and so it is obtained:

$$\left\{R^e\right\} = \int_V [B]^T \{\sigma\} dV - \int_V [N]^T \{b\} dV \tag{2.18}$$

with:

$$\{\sigma\} = [C]\left(\{\varepsilon\} - \{\varepsilon_0\}\right) + \{\sigma_0\} \tag{2.19}$$

$$\left\{R^e\right\} = \int_V [B]^T [C]\{\varepsilon\} dV - \int_V [B]^T [C]\{\varepsilon_0\} dV + \int_V [B]^T \{\sigma_0\} dV - \int_V [N]^T \{b\} dV \tag{2.20}$$

where $[C]$ is the elastic constitutive matrix , $[N]$ is the shape functions matrix and $[B]$ is a matrix operator, $\{\sigma_0\}$ is the initial stress vector.

From:

$$\{\varepsilon\} = [B]\{a_i^{(e)}\} \tag{2.21}$$

where $\{a_i^{(e)}\}$ are the nodal displacements, finally, for each element results:

$$\{R^e\} = \int_V [B]^T [C][B]\{a_i^{(e)}\}\, dV - \int_V [B]^T [C]\{\varepsilon_0\}\, dV + \int_V [B]^T \{\sigma_0\}\, dV - \int_V [N]^T \{b\}\, dV \tag{2.22}$$
$$= [K^e]\{a_i^{(e)}\} + \{F^e\}$$

with:

$$[K^e] = \int_V [B]^T [C][B] dv \tag{2.23}$$

$$\{f^e\} = \int_V [B]^T [C]\{\varepsilon_0\}\, dV + \int_V [B]^T \{\sigma_0\}\, dV - \int_V [N]^T \{b\}\, dV \tag{2.24}$$

Summarizing, for each element, the discretization process yields to the following relationships:

$$\{a_e\} = [N]\{a_i^{(e)}\} \tag{2.25}$$

Displacement field vector as function of only nodal displacements

$$\{\varepsilon\} = [L]\{a_e\} \tag{2.26}$$

where $[L]$ is a matrix operator of derivation.

Strain-displacement fields relationship

$$\{\varepsilon\} = [L][N]\{a_i^{(e)}\} = [B]\{a_i^{(e)}\} \tag{2.27}$$

Strain-nodal displacement fields relationship

$$\{R^e\} = [K^e]\{a_i^{(e)}\} + \{f^e\} \tag{2.28}$$

Equivalent nodal forces as functions of nodal displacements

$$\{\sigma\} = [C]\{\varepsilon - \varepsilon_0\} + \{\sigma_0\} \tag{2.29}$$

Stress-strain field relationship.

The last relationship leads to:

$$\{\sigma\} = [C]\{\varepsilon\} - [C]\{\varepsilon_0\} + \{\sigma_0\} = [C][B]\{a_i^{(e)}\} - [C]\{\varepsilon_0\} + \{\sigma_0\} \tag{2.30}$$

So if, $\{\varepsilon_0\} = \{\sigma_0\} = 0$ as usual:

$$\{\sigma\} = [C][B]\{a_i^{(e)}\} = [S]\{a_i^{(e)}\} \tag{2.31}$$

where:

$$[S] = [C][B] \tag{2.32}$$

is the stress matrix.

The following relationship

$$\left\{R_{i,l}{}^{e}\right\}=\left[K_{i,l}{}^{e}\right]\left\{a_{i,l}{}^{e}\right\} \tag{2.33}$$

demonstrated for one element (e_i) and valid in the local (l) system, can be rewritten as a function of all the nodal displacements of the structure $\left\{a_g\right\}$. Expanding the vector $\left\{R_{i,l}{}^{e}\right\}$ and the matrix $\left[K_{i,l}{}^{e}\right]$ of each element to the global system, this yields:

$$\begin{aligned}
&(a)\ \left\{R_{1,g}{}^{e}\right\}=\left[K_{1,g}{}^{e}\right]\left\{a_g\right\};\\
&(b)\ \left\{R_{2,g}{}^{e}\right\}=\left[K_{2,g}{}^{e}\right]\left\{a_g\right\};\\
&\text{.....;}\\
&(c)\ \left\{R_{n,g}{}^{e}\right\}=\left[K_{n,g}{}^{e}\right]\left\{a_g\right\}
\end{aligned} \tag{2.34}$$

where indexes from 1 to n define the number of each element generated in the discretization process (finite element mesh of the continuum).

Finally, summing the single linear system of equations resulting from the finite element process, the equilibrium equation is obtained:

$$\sum_{i=1}^{n}\left\{R_{i,g}{}^{e}\right\}=\left(\sum_{i=1}^{n}\left[K_{i,g}^{e}\right]\right)\left\{a_g\right\}=\left[K_g\right]\left\{a_g\right\}=\left\{R_g\right\} \tag{2.35}$$

where $\left[K_g\right]$ is the global stiffness matrix found assembling the expanded local stiffness matrix $\left[K_{i,g}^{e}\right]$ of each element.

2.4.2.1 Linear analysis and masonry structures

Linear elastic finite element models have been widely used for analyzing existing masonry constructions. In particular, depending on the desired level of accuracy, it is possible to use several strategies to model masonry: bricks and mortar can be both represented by different continuum elements while brick-mortar interface by discontinuous element (detailed micro-modeling), or expanded brick (including in the geometry dimensions half mortar-joint for each side) can be represented by continuous elements while mortar-joints and brick-mortar interface behavior is lumped in only one interface discontinuous element (simplified micro-modeling, Fig. 2.20) or finally bricks, mortar and brick-mortar interfaces can be smeared out in a continuum element by means of homogenization theory (macro-modeling), see Lourenço 1996.

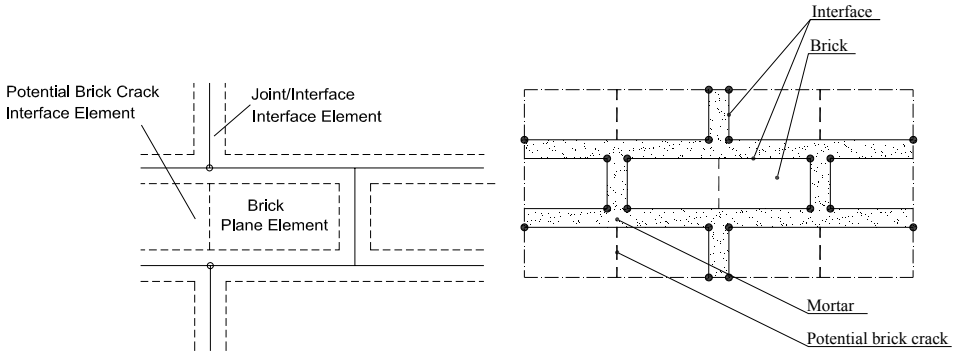

Fig. 2.20 Micro-modeling of masonry structures using interface elements

According to the simplified micro-modeling described previously, the mesh adopted in the analyses includes e.g. eight-node plane stress elements to represent the masonry units (brick + mortar) and six-nodes interface elements to simulate the brick-mortar interface and to allow some discontinuities in the displacement field. Zero thickness is assumed for the interface elements representing each joint.

The plane stress element used for the masonry, Fig. 2.21, can be an eight-node quadrilateral isoparametric element, based on quadratic interpolation and Gauss integration. The polynomial for the displacements u_x and u_y is expressed as:

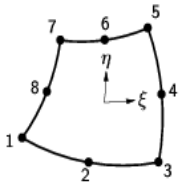

$$u_i(\xi,\eta)=a_0 + a_1\xi + a_2\,\eta + a_3\,\xi\eta + a_4\xi^2 + a_5\,\eta^2 + a_6\,\xi^2\eta + a_7\,\xi\eta^2$$

Fig. 2.21 Plane stress element used to model the units (bricks + mortar)

Typically, this polynomial yields a strain ε_{xx} which varies linearly in *x* direction and quadratically in *y* direction, while the strain ε_{yy} varies linearly in *y* direction and quadratically in *x* direction and the shear strain γ_{xy} varies quadratically in both directions.

For the interface elements, a three plus three curved interface element between two lines in a two-dimensional configuration can be used, Fig. 2.22. The local *xy* axes for the displacements are evaluated in the first node with *x* from node 1 to node 2. Variables are oriented in the *xy* axes. The element is based on quadratic interpolation. A 4-point Newton-Cotes integration scheme or a 3 point Lobatto integration scheme are possible.

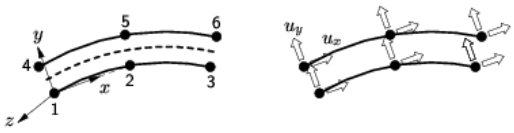

Fig. 2.22 Interface element used to model the brick-mortar joint

As a first-order calculation, the simple linear finite element analysis (FEA) can only provide the displacement field of the structure and predict the stress level in the material based on linear elastic behavior, Fig. 2.23

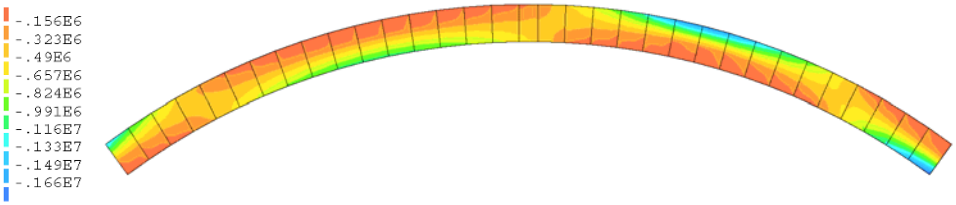

Fig. 2.23 Linear analysis of unstrengthened masonry arch modeled with interface elements (Contour Levels of the principal compressive stresses, kPa)

Simplified linear FEA shows one possible stress state in the material, but does not say anything about the stability or collapse of the arch. This is a very simple and well-known problem that immediately show how hard is to draw significant conclusions using linear FEA, even for simple two-dimensional problems. Therefore, the use of linear elastic analyses is debatable, taking into account the advanced tools today available to solve engineering problems.

2.4.3 Nonlinear behavior

The solution of nonlinear problems can be found by an iterative application of the linear procedures introduced in the previous section until the final stage. The nonlinearity employed in this work arises in materials having inelastic constitutive laws (the masonry and the interfaces between different materials, namely the masonry and the FRP in this work), where stress depends from strain according to a complex constitutive law. A nonlinear problem does not necessarily have a solution and if this exists it is not necessarily unique. The main way to assess a real solution is to apply the external load in small step-increments. This aspect is more important if the stress-strain behavior is path dependent.

In nonlinear problems the stiffness matrix $\left[K_g\right]$ depends from the unknown nodal displacements, therefore the equilibrium equation becomes:

$$[K_g(a_g)]\cdot\{a_g\}=\{R_g\} \tag{2.36}$$

and therefore an incremental-iterative procedure is required to solve the problem. First, the previous equation needs to be rewritten in incremental form considering load increments, displacement increments and the tangential stiffness matrix, yielding to:

$$[K_t(\delta a_g)]\cdot\{\delta a_g\}=\{\delta R_g\} \tag{2.37}$$

According to the formulation by Zienkiewicz, Taylor et al. 2005, a non linear problem can be formulated in terms of a discretization set $\{a_g\}$ collecting all the nodal displacements. The system of nonlinear equations that results from the finite element discretization is solved with an incremental-iterative Newton-Raphson method.

As follows, the procedure employed will be briefly described.

2.4.3.1 Newton-Raphson method

The starting point is the linear elastic solution, where the relationship between stress and strain is defined from the constitutive matrix $[C]$. When the first increment of load $\{\delta R_1\}$ is applied, the increment counter m will be equal to 1, the iteration counter i will be posed also equal to 1, the starting tangent constitutive matrix $[C_t^1]$ will be the elastic constitutive matrix $[C]$: $[C_t^1]=[C]$, the shape function matrix $[B]$ will be calculated according to the element types (meaning their shape functions) employed in the finite element model developed. So, all the parameters required as input are known and therefore this allows to determine $[K_{t_1}^{(1)}]=\int_v [B^T][C][B]dV$, $\{\delta a_1^{(1)}\}$, $\{\varepsilon_1^{(1)}\}$, $\{\sigma_1^{(1)}\}$. Then, the evolution of the plasticity state will be determined by means of a comparison of the current stress state defined by vector "σ" (relating to the three-dimensional stress-strain evolution of the structural system analyzed) and the yielding stress values $\sigma^{(1)}{}_{pl1}$, $\sigma^{(1)}{}_{pl2}$, ..., $\sigma^{(1)}{}_{pl3}$ (only two if 2 surface plasticity are used in the model) that indicate the attainment of the plasticity condition: meaning the intersection with the plasticity functions employed in the analysis. If this occurs, the stress has to be updated in such a way that the plastic-domain and the hardening and softening laws hypothesized are respected. Then a tangent constitutive matrix $\left[C_{t_1}^{(1)}\right]$ will be determined according to the current stress/strain condition. Once the tangent

constitutive matrix $\left[C_{t_1}^{(1)}\right]$ is obtained, the new global tangent stiffness matrix of the system can be determined in the next iteration step: $\left[K_{t_1}^{(2)}\right]=\int_v [B^T][C_{t_1}^{(1)}][B]dV$. The iteration process will go forward until a special convergence criterion will be fulfilled. Three different possible criteria are presented:

$$\frac{\|\{R_1\}-\{F_1^{(1)}\}\|}{\|\{\Delta R_1\}\|}\le \delta_1 \tag{2.38}$$

if the residual force $\|\{R_1\}-\{F_1^{(1)}\}\|$ over the incremental external load $\|\{\Delta R_1\}\|$ is considered,

$$\frac{\|\{d\Delta^{(i)}\}\|}{\|\{\Delta^{(i)}\}\|}\le \delta_2 \tag{2.39}$$

if the incremental displacement $\|\{d\Delta^{(i)}\}\|$ over the current displacement $\|\{\Delta^{(i)}\}\|$ is considered

$$\frac{\|\left(\{R\}-\{F^{(i)}\}\right)^T\{d\Delta^{(i)}\}\|}{\|\left(\{R\}-\{F^{(1)}\}\right)^T\{d\Delta^{(1)}\}\|}\le \delta_3 \tag{2.40}$$

if the ith-work increment $\|\left(\{R\}-\{F^{(i)}\}\right)^T\{d\Delta^{(i)}\}\|$ over the first work increment $\|\left(\{R\}-\{F^{(1)}\}\right)^T\{d\Delta^{(1)}\}\|$ is considered.

Generalizing this procedure, Zienkiewicz, Taylor et al. 2005, the system of equations to be solved becomes at the stage n+1:

$$\{\Psi(a_{n+1}^{i+1})\}=\{R_{n+1}\}-\{F(a_{n+1}^{i})\}\approx\{\Psi(a_{n+1}^{i})\}+\left\{\left(\frac{\partial\Psi}{\partial a}\right)^i_{n+1}\right\}\cdot\{\delta a_{n+1}^{i+1}\}=\{\Psi(a_{n+1}^{i})\}+\left(\left[K_t\right]\right)^i_{n+1}\cdot\{\delta a_{n+1}^{i+1}\}=0 \tag{2.41}$$

$$\Rightarrow\ \{\delta a_{n+1}^{i+1}\}=-(\left[K_t^{-1}\right])^i_{n+1}\{\Psi^i_{n+1}\} \tag{2.42}$$

where $\{\Psi\}$ is the vector of residuals (unbalanced forces), $\{R\}$ is the vector of external forces and $\{F\}$ is the vector of internal forces. Therefore, known the near equilibrium solution of the previous stage *n*, results:

$$\{R_{n+1}\}=\{R_n\}+\{\Delta R_{n+1}\} \tag{2.43a}$$

$$\{\delta a^{i+1}_{n+1}\}=-\left(\left[K_t^{-1}\right]\right)^i_{n+1}\{\Psi^i_{n+1}\}) \tag{2.43b}$$

$$\{\Delta a^{i+1}_{n+1}\}=\sum_{k=1}^{i+1}\{\delta a^k_{n+1}\} \tag{2.44a}$$

$$\{a_{n+1}\}=\{a_n\}+\{\Delta a_{n+1}\} \tag{2.44b}$$

$$\left\{\delta\varepsilon_{n+1}^{i+1}\right\}=\left[B\right]\left\{\delta a_{n+1}^{i+1}\right\} \quad (2.45_a) \qquad \left\{\delta\sigma_{n+1}^{i+1}\right\}=\left[C_{t_{n+1}}^{(i)}\right]\left\{\delta\varepsilon_{n+1}^{i+1}\right\} \quad (2.45_b)$$

$$\left\{\Delta\varepsilon_{n+1}^{i+1}\right\}=\sum_{k=1}^{i+1}\left\{\delta\varepsilon_{n+1}^{k}\right\} \quad (2.46_a) \qquad \left\{\Delta\sigma_{n+1}^{i+1}\right\}=\sum_{k=1}^{i+1}\left(\left[C_{t_{m+1}}^{i}\right]\right)\left\{\delta\varepsilon_{n+1}^{k}\right\} \quad (2.46_b)$$

It is worth underlining that load increments

$$\left\{\Delta R_{n+1}\right\}=\left\{R_{n+1}\right\}-\left\{R_{n}\right\} \quad (2.47)$$

have to be small because the aim is to catch the path dependence of the process. Moreover, small steps allow getting a solution in a not excessive number of iterations. Sometimes manual adjustment of the load increments are required to overpass critical points. It can be demonstrated that, according to the previous formulation, it is possible to describe the full nonlinear evolution of the system in terms of strains, stresses, and the load-displacement curve.

2.4.3.2 Special techniques to follow path-dependent system evolution

Line search techniques are required to assess the solution outside the radius of convergence of the Newton-Raphson method. A new factor μ has to be defined to scale the incremental displacement field and this factor is determined imposing the projection of residuals in the search direction to be zero:

$$\left(\left\{\delta a_{n+1}^{i+1}\right\}\right)^{T}\left\{\Psi(a_{n+1}^{i}+\mu_{ij}\delta a_{n+1}^{i+1})\right\}=0\Rightarrow\mu_{ij} \quad (2.48)$$

where j is the counter of line searches.

Very often in structural problems, load increments are defined by means of a load factor:

$$\left\{\Delta R_{n+1}\right\}=\Delta\lambda_{n+1}\cdot\left\{R_{0}\right\} \quad (2.49)$$

where $\left\{\Delta R_{n+1}\right\}$ is the external force vector increments, $\Delta\lambda_{n+1}$ is the load factor used, and $\left\{R_{0}\right\}$ is the normalized force vector. If standard load control is used, the numerical procedure is unable to overpass critical points, therefore arc-length procedures are required to solve this kind of problems.

The original problem is reformulated by means of a constraint equation:

$$\begin{cases}\left\{\Psi_{n+1}\right\}=-(\lambda_{n}+\Delta\lambda_{n+1})\left\{R_{0}\right\}-\left\{F(a_{n}+a_{n+1})\right\}=0\\ \left\{R(\Delta\lambda_{n+1},\ \Delta a_{n+1})\right\}=0\end{cases} \quad (2.50)$$

Where $\Delta\lambda_{n+1}$ is an additional variable. This can be simply found knowing the expression of the nodal displacement update, in fact according to previous formulation eq. 2.43_b becomes

$$\begin{aligned}&\left\{\delta a_{n+1}^{i+1}\right\} = -\left(\left[K_t^{-1}\right]\right)_{n+1}^{i}\left\{\Psi_{n+1}^{i}\right\} = -\left(\left[K_t^{-1}\right]\right)_{n+1}^{i}\left(\left\{R_{n+1}^{i}\right\} - \left\{F_n\right\}\right) - \Delta\lambda_{n+1}^{i+1}\left\{R_0\right\} = \\ &\left\{-\left(\left[K_t^{-1}\right]\right)_{n+1}^{i}\left(\left\{F_n\right\} - \left\{R_{n+1}^{i}\right\}\right)\right\} + \Delta\lambda_{n+1}^{i+1}\left\{\left(\left[K_t^{-1}\right]\right)_{n+1}^{i}\left\{R_0\right\}\right\} = \left\{\delta^I a_{n+1}^{i+1}\right\} + \Delta\lambda_{n+1}^{i+1}\cdot\left\{\delta^{II} a_{n+1}^{i+1}\right\} = f\left(\Delta\lambda_{n+1}^{i+1}\right)\end{aligned} \tag{2.51}$$

To overcome limit points, the Newton-Raphson method has to be constrained with the updated-normal-plane method, therefore imposing the constraint condition, i.e. in this case the orthogonality between the tangent vector $\left\{\delta a_{n+1}^{i+1}\right\}$ and the update vectors $\left\{\Delta a_{n+1}^{i}\right\}$:

$$\left(\left\{\Delta a_{n+1}^{i}\right\}\right)^T\left\{\delta a_{n+1}^{i+1}\right\} = 0 \tag{2.52}$$

this yields:

$$\Delta\lambda_{n+1}^{i+1} = -\frac{\left(\left\{\Delta a_{n+1}^{i}\right\}\right)^T\left\{\delta^I a_{n+1}^{i+1}\right\}}{\left(\left\{\Delta a_{n+1}^{i}\right\}\right)^T\left\{\delta^{II} a_{n+1}^{i+1}\right\}} \tag{2.53}$$

Moreover, for problems where cracking and sliding are important, it is recommended to select two displacements at both sides of an active crack or slip line restricting the number of degrees of freedom in the constraint equation. Subtracting these two displacements leads to some mode I or mode II Crack Mouth Opening Displacement (CMOD) as a scalar parameter. eq. 2.53 then becomes:

$$\Delta\lambda_{n+1}^{i+1} = -\frac{\left\{COD_{n+1}^{i+1}\right\}\cdot\left\{\delta^I a_{n+1}^{i+1}\right\}}{\left\{COD_{n+1}^{i+1}\right\}\left\{\delta^{II} a_{n+1}^{i+1}\right\}} \tag{2.54}$$

This technique is defined also as indirect displacement control method.

2.5 Plasticity theory

This paragraph introduces the fundamental aspects of the theory of plasticity such as: the yielding condition, the plastic multiplier, the flow rule, the normality hypothesis, the consistency condition, the concept of isotropic and kinematic hardening. This general formulation is necessary to understand the constitutive models developed in chapter 3 and 4, the first within the framework provided from the theory of multi-surface plasticity and the second of cyclic plasticity.

2.5.1.1 Yielding functions

Numerical implementation of plasticity theory requires the definition of the yield functions bounding the elastic domain. When stresses $[\sigma]$ satisfy the yielding criterion employed, yielding occurs. The best way to introduce the concept of the yielding function is to analyze the spring-sliding system of Fig. 2.24.

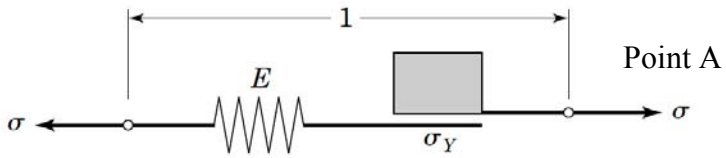

Fig. 2.24 The zero length spring (ZLH) model: elastic part and friction part

The horizontal displacement of point A is first due to the elongation of the spring, since, for low force levels, the adhesion and the friction between the block and the floor will prevent any sliding of the block (De Borst 1991) . The block will start sliding only when the maximum shear force due to both adhesion and friction is exhausted and the yielding function allows to define this moment. For the simple system considered above there are only two force components: H and V. The simplest assumption that sliding starts when the Coulomb friction augmented with some adhesion is fully mobilised leads to:

$$H + V\tan\phi - c = 0 \tag{2.55}$$

with ϕ the so-called friction angle and c the adhesion. If

$$H + V\tan\phi - c < 0 \tag{2.56}$$

only elastic deformations will take place. A combination of forces in which

$$H + V\tan\phi - c > 0 \tag{2.57}$$

is physically impossible, since the maximum horizontal force is bounded by the restriction (2.55). If we assume that ϕ and c are constants, this leads after differentiation to

$$f(\sigma) = H + V\tan\phi - c = 0 \;\rightarrow\; \dot{H} + \dot{V}\tan\phi = 0 \tag{2.58}$$

It is observed here that due to the difficulties to describe completely the material behaviour with a single yield surface, the theory of multi-surface plasticity needs to be introduced. In this study several yield functions are used. The tension cut-off criterion,

assuming exponential softening for the tension mode failure according to experiments, leads to this yield function:

$$f_1(\sigma, k_1) = \sigma - \sigma_1^{pl}(k_1) = \sigma - f_t \cdot \exp\left(-\frac{f_t}{G_f^I} \cdot k_1\right) \tag{2.59}$$

where f_t is the tensile strength of the unit-mortar interface and G_f^I is the mode I fracture energy. For the coulomb-friction criterion, the yield function reads:

$$f_2(\sigma, k_2) = |\tau| + \sigma \tan\phi(k_2) - \sigma_2^{pl}(k_2) = |\tau| + \sigma \tan\phi(k_2) - c \cdot \exp\left(-\frac{c}{G_f^{II}} \cdot k_2\right) \tag{2.60}$$

where

$$\tan\varphi = \tan\varphi_0 + (\tan\varphi_r - \tan\varphi_0)\frac{c - \sigma_2^{pl}}{c} \tag{2.61}$$

c is the cohesion of the unit-mortar interface, ϕ_0 is the initial friction angle, ϕ_r is the residual friction angle and G_f^{II} is the mode II fracture energy. For the compressive cap criterion an ellipsoidal interface model is used and the yield function reads for a 2D configuration:

$$f_3(\sigma, k_3) = C_{nn}\ \sigma^2 + C_{ss}\tau^2 + C_n\sigma - (\sigma_3^{pl}(k_3))^2 \tag{2.62}$$

where C_{nn} , C_{ss} , C_n are a set of material parameters and $\sigma_1^{pl}, \sigma_2^{pl}, \sigma_3^{pl}$ are the yielding values according Lourenço 1996.

2.5.1.2 Consistency Condition

In the preceding description the concept of a yield function has been introduced as the function that defines the surface in the n-dimensional stress space which separates permissible from non-permissible stress states. Plastic strain occurs if only the following two conditions are simultaneously met:

$$f = 0\,;\ \dot{f} = 0 \tag{2.63}$$

Eq. 2.63 is usually called Prager Consistency Condition.

2.5.1.3 The plastic multiplier and the tangent stiffness matrix

The best way to introduce the concept of the plastic multiplier and the tangent stiffness matrix is to analyze again the spring-sliding system of Fig. 2.24. The horizontal

displacement of point A is first due to the elongation of the spring, and second due to the sliding of the block when the adhesion and friction are exhausted. The total displacement is therefore obtained adding the elastic reversible part to the plastic, irreversible part:

$$\varepsilon = \varepsilon_e + \varepsilon_p \tag{2.64}$$

Moreover, the dependence of the stress vector on the elastic strain vector ε_e can be expressed as:

$$\sigma = D_e \, \varepsilon_e \tag{2.65}$$

with D_e the elastic stiffness matrix. Moreover, the plastic strain vector can be written as the product of a scalar $\dot{\lambda}$ defined as the plastic multiplier and a vector *m*:

$$\dot{\varepsilon}_p = \dot{\lambda} m \tag{2.66}$$

In eq. (2.66) $\dot{\lambda}$ determines the magnitude of the plastic flow, while *m* describes the direction of the plastic flow. Since the yield function *f* has been assumed to be solely a function of the stress tensor, the consistency condition can be elaborated as

$$n^T \dot{\sigma} = 0 \tag{2.67}$$

with *n* the gradient vector of the yield function, i.e. the vector that is perpendicular to the yield surface at the current stress point (see Fig. 2.25).

$$n = \frac{\partial f}{\partial \sigma} \tag{2.68}$$

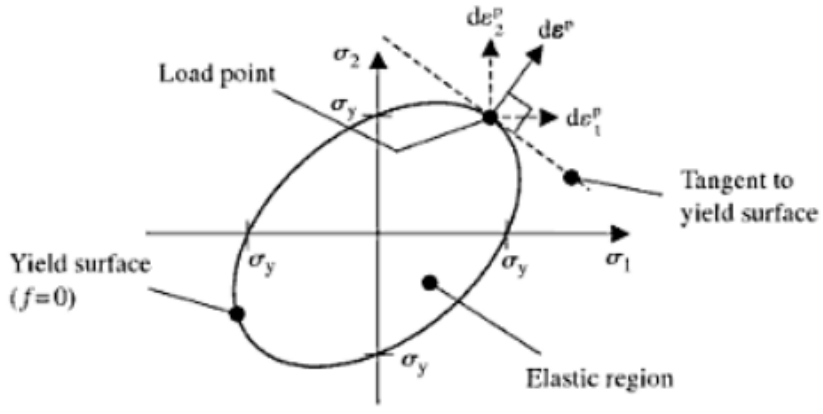

Fig. 2.25 Orthogonality of the gradient vector n to the yield surface f = 0, (see Dunne and Petrinic 2006)

Differentiation of eq. 2.65 and combination of the result with eqs. 2.66 and 2.67 yields an explicit expression for the magnitude of the plastic flow

$$\dot{\lambda} = \frac{n^T D_e \dot{\varepsilon}}{n^T D_e m} \tag{2.69}$$

For the simple spring-sliding system, eq. 2.68 can be expressed with the vector

$$n^T = \begin{bmatrix} 1 & \tan\phi \end{bmatrix} ; \tag{2.70}$$

while eq. 2.67 can be written symbolically as:

$$n^T \dot{f} = 0 \tag{2.71}$$

where

$$\begin{bmatrix} 1 & \tan\phi \end{bmatrix} = n^T ; \quad \begin{bmatrix} \dot{H} & \dot{V} \end{bmatrix}^T = \dot{f} = \dot{\sigma} \tag{2.72}$$

In fact it results with a simple differentiation:

$$H + V\tan\phi - c = 0 \rightarrow \dot{H} + \dot{V}\tan\phi = 0 \rightarrow \begin{bmatrix} 1 & \tan\phi \end{bmatrix} \begin{bmatrix} \dot{H} & \dot{V} \end{bmatrix}^T = 0 \tag{2.73}$$

Premultiplying eq. 2.65 with n^T and utilising the fact that during plastic flow eq. 2.71 must hold, the following explicit expression is obtained for the (plastic) multiplier $\dot{\lambda}$

$$n^T \dot{f} = n^T D_e \begin{bmatrix} \dot{\varepsilon} - \dot{\lambda} m \end{bmatrix} \rightarrow \tag{2.74}$$

$$\dot{\lambda} = \frac{n^T D_e \dot{\varepsilon}}{n^T D_e m} \tag{2.75}$$

This can be inserted in eq. 2.74 to yield an explicit relation between stress rate and the strain rate:

$$\dot{\sigma} = \left[D_e - \frac{D_e m\, n^T D_e}{n^T D_e m} \right] \dot{\varepsilon} \tag{2.76}$$

Finally the tangent stiffness matrix $\mathbf{D}^{ep}$ can be defined:

$$\mathbf{D}^{ep} = \left. \frac{d\sigma_{n+1}}{d\varepsilon_{n+1}} \right|_{n+1} = \left[D_e - \frac{D_e m\, n^T D_e}{n^T D_e m} \right] ; \tag{2.77}$$

2.5.1.4 The flow rule

The definition of the plastic flow direction *m* can be assessed with the Drucker assumption that mathematically, it states that:

$$\dot{\sigma}^T \dot{\varepsilon}_p = 0 \tag{2.78}$$

Comparing this result with the consistency condition shows that

$$\dot{\sigma}^T \dot{\varepsilon}_p = 0 \rightarrow \dot{\sigma}^T \dot{\lambda} m = 0 \rightarrow m^T \dot{\sigma} = 0 \tag{2.79}$$

$$m = \mu n \tag{2.80}$$

with μ an undetermined scalar quantity. Accordingly, the expression for computing the plastic strain rate transforms into the so-called associated flow rule of plasticity

$$\dot{\varepsilon}_p = \dot{\lambda} m \rightarrow \dot{\lambda} \mu n \tag{2.81}$$

Since the plastic flow direction is now normal to the yield surface, the associated flow rule is also referred to as normality rule. Instead, the assumption of a non-associated flow rule for single surface plasticity requires the definition of a plastic potential *g* so that:

$$\dot{\varepsilon}_p = \dot{\lambda} \frac{\partial g}{\partial \sigma} \tag{2.82}$$

where *g* is the plastic potential. Usually, simplified algorithms are obtained if the plastic potential *g* has separate variables, i.e. it can be written as:

$$g(\sigma, \kappa) = \Phi(\sigma) + \Omega(\kappa) \tag{2.83}$$

where Φ and Ω represent generic functions. In this case the tangent stiffness matrix does not preserve the symmetry.

In general, however, since it is extremely complex to describe the material behavior with a single yield surface in an appropriate manner, the theory of multisurface plasticity become necessary. In this case the elastic domain is defined by a number of functions $f_i < 0$ which define a composite yield surface. An important issue, for multisurface plasticity model is the intersection of different yield surfaces that defines corners, see Fig. 2.26**,** and according to Koiter 1953, the plastic strain rate $\dot{\varepsilon}_p$ in the corner is obtained from a linear combination of the plastic strain rates of the two yield surfaces, reading:

$$\dot{\varepsilon} = \dot{\varepsilon}_1^p + \dot{\varepsilon}_2^p = \dot{\lambda}_1 \frac{\partial g_1}{\partial \sigma} + \dot{\lambda}_2 \frac{\partial g_2}{\partial \sigma} \tag{2.84}$$

The yield surfaces can also be explicitly coupled by introducing composite hardening scalar rates $\dot{\kappa}_1^c$ and $\dot{\kappa}_2^c$

$$\dot{\kappa}_1^c = \dot{\kappa}_1^c(\dot{\kappa}_1 + \dot{\kappa}_2) \qquad \dot{\kappa}_2^c = \dot{\kappa}_2^c(\dot{\kappa}_1 + \dot{\kappa}_2) \tag{2.85}$$

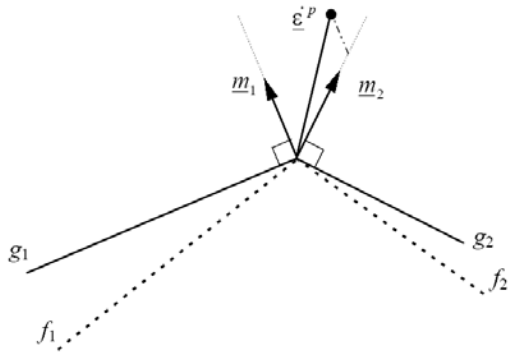

Fig. 2.26 Corner in the yield surface and/or plastic potential function.

2.5.1.5 Hardening behavior – general formulation

So far, it has been assumed that the yield function only depends on the stress tensor. Also in the simple slip model the assumption was made that the friction coefficient was a constant and did not depend upon the previous loading history. Such a dependence, however, can easily be envisaged, e.g. due to breaking-off of the asperities between the block and the surface. The simplest extension beyond the model of ideal plasticity as adopted in the preceding paragraphs is to make the yield function also dependent on a scalar measure of the plastic strain tensor:

$$f\ (\sigma, \bar{\sigma}(\kappa)) = 0 \tag{2.86}$$

where the yield stress value $\bar{\sigma}$ is a function, commonly named hardening law, of the scalar κ, which is introduced as a measure for the amount of hardening or softening.
Two types of hardening laws are commonly used in the practice: isotropic hardening if the yielding surface shrinks or expands in the stress space, kinematic hardening if it moves in the stress space, see Fig. 2.27.

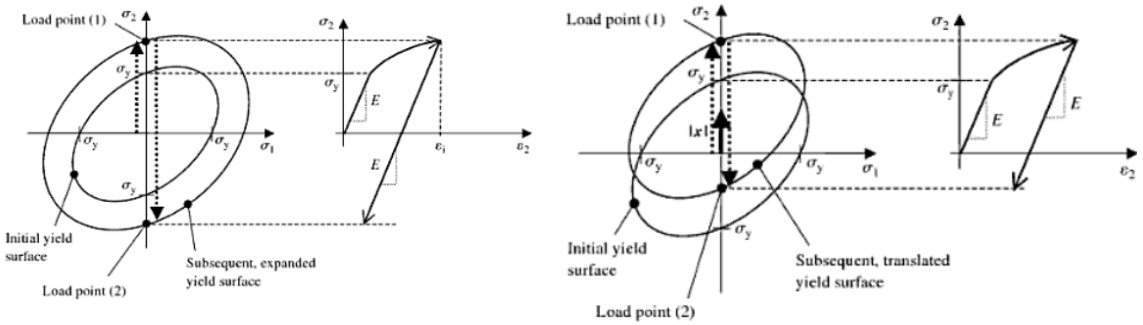

Fig. 2.27 Hardening behavior: (a) isotropic; (b) kinematic, (see Dunne and Petrinic 2006)

Loading/unloading can be conveniently established in standard Kuhn-Tucker form by means of the conditions:

$$\dot{\lambda}_i \geq 0; \quad f_i \leq 0; \quad \dot{\lambda}_i \, f_i = 0 \tag{2.87}$$

where $\dot{\lambda}_i$ is the plastic multiplier rate. In the case of strain hardening (or softening) the scalar $\dot{\kappa}$ reads

$$\dot{\kappa} = \dot{\varepsilon}_{eps} \tag{2.88}$$

where the equivalent plastic strain rate $\dot{\varepsilon}_{eps}$ must always be positive and increasing. The simplest combination of this kind which is dimensionally correct is

$$\dot{\kappa} = \dot{\varepsilon}_{eps} = \sqrt{(\dot{\varepsilon}_p)^T \dot{\varepsilon}_p} \tag{2.89}$$

Another possibility is to define the equivalent plastic strain rate from the plastic work per unit of volume in the form

$$\dot{W}_p = \sigma^T \dot{\varepsilon}_p \Leftrightarrow \bar{\sigma} \dot{\varepsilon}_{eps} \tag{2.90}$$

which gives

$$\dot{\kappa} = \dot{\varepsilon}_{eps} = \frac{1}{\bar{\sigma}} \sigma^T \dot{\varepsilon}_p \tag{2.91}$$

In the case of work hardening (or softening), the scalar $\dot{\kappa}$ should be a work measure and simply read

$$\dot{\kappa} = \dot{W}_p = \sigma^T \dot{\varepsilon}_p \tag{2.92}$$

2.5.1.6 Cyclic plasticity

A combined isotropic and kinematic hardening formulation is necessary for applications to cyclic plasticity where within an individual cycle, kinematic hardening is the dominant hardening process but over each cycle, the material also hardens or soft isotropically such that the peak tension and compression stresses in a given cycle increase/decrease from one cycle to the next until saturation is achieved, see Fig. 2.28. The MultiFan model for cyclic loads will be developed in this theoretical framework.

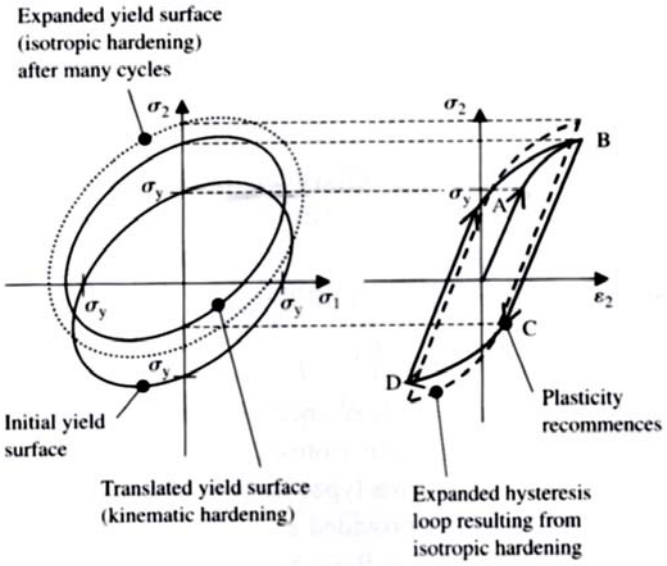

Fig. 2.28 Cyclic behavior: kinematic and isotropic hardening are combined, (see Dunne and Petrinic 2006)

2.5.1.7 Algorithmic aspects

Eq. 2.76 sets a linear relation between the stress-rate tensor and the strain-rate tensor.

To obtain the strains and stresses in a structure that are coupled with a generic loading stage eq. 2.76 must therefore be integrated along the loading path. The integration of the rate equations is a problem of evolution and this means that at a stage *n* the total strain field and the plastic strain field as well as the hardening parameter(s) are known:

$$\left\{\varepsilon_n, \varepsilon_n^p, \kappa_{i,n}\right\} \tag{2.93}$$

The elastic strain and stress fields are regarded as dependent variables which can always be obtained from the basic variables through the relations

$$\varepsilon_n^e = \varepsilon_n - \varepsilon_n^p \tag{2.94}$$

$$\sigma_n = \mathbf{D}\varepsilon_n^e \tag{2.95}$$

Therefore, the stress field at a stage $n + 1$ is computed once the strain field is known. The problem is strain driven in the sense that the total strain ε is trivially updated according to the exact formula

$$\varepsilon_{n+1} = \varepsilon_n + \Delta\varepsilon_{n+1} \tag{2.96}$$

It remains to update the plastic strains and the hardening parameter(s). These quantities are determined by integration of the flow rule(s) and hardening law(s) over the step $n \to n+1$. For single surface plasticity, in the general case of $g = g(\sigma, \kappa)$, this algorithm results in the following set of nonlinear equations in the presence of yielding, see Lourenço 1996:

$$\begin{cases} D^{-1}(\sigma_{n+1} - \sigma^{trial}) + \Delta\varepsilon^{p}_{n+1} = 0 \\ \Delta\kappa_{n+1} = \Delta\kappa_{n+1}(\sigma_{n+1}, \Delta\varepsilon^{p}_{n+1}) \\ f_{n+1}(\sigma_{n+1}, \kappa_{n+1}) = 0 \end{cases} \tag{2.97}$$

in which $\Delta\varepsilon^{p}_{n+1}$ reads

$$\Delta\varepsilon^{p}_{n+1} = \Delta\lambda_{n+1}\left(\frac{\partial g}{\partial\sigma}\right)_{n+1} \tag{2.98}$$

$\Delta\kappa_{n+1}$ results from the integration of one of the rate equations and the elastic predictor step returns the value of the elastic trial stress σ^{trial}

$$\sigma^{trial} = \sigma_n + \mathbf{D}\Delta\varepsilon_{n+1} \tag{2.99}$$

The unknowns of the system of nonlinear equations are the components of the stress vector σ_{n+1} plus the state variables $\Delta\kappa_{n+1}$ and $\Delta\lambda_{n+1}$. The system is solved with a regular Newton-Raphson method where the starting point is given by the elastic predictor: $\sigma_{n+1} = \sigma^{trial}$, $\Delta\kappa_{n+1} = 0$ and $\Delta\lambda_{n+1} = 0$. Yielding occurs because the elastic trial stress σ^{trial} lies outside the current (at step *n*) elastic domain. The plastic corrector, given by eq. 2.82, "brings back" the stress update to the yield surface and is thus termed return mapping. If the plastic potential has separate variables, in most cases, and for the yield functions used later in chapter 3, eq. 2.97 can be solved in order to obtain explicitly the updated stress value as a function of the updated plastic multiplier

$$\sigma_{n+1} = \sigma_{n+1}(\Delta\lambda_{n+1}) \tag{2.100}$$

Furthermore, inserting eq. 2.98 in eq. 2.97_2 yields

$$\Delta\kappa_{n+1} = \Delta\kappa_{n+1}(\sigma_{n+1}, \Delta\lambda_{n+1}) \tag{2.101}$$

Substitution of these two equations in the yield function, cf. eq. 2.97_3, leads to a nonlinear equation in one variable, namely $\Delta\lambda_{n+1}$: $f_{n+1}(\Delta\lambda_{n+1}) = 0$. This constitutive equation is solved again with a local Newton-Raphson method. The derivative of $f_{n+1}(\Delta\lambda_{n+1})$ with respect to $\Delta\lambda_{n+1}$, can be determined after some manipulation as:

$$\left(\frac{\partial f}{\partial\Delta\lambda}\right)_{n+1} = \gamma^{T}\frac{\partial\sigma}{\partial\Delta\lambda} - h \tag{2.102}$$

where the modified yield surface gradient γ and the hardening modulus h are given by

$$\gamma = \frac{\partial f}{\partial \sigma} + \frac{\partial f}{\partial k}\left(\frac{\partial \kappa}{\partial \sigma}\right)_{n+1}$$
$$h = -\frac{\partial f}{\partial \kappa}\left(\frac{\partial \kappa}{\partial \Delta\lambda}\right)_{n+1} \tag{2.103}$$

For multi-surface plasticity, in the general case of $g = g(\sigma, \kappa)$, the Euler backward algorithm results in the following set of nonlinear equations in the presence of yielding, see again Lourenço 1996 for a complete discussion:

$$\begin{cases} D^{-1}(\sigma_{n+1} - \sigma^{trial}) + \Delta\varepsilon^{p}_{1,n+1} + \Delta\varepsilon^{p}_{2,n+1} = 0 \\ \Delta\kappa^{c}_{1,n+1} = \Delta\kappa^{c}_{1,n+1}(\sigma_{n+1}, \Delta\varepsilon^{p}_{1,n+1}, \Delta\varepsilon^{p}_{2,n+1}) \\ \Delta\kappa^{c}_{2,n+1} = \Delta\kappa^{c}_{2,n+1}(\sigma_{n+1}, \Delta\varepsilon^{p}_{1,n+1}, \Delta\varepsilon^{p}_{2,n+1}) \\ f_{1,n+1}(\sigma_{n+1}, \kappa^{c}_{1,n+1}) = 0 \\ f_{2,n+1}(\sigma_{n+1}, \kappa^{c}_{2,n+1}) = 0 \end{cases} \tag{2.104}$$

2.5.1.8 Evaluation of the tangent operator

Similarly to the previous formulation, see Lourenço et al. 1994, an expression for the stiffness matrix can be determined also for multisurface plasticity and reads

$$\mathbf{D}^{ep} = \left.\frac{d\sigma_{n+1}}{d\varepsilon_{n+1}}\right|_{n+1} = H - HU\left(E + V^{T}HU\right)^{-1}V^{T}H \tag{2.105}$$

where the modified stiffness matrix reads

$$\mathbf{H} = \left[\mathbf{D}^{-1} + \Delta\lambda_{1,n+1}\frac{\partial^2 g_1}{\partial\sigma^2} + \Delta\lambda_{2,n+1}\frac{\partial^2 g_2}{\partial\sigma^2}\right]^{-1} \tag{2.106}$$

and the gradient matrices read

$$\mathbf{U} = \begin{bmatrix} \dfrac{\partial g_1}{\partial\sigma} & \dfrac{\partial g_2}{\partial\sigma} \end{bmatrix} \tag{2.107}$$

$$\mathbf{V} = \begin{bmatrix} \gamma_1 & \gamma_2 \end{bmatrix} \tag{2.108}$$

and the hardening matrix reads

$$E = \begin{bmatrix} -h_1 & \dfrac{\partial f_1}{\partial k^{c}_1} & \dfrac{\partial k^{c}_1}{\partial \Delta\lambda_2} \\ \dfrac{\partial f_2}{\partial k^{c}_2} & \dfrac{\partial k^{c}_2}{\partial \Delta\lambda_1} & -h_2 \end{bmatrix} \tag{2.109}$$

Where γ_i is the modified yield surface gradient and h_i is the hardening modulus for each branch of the composite yielding surface.

2.6 Methods of analysis in earthquake engineering

Up to now, in the design of buildings, the seismic effects and the effects of the other actions included in the seismic design situation may be determined on the basis of four different methods:

- Linear static procedures
- Mode superposition procedures
- Non linear static (pushover) procedures
- Non linear dynamic (time history) procedures

The reference method for determining the seismic effects is the modal response spectrum analysis, using a linear-elastic model of the structure and a design spectrum determined according the procedure in the next section.

2.6.1 Elastic Response Spectra and behavior factor

The reference model for the description of earthquake motion at a point on the ground surface is represented by an elastic ground acceleration response spectrum, hereinafter called "elastic response spectrum". For certain applications, the earthquake motion may be described by acceleration time series (accelerograms). The horizontal earthquake motion consists of two independent perpendicular components, having the same response spectrum. In the absence of documented specific information, the vertical component of earthquake ground motion shall be represented through an elastic response spectrum different from that of the horizontal components. The elastic response spectrum is composed of a spectral shape (normalized spectrum), assumed to be independent of the level of seismic magnitude, and multiplied by the peak horizontal ground acceleration applicable at the construction site.

The horizontal elastic response spectrum, see Fig. 2.28, is defined by the following expressions where a_g indicates the ground acceleration:

$$
\begin{aligned}
&0 \le T < T_B && S_e(T) = a_g \cdot S \cdot \left(1 + \frac{T}{T_B} \cdot (\eta \cdot 2.5 - 1)\right) \\
&T_B \le T < T_C && S_e(T) = a_g \cdot S \cdot \eta \cdot 2.5 \\
&T_C \le T < T_D && S_e(T) = a_g \cdot S \cdot \eta \cdot 2.5 \left(\frac{T_C}{T} \cdot\right) \\
&T_D \le T && S_e(T) = a_g \cdot S \cdot \eta \cdot 2.5 \cdot \left(\frac{T_C T_D}{T^2}\right)
\end{aligned}
\qquad (2.110)
$$

where S_e = elastic response spectrum

S = soil amplification factor (independent of the vibration period);

η = damping correction factor with reference value η = 1 for 5% viscous damping, which may be determined by the expression:

$$\eta = \sqrt{10/(5+\xi)} \geq 0{,}55 \qquad (2.111)$$

where ξ = viscous damping ratio of the structure, expressed in percent age;

T = natural period of vibration of the simple oscillator;

T_B, T_C = limits of the constant spectral acceleration branch, depending on ground type;

T_D = value at which the constant displacement response range of the spectrum begins.

In the absence of detailed experimental data, the values of T_B, T_C, T_D and S for the horizontal components of motion and for the ground types given in the Tab. 2.2 may be used.

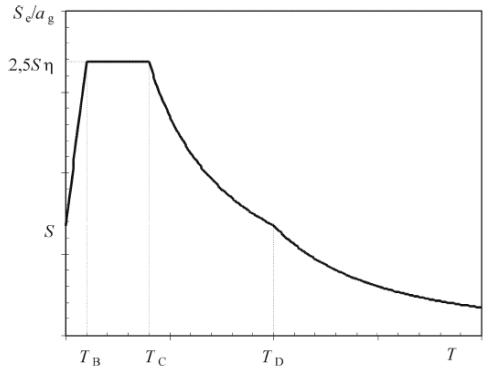

Fig. 2.29 – Shape of elastic response spectrum

Tab. 2.2 - Values of the parameters describing the horizontal response spectrum

Ground type	S	T_B	T_C	T_D
A	1.0	0.15	0.40	2.0
B, C, E	1.25	0.15	0.50	2.0
D	1.35	0.20	0.80	2.0

When the ground profile at the construction site cannot be clearly assigned to one of the ground types defined, ground type D shall generally be adopted. If attribution to either one of two ground types is uncertain, the most conservative condition shall be adopted.

To avoid explicit inelastic structural analysis in design, the capacity of the structure to dissipate energy through mainly ductile behavior may be taken into account by performing an elastic analysis based on a response spectrum reduced with respect to the

elastic one, hereafter called "design spectrum". This reduction is accomplished by introducing a factor reducing the elastic forces, denominated behavior factor q.

In the absence of specific supporting analyses, for the vertical component of the seismic action a behavior factor q = 1.5 should normally be adopted for all materials and structural systems.

2.6.2 Linear Static Procedures

This type of analysis may be applied to buildings the response of which is not significantly affected by contributions from higher modes of vibration. These requirements are deemed to be satisfied in buildings which fulfill both of the following two conditions:

a) they have fundamental periods of vibration T_1 in the two main directions less than the following values

$$T_1 \le \begin{cases} 4 \cdot T_C \\ 2{,}0\,\mathrm{s} \end{cases} \qquad \text{where } T_C \text{ is given in Tab. 2.2} \tag{2.112}$$

b) they meet the criteria for regularity in elevation.

The seismic base shear force F_b, for each horizontal direction in which the building is analyzed, is determined as follows:

$$F_b = S_d(T_1) \cdot m \cdot \lambda \tag{2.113}$$

where $S_d(T_1)$ = ordinate of the design spectrum at period T_1

T_1 = fundamental period of vibration of the building for lateral motion in the direction considered

m = total mass of the building

λ = correction factor, the value of which is equal to:

λ = 0,85 if $T_1 \le 2\ T_C$ and the building has more than two storey, or λ = 1,0 otherwise.

For the determination of the fundamental vibration period T_1 of the building, expressions based on methods of structural dynamics (e.g. by Rayleigh method) may be

used. For buildings with heights up to 40 m the value of T_1 (in s) may be approximated by the following expression:

$$T_1 = C_t \cdot H^{3/4} \tag{2.114}$$

where C_t = 0,085 for moment resistant space steel frames; 0,075 for moment resistant space concrete frames and for eccentrically braced steel frames; 0,050 for all other structures

H = height of the building, in m, from the foundation or from the top of a rigid basement;

2.6.2.1 Distribution of the horizontal seismic forces

The fundamental mode shapes in the horizontal directions of analysis of the building may be calculated using methods of structural dynamics or may be approximated by horizontal displacements increasing linearly along the height of the building.

The seismic action effects shall be determined by applying, to the two planar models, horizontal forces F_i to all storey masses m_i.

$$F_i = F_b \cdot \frac{s_i \cdot m_i}{\Sigma s_j \cdot m_j} \tag{2.115}$$

where: F_i = horizontal force acting on storey i

F_b = seismic base shear according to eq. 2.113

s_i, s_j = Displacements of masses m_i, m_j in the fundamental mode shape.

When the fundamental mode shape is approximated by horizontal displacements increasing linearly along the height, the horizontal forces F_i are given by:

$$F_i = F_b \cdot \frac{z_i \cdot m_i}{\Sigma z_j \cdot m_j} \tag{2.116}$$

where z_i, z_j = heights of the masses m_i, m_j above the level of application of the seismic action (foundation).

The horizontal forces F_i determined according to this formulation shall be distributed to the lateral load resisting system assuming rigid floors.

2.6.2.2 Simplified procedures

The analysis may be performed using two planar models, one for each main horizontal direction, if the criteria for regularity in plan are satisfied. Buildings not complying with these criteria shall be analyzed using a spatial model. Whenever a spatial model is used, the design seismic action shall be applied along all relevant horizontal directions (with regard to the structural layout of the building) and their orthogonal horizontal axes. For buildings with resisting elements in two perpendicular directions these two directions are considered as the relevant ones.

2.6.3 Mode superposition methods

The mode superposition type of analysis shall be applied to buildings which do not satisfy the conditions of regularity for applying the lateral force method of analysis, and is applicable to all types of structures. The response of all modes of vibration contributing significantly to the global response of the building shall be taken into account.

This requirement may be satisfied by either of the following:

- By demonstrating that the sum of the effective modal masses for the modes taken into account amounts to at least 90% of the total mass of the structure.
- By demonstrating that all modes with effective modal masses greater than 5% of the total mass are considered.

The response in two vibration modes i and j (including both translational and torsional modes) may be considered as independent of each other, if their periods T_i and T_j satisfy (with $T_j \leq T_i$) the following condition:

$$T_j \leq 0{,}9 \cdot T_i \tag{2.117}$$

Whenever all relevant modal responses (see above) may be regarded as independent of each other, the maximum value E_E of a seismic action effect may be taken as

$$E_E = \sqrt{\Sigma\, E_{Ei}{}^2} \tag{2.118}$$

where: E_E = seismic action effect under consideration (force, displacement, etc.)

E_{Ei} = value of this seismic action effect due to the vibration mode i.

If previous equation is not satisfied, more accurate procedures for the combination of the modal maximum shall be adopted, e.g. using procedures such as the "Complete Quadratic Combination".

2.6.4 Nonlinear static (pushover) analysis

Pushover analysis is a nonlinear static analysis under constant gravity loads and monotonically increasing horizontal loads. It may be applied to verify the structural performance of newly designed and of existing buildings for the following purposes:

- to verify or revise the values of the overstrength ratio α_u/α_1;
- to estimate expected plastic mechanisms and the distribution of damage;
- to assess the structural performance of existing or retrofitted buildings;
- as an alternative to design based on linear-elastic analysis which uses the behavior factor q.

Buildings not complying with the regularity criteria shall be analyzed using a spatial model. For buildings complying with the regularity criteria the analysis may be performed using two planar models, one for each main horizontal direction. For low-rise masonry buildings, in which structural wall behavior is dominated by shear (e.g. if the number of storey is 3 or less and if the average aspect (height to width) ratio of structural walls is less than 1.0), each storey may be analyzed independently.

At least two vertical distributions of lateral loads should be applied: a uniform pattern based on lateral forces that are proportional to mass regardless of elevation (uniform response acceleration), and a modal pattern, proportional to lateral forces consistent with the lateral force distribution determined in elastic analysis. Lateral loads shall be applied at the location of the masses in the model. Accidental eccentricity shall be considered. The relation between base shear force and the control displacement (the “capacity curve”) should be determined by pushover analysis for values of the control displacement ranging between zero and the value corresponding to 150% of the target displacement. The control displacement may be taken at the centre of mass at the roof of the building. Target displacement is defined as the seismic demand derived from the elastic response spectrum in terms of the displacement of an equivalent single-degree-of-freedom system. Pushover analysis may significantly underestimate deformations at the stiff/strong side of a torsionally flexible structure, i.e. a structure with first mode predominately torsional. The same applies for the stiff/strong side deformations in one

direction of a structure with second mode predominately torsional. For such structures, displacements at the stiff/strong side should be increased, compared to those in the corresponding torsionally balanced structure. The requirement above is deemed to be satisfied if the amplification factor to be applied to the displacements of the stiff/strong side is based on results of elastic modal analysis of the spatial model. If two planar models are used for analysis of structures regular in plan, the torsional effects need to be estimated. In this study, finite element approaches suitable for the pushover analysis of masonry building under seismic loads will be developed in chapter 3 and 4.

2.6.5 Non-linear time-history analysis

The time-dependent response of the structure may be obtained through direct numerical integration of its differential equations of motion, using the acceleration time series to represent the ground motions. The element models should be supplemented with rules describing the element behavior under post-elastic unloading-reloading cycles. These rules should reflect realistically the energy dissipation in the element over the range of displacement amplitudes expected in the seismic design situation.

If the response is obtained from at least 7 nonlinear time-history analyses to ground motions (Monti, Maruccio et al. 2010) the average of the response quantities from all these analyses should be used as action effect E_d. Otherwise, the most unfavorable value of the response quantity among the analyses should be used as E_d.

2.7 Summary

First, a short description of the typical damages suffered by masonry buildings during the L'Aquila earthquake is presented since it represents a suitable introduction to the next topic of this thesis: namely the seismic assessment of existing masonry buildings and the development of numerical strategies to assess the strengthening effect due to FRP retrofitting. Second, the possible mathematical descriptions of the material behavior which yields the relation between the stress and strain tensor in a material point of the body (constitutive models) are discussed. In particular it is stressed that the use of FRP material leads to new and important modeling problems despite the fact that several material modeling strategies are available: micromechanical and multiscale models, macro mechanical models based on phenomenological constitutive laws and macro elements characterized by few parameters and a reduced computational effort

regarding the modeling and the structural analysis phases. Then, a brief description of the advanced numerical techniques that are the starting point of the research work is detailed: in particular the finite element formulation of the continuum mechanics equations and the theory of plasticity. Finally, a general description of the techniques available in earthquake engineering for the analysis of masonry buildings is provided (linear, modal, nonlinear and nonlinear-dynamic analyses). The different approaches are detailed and the nonlinear procedures suitable for this study introduced. Moreover the strengthening technique based on the use of FRP composite is briefly introduced.

3 A Micro-modeling approach for FRP-Strengthened masonry structures

3.1 Introduction

A significant issue in actual research is the need for efficient strengthening techniques to re-establish the performance of masonry structures and preventing their brittle collapse when subjected to ultimate state limit loads. However, the design of any intervention in existing masonry constructions should be based on modern principles that include aspects like reversibility, respect by the original conception, safety, durability and compatibility of the materials, see Icomos 2001.

For this purpose, fiber-reinforced polymer (FRP) composites in the form of bonded laminates applied to the external surface with the wet lay-up technique are an effective solution, as demonstrated by the available experimental and theoretical studies in technical literature (Triantafillou 1998; Valluzzi, Valdemarca et al. 2001; Foraboschi 2004; De Lorenzis, Dimitri et al. 2007). In addition to being structurally effective, FRPs present several advantages over conventional techniques: they add no extra weight to the structure, are corrosion-resistant, have minimal aesthetic impact, and can be easily removed (Aiello, Micelli et al. 2007 and 2009; Barros 2006; Brencich and Gambarotta 2005). Therefore, these materials may be considered to ensure minimal invasiveness and reversibility of the intervention in the strengthening of existing masonry structures.

In particular, the bond mechanism between masonry and FRP has been investigated by several researchers in the last years (Basilio 2008; Grande, Imbimbo et al. 2011; Marfia, Ricamato et al. 2008) and it is a key issue when dealing with the strengthening of masonry construction. Some tests have shown that debonding of FRP is the predominant mode of failure (Oliveira, Basilio et al. 2011; Moon 2004; Tumialan 2001), so the bond strength assessment of a FRP-masonry joint is of major significance. Further studies stressed that the bond behavior of FRP-masonry joints seems different from the one of FRP-concrete in terms of strength and stress distribution at the interface (Aiello and Sciolti 2006), meaning that further experimental and numerical studies are required.

On the other hand, several theoretical models have been developed to predict the bond strength of FRP-concrete joints, generally on the basis of pull tests (Lu, Jiang et

al. 2006; Lu, Teng et al. 2005; Lu, Ye et al. 2005; Dai, Ueda et al. 2005). Evaluating the accuracy of the existing theoretical models, the predictions show that the accuracy improves as more significant parameters are considered, being the cohesion and the fracture energy of the interface the most important. Since it is difficult to obtain accurate bond-slip curves directly from strain measurements in a pull test, recently some researchers explored numerical procedures to obtain the bond-slip curve at any point along the interface (De Lorenzis, Teng et al. 2006; De Lorenzis and Zavarise 2008; Yuan, Chen et al. 2007).

Following this approach, a material model is proposed and implemented in the finite element program Diana 8 with a user subroutine aiming to accurately model the FRP-masonry interface: both for planar and curved substrates. The material model allows to obtain the global full shear force-displacement path and also to simulate the stress distribution at the interface for flat and curved substrates. Moreover, aiming to provide a better knowledge of FRP-masonry bond behavior and to challenge the performance of sophisticated nonlinear techniques, two different approaches are discussed and validated through experimental results. First, a simplified bilinear bond-slip model is used for the interface again using the software Diana with an internal routine, and second an analytical study is developed according the formulation proposed in Yuan, Teng et al. 2004. Afterwards , the solutions are compared among them. The developed material model is then applied to analyze the structural response of masonry arches strengthened with FRP reinforcement in the form of strips bonded at the extrados and/or intrados, considering strips arrangements that prevent hinged-mode failure. In order to estimate their maximum resistant loads, deformation patterns and collapse mechanisms, based on experimental results, detailed finite element models are developed. The arches considered here have a semicircular shape and are submitted to a concentrate load applied at quarter span. Finally, a case study is presented where the material model developed is used to design the strengthening effect of a 16 meter span arch bridge using FRP at the bottom layer.

3.2 Experimental bond tests

Within the scope of a research project, several bond specimens submitted to monotonic loading were recently performed, see Basilio 2007. Four clay bricks were used to build

the masonry specimens to be tested, whereas mortar joints were kept at an approximate thickness of 15-20 mm. Masonry prisms with an average dimension of 150×95×25 mm^3 were therefore obtained. Handmade bricks and weak mortar were used in all specimens in order to replicate old masonry constructions. The FRP was externally bonded to masonry. A couple of strain gauges were glued along the external surface of the FRP bond length, dividing it into three equal parts. Moreover, the instrumentation included three linear variable differential transformers (lvdts) to measure relative displacements between masonry and FRP. In this way the strain and stress could be known in four sections along the bond length. A Universal Instron testing machine and axial displacement control were employed in the tests. A masonry specimen strengthened with a 25mm width and 150mm length FRP strip was considered as the standard specimen, and additional variations were considered to evaluate the influence of the major parameters controlling the bond behavior of masonry-FRP interface namely: variable anchorage types, different bond lengths (100mm, 150mm and 200mm) and strengthening materials (glass or carbon fibers). The tests consisted of the uniaxial direct strip composite pulled from the masonry specimen, see Fig. 3.1. For further details on the experimental tests, the reader is referred to Basilio 2007.

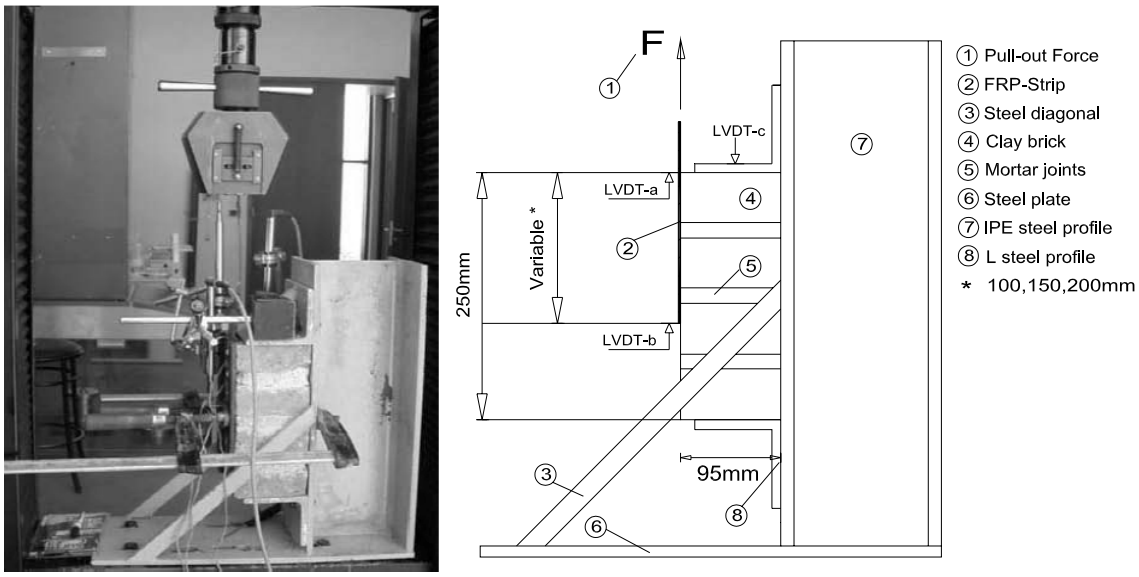

Fig. 3.1 Bond test setup: schematic view and test to be started

3.3 Advanced numerical modeling

In order to reproduce the main characteristics related to bond phenomena, an advanced numerical approach is proposed. A geometric model of the specimens was created and a two-dimensional plane stress model is used. The application of a micro-modeling strategy to the analysis of bond tests requires the use of continuum elements and line interface elements. Usually, continuum elements are assumed to behave elastically whereas nonlinear behavior is concentrated in the interface elements. Different bond lengths of the FRP sheet were considered: 100mm, 150mm, 200mm, which according to previous tests (Basilio 2007), are respectively shorter, close and longer than the effective bond length. A rectangular cross section of 25x0.15mm^2 was used for the FRP strip.

The mesh adopted in the analysis includes eight-node quadrilateral isoparametric plane stress elements to represent masonry (brick and mortar), three-node curved beam elements (based on Mindlin-Reissner theory allowing to consider shear deformations) to represent the FRP, and six-node curved zero-thickness interface elements to simulate the FRP-masonry interface. For the evaluation of strains and stresses, quadratic interpolation and Gauss integration is applied for the first and second element and three points Lobatto integration for the interface. The use of an incremental load applied at the end of the FRP loaded end with arc-length and crack mouth opening displacement (CMOD) control allowed overpass critical points and simulate the experimental results accurately.

3.3.1 Constitutive model

The constitutive model is fully based on an incremental formulation of plasticity theory developed for masonry joints which includes all the modern concepts used in computational plasticity, such as implicit return mappings and consistent tangent operators, (Lourenço 1996). The monotonic constitutive interface model is defined by a convex composite yield criterion, composed by three individual yield functions, where softening behavior has been included for all modes reading, see eq. 3.1:

Tensile criterion:

$$f_t\left(\sigma,\kappa_t\right)=\sigma-\bar{\sigma}_t(\kappa_t)$$

Shear criterion:

$$f_s(\sigma,\kappa_s)=\left|\tau\right|+\sigma\tan\varphi-\bar{\sigma}_s(\kappa_s) \tag{3.1}$$

Compressive criterion:

$$f_c(\sigma,\kappa_c)=(\sigma^T P\,\sigma)^{1/2}-\bar{\sigma}_c(\kappa_c)$$

Here, ϕ represents the friction angle and P is a projection diagonal matrix, based on material parameters. $\bar{\sigma}_t$, $\bar{\sigma}_s$ and $\bar{\sigma}_c$ are the isotropic effective stresses of each of the adopted yield functions, ruled by the scalar internal variables κ_t, κ_s and κ_c. Fig. 3.2 schematically represents the three individual yield surfaces in the stress space.

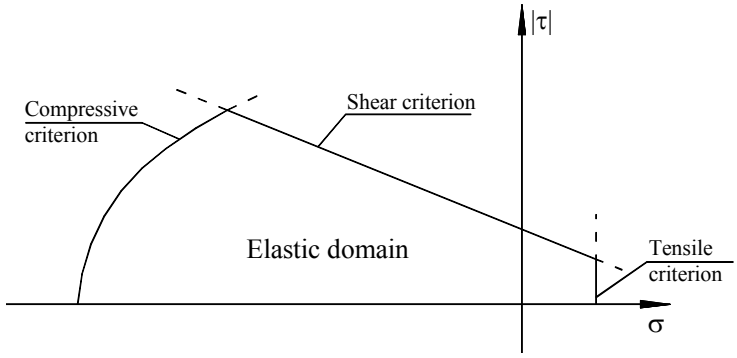

Fig. 3.2 Existing multi-surface interface model (stress space)

Associated flow rules were assumed for tensile and compressive modes and a non-associated plastic potential was adopted for the shear mode with dilatancy angle ψ and cohesion c. For further details the reader is referred to Lourenço and Rots 1997.

Adopted material properties are provided in Tab. 3.1 and Tab. 3.2.

Tab. 3.1 Elastic properties of the masonry, the FRP, and the joint

Masonry		FRP		Joint	
E_m	ν	E_{FRP}	ν	k_n	k_s
1500 [N/mm²]	0,15	80000 [N/mm²]	0,2	20 [N/mm³]	48 [N/mm³]

Tab. 3.2 Inelastic properties of the joint

Tension		Shear				Cap	
f_t^m	G_f^I	c	$\tan\phi$	$\tan\psi$	G_f^{II}	f_c^m	G_{fc}
1,1 [N/mm²]	0,02 [Nmm/mm²]	1,3 [N/mm²]	0,75	0	1,25 [Nmm/mm²]	7,1 [N/mm²]	5 [Nmm/mm²]

f_t^m, f_c^m are respectively the tensile strength of the interface (assessed through eight pull off tests) and the compressive strength of masonry (obtained from experiments) while G_f^I, G_f^{II}, G_{fc} are the tensile, shear and compressive fracture energies of the interface. The first and third value were assumed according to Lourenço 1996, while the second was assessed through numerical analysis, as done for the cohesion of the interface c, due to the difficulties to perform tests to determine them. ϕ and ψ are the friction and dilatancy angles of the interface and were assumed again as proposed in Lourenço 1996. Further parameters to be considered are the tensile strength of the GFRP f_t^{GFRP} (1473 N/mm^{2,} assessed by tests) and the elastic stiffness of the interface layer, which had to be numerically adjusted to reproduce the stiffness of the experiments since it was unknown. In particular only the value of the shear elastic stiffness k_s was calibrated, while for tension, k_n was taken according to elasticity theory, see eq. 3.2:

$$k_n = 2(1+\nu)\, k_s \tag{3.2}$$

The same set of input parameters was used in all cases to reproduce the bond mechanism.

3.3.2 Parametric study

A comprehensive parametric study was carried out to assess the local bond-slip behavior of the interface as a function of a number of key parameters. The distributions of the numerical data in terms of different mechanical properties was considered: the shear stiffness k_s, the cohesion c and the shear fracture energy G_f^{II} of the interface. Similarly, for the following geometrical variables: the bond length L and the FRP plate width w^{FRP}. In the following $c_0, G_{f0}^{II}, k_{s0}, w_0, L_0$ are the values employed to reproduce numerically the experimental bond behavior of the previously defined standard specimen. All the graphs are shown until reaching the failure in the numerical analysis due to debonding or achievement of the maximum tensile strength of the FRP strip.

The parametric study identifies the cohesion c of the interface as the main parameter influencing the applied load – relative displacement at the loaded end curve, see Fig. 3.3.

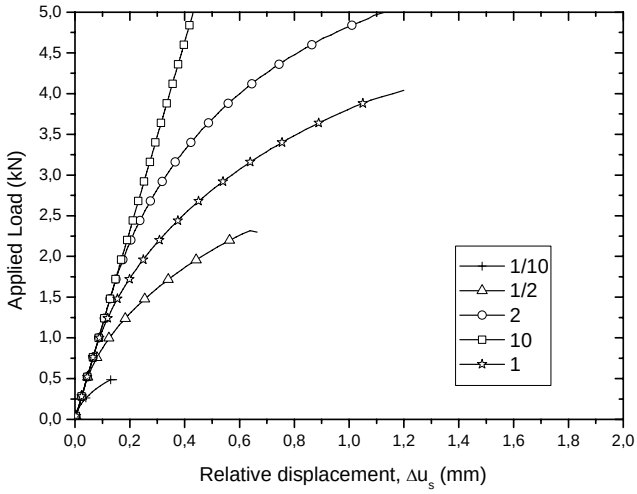

Fig. 3.3 Influence of the cohesion on the load – displacement curve at the loaded end

If the value of c is reduced to 1/10 c_0, this results in an 8-times decrease of the peak load, while c=10 c_0 causes a 25% increase. As shown in Fig. 3.4, the peak load saturates at high c values (larger than $2c_0$). The reason of this behavior is a change in the failure pattern.

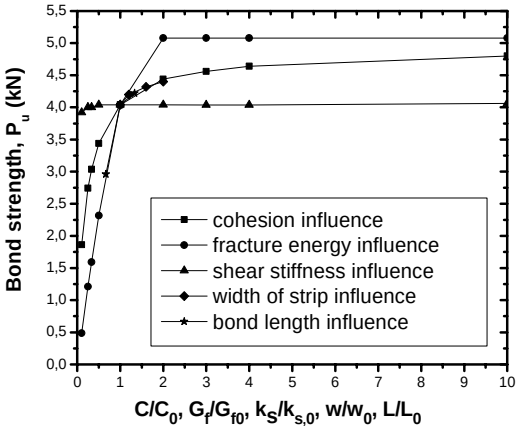

Fig. 3.4 Influence of cohesion, fracture energy, bond length, width of strip, shear stiffness on bond strength (kN)

For a low cohesion, failure is due to a loss of bond between FRP and masonry, whereas for high c values, the attainment of the ultimate tensile strength of the FRP is the

dominant failure mechanism. The interplay between the cohesion of the interface (depending on the properties of both adherent and adherend materials) and the tensile strength of the reinforcement material is crucial for the determination of the failure pattern and the peak load. CFRP strips were also used in the experiments without any appreciable increase of the peak load since their larger ultimate tensile strength was un-effective because failure was always achieved due to debonding. More effective results can be obtained by coupling similar materials (with closer elastic module). The cohesion strongly influences also the slope of the applied load - relative displacement curve. In particular for low c values, such curve exhibits a highly nonlinear behavior, while for increasing c, the linear region of the plot extends and the nonlinear region is reduced until it disappears when c=10 c_0. This can be ascribed to the localization of the stress transfer from FRP to masonry in a very small portion of the bond length, meaning that when the cohesion is high, the displacement obtained in the numerical applied load–relative displacement curve is mainly due to the elastic deformation of the FRP. For lower c values, the migration of the shear stresses along the bond length related to the nonlinear behavior can be observed as it will be clarified later. Concerning the influence of the debonding process on the joint ductility (which can be assessed as the final displacement divided by the maximum elastic displacement ratio), an effective c value exists coinciding with the calibrated one. The ductility in fact becomes 4.5 times smaller when reducing c to 1/10 c_0 and 2.6 times smaller when increasing it to 10 c_0, see Fig. 3.3.

Recently, some numerical studies were carried out to assess the influence of the interface shear stiffness on bond failure in FRP strengthened concrete structures (Dai, Ueda et al. 2005). Also in this study, several shear stiffness values were used to represent a normal-adhesive bonded joint. The parametric study described here points out that the interface shear stiffness does not influence considerably the applied load - relative displacement curve. Values of the shear stiffness k_s ten times smaller than the calibrated value k_{s0} are necessary to generate a deviation from the calibrated curve, while in the range between 1/2 k_{s0} and 10 k_{s0} the behavior is almost unchanged without an appreciable reduction of the peak load (4 kN), see Fig. 3.4. Inside the range

1\2-10 k_{s0}, the behavior is highly nonlinear while reducing the stiffness to 1\10 k_{s0} the linear phase and the nonlinear phase have similar extensions.

Further research (Lu, Ye et al. 2005), has shown that the ultimate load P_u of a FRP-concrete bonded joint is directly proportional to the square root of the shear interfacial fracture energy G_f^{II} regardless of the shape of the bond-slip curve, so a comparison of the bond strength is equivalent to a comparison of the shear interfacial fracture energy. For the FRP-masonry bonded joint considered in this work, the parametric study on the shear fracture energy shows as a 90% reduction results in a 57% decrease of P_u, while a 10-times larger value leads to a 25% increase of P_u, see Fig. 3.5.

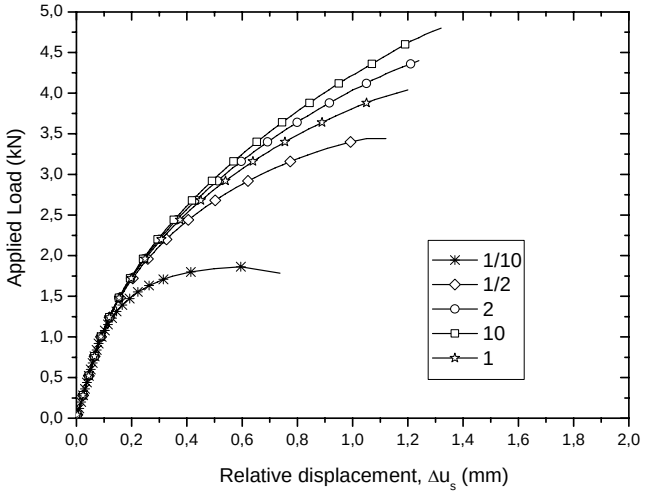

Fig. 3.5 Influence of the shear fracture energy on the load – displacement curve at the loaded end

Moreover, the fracture energy does not affect the slope of the linear (elastic) region in the applied load - relative displacement curve in the investigated range, while concerning the nonlinear behavior only a small difference in stiffness exists in the range (0.5-10 G_{f0}^{II}) but it becomes significant if G_f^{II} = 1/10 G_{f0}^{II} , where an horizontal asymptote is visible. The nonlinear region and the ductility of the system increases obviously with the fracture energy since it increases the capacity to transfer the stresses along the bond length due to the larger energy involved in this process. However, this is not observed in all the graphs since according to the numerical and experimental results, the debonding process is quite brittle in the proximity of the ultimate load and

thus influenced more by the cohesion than by the fracture energy. The value of the fracture energy, beyond which there are no more significant increments of the ultimate load and of the ductility, is around $0.5\,G_{f0}^{II}$.

Three different bond lengths were analyzed: 100mm, 150mm and 200mm in order to allow a direct comparison between experiments and numerical results. The bond length is again a parameter having a large influence on the peak load. For a bond length L=100mm, the peak load is reduced by 25% when compared to the standard 150mm length. The applied load - relative displacement curve displayed in Fig. 3.6 remains almost unchanged until 3kN and there is no influence of the bond length on the slope.

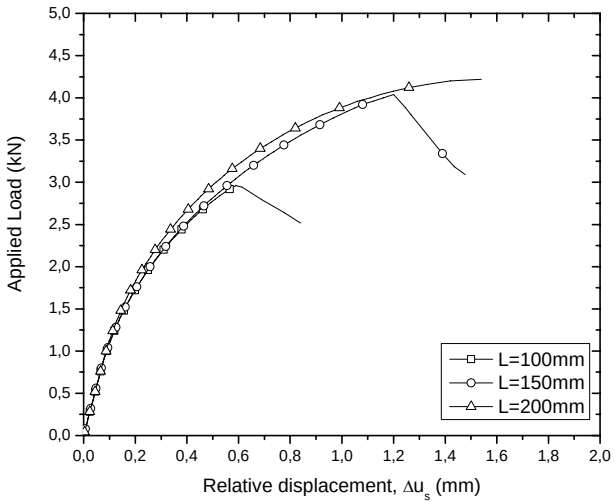

Fig. 3.6 Influence of the bond length on the load – displacement curve at the loaded end

Both for lower and higher bond length values, the behavior is highly nonlinear but almost coincident for the three cases. The linear region is very small and always ends at displacement values as low as 0.2 mm. Thus, this value was subsequently used to calibrate the analytical model according to the Yuan, Teng et al. 2004 formulation. Fig. 3.6 shows a 53% increment of the ductility when changing from 100mm to 150mm and 19% when changing from 150mm to 200mm. However, the slip at the elastic limit seems independent from the bond length.

Four different FRP strip widths were considered: 25mm, 30mm, 40mm, and 50mm. As expected according the plane stress model developed, an increase in width causes an increase of the peak load and of the stiffness, while the ultimate slip keep unchanged, see Fig. 3.7.

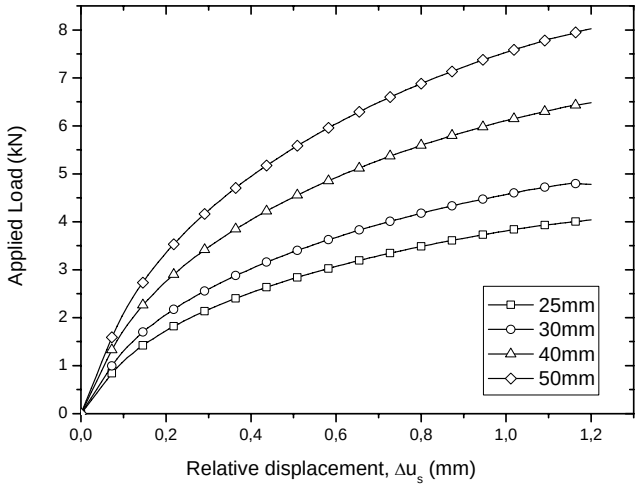

Fig. 3.7 Influence of the width of the FRP strip on the load – displacement curve at the loaded end

3.4 Simplified numerical model and analytical study

In order to establish a comparison with the results obtained using the combined cracking/shearing/crushing model in terms of applied load – relative displacement curves, two other approaches are also used: the first concerns the substitution of the plasticity model of the interface by a simplified bond slip curve, the second is the solution of the differential equations governing the bond mechanism according to the formulation of Yuan, Teng et al. 2004. According to the latter approach four states are successively found (see continuous curves in Fig. 3.8 a, b, c): an elastic state (linear behavior, increasing branch [AB]) , an elastic softening state (nonlinear behavior, increasing branch until peak load [BC]), a softening debonding state (nonlinear behavior with soft decreasing branch [CD]), and a debonding propagation state (linear behavior, decreasing branch [DE]).

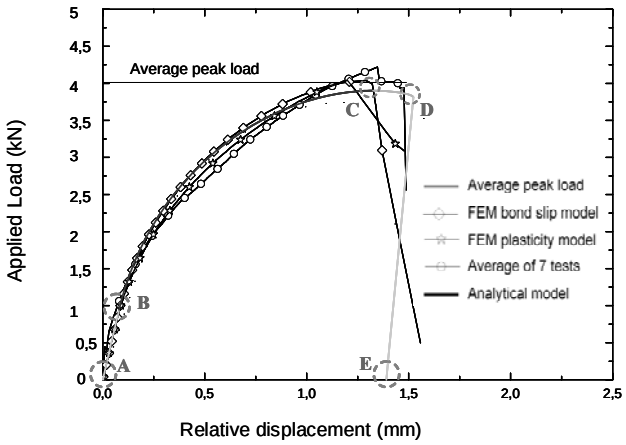

Fig. 3.8a Applied load – Relative displacement diagram for a bond length L=150mm;

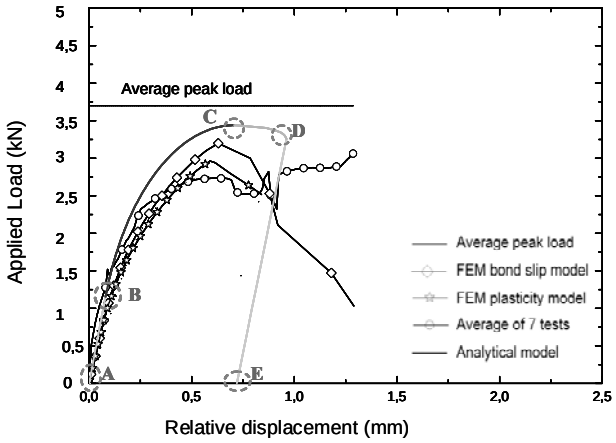

Fig. 3.8b Applied load – Relative displacement diagram for a bond length L=100mm;

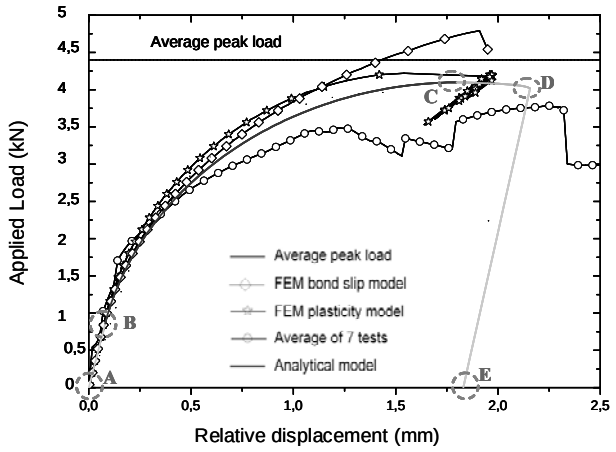

Fig. 3.8c Applied load – Relative displacement diagram for a bond length L=200mm;

Two different bond slip models were employed in the simplified numerical analyses, see Fig. 3.9

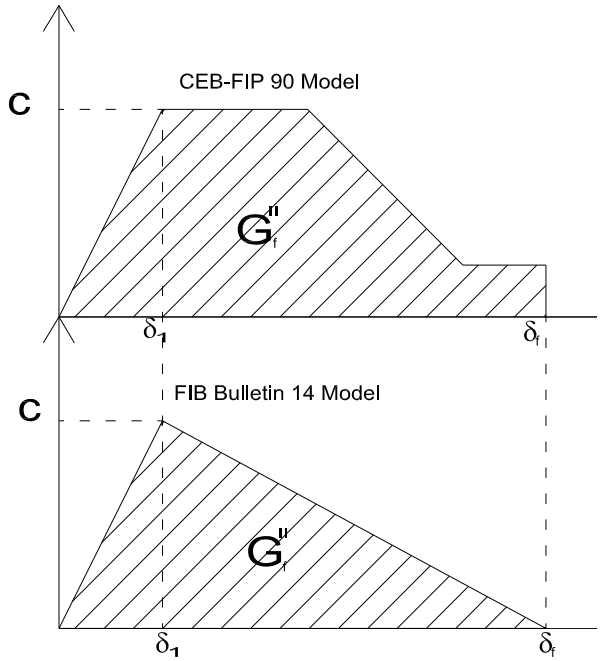

Fig. 3.9 Bond slip models used in the simplified numerical analyses according to CEB-FIP 90 Model and FIB Bulletin 14 Model

In the first part of the calibration the bond slip curve of the interface has been taken according to CEB-FIP Model Code 1990, aiming to understand if the masonry-FRP interface could exhibit a plastic behavior, to determine its extension and to check if the use of a residual friction value was reasonable. Through the analyses, it was possible to observe that the value of the residual stress is generally around 10% of the peak value, since friction at the interface is quite low once the micro-cracks in the masonry are generated. According to these observations, in the second part of the calibration the bond slip curve of the interface was simplified adopting a simple bilinear bond-slip curve according Fib bulletin 14, 2001, see Fig. 3.9. This bilinear model has the same local bond strength and total interfacial fracture energy of the combined cracking/shearing/crushing model in order to do not affect the bond strength by this simplification. Moreover, this allows reducing the number of unknown parameters to be calibrated in the nonlinear FE analysis since the fracture energy is no longer unknown, but related with cohesion, slip and interface stiffness through the area of the triangle in

the bilinear bond stress-slip curve. Finally, the utility of assessing the capability of a simplified bilinear bond slip model is evident since for bond of FRP to concrete the European design guidelines on FRP strengthening, i.e. Fib bulletin 14, 2001, proposes a simplified bilinear model for design phase. Additionally, the complete solution of the bond differential equations according to Yuan, Teng et al. 2004 is possible only if a bilinear bond-slip model is used.

3.5 Discussion of results

The ability of the numerical model to reproduce the main features characterizing the masonry-FRP bond behavior as well as to reproduce experimental results is assessed in this section. The numerical results are also employed as input for an analytical process in order to extract curves representing the distributions of strains, bond stresses and slip along the bond-length to compare with the experimental values. However, due to their discrete nature, such analytical curves provide only some hints about the average values of the considered entities.

3.5.1 Bond Strength

In Fig. 3.8 the load applied to the FRP strip is related with the relative displacement between the masonry surface and the FRP strip measured at the loaded end. The bond strength predicted using the proposed approaches are compared with the results of the experimental bond tests for three different bond lengths. The results demonstrate that the trends exhibited by experimental results are reasonably well described by all the numerical models considered. Both results of the advanced plasticity model and the simplified bilinear bond-slip model are shown. They are in close agreement with the average of seven tests, with the advanced model performing slightly better. The pre-peak branch is dominated by a clearly nonlinear behavior, which is initiated for a relatively low stress-level (point B). The scattering in the experimental data was high due to the particular brittle behavior of masonry. The combined cracking/shearing/crushing model provides an accurate estimation of the ultimate load independently from the bond length, moreover this value is always lower than the average peak load evaluated at a different displacement Δu_s and represented by a horizontal continuous line. The simplified bilinear bond slip model provides still reasonable approximation except a slightly overestimation of the maximum average

peak load for the 200mm bond length. The analytical approach (continuous curve) allows clarifying some interesting aspects of the results like the use in the constitutive model of a bilinear bond slip curve with large slip values (ultimate local slip Δu_s=0.2 mm for FRP-concrete joints and 1.2mm for the FRP-masonry joints). This assumption is validated being the softening debonding state ([CD] branch) almost absent in the experimental curves. This means that for the FRP-masonry interface, the phenomenon of stress propagation along the bond length is less localized than in the bond between FRP and concrete, probably because the tensile and compressive strengths of historical masonry used in the tests are low and the ratio of the elastic stiffness of GFRP and masonry large. Hence, bond stresses interest large regions of the bond length even for a low percentage of the peak load (50%) as contour plots point out in Fig. 3.10. In the first part of the calibration the bond slip curve of the interface has been taken according to CEB-FIP Model Code 1990. With simple equilibrium considerations, the previous evidence also explains why bond stress peak values are lower than values available in literature, Yuan, Teng et al. 2005, regarding FRP-concrete bond joints (7-10 N/mm^2 for FRP-concrete joints; 1.3 N/mm^2 for FRP-masonry joints). Reasonably, these values are closer to the average stress at the FRP-masonry interface, while in previous works the values represent a localized peak stress acting in the point at the interface where detachment has to occur. The effective bond length in the elastic softening stage is assessed according to Yuan, Teng et al. 2004, with the formula in eq. 3.3:

$$l_e = a + \frac{1}{2\lambda_1}\ln[\frac{\lambda_1 + \lambda_2 \tan(\lambda_2 a)}{\lambda_1 - \lambda_2 \tan(\lambda_2 a)} \tag{3.3}$$

where each term is obtained according to eq. 3.4, eq. 3.5 and eq. 3.6:

$$\lambda_1^2 = \lambda^2 \cdot \frac{2G_f}{\delta_1 \cdot \tau_f};\ \lambda_2^2 = \lambda^2 \cdot \frac{2G_f}{(\delta_f - \delta_1)\cdot \tau_f};\ \lambda^2 = \frac{\tau_f^2}{2G_f}\left(\frac{1}{E_{FRP}t_{FRP}} + \frac{b_{FRP}}{b_m E_m t_m}\right); \tag{3.4}$$

$$G_f^{II} = \frac{\delta_f \cdot \tau_f}{2};\ \tau_f = \frac{P_2^2}{E_{FRP}t_{FRP}b_{FRP}^2 u_2}; \tag{3.5}$$

$$\delta_1 = u_1 = \frac{P_1^2}{E_{FRP}t_{FRP}b_{FRP}^2 \tau_f};\ \delta_f = u_2 \tag{3.6}$$

P_1 and P_2 such as u_1 and u_2 are determined from the experimental or numerical curves and represent respectively the displacements and the loads at the end of the elastic stage (point B) and the elastic softening stage (point C);

while t_{FRP} , t_m, b_{FRP}, b_m, E_{FRP}, E_m are respectively the thickness, the width and the elastic modulus of the FRP and the masonry. The formula to obtain the value a changes according to the state in the debonding process according to Yuan, Teng et al. 2004 and is not reported here for briefness.

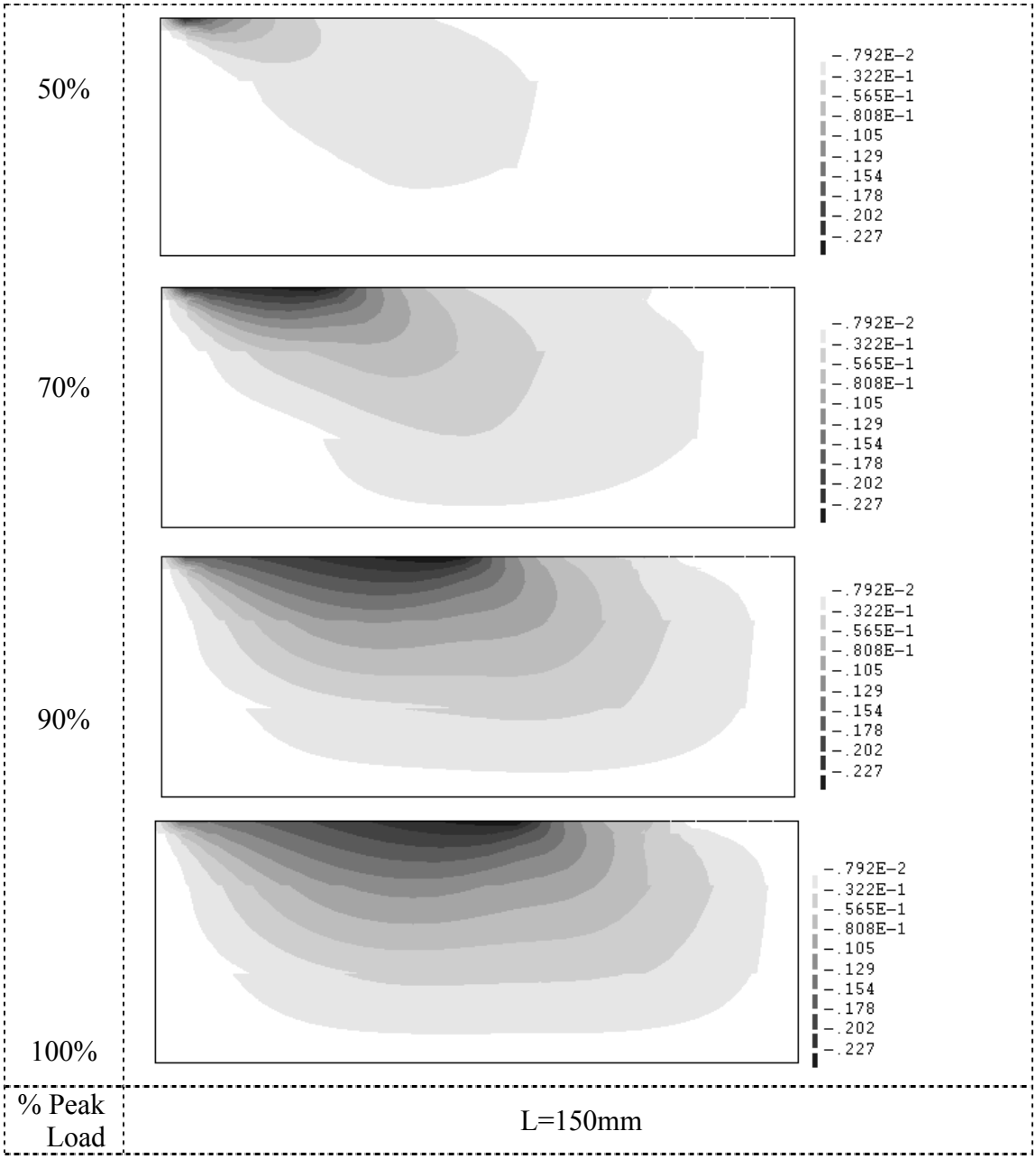

Fig. 3.10 Contour levels of shear bond stress in the masonry specimen for a bond length L=150mm (values in N/mm^2)

Using this formulation, the effective bond length in the elastic softening stage increases with the total bond length covering it entirely also when the failure pattern is stable and

due to the attainment of the tensile strength of the FRP strip (for 150mm and 200mm bond lengths). Moreover, comparison of numerical, experimental and analytical results, see Fig. 3.8, shows that an increasing of the bond length does not cause always an increase of the bond strength, becoming P_u around 3.5 kN, 4.1 kN and 4.2 kN respectively for 100mm, 150mm and 200mm due to a change in the failure behavior (from sliding to tensile strength) which is observed only when passing from 100mm to 150mm. According the numerical analysis, a solution to increase the bond strength can be an increase of the width of the FRP strip, because in this way the failure behavior due to the achievement of the tensile strength of the FRP is prevented.

3.6 Further comparisons

Other aspects of the bond behavior can be numerically reproduced using advanced nonlinear finite element analysis. Using three specimens randomly selected for each bond length as an example, the strain, stress and slip distributions predicted with the advanced numerical model are compared with the test results. Comparisons were done at the same applied load to peak load ratios: 25%, 50%, 75% and 100%. 100, 150, 200 are the bond-lengths in mm; a, b and c refer to 3 different specimens, 1/3, 2/3, 3/3 mean respectively the relative location along the bond-length considered.

Fig. 3.11 shows the points along the bond length where strains were experimentally measured. At the free end it is assumed that there is no deformation, while at 1/3 and 2/3 of the bond length the strain value was measured with strain gauges, finally the strain at the loaded end can be determined measuring with an lvdt the relative displacement between the masonry prism and the FRP strip.

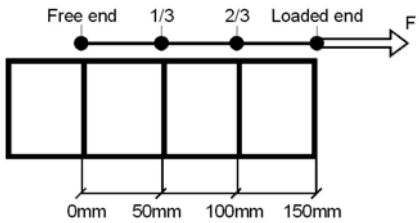

Fig. 3.11 Points along the bond length where strains were experimentally measured

In Fig. 3.12 the FRP normal strain is normalized by the maximum experimental peak strain and is evaluated along the bond length for the four aforementioned percentages of the peak load. The typical evolution is reported only for a 150mm bond length for briefness but similar results were obtained for L=100mm and L=200mm. For each

percentage of the peak load considered, the numerical curve falls inside the experimental ones independently from the location along the bond length where the experimental strain is assessed, providing a good estimation of the physical phenomena.

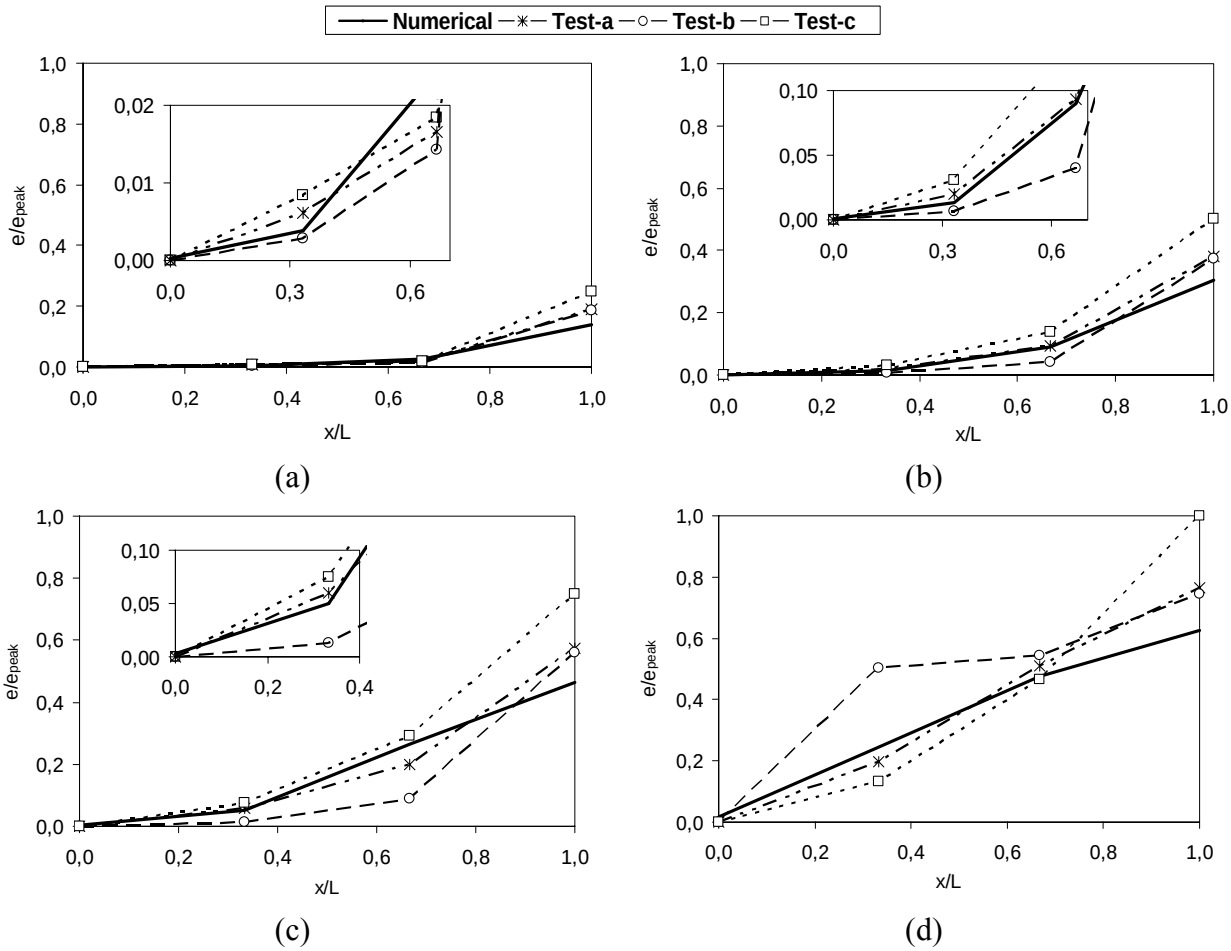

Fig. 3.12 Comparison between numerical and experimental FRP strain distribution along the bond length (150mm) for an applied load to peak load ratio of: a) 25% b) 50% c) 75% d) 100%

In Fig. 3.13 instead, the typical evolution of the strains along the FRP strip as a function of the load variation is presented at 1/3 (a), 2/3 (b) and 3/3 (c) of the bond length according to Fig. 3.11. A very good agreement between experimental and numerical results at the loaded end (3/3) can be observed, while the numerical curves show a trend away from the experimental results at 1/3 and 2/3 of the bond length. This means that the absolute values of the strains can still be well predicted by the numerical model but generally when comparing with experimental results, the values in the numerical analysis are achieved for a lower value of the external applied load.

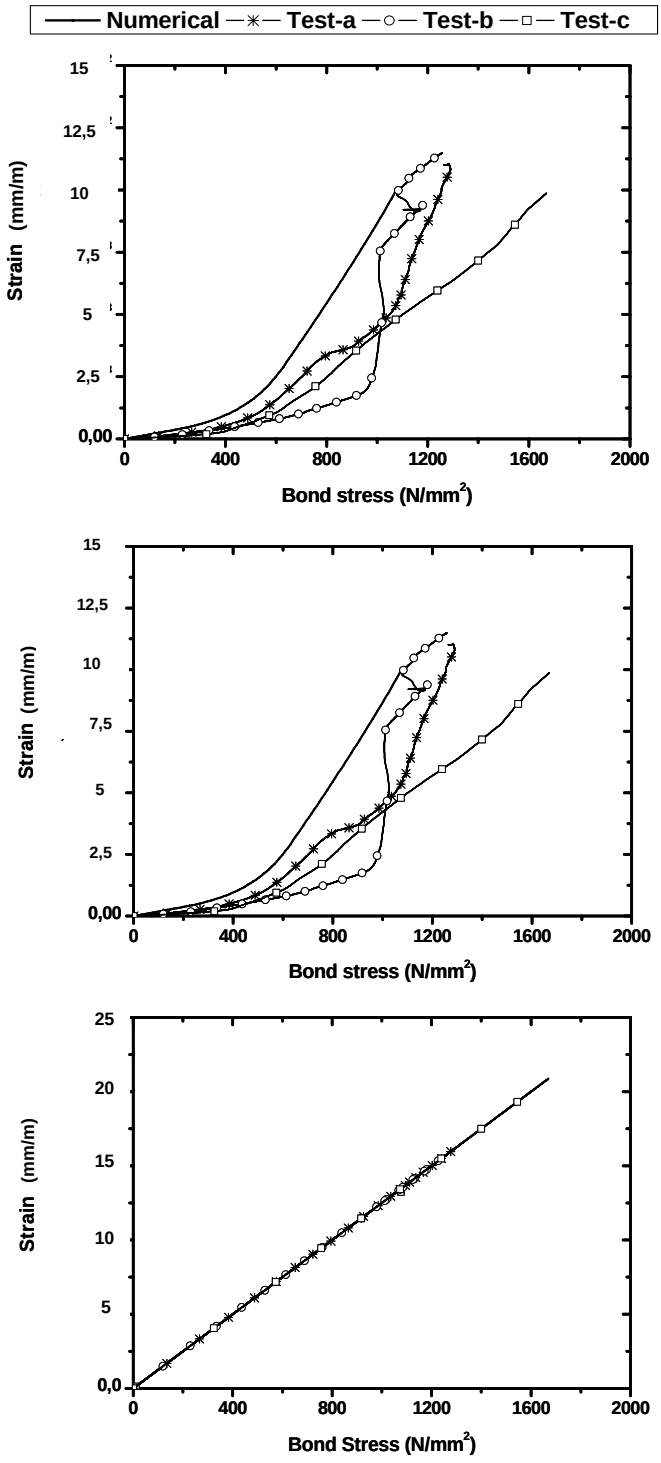

Fig. 3.13 Comparison between numerical and experimental deformations in the three points where strains were experimentally measured: a) 1/3, b) 2/3, c) 3/3

To determine the distribution of the bond shear stresses at the interface, the equilibrium equation of one element of fiber between two consecutive strain gauges can be used giving:

$$t_{FRP}(\sigma_{i+1} - \sigma_i) = \tau(x)(x_{i+1} - x_i) \tag{3.7}$$

Moreover, considering the elastic behavior of the FRP:

$$\sigma_i(x) = E_{FRP}\varepsilon_i(x) \tag{3.8}$$

and substituting eq. 3.8 into eq. 3.7, this yields:

$$\tau(x) = \frac{t_{FRP}E_{FRP}(\varepsilon_{i+1} - \varepsilon_i)}{(x_{i+1} - x_i)} \tag{3.9}$$

where t_{FRP} is the FRP strip thickness, ε_i is the deformation where strain gauges are located, x_i is their position and σ_i is the stress in the FRP corresponding to the location x_i. The typical dependence of the stress on the location as obtained using eq. 3.9 is compared for the three bond lengths at the peak load level (100%) in Fig. 3.14. Once again, the numerical curves fall inside the experimental ones, even if important scattering of the experimental data is observed, together with the incapability of the numerical model to predict the peak values measured experimentally. Similar results were obtained even for applied load to peak load ratio equal to 25%, 50% and 75%.

In Fig. 3.15, the bond stresses are plotted against the load factor for four different sections. This picture shows the migration of adhesion areas in the model when the load factor (x-axis) is increased. Looking at the loaded end section, when increasing the load, an increasing branch is detected followed by a decreasing one, once the cohesion value is reached. If load is increased continuously, a simultaneous increase of the bond stress in the adjacent zones is depicted in the section at 2/3 of the bond length and so on, until the bond stress reaches the free end. The decreasing branch is related to crack propagation at the interface in this zone, while the simultaneous increase in the closer zones indicates that the shear stress is moving toward these zones.

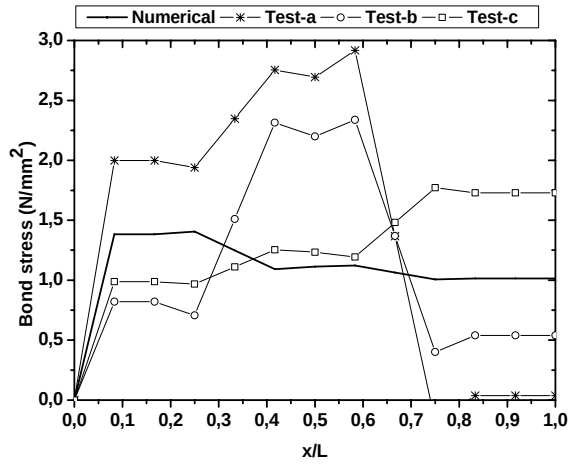

(a)

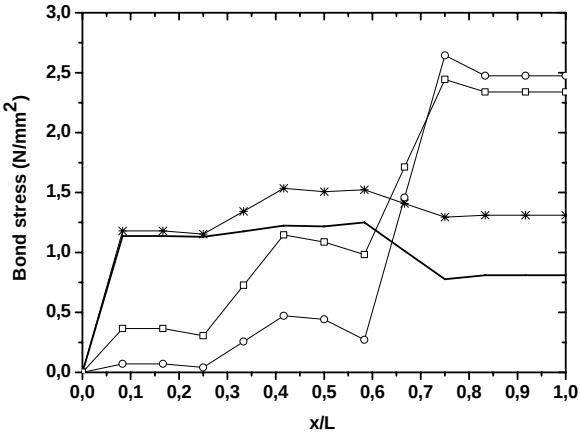

(b)

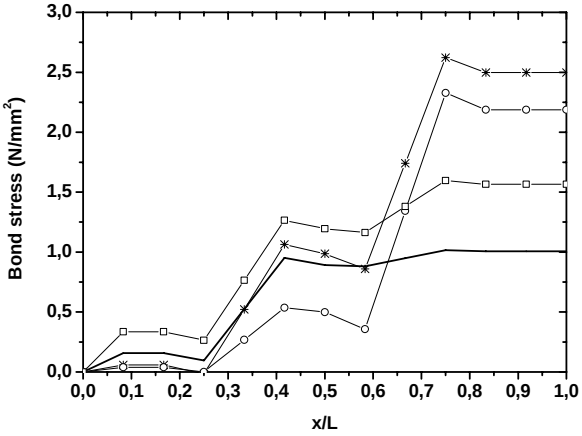

(c)

Fig. 3.14 Comparison between numerical and experimental bond stress distribution along the bond length at the peak load: (a) L=100mm; (b) L=150mm; (c) L=200mm

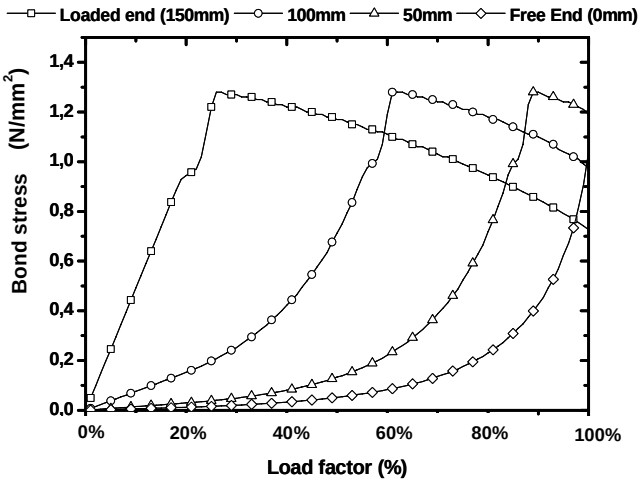

Fig. 3.15 Bond stress versus load factor

It is possible to calculate the slip as a function of the position by numerically integrating the deformation-location curves. If an infinitesimal element dx of FRP bonded to the masonry is considered, deformation compatibility yields:

$$d\Delta u_s / dx = \varepsilon_{FRP}(x) - \varepsilon_m(x) \tag{3.10}$$

where Δu_s is the FRP-masonry relative slip, ε_{FRP} is the FRP deformation and ε_m is the masonry deformation. Neglecting the deformation of masonry, the slip at the loaded end can be calculated by integration along the bond length according to:

$$\Delta u_s(x) = \int_0^L \varepsilon_{FRP}(x)dx + \Delta u_s(0) \tag{3.11}$$

Assuming zero slip at the free end, numerical integration yields:

$$\Delta u_s(L) = \sum_i \varepsilon_{FRP}(i)\Delta x_i \tag{3.12}$$

where Δx_i is the distance between two adjacent strain gauges, in which the deformation is assumed constant. In Fig. 3.16, the typical dependence of the slip versus the location obtained using eq. 3.12 is compared for the three bond lengths at the peak load (100%). The numerical results fit quite well the experimental values obtained during the tests even if they slightly overestimate results obtained from tests b and c at a bond length equal to 100mm and 150mm. On the other hand, numerical results approximate well the average experimental values when compared for a bond length equal to 200mm. Again, similar results were obtained for applied load to peak load ratio equal to 25%, 50% and 75%.

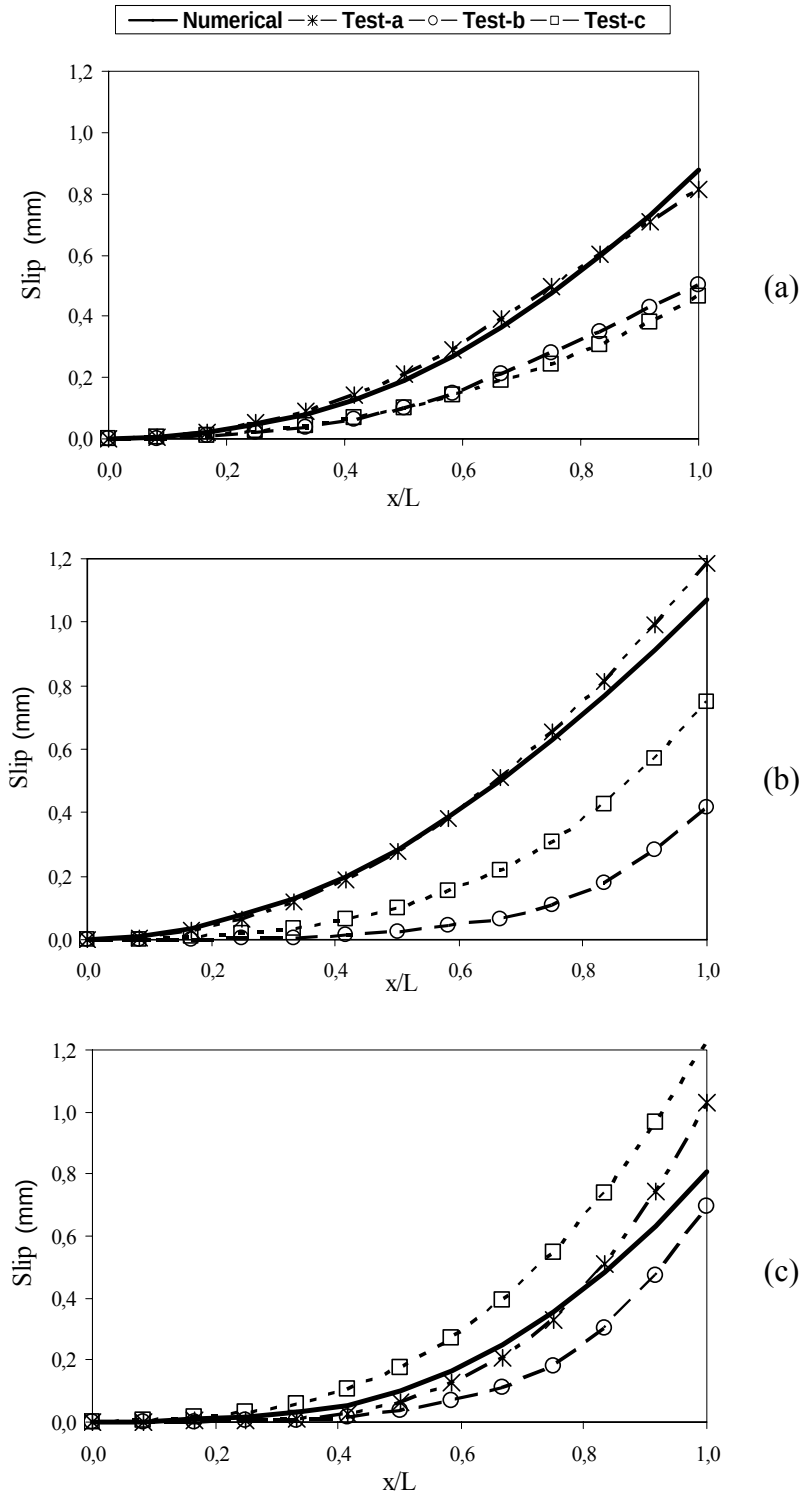

Fig. 3.16 Comparison between numerical and experimental slip distribution along the bond length: (a) L=100mm; (b) L=150mm; (c) L=200mm

Finally, in Fig. 3.17 the typical diagram of the shear bond stress as a function of slip Δu_s, evaluated according equations 3.9 and 3.12 at 1/3, 2/3 and 3/3 of the bond length,

is depicted. The difference between the experimental data and the numerical predictions can be explained considering that the axial strains measured on the thin FRP plate with strain gauges may show strong variations as a result of the discrete nature of masonry cracks, heterogeneities of materials and the roughness of the underside of the debonded FRP strip. For example, a strain gauge located above a crack will have a much greater strain than other placed above a large aggregate particle, so the shear stress deduced from such axial strains is not reliable enough and prone to large variations, while these aspects can be over-passed using the numerical model.

3.7 Modification of the interface model to account for FRP strengthening

3.7.1 An existing constitutive interface model

The micro-modeling strategy for masonry, in which the units are discretized with continuum elements and the joints are discretized with interface elements, as demonstrated in detail in previous subsections is also a very powerful tool to understand the behavior of the FRP-masonry interface (Maruccio, Oliveira et al. 2008 and 2009; Maruccio, Basilio et al. 2009). A general description of the existing interface model was provided in subsection 3.3. Moreover in section 3.4, 3.5, 3.6 the existing model has been used to simulate the interfacial behavior of flat FRP-masonry joints showing that a good agreement with experimental and analytical results can be achieved in the simulation of shear bond test. Further results, Basilio 2007, show that the model is less accurate in the simulation of the strengthening effects of FRP strips on masonry arches. This is due to the coupling of shear stresses and tensile stresses when the interface has a curved shape. Existing research (Valluzzi, Valdemarca et al. 2001), show that due to mechanical equilibrium of forces at the interface of curved substrates, compressive normal stresses will be present for extrados strengthening and tensile stresses will be present for intrados strengthening. Therefore, a detailed experimental characterization of the mechanical behavior of curved interfaces is needed and an advanced numerical approach is required to properly describe the different effects existing due to shear and tension failure.

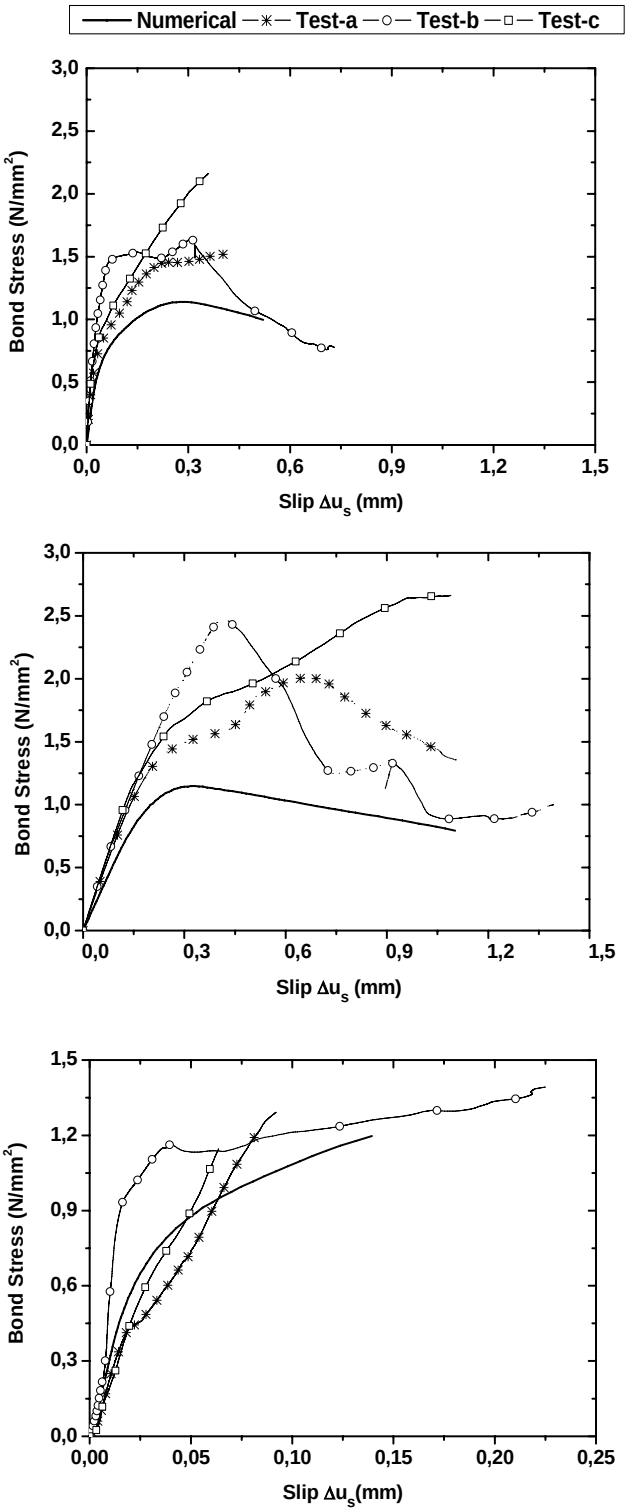

Fig. 3.17 Comparison between numerical and experimental deformations in the three points where strains were experimentally measured: (a) 1/3; b) 2/3; c) 3/3

The aim of this section is the improvement of the existing interface model in such a way to accurately simulate the experimental results obtained for FRP-strengthened masonry arches. First, a detailed description of the theoretical features characterizing the model is provided with particular attention to his application to the FRP-masonry interface. Second, the effects of relevant parameters on the shape of the yielding functions is investigated and improvement are proposed. In particular it will be shown that exponential softening for the tension mode can be accepted both for brick mortar joints and FRP-masonry interface, but not for the Coulomb mode since exponential softening is not able to describe properly the high fracture energy involved in the debonding process (see section 3.4). Third, a new multi-linear hardening law will be proposed for shear and tension failure and implemented in Diana 8. Uncoupled behavior for tension mode and shear mode will be considered in the implementation. The constitutive model with the new hardening law is used to simulate the stress distribution on curved interfaces for different bond lengths and applied to simulate the strengthening effects of FRP strengthened masonry arches. As detailed in subsection 3.3, the monotonic constitutive interface model is defined by a convex composite yield criterion, composed by three individual yield functions, where softening behavior has been included for all mode. Fig. 3.18 schematically represents the three individual yield surfaces in the stress space for a given set of input parameter, while Fig. 3.19 represents the inelastic laws considered in the implementation.

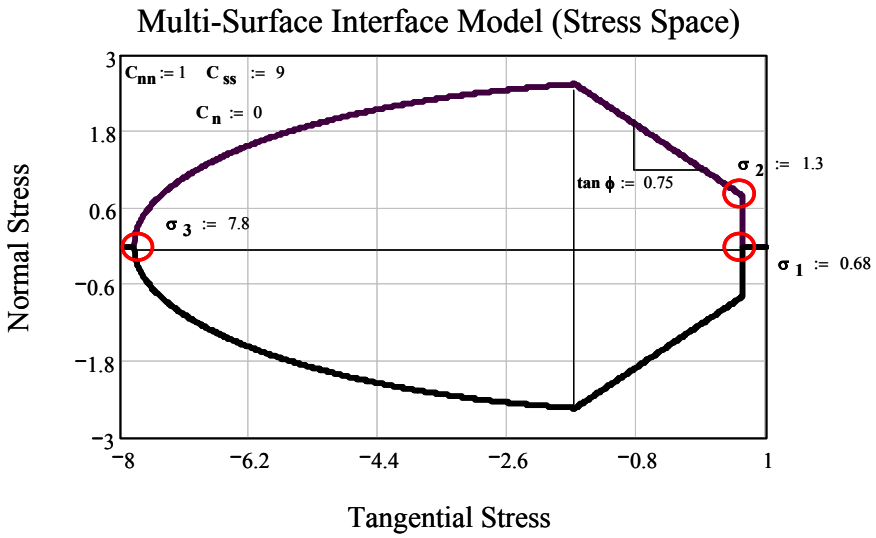

Fig. 3.18 Multi-surface interface model (stress space)

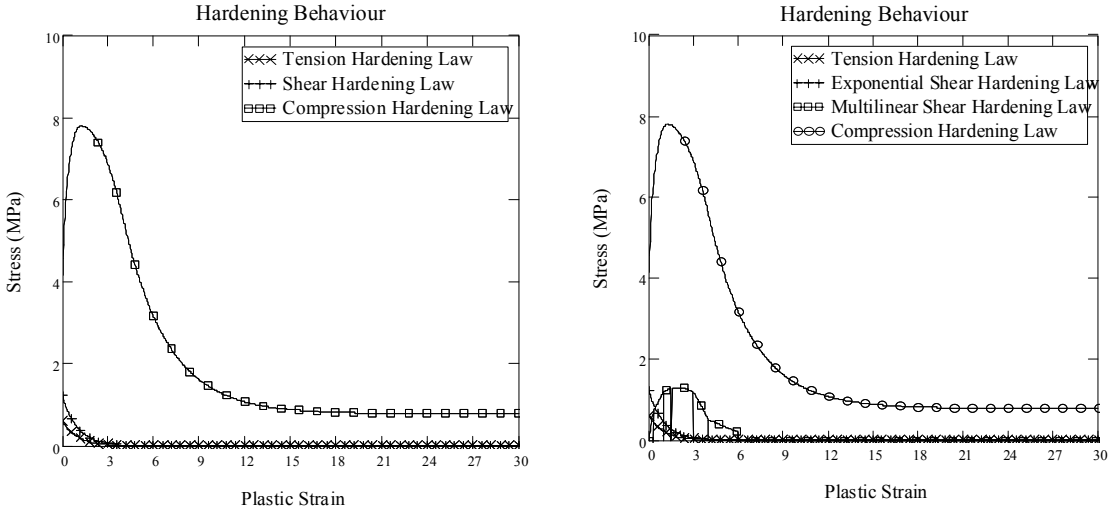

(a) (b)

Fig. 3.19 Inelastic behavior: (a) exponential softening; b) exponential softening and multi-linear hardening or softening

Further details about the theoretical aspects of the existing model are provided in the next sections.

3.7.2 The tension-cut off criterion

For the tension mode, exponential softening of the tensile strength is assumed according to mode I experiments, namely pull off test, see Fig. 3.20. The yield function reads

$$f_1(\sigma,\kappa_1) = \sigma - \bar{\sigma}_1(\kappa_1) \tag{3.13}$$

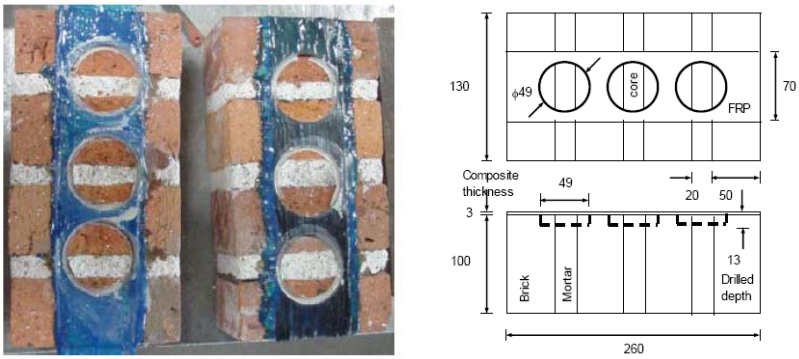

Specimen	Stress (MPa)
GPO-1	1.1
GPO-2	1.3
GPO-3	0.9
GPO-4	1.4
GPO-5	1.0
Average	1.1
CV (%)	18.2

(a) (b) (c)

Fig. 3.20 Pull off tests: (a) specimen; (b) specification of test; (c) results for f_t

where the yield value $\overline{\sigma_1}$ is

$$\overline{\sigma_1} = f_t \exp\left(-\frac{f_t}{G_f^I}\kappa_1\right) \tag{3.14}$$

In the above f_t is the tensile strength of the joint or, more precisely, of the masonry-FRP interface and G_f^I is the mode I fracture energy.

The shape of the yield value $\overline{\sigma_1}$ is provided in Fig. 3.21 for a given set of values for f_t and G_f^I. The dependence of the exponential curve $\overline{\sigma_1}$ from the fracture energy considered in the model is evident.

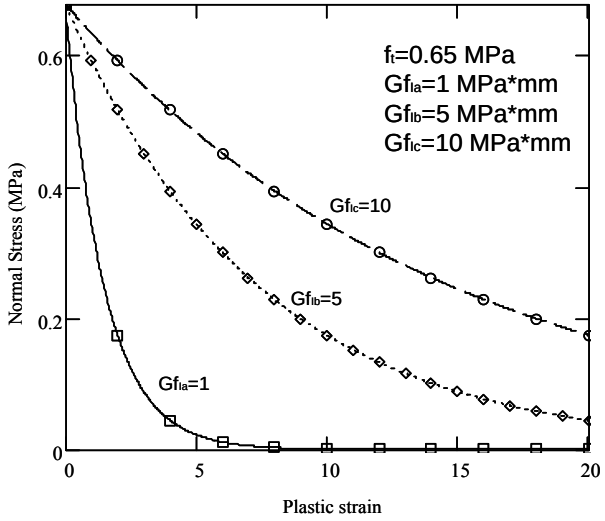

Fig. 3.21 Yield value $\overline{\sigma_1}$ as a function of the fracture energy

An associated flow rule and a strain softening hypothesis are considered. Assuming that only the normal plastic relative displacement controls the softening behavior, results

$$\dot{\kappa}_1 = \left|\dot{\Delta u}_n^p\right| = \dot{\lambda}_1 \tag{3.15}$$

The stress update equations read

$$\begin{cases} \sigma_{n+1} = \sigma^{trial} - \Delta\lambda_{1,n+1} k_n \\ \tau_{n+1} = \tau^{trial} \end{cases} \tag{3.16}$$

and the derivative necessary for the iterative local Newton-Raphson method according general formulation in chapter 2 is:

$$\left(\frac{\partial f_1}{\partial \Delta\lambda_1}\right)_{n+1} = -k_n - h_1 \tag{3.17}$$

where

$$h_1 = \frac{\partial \overline{\sigma_1}}{\partial \kappa_1} \tag{3.18}$$

and the consistent tangent stiffness matrix reads

$$\mathrm{D}_1^{ep} = \left(\frac{\partial \sigma}{\partial \varepsilon} \right)_{n+1} = \begin{bmatrix} \frac{h_1 \, k_n}{h_1 + k_n} & 0 \\ 0 & k_s \end{bmatrix} \tag{3.19}$$

3.7.3 The Coulomb-friction criterion

For the Coulomb friction mode, the yield function reads

$$f_2(\sigma, \kappa_2) = |\tau| + \sigma \tan\phi(\kappa_2) - \overline{\sigma}_2(\kappa_2) \tag{3.20}$$

where the yield value $\overline{\sigma_2}$, see Fig. 3.22, reads

$$\overline{\sigma_2} = c \exp\left(-\frac{c}{G_f^{II}} \kappa_2 \right) \tag{3.21}$$

and the friction angle is coupled with cohesion softening via the expression

$$\tan\phi = \tan\phi_0 + (\tan\phi_r - \tan\phi_0) \frac{c - \overline{\sigma}_2}{c} \tag{3.22}$$

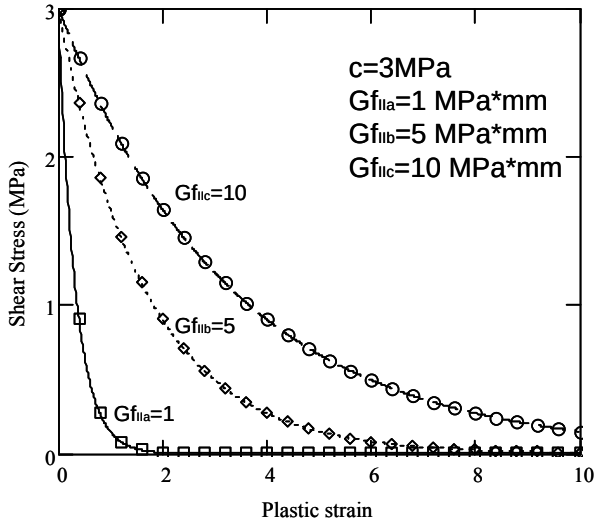

Fig. 3.22 Yield value $\overline{\sigma_2}$ as a function of the fracture energy

In the above *c* is the cohesion of the unit-mortar interface, ϕ_0 is the initial friction angle, ϕ_r is the residual friction angle and G_f^{II} is the mode II fracture energy. Exponential softening is assumed for the cohesion, and, for simplicity, the softening of the friction angle is taken proportional to the softening of the cohesion.

A non-associated plastic potential g_2,

$$g_2 = |\tau| + \sigma \tan\psi - c \tag{3.23}$$

with a dilatancy angle ψ and a strain softening hypothesis are considered. In the computational implementation of the model, the dilatancy angle is considered as a function of the plastic relative shear displacement and the normal confining pressure.

Assuming that the softening behavior is controlled by the shear plastic relative displacement, yields

$$\dot{\kappa}_2 = \left|\Delta \dot{u}_s^{\,p}\right| = \dot{\lambda}_2 \tag{3.24}$$

The stress update equations read

$$\begin{cases} \sigma_{n+1} = \sigma^{trial} - \Delta\lambda_{2,n+1} k_n \tan\psi \\ \tau_{n+1} = \tau^{trial} - \Delta\lambda_{2,n+1} k_s \dfrac{\tau^{trial}}{\left|\tau^{trial}\right|} \end{cases} \tag{3.25}$$

and the derivative necessary for the iterative local Newton-Raphson method is

$$\left(\frac{\partial f_2}{\partial \Delta\lambda_2}\right)_{n+1} = -k_n \tan\phi \tan\psi - k_s - h_2 \tag{3.26}$$

where

$$h_2 = \left[\sigma_{n+1}\left(\frac{\tan\phi_r - \tan\phi_0}{c} + 1\right)\right]\frac{\partial \overline{\sigma_2}}{\partial \kappa_2} \tag{3.27}$$

and the consistent tangent stiffness matrix reads

$$\mathrm{D}_2^{\mathrm{ep}} = \left(\frac{\partial \sigma}{\partial \varepsilon}\right)_{n+1} = \frac{1}{h_2 + k_n \tan\phi \tan\psi + k_s} * \begin{bmatrix} k_n(h_2 + k_s) & -k_n k_s \tan\psi \dfrac{\tau_{n+1}}{|\tau_{n+1}|} \\ -k_n k_s \tan\phi \dfrac{\tau_{n+1}}{|\tau_{n+1}|} & (h_2 + k_n \tan\phi \tan\psi) k_s \end{bmatrix} \tag{3.28}$$

Fig. 3.22 shows the dependence of $\overline{\sigma_2}$ from the values of fracture energy considered in the model. Aiming to investigate the interfacial shear behavior of FRP-masonry joints, an experimental campaign was developed recently at the University of Minho, Basilio 2007, see Fig. 3.23.

Moreover, Lu, Teng et al. 2005, showed that the exponential softening law for mode II would not be appropriate, even if applied in the past for FRP-concrete joints, see Fig. 3.24

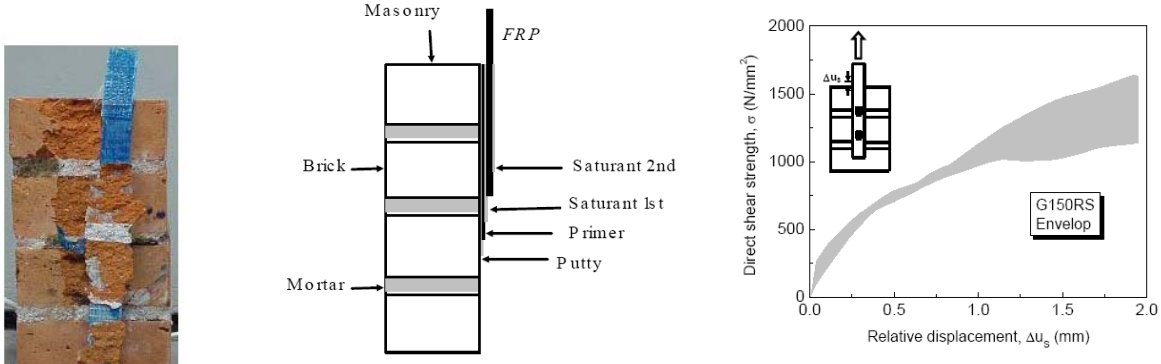

Fig. 3.23 Bond tests: (a) specimen; (b) specification of test; (c) results, see Basilio 2007

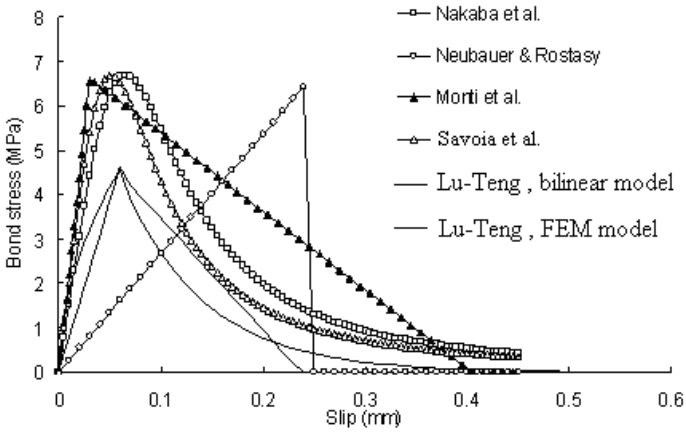

Fig. 3.24 Bond-slip curves from existing bond-slip models (concrete-FRP interface)

Since the value of the cohesion *c* and the experimental shape of $\overline{\sigma_2}$ cannot be easily determined by experiments due to the brittle behavior of the interface, an indirect method was used in this study. In fact, the experimental behavior was determined by means of the numerical analysis detailed in section 3.3. In particular the bond strength of the FRP-masonry joints is a function of several parameters as it detailed in Tab. 3.3.

Tab. 3.3 Influence of cohesion, shear fracture energy and shear stiffness on the bond strength

Parametric study L=150 mm			
Parametric Value / Calibrated Value	Shear Fracture Energy (Nmm/mm^2)	Shear Stiffness (N/mm^3)	Cohesion (N/mm^2)
	Peak Load (kN)	Peak Load (kN)	Peak Load (kN)
1/10	1.82	3.92	0.48
1/4	2.74	4.01	1.21
1/3	3.03	4.02	1.59
1/2	3.44	4.04	2.31
1	4.04	4.04	4.04
2	4.44	4.04	5.08
3	4.56	4.03	5.08
4	4.64	4.03	5.08
10	4.80	4.06	5.08

By means of a parametric study, the correct set of parameters to be used in the numerical analysis was determined and the numerical shape of $\overline{\sigma_2}$ assessed. Therefore, aiming to be more general, a multi-linear hardening/softening law can be used to describe the ductility of the FRP-masonry joint. The law implemented in this study, see Fig. 3.25, defines $\overline{\sigma_2}$ as a function of 10 parameters including the cohesion and the fracture energy of the interface, see appendix 1.

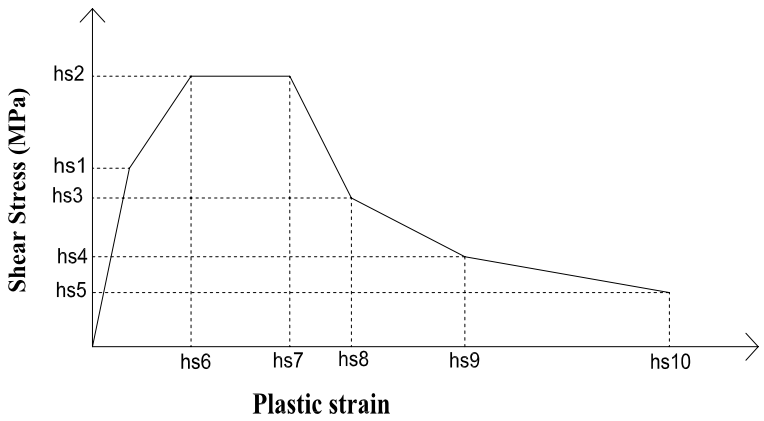

Fig. 3.25 New hardening/softening law to describe the evolution of the yield value $\overline{\sigma_2}$ as a function of κ_2

The application of this approach to simulate bond tests on curved substrates and FRP strengthening effects on masonry arch is provided in the following sections.

3.7.4 The compressive-cap criterion

For the cap mode, the ellipsoid interface model firstly introduced by Schellekens and De Borst 1993 for orthotropic plasticity in a 3D configuration is used. For the compressive-cap mode, the yield function reads

$$f_3(\sigma,\kappa_3) = C_{nn}\sigma^2 + C_{ss}\tau^2 + C_n\sigma - \left(\overline{\sigma}_3(\kappa_3)\right)^2 \tag{3.29}$$

with C_{nn}, C_{ss} and C_n a set of material parameters and $\overline{\sigma}_3$ the yield value. The parameters C_{nn} and C_n control the center of the cap and its intersection with the tensile part of the normal stress axis whereas the parameter C_{ss} controls the contribution of the shear stress to failure, see Fig. 3.28. In this study a centered cap with $C_{nn} = 1$ and $C_n = 0$ is adopted because a tension cut-off is included in the composite yield surface. For the hardening/softening behavior the law shown in Fig. 3.26 and eq. 3.30 is adopted, where the subscripts *i*, *m*, *p* and *r* of the yield value $\overline{\sigma}$ denote respectively, the *i*nitial, *m*edium, *p*eak and *r*esidual values. The peak value $\overline{\sigma}_p$ equals the masonry compressive strength f_m.

$$\begin{aligned}
&\overline{\sigma_a}(\kappa_3) = \overline{\sigma_i} + (\overline{\sigma_p} - \overline{\sigma_i})\sqrt{\frac{2\kappa_3}{\kappa_p} - \frac{\kappa_3^2}{\kappa_p^2}} \quad \text{if } \kappa_3 < \kappa_p \\
&\overline{\sigma_b}(\kappa_3) = \overline{\sigma_p} + (\overline{\sigma_m} - \overline{\sigma_p})\left(\frac{\kappa_3 - \kappa_p}{\kappa_m - \kappa_p}\right)^2 \quad \text{if } \kappa_p < \kappa_3 < \kappa_m \\
&\overline{\sigma_c}(\kappa_3) = \overline{\sigma_r} + (\overline{\sigma_m} - \overline{\sigma_r})\exp\left(m\frac{\kappa_3 - \kappa_m}{\overline{\sigma_m} - \overline{\sigma_r}}\right)^2 \quad \text{if } \kappa_3 > \kappa_m \\
&m = 2\frac{\overline{\sigma_m} - \overline{\sigma_p}}{\kappa_m - \kappa_p}
\end{aligned} \tag{3.30}$$

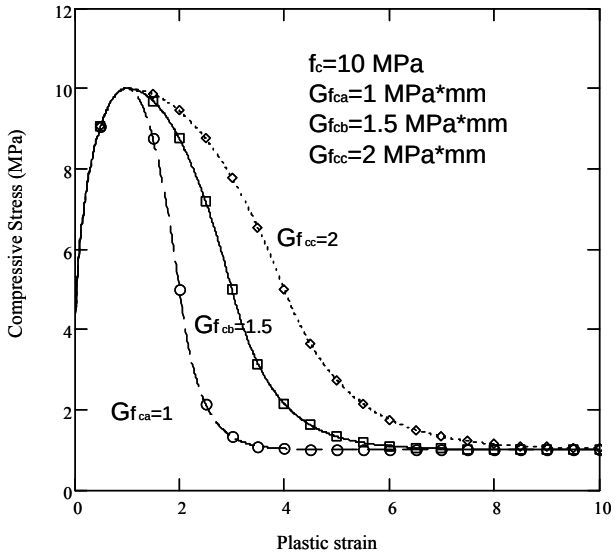

Fig. 3.26 Yield value $\overline{\sigma_3}$ as a function of the fracture energy

To ensure that the intersection between the cap and shear modes always occurs before the intersection between the cap and the tensile modes, see Fig. 3.27, the residual value has to be:

$$\overline{\sigma}_r > \sqrt{C_{nn} f_t^2 + C_{ss}(c - f_t \tan\phi_0)^2 + C_n f_t} \tag{3.31}$$

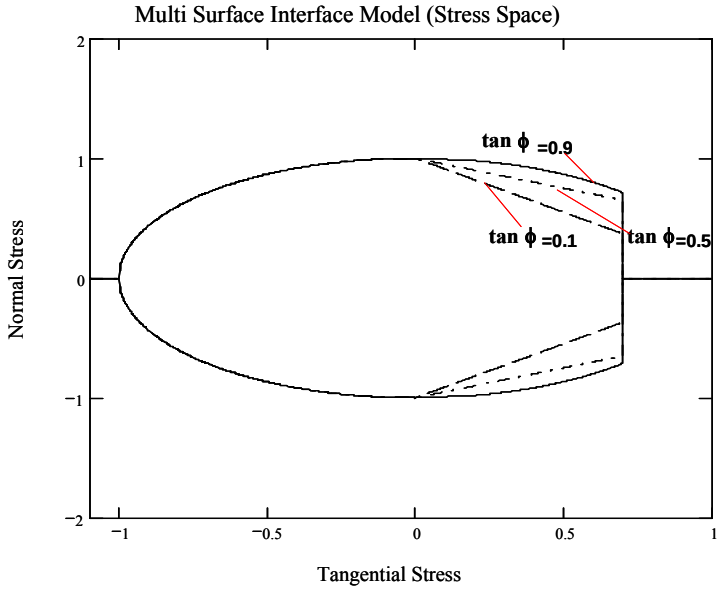

Fig. 3.27 Intersection between the cap and the tensile modes for tan $\phi = 0.9$

Using matrix notation, eq. 3.32 can be rewritten in a form more amenable to computational implementation, as

$$f_3(\sigma,\kappa_3)=\frac{1}{2}\sigma^T P\sigma+p^T\sigma-\left(\bar{\sigma}_3(\kappa_3)\right)^2 \tag{3.32}$$

where the projection matrix P and the projection vector p reads

$$P=\begin{bmatrix}2C_{nn} & 0\\ 0 & 2C_{ss}\end{bmatrix};\ p=\begin{Bmatrix}C_n\\ 0\end{Bmatrix} \tag{3.33}$$

An associated flow rule and a strain hardening/softening hypothesis are considered. This yields

$$\dot{\kappa}_3=\dot{\lambda}_3\sqrt{(P\sigma+p)^T(P\sigma+p)} \tag{3.34}$$

The stress update equations, can be manipulated to obtain

$$\begin{cases}\sigma_{n+1}=(D^{-1}+\Delta\lambda_{3,n+1}P)^{-1}(\varepsilon^e_{trial}-\Delta\lambda_{3,n+1}p)\\ \varepsilon^e_{trial}=D^{-1}\sigma^{trial}\end{cases} \tag{3.35}$$

The derivative necessary for the iterative local Newton-Raphson method reads

$$\left(\frac{\partial f_3}{\partial\Delta\lambda_3}\right)_{n+1}=\left(\frac{\partial f_3}{\partial\boldsymbol{\sigma}}+\frac{\partial f_3}{\partial\kappa_3}\frac{\partial\kappa_3}{\partial\boldsymbol{\sigma}}\right)^T\frac{\partial\boldsymbol{\sigma}}{\partial\Delta\lambda_3}-h_3 \tag{3.36}$$

where:

$$\frac{\partial f_3}{\partial\boldsymbol{\sigma}}=\mathbf{P}\boldsymbol{\sigma}_{n+1}+\mathbf{p} \tag{3.37}$$

$$\frac{\partial\kappa_3}{\partial\boldsymbol{\sigma}}=\Delta\lambda_{3,n+1}\frac{\mathbf{P}(\mathbf{P}\boldsymbol{\sigma}_{n+1}+\mathbf{p})}{\sqrt{(\mathbf{P}\boldsymbol{\sigma}_{n+1}+\mathbf{p})^T(\mathbf{P}\boldsymbol{\sigma}_{n+1}+\mathbf{p})}} \tag{3.38}$$

$$\frac{\partial f_3}{\partial\kappa_3}=-2\bar{\sigma}_{3,n+1}\frac{\partial\bar{\sigma}_3}{\partial\kappa_3} \tag{3.39}$$

$$\frac{\partial\boldsymbol{\sigma}}{\partial\Delta\lambda_3}=-(\mathbf{D}^{-1}+\Delta\lambda_{3,n+1}\mathbf{P})^{-1}(\mathbf{P}\boldsymbol{\sigma}_{n+1}+\mathbf{p}) \tag{3.40}$$

and the hardening modulus:

$$h_3=-\frac{\partial f}{\partial\kappa}\frac{\partial\kappa}{\partial\Delta\lambda}\bigg|_{n+1}=-\frac{\partial f_3}{\partial\kappa_3}\frac{\partial\kappa}{\partial\Delta\lambda}\sqrt{(P\sigma_{n+1}+p)^T(P\sigma_{n+1}+p)} \tag{3.41}$$

The consistent tangent stiffness matrix cannot be written in a simple form and is evaluated according to the general formulation given in chapter 3.

$$\mathbf{D}^{ep}=\frac{d\sigma_{n+1}}{d\varepsilon_{n+1}}\bigg|_{n+1}=\mathbf{H}-\frac{\mathbf{H}\dfrac{\partial g}{\partial\sigma}\gamma^T\mathbf{H}}{h+\gamma^T\mathbf{H}\dfrac{\partial g}{\partial\sigma}};\ \tag{3.42}$$

where the modified stiffness matrix reads

$$\mathbf{H} = \left[\mathbf{D}^{-1} + \Delta\lambda_{n+1} \frac{\partial^2 g}{\partial \boldsymbol{\sigma}^2} \right]^{-1} = \left[\mathbf{D}^{-1} + \Delta\lambda_{3,n+1} \mathbf{P} \right]^{-1} \tag{3.43}$$

and the modified yield surface gradient reads:

$$\gamma = \frac{\partial f_3}{\partial \boldsymbol{\sigma}} + \frac{\partial f_3}{\partial \kappa_3} \frac{\partial \kappa_3}{\partial \boldsymbol{\sigma}} \Bigg|_{n+1} \tag{3.44}$$

Fig. 3.28 illustrate the effect of several parameter changes in the cap mode of failure: namely C_{nn}, C_n, C_{ss}, $\overline{\sigma_3}$.

3.7.5 Corners

Corners of the composite yield surface are singular points that have to be handled according to the general procedures reviewed in chapter 3, see Lourenço 1996, for a full description.

3.8 Validation of the model

In this section, the capabilities of the interface model with the new multi-linear hardening law implemented are assessed aiming to numerically simulate the main features characterizing the masonry-FRP interfacial behavior. First, the model will be applied to simulate the debonding process in curved FRP-masonry substrates and second to simulate the failure pattern of FRP strengthened masonry arches at the intrados and extrados loaded at a quarter of their span.

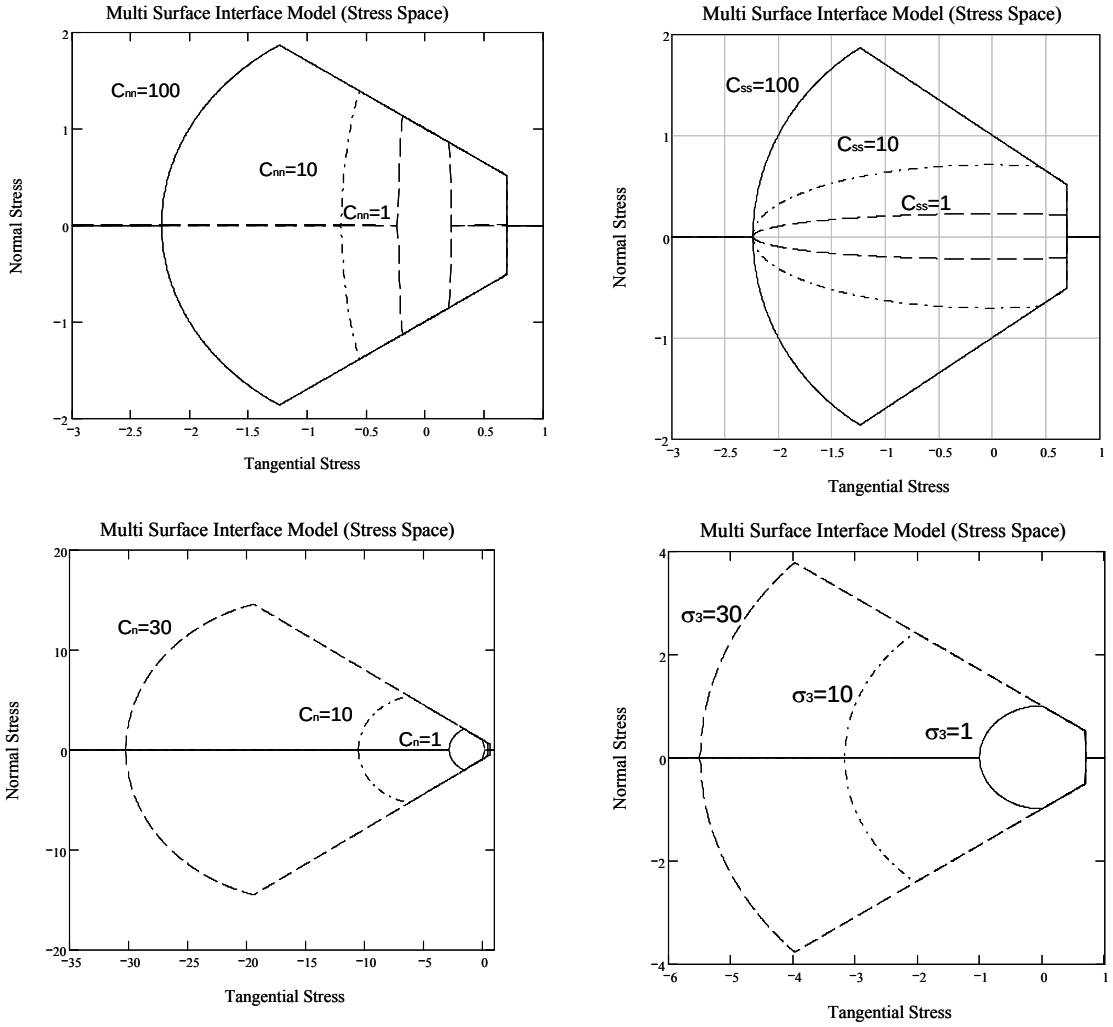

Fig. 3.28 Influence of C_{nn}, C_n, C_{ss}, $\overline{\sigma_3}$ .on the shape of the yielding function

3.8.1 Application to the bond test of curved substrates

The aim of the numerical analysis of the debonding process in curved substrates detailed in the following is to evaluate the stresses acting at the interface, namely tensile and shear, since they represent the critical aspect that needs to be captured from the constitutive model at local level, if FRP strengthening effects on real arched or vaulted structure is be simulated. In particular, the implementation, according to the numerical analysis provided in previous sections, showed good results when simulating simple shear bond test but provide a less good estimation in the case of strengthened masonry arches. This feature represents a drawback of the existing model and probably can be ascribed to a less correct representation of the hardening and softening behavior of the interface in the case of mixed mode debonding. This is particularly important for the

case of the intrados FRP strengthened masonry arch since in this case tensile stresses will born at the interface encouraging the debonding processes. The case of extrados FRP strengthened masonry arch is numerically less important since in this case compressive stresses will be generated at the interface. Note that the compressive strength of the interface (equal to the masonry compressive strength) has values much higher than the tensile strength of the interface. A schematic representation of the pull out test on curved substrates is provided in Fig. 3.29. Again in the numerical analysis three bond lengths where considered: 100mm, 150 mm and 200mm

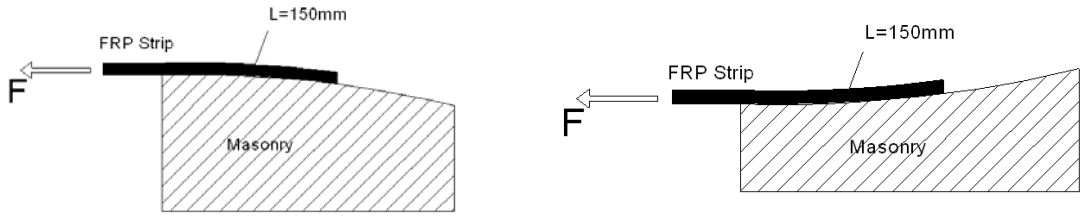

(a) (b)

Fig. 3.29 Schematic representation of the pull out test on curved substrates: (a) extrados; (b) intrados

The material properties used in the numerical analysis are the same as for the flat interface. Again, the same set of input parameters was used in all cases to reproduce the bond mechanism with a plane stress finite element model.

The comparison between the three bond lengths is done in terms of applied load – relative displacement diagrams, see Fig. 3.30, and shear and normal stresses distribution along the interface, see Fig. 3.31.

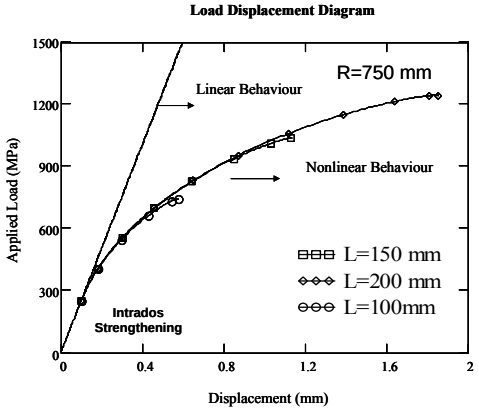

Fig. 3.30 Numerical load displacement diagrams to predict the bond strength of curved FRP-Masonry joints (intrados strengthening).

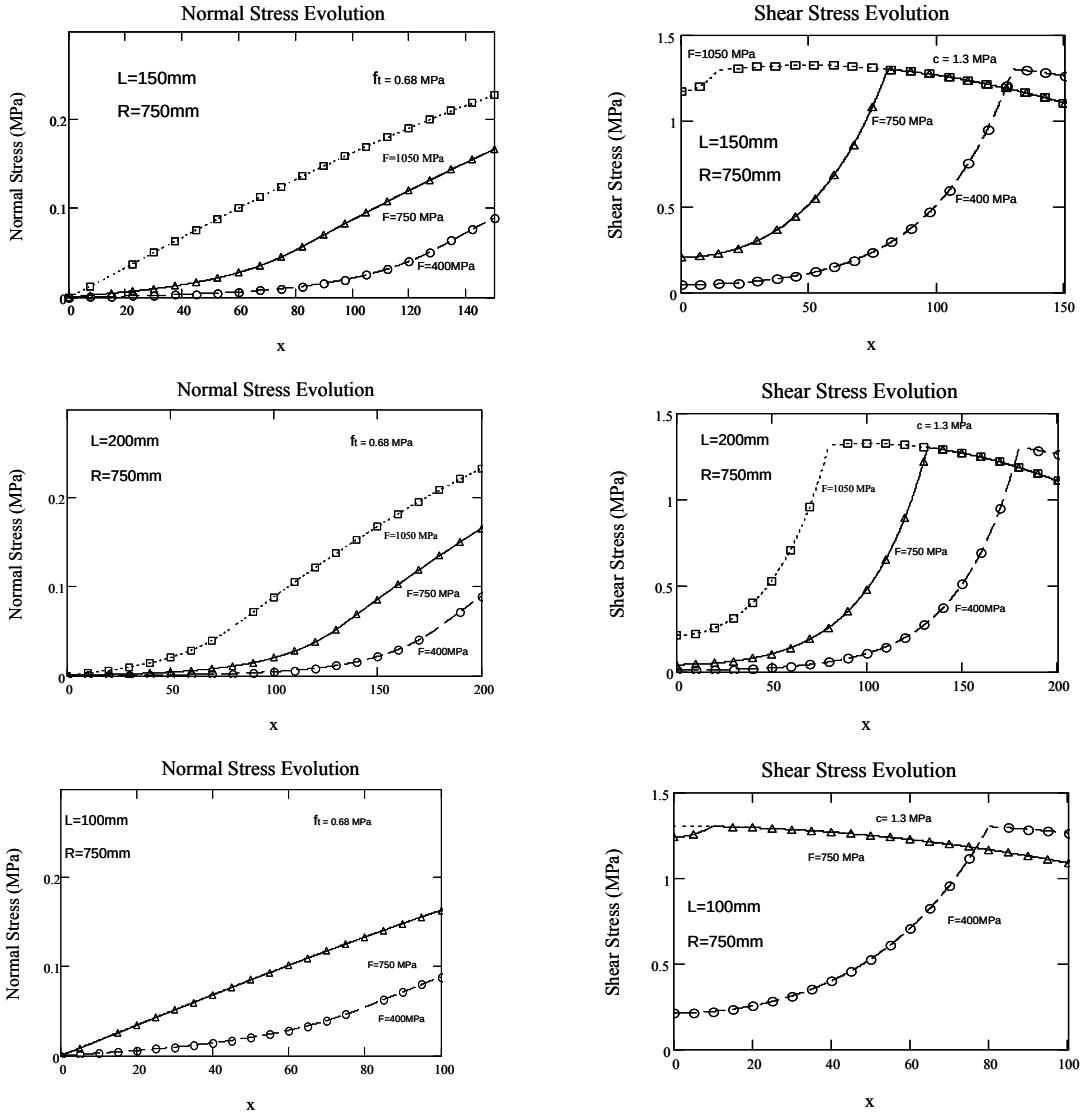

Fig. 3.31 Shear and normal stresses distribution along the interface for different bond lengths (intrados strengthening)

The new hardening law allows describing accurately the evolution of the debonding with the applied load both in terms of stresses and strain at the interface. An increase in the bond strength is found with the bond length also for mixed mode debonding in curved substrates. An important result consist in the observation that debonding is always due to attainment of the shear strength of the interface (c=1.3 MPa) being the normal stresses always less than the tensile strength of the interface (f_t=0.68 MPa).

3.8.2 Comparison with tests of strengthened arches

3.8.2.1 Structural model for masonry arches

The approach followed here concerning modeling was based on the micro-modeling strategy, where units behave in a linear fashion and the damage is concentrated in the relative weak masonry joints. The composite interface model has been widely described in section from 3.2 to 3.8. The semicircular masonry arches here had a 750 mm radius, 450 mm width and 50 mm ring thickness. The displacements at the abutments were restrained in both orthogonal directions, see Fig. 3.32a. The complete setup description can be found in Oliveira, Basilio et al. 2010. Numerical analyses were performed with a nonlinear finite element program including discontinuities by means of interfaces. The two dimensional mesh adopted in the analysis includes again eight-node plane stress elements to represent the masonry units, six-node interface elements to simulate the mortar and GFRP-masonry joints and three-node beam elements to represent the GFRP, see Fig. 3.32b. Each masonry unit was modeled with four elements. In this case zero thickness interfaces were assumed for all the joints. Most of the properties used to simulate the mortar and GFRP-masonry interfaces were determined during the previous analyses, either from experimental work, or from numerical calibration.

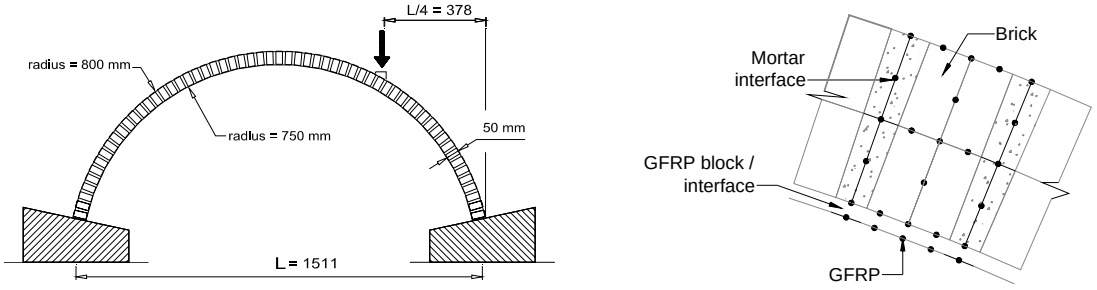

Fig. 3.32 Modeling of semicircular arches: (a) Elevation view (in mm), (b) Mesh detail of the masonry arch and GFRP strip, Basilio 2007.

3.8.2.2 Unstrengthened arches

In order to identify the structural behavior, the maximum load capacity and the mechanism of collapse, an analysis of plain arches was carried out. This analysis gave a general overview about how the structure behaved under an increasing load applied at the quarter span, without any strengthening. The deformed shape provided an indication

on its behavior, showing where subsequent arches should be reinforced. The numerical model shows a reasonable agreement with the experiments in the sense that it reproduces the initial stiffness and peak load, as illustrated in Fig. 3.33.

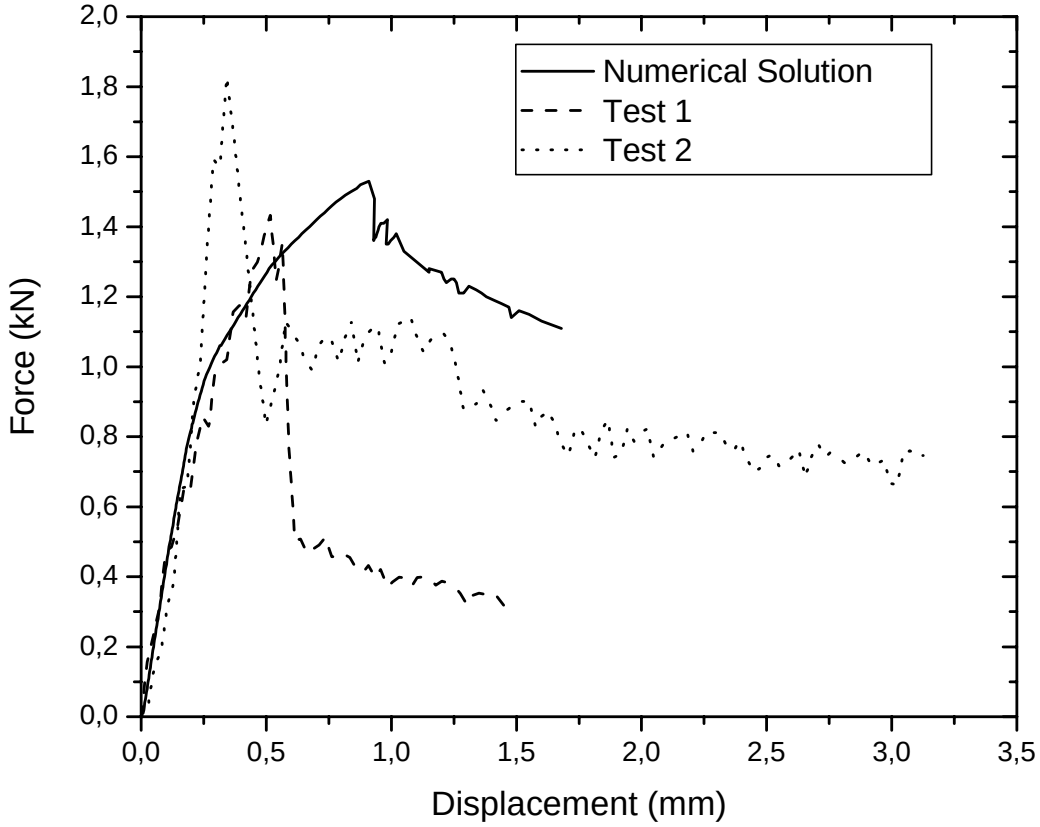

Fig. 3.33 Unstrengthened arches: Test 1 and Test 2 results compared with its corresponding numerical response with indication of plastic hinges sequence on the load-displacement diagram

As observed experimentally, a sudden drop in the load carrying capacity after reaching the peak load was obtained. Failure was characterized by brittle behavior. For a better perception of the structural behavior, hinges appearance sequence is shown on the numerical load-displacement curve outlined in Fig. 3.34.

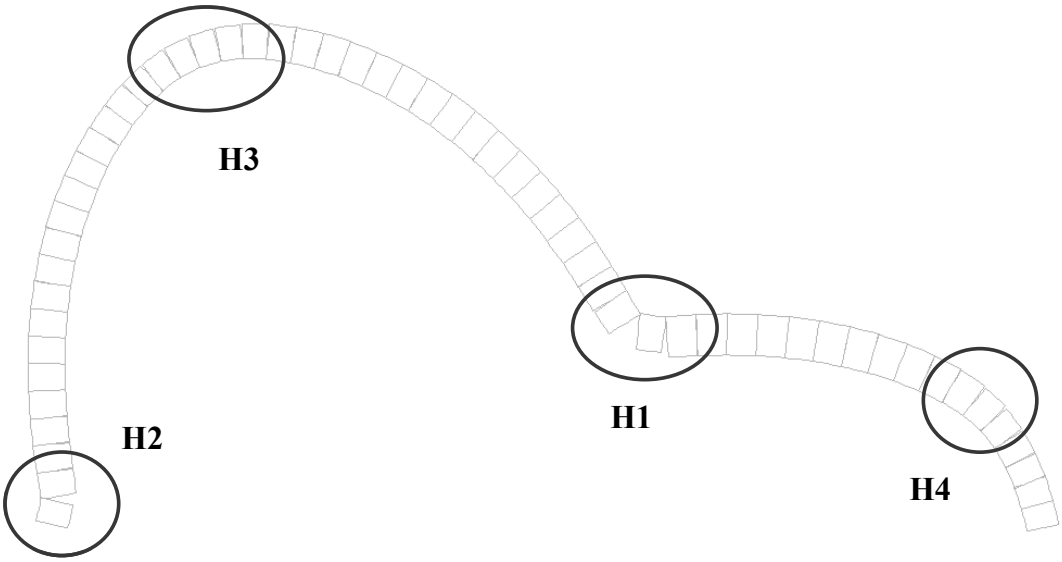

Fig. 3.34 Numerical hinge development sequence for the unstrengthened masonry arch described on the incremental deformed mesh.

Each hinge, marked with a circle, results in slight stiffness changes along the structural response path. All four hinges were formed before the peak load was reached.

3.8.2.3 Comparison with tests carried out over the strengthened arches

When strengthening masonry arches with composite materials, some relevant issues have to be taken into account. Both numerical and experimental study demonstrate that, in the case of a continuous strengthening only at one face (intrados or extrados), modifications to the statically determinate structure occur, presenting just three hinges and a possible other release, whose location depends on the surface considered for application of reinforcement. Both cases presented hinges at the supports. The first hinge appears below the loading point for the extrados strengthened structures, and at the opposite side of the load application point for the intrados-strengthened arches.

A reinforcement consisting in an FRP-strip located at the extrados disables hinge development at the extrados. The opposite happens for the intrados-reinforced arches, where this kind of reinforcement disables hinges development at the intrados beneath the application load. Particularly, in the zones where the first hinge appears, cracking along the masonry joint starts to propagate spreading until arches feet before local sliding occurred. This behavior is well simulated by the numerical model. The values employed for tensile and shear strength of masonry joint are responsible for the above-

discussed features. The numerical models show clearly collapse and in the mechanism how the location of the plastic hinges moves towards the zone where reinforcement ends up. Results related to the full length reinforcement at the extrados are shown in Fig. 3.35 and at the intrados in Fig. 3.36 in terms of hinge-location evolution and principal compressive stresses (kN/m^2) depicted vs. the incremental deformed shape.

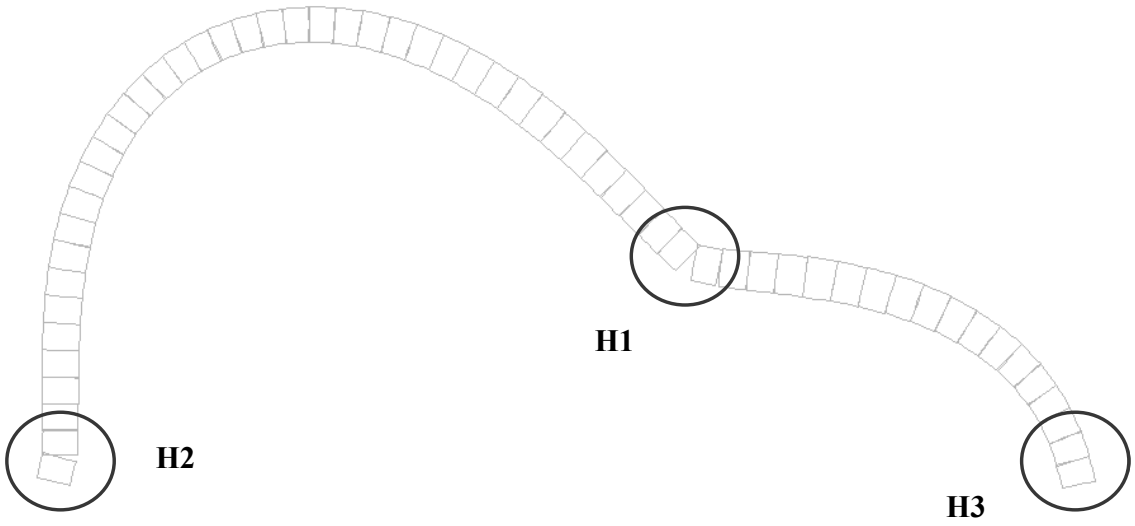

(a)

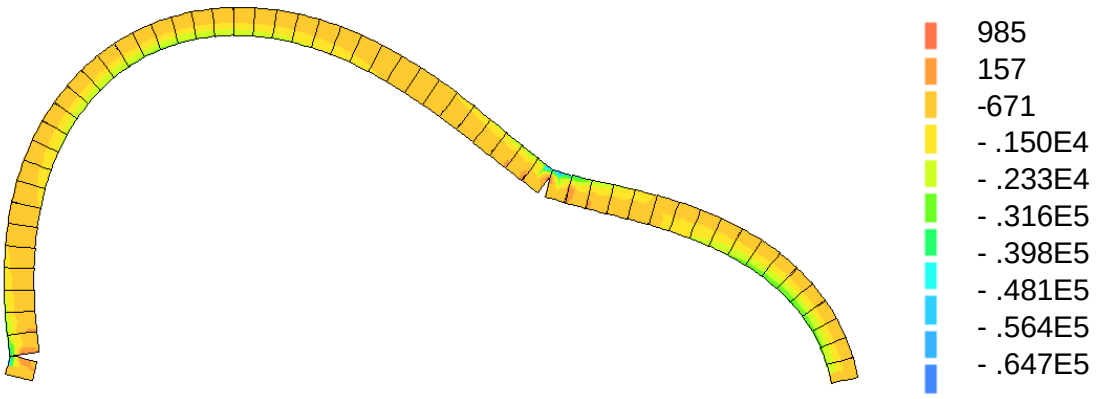

(b)

Fig. 3.35 (a) Numerical hinge development sequence for the composite strengthened in the extrados arch, including (b) Principal compressive stresses (kN/m^2) depicted on the incremental deformed mesh.

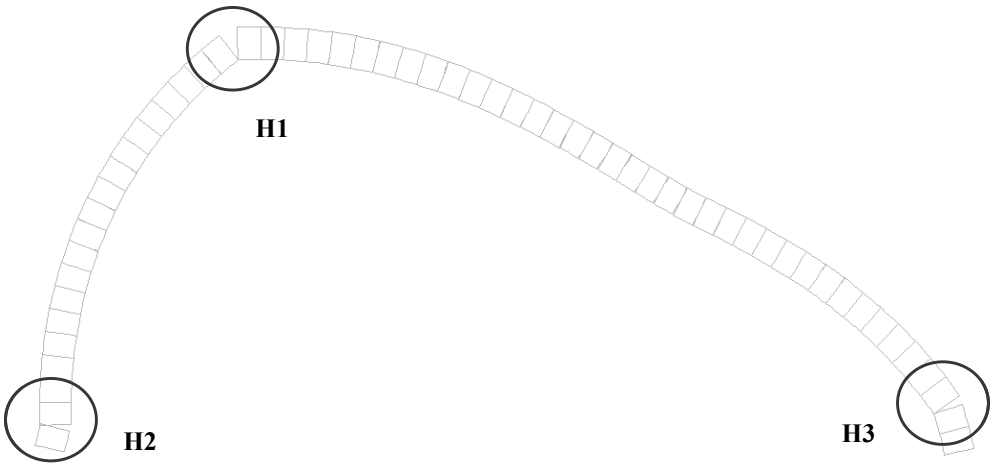

(a)

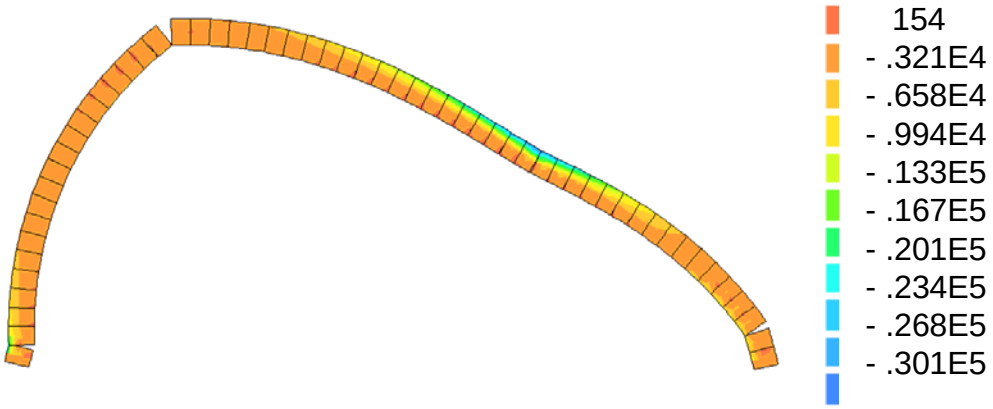

(b)

Fig. 3.36 (a) Numerical hinge development sequence for the numerical composite strengthened in the intrados arch, including (b) Principal compressive stresses (kN/m2) depicted on the incremental deformed mesh.

In the case of intrados-reinforcement, failure is characterized by the opening of the joints in the opposite surface when compared with the extrados, because the FRP-reinforcement contributes to holding the bricks together. In the numerical model, however, a discrepancy exists near the collapse load, due to the (incorrect) opening of a masonry joint in the position (bottom-left), where the reinforcement (at the intrados) is located. On the contrary, in experiments, sliding was observed in that position. The mechanism of collapse produced by these openings (hinges), together with masonry crushing or interface debonding, prevents the arch from continuing to carry an increasing load. Concluding, Figs. 3.37 and 3.38 compare the different results obtained

with the two strengthening procedures in terms of load displacement diagram. The comparison is done versus experimental results.

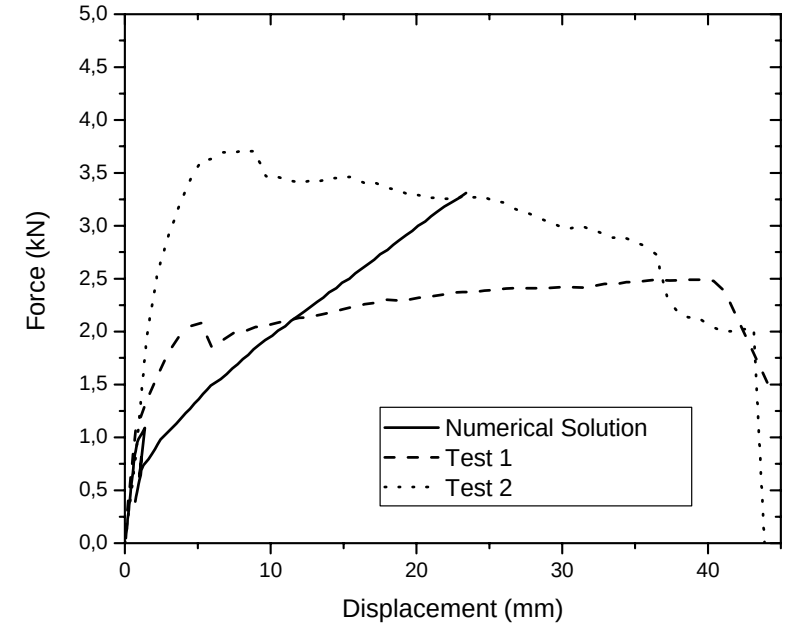

(a)

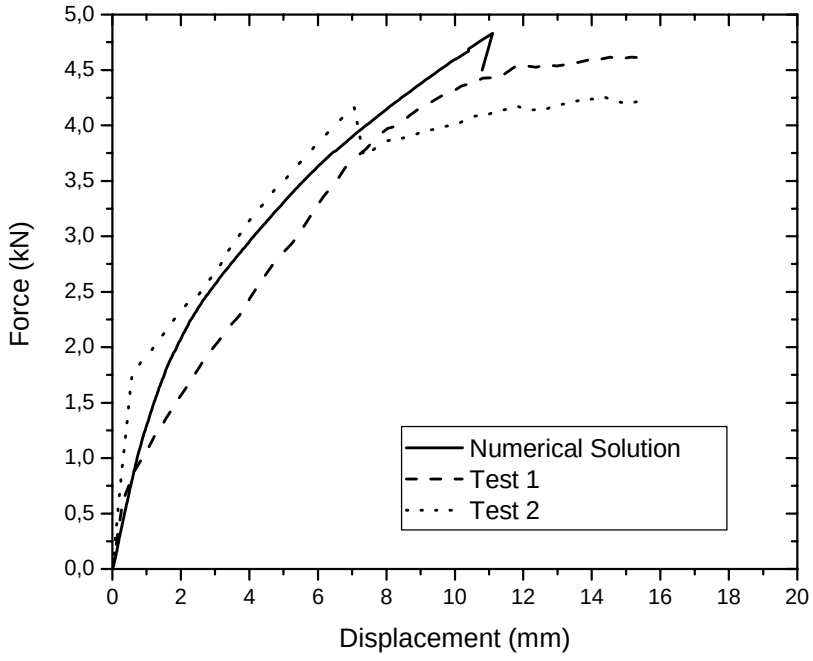

(b)

Fig. 3.37 Continuously strengthened arches, Test 1 and Test 2 results compared with the corresponding numerical response: (a) extrados; (b) intrados

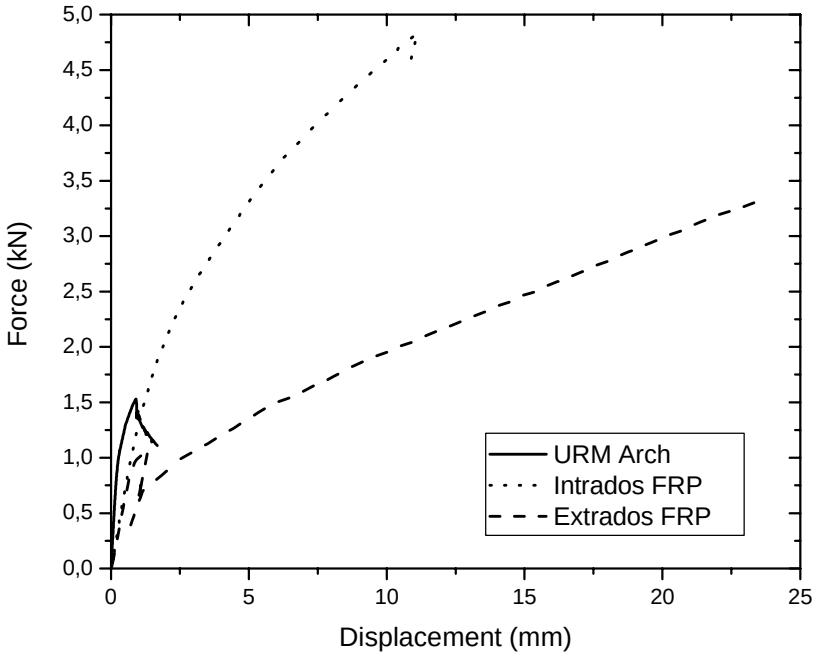

Fig. 3.38 Comparison of numerical results for the URM arch and the continuously strengthened arches at the intrados and extrados

Numerical analyses show that arches with full length GFRP reinforcement placed at the intrados present higher peak load values, when they are compared with full length GFRP reinforcement placed at the extrados, the opposite is valid when the comparison is done in terms of ductility. Independently from the damage stage, a reasonable increment on the peak load might be reached and ductility is gained by means of the application of FRP strips both at the extrados and/or the intrados. Fig. 3.39 shows the failure modes obtained with the numerical analysis at the last step, shown in terms of incremental displacement. In particular failure is due to debonding between the FRP and masonry substrate for arch with FRP at the intrados (Fig. 3.39a) and shear between masonry joints after debonding at the FRP-masonry interface (Fig. 3.39b) for the arch with reinforcement at the intrados.

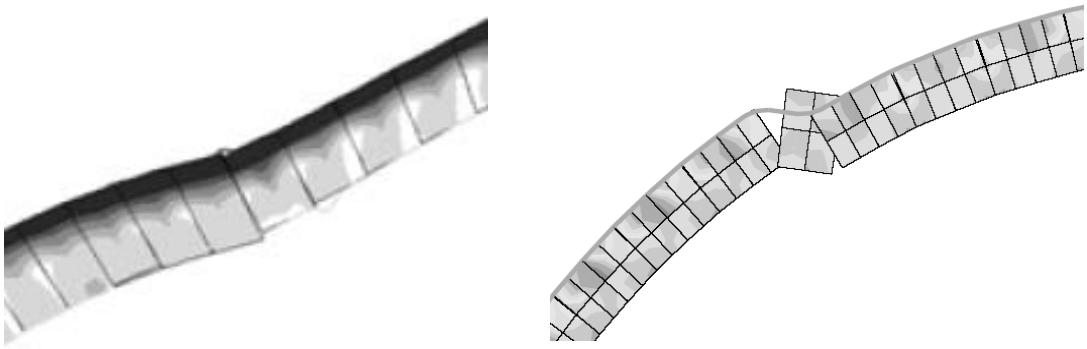

(a) (b)

Fig. 3.39 Continuously strengthened arches at the intrados (a) and extrados (b)

3.9 Case study: Leiria Bridge

This last section deals with the numerical analysis of a masonry arch bridge considered as a case study. The bridge, dated from early 20th century, is made of limestone masonry and is located in the city centre of Leiria, Portugal, Fig. 3.40.

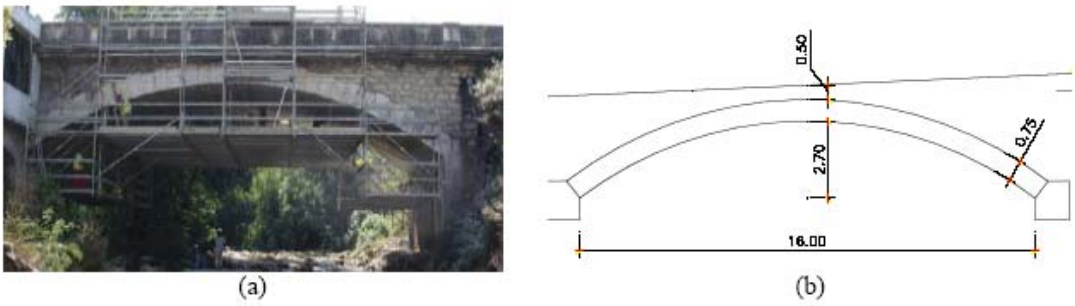

Fig. 3.40 Elevation view (downstream side): (a) photo; (b) model

In the framework of a governmental urban rehabilitation program, the part of the city involving the bridge was under rehabilitation works. Therefore, a detailed characterization of the bridge state was needed. The purpose of the modeling described in this section is related to the simulation of three load tests carried out, as well as the assessment of the load carrying capacity of the bridge and design of a possible strengthening solution using FRP materials. According to the previous description of the possible modeling strategies of masonry constructions, in this section both linear analysis, limit analysis and nonlinear analysis will be used aiming to provide a different level of insight into the structural behavior of the masonry arch bridge analyzed.

3.9.1 General considerations

The data available with regard to the elastic properties ($E_c = 56.7$ GPa) and the mechanical properties ($f_c = 59.9$ MPa) were obtained through uni-axial compression tests on masonry specimens, see Fig. 3.41.

Fig. 3.41 Masonry specimen extracted from the arch bridge

The tests allow asserting that the material is hard limestone ($f_c > 30$ MPa). These results cannot be directly used to assess the parameters to be used in the numerical models because they are referred to limestone cylinders extracted from the bottom part of the bridge, while masonry blocks behave in a different way. Therefore, starting from the results above mentioned and considering the absence of other values characterizing the material and mechanical properties of the masonry stones that constitute the arch bridge and the infill, standard values available for this type of structure were used (Orduna and Lourenço 2003). In particular, a value of 4 MPa was adopted for the masonry compressive strength according Piet 1970. This value selected for the compressive strength of masonry take into account the type of material (hard limestone) and the existence of joints between stones. The properties are reported in Tab. 3.4.

Tab. 3.4 Material and mechanical properties used

Masonry stone	**Infill Material**
Density = 25 kN/ m^3	Density = 20 kN/ m^3
Friction angle of joints = 31º	Friction angle of soil = 30º
Compression strength = 4 MPa	Friction angle arch-soil = 20º

The values used for the compressive strength of the masonry take into account the type of material characterized with the mechanical tests (hard limestone), the existence of joints between stones and the reduction of the strength due to the transversal fissures observed during the visual inspection of the bridge in the preliminaries phases, see Fig. 3.42, Piet 1970.

Fig. 3.42 Visual inspection: vertical cracks in the masonry blocks

Considering that in this type of bridges, the infill material causes a redistribution of the concentrated loads applied on the top surface, in this work it was supposed that the vertical loads are dispersed inside the soil with an angle of 30º according Boussinesq theory. The effects of any other type of damage were not included in the numerical model.

3.9.2 Numerical analysis of the static tests

In this subsection the numerical analysis of the static tests performed is presented and discussed. The most critical loads conditions were assessed according the Portuguese codes, RSA 1983. A finite element model was developed assuming the hypothesis of linear elastic behavior of the materials. Despite the fact that masonry, in general, exhibits a nonlinear behavior since early load levels, the load and of the deformation recorded during the static tests allow to accept the assumption of elastic behavior of the materials. In the following sections, the displacements obtained through the numerical analysis and the ones recorded during the static tests are compared in three control sections: the section at the crown of the arch and the sections at the quarters of the bridge span.

3.9.3 Structural model

The bridge was modeled through a finite element model using eight nodes elements in plane stress conditions. The resistant elements considered are both the masonry arch and the spandrels as illustrated in Fig. 3.43. For low load levels, the spandrels can have an important influence on the structural behavior of the bridge, while for higher load levels these effects are reduced due to the accumulated damages that generate a loss of connection with the arch.

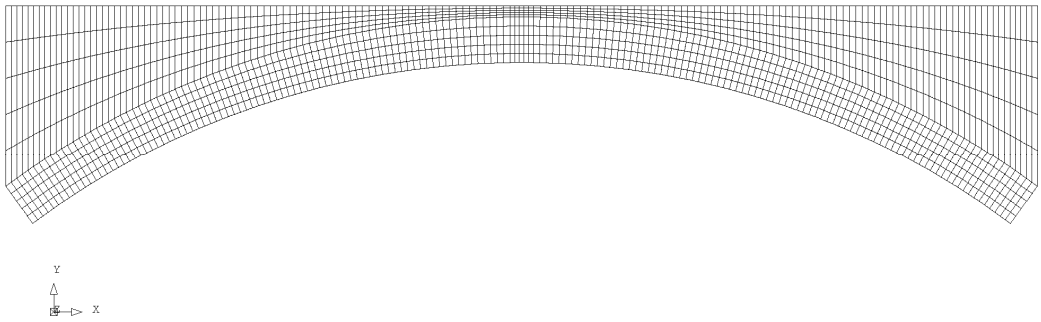

Fig. 3.43 Finite element mesh used to model arch and spandrels**.**

3.9.4 Characterization of the materials

Material properties of the masonry arch and of the infill material considered in the numerical model are indicated in Tab. 3.4. The properties are the followings: E_{arch} = 15 GPa e $S_{pandrel}$ = 3 GPa. Due to the small displacements generated from the static tests, it was assumed that the passive thrust of the soil was only partly activated.

3.9.5 Load conditions

To characterize the global behavior of the bridge and assess his load capacity, three different static loads tests were realized. Two different trucks were used to generate the load cases, respectively indicated as truck 1 (front axis: 17.6 kN and back axis: 22.3 kN) and truck 2 (front axis: 18.3 kN and back axis: 24.3 kN), as indicated in Fig. 3.44.

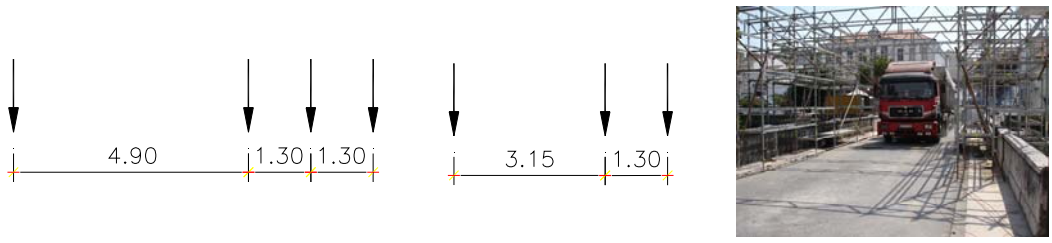

(a) (b) (c)

Fig. 3.44 Load test: trucks used in the static tests: (a) truck 1; (b) truck 2**;** (c) truck during a load test

The experimental characterization of the bridge under static loads needed three different tests as described in the following:

- Test 1: the two trucks were set facing the back parts (distance between the axis of the trucks approximately equal to 2,70 m), centered in the middle of the bridge span, (E2);

- Test 2: the two trucks were set facing the back parts (distance between the axis of the trucks approximately equal to 2,70 m), centered in the quarter of the bridge span on the South-East part, left side, (E3);
- Test 3: truck 1 was on the North-East side, with the power axis centered in the quarter of the bridge span on the North-East part, right side, (E4).

Fig. 3.45 shows in schematic form the positions of the trucks for each static load conditions.

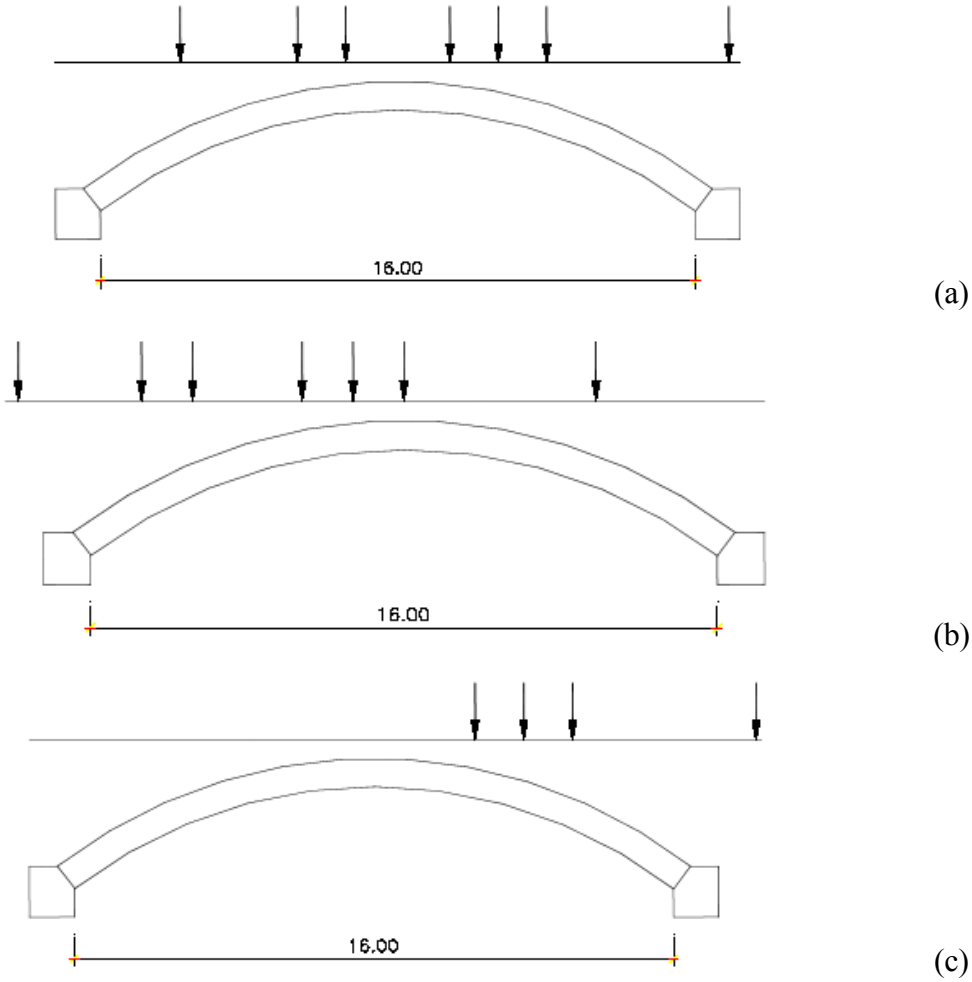

Fig. 3.45 Schematic representation of each static load test performed: (a) load condition 1; (b) load condition 2; (c) load condition 3

3.9.6 Analysis and discussion of the results

3.9.6.1 Linear finite element analysis

The comparison between the experimental and numerical results is done with respect to the following displacements:

- Displacement d_1: vertical arch displacement, measured at the South-East quarter of the bridge span (left side);
- Displacement d_2: vertical arch displacement, measured at the middle of the bridge span. Experimentally, two different vertical displacements were measured in the middle of the bridge span (one for each side of the bridge width) and therefore the average value is considered for the comparison with the numerical value;
- Displacement d_3: vertical arch displacement, measured at the North-East quarter of the bridge span (right side).

The displacements were measured by means of steel cables and added masses in contact with Lvdts fixed to the soil. Because of this, the errors related to the instrumentation used during the experimental tests are larger than the precision of the LVDT (around 0.01 mm). The experimental displacements are quite small, see Tab. 3.5. The analysis of these values shows that the maximum displacements are due to the load condition 1, while for the load condition 3 the observed displacements are quite close to the error of the instrumentation. Tab. 3.5 also contains the comparison between the numerical and experimental displacements for the other load condition.

Tab. 3.5 Experimental and numerical displacements for the three different static loads tests.

Test	Experimental [mm]			Numerical [mm]		
	d_1	d_2	D_3	d_1	d_2	d_3
Test 1	–0.14	–0.27	–0.18	–0.162	–0.201	–0.134
Test 2	–0.10	–0.12	–0.10	–0.155	–0.148	–0.075
Test 3	+0.03	–0.03	–0.04	+0.104	–0.046	–0.214

(The sign "+" indicates the upward vertical displacement)

The maximum differences between experimental and numerical results, obtained for the load conditions 1 and 2, (respectively 0.07 mm e 0.06 mm) are very similar to the margins of uncertainty of the instrumentation and therefore can be considered reasonable.

Moreover, the maximum difference obtained for the load condition 3 (0.17 mm) cannot be validated because the experimental displacements for this load condition are very small and therefore the values fall in the margin of error of the instrumentation. Finally, analyzing the values in Tab. 3.5, it is possible to verify that the numerical displacements obtained can well approximate the ones determined through the tests. To improve the agreement between numerical and experimental analysis, a more complex numerical model able to assess the influence of the layer of reinforced concrete and the effects of the infill. This level of accuracy could be achieved only determining the mechanical properties of the soil and of the reinforced concrete through other experimental investigation. Fig. 3.46 shows the minimum compressive stresses generated due to the dead weight of the bridge including the effects of the infill material and of the pavement. With exceptions for the elastic peaks of stresses near to the abutments, the maximum compressive strength is around 1.2 MPa. This value can hence be accepted for this type of structure.

Fig. 3.46 Minimum compressive stresses due to the dead weight of the bridge represented on the undeformed mesh (values in [Pa]).

Considering again the static load tests, Fig. 3.47 shows the minimum compressive stresses, generated due to the dead weight of the bridge and each single static load condition. From these figures it is possible to assess that the maximum compressive stresses have a magnitude of around 1.5 MPa, excluding the elastic peaks that can generate punctual zones where the materials enter in the nonlinear range. The maximum tensile stresses are instead around 50 kPa (obtained for the third load condition). This result confirms that the hypothesis of elastic behavior of the material is reasonable for this numerical analysis.

3.9.7 Load carrying capacity

3.9.7.1 Limit analysis

Besides the simulation of the load tests, also a numerical assessment in terms of carrying capacity was required in order to assess the safety conditions of the bridge in order to be used by vehicles. The objective here is to provide a good estimation of the maximum load that the bridge can sustain prior to failure. Among the available computational methods proposed in literature to compute the carrying capacity of masonry arch bridges, from hand-based methods to advanced nonlinear tools, the limit analysis method is the most generally applicable, see Gilbert 2005, for further details. Within the limit analysis method, the load distribution is known but the load magnitude that the bridge can carry is unknown, but it can be computed. Therefore, limit analysis is a very practical tool since it only requires a reduced number of material parameters and it can provide a good insight into the failure pattern and limit load.

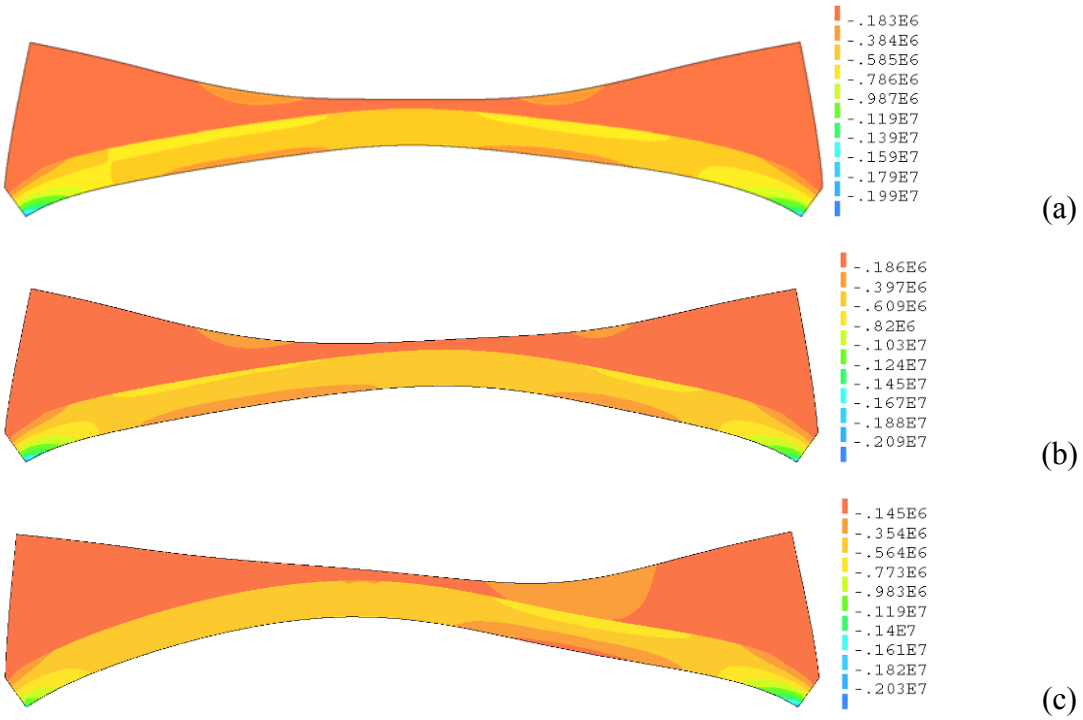

Fig. 3.47 Minimum compression stresses (values in [Pa]), represented on the incremental deformed shaped due to the dead weight of the bridge and different static load conditions: respectively (a) load condition 1; (b) load condition 2; (c) load condition 3.

Here, the bridge was modeled as an in-plane single span segmental arch, see Fig. 3.48. For the horizontal passive pressure, a conservative value equal to half of the classical value given by Rankine theory was used. Besides the self-weight of the materials (masonry and fill), a movable load composed by the Portuguese standard vehicle was considered, RSA 1983. This standard vehicle is composed by three axles equally spaced by 1.50 m and with a 200 kN load per axle. Using the computer program Ring, developed within the rigid block limit analysis method, Gilbert 2005, the minimum failure load factor was found to be equal to 4.47. This load factor was found for the vehicle central axle positioned at 31.9 % of the free span. Fig. 3.48 illustrates the associated four hinges failure mechanism found, where both the dead and live load pressures applied to the arch, the hinges and the thrust-line are shown. The load factor obtained seems to indicate that the bridge can be safely crossed by traffic.

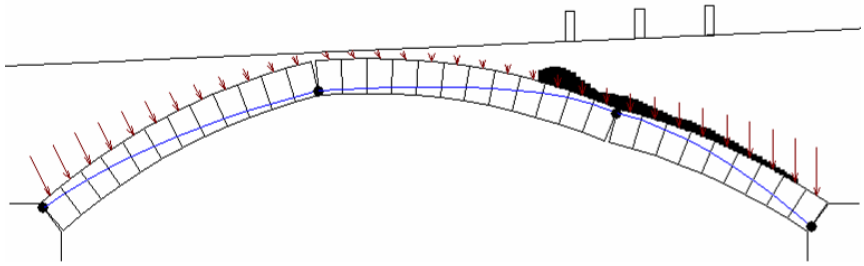

Fig. 3.48 Collapse mechanism for the minimum failure load.

3.9.7.2 Nonlinear finite element analysis

Aiming to evaluate the ultimate strength capacity of the bridge, for the same load condition considered in the limit analysis, finite element models are developed again but this time including in the model the material nonlinear behavior. The material properties used are according to the values used for the linear and limit analysis previously detailed. The ultimate load factor obtained with a smeared cracking approach is about 4 and therefore less than the value obtained with the limit analysis approach. In Fig. 3.49 the values of the maximum compressive stresses before collapse on the deformed configuration are plotted expressed in MPa.

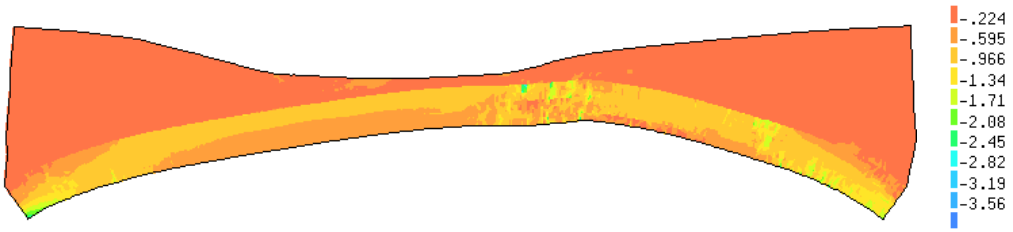

Fig. 3.49 Contour plot of the maximum compressive stresses before collapse

Fig. 3.50 gives the load displacement diagram representing the load history of the bridge obtained with a finite element model with interfaces between the blocks. The analysis was performed considering also the presence of FRP strips at the intrados of the arch bridge modeled using the constitutive model described in previous sections. The displacement shown in Fig. 3.50 is at a quarter of the span bridge opposite to the part where the load is applied. The difference in terms of collapse load between the strengthened, Fig. 3.52**,** and unstrengthened, Fig. 3.51**,** configuration is around 600 kN, as collapse is much controlled by masonry crushing. Note that the adopted compressive strength is low and the arch is shallow, inducing higher normal stresses.

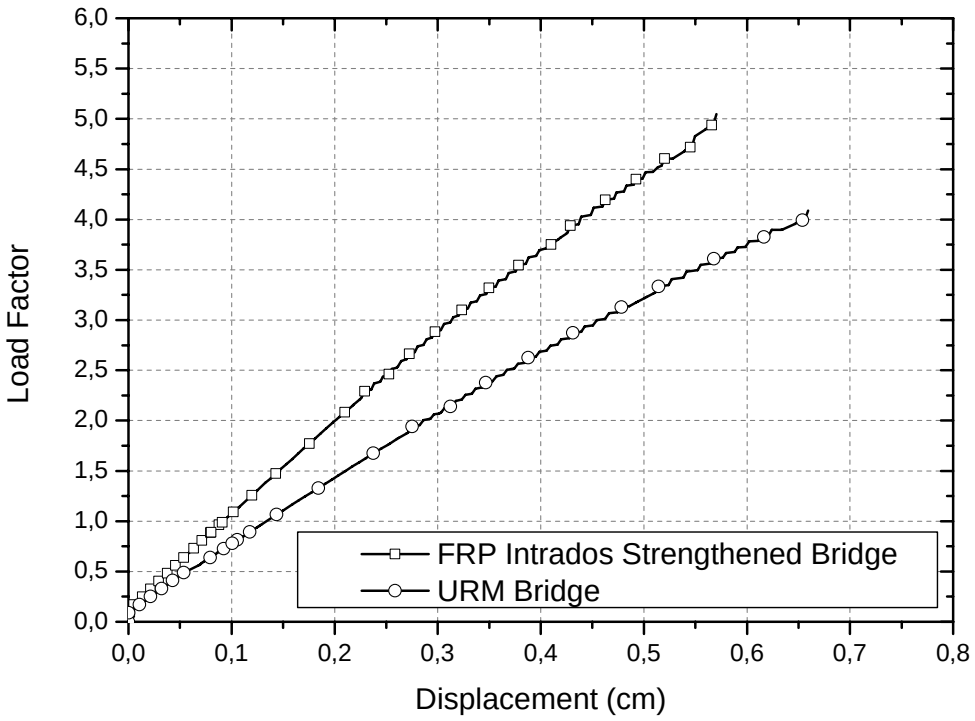

Fig. 3.50 Load-displacement diagram at a quarter of the bridge span

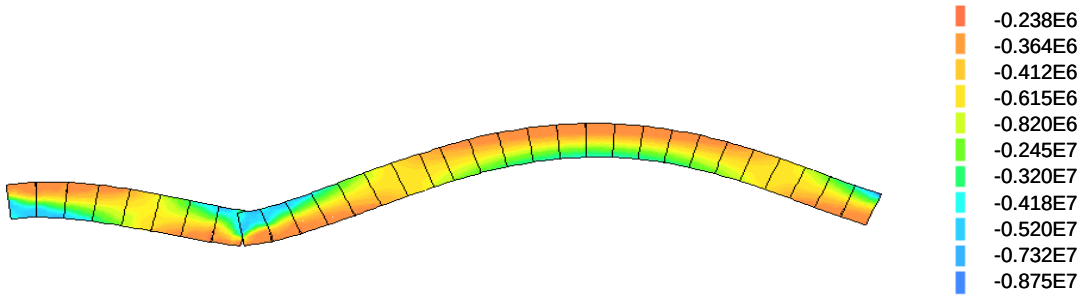

Fig. 3.51 Failure mode - bridge without strengthening (Pa)

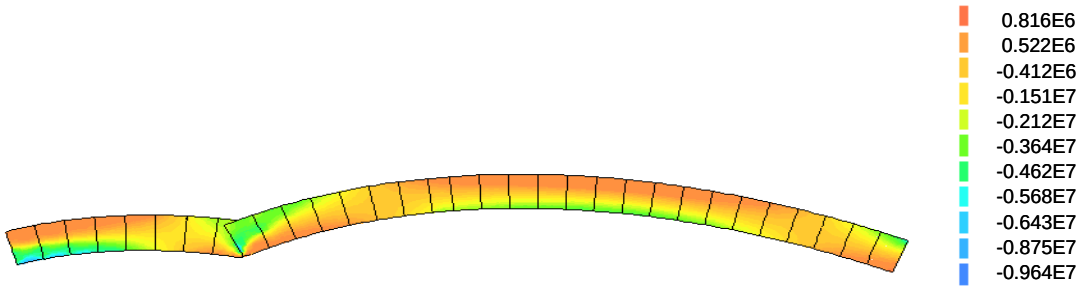

Fig. 3.52 Failure mode - bridge with strengthening (Pa)

3.10 Summary

In this chapter, a finite element model has been presented for the simulation of the interfacial behavior of FRP bonded to masonry. Since results in this area are scarce, research efforts are needed. An approach based on the incremental theory of multi-surface plasticity is presented. Zero-thickness interface elements are used to capture the development and propagation of debonding in the masonry layer adjacent to the adhesive layer. The monotonic constitutive model of the interface is defined by a convex composite yield criterion, composed by three individual yield functions, where softening behavior has been considered for all modes (tension, shear and compression). The model is able to assess the influence of several parameters on the FRP-masonry interfacial behavior, showing that the cohesion and the shear fracture energy of the interface are the most important parameters. Also the change of inelastic laws in shear and tension is detailed, showing that the material model proposed and implemented in the finite element program Diana, is useful to model the FRP-masonry interface, for both planar and curved substrates. It allows to obtain the global full shear force-displacement path and also to simulate the stress distribution at the interface in the

tangential and normal direction. Then the material model developed is used to assess the structural behavior of semi-circular masonry arches strengthened with composite materials. The details of the modeling have been explained and discussed. With this model, it was possible to obtain peak loads and mechanisms of failure similar to a previous experimental investigation performed at the University of Minho. However, improvements in the coupling of shear and tension modes of failure of the proposed constitutive law are still necessary. In the final part of this chapter the micro-modeling approach is used to analyze the structural behavior of a masonry arch bridge aiming to simulate a load test, to assess its carrying capacity and the FRP strengthening effect on the bridge loading capacity. To accomplish both of the objectives, three different models were used, namely a model based on an elastic analysis to simulate the load tests, a plastic-based (limit analysis) model to assess the ultimate load capacity and a model based on nonlinear analysis (micro modeling) to catch the load dependency of the structural behavior of the bridge passing from linear behavior to cracking until collapse is achieved and to assess strengthening.

4 A macro-modeling approach for FRP-Strengthened masonry structures

4.1 Introduction

The possibility of using struts and tie models to assess the ultimate response of plain masonry walls or buildings has not received much attention in the scientific community despite the fact that this approach is accepted by modern concrete codes and often used for practical design and strength assessment in this field. However this approach is not completely unexplored: Ganz and Thurlimann 1983 and Roca 2006 more recently, have proposed approaches based on this methodology to assess the ultimate capacity of masonry shear walls and facades. This chapter presents a description about the possibility of using strut and tie schemes to determine the stiffness matrix of a finite element oriented to the analysis of ancient masonry buildings subjected to a combination of vertical and horizontal forces. The ability of the proposed approach to estimate the ultimate capacity of masonry walls has been analyzed by comparing its predictions with the experimental results available in literature and their micro-modeling interpretation, according to the procedures described in chapter 3.

4.2 Implementation of the model: Monotonic formulation

The monotonic MultiFan element was originally developed by Braga and Liberatore 1990$_{a,b}$. Each masonry panel in the structure can be accurately modeled by a single element. Panel here is taken to represent a rectangular part of the wall with free lateral edges. It is assumed that the stress field of the panel follows a MultiFan pattern, see Fig. 4.1. In addition, it is assumed that: the upper and lower faces of the panel are rigid, and there is no interaction in the circumferential direction between the infinitesimal fans.

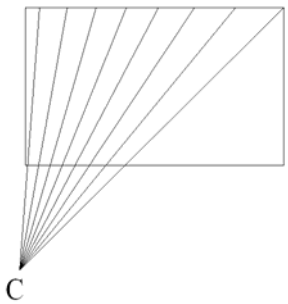

Fig. 4.1 Fan stress field

The unknowns about the element are the displacements of the first and second cross-section denoted by u_1, v_1, $Ø_1$ and u_2, v_2 and $Ø_2$, see Fig. 4.2, associated with the internal forces: axial force N_i, shear force T_i and bending moment M_i, with i = 1,2.

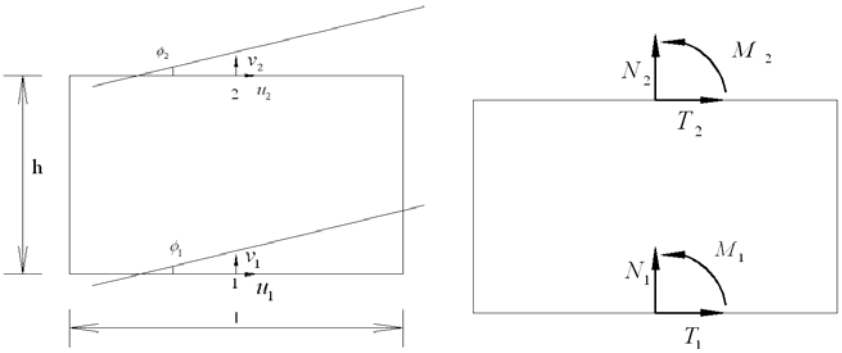

Fig. 4.2 Unknown displacements and forces

4.2.1 Equilibrium equations

The equilibrium equations can be formulated in a system of polar coordinates r, θ whose origin C is the vertex of the stress fan, see Fig. 4.3

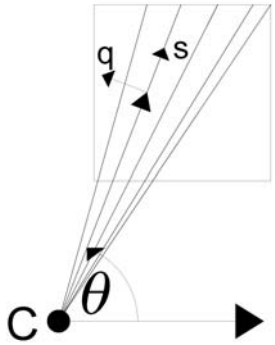

Fig. 4.3 System of polar coordinates

In the case that no forces are applied to internal points of the panel, the equilibrium equations read:

$$\begin{aligned} &\sigma_{r,r} + \frac{1}{r}\left(\sigma_r - \sigma_\theta + \tau_{r\theta,\theta}\right) = 0 \\ &\tau_{r\theta,r} + \frac{1}{r}\left(\sigma_{\theta,\theta} + 2\tau_{r\theta}\right) = 0 \end{aligned} \tag{4.1}$$

where the comma denotes partial derivative with respect to subsequent variable and $\sigma_r, \sigma_\theta, \tau_{r\theta}$ identify respectively the radial stress, the circumferential stress, and the shear stress. The assumption that no circumferential interaction exist between infinitesimal fans leads to zero circumferential and shear stresses reading:

$$\sigma_\theta = 0 \qquad (4.2)$$
$$\tau_{r\theta} = 0$$

Consequently the second equilibrium equation is trivially satisfied while the first simplifies to:

$$\sigma_{r,r} + \frac{1}{r}\sigma_r = 0 \qquad (4.3)$$

4.2.2 Constitutive relationships

Again the constitutive equations can be formulated in a system of polar coordinates r, θ whose origin C is the vertex of the stress fan. The basic assumption of this study is that the material behavior is linear elastic in compression and no tension. Therefore, the general expression of the constitutive relationships for a radial compression stress field simplify to:

$$\begin{aligned} &\varepsilon_r = \frac{1}{E}\left[\sigma_r - \mu\sigma_\theta\right] \\ &\varepsilon_\theta = \frac{1}{E}\left[\sigma_\theta - \mu\sigma_r\right] \quad \textbf{if} \quad \sigma_\theta = 0 \longrightarrow \\ &\gamma_{r\theta} = \frac{1}{G}\tau_{r\theta} = \frac{2(1+\mu)}{E}\tau_{r\theta} \end{aligned} \quad \begin{aligned} &\varepsilon_r = \frac{1}{E}\sigma_r \\ &\varepsilon_\theta \geq \frac{1}{E}(-\mu\sigma_r) \end{aligned} \qquad (4.4)$$

where, the first equation holds only for the fans under compression and fans in tension are eliminated. The second equation is the cracking condition.

4.2.3 Kinematic equations

The expression of the kinematic equations is very simple and reads:

$$\begin{aligned} &\varepsilon_r = s_{,r} \\ &\varepsilon_\theta = \frac{1}{r}\left(s + q_{,\theta}\right) \\ &\gamma_{r\theta} = q_{,r} + \frac{1}{r}\left(s_{,\theta} - q\right) \end{aligned} \qquad (4.5)$$

where s and q represent respectively the radial and circumferential component of the displacement field.

4.2.4 Forces and total complementary energy

After solving the differential equations introduced above and applying the boundary conditions, the generalized forces acting at the end cross-sections have the expressions:

$$N_K = t\int_{\theta_1}^{\theta_2} f_{rk} r_k \left|\sin\theta\right| d\theta$$

$$T_K = t\int_{\theta_1}^{\theta_2} f_{rk} r_k \cos\theta \cdot sign(\sin\theta) d\theta \tag{4.6}$$

$$M_K = t\int_{\theta_1}^{\theta_2} f_{rk} r_k x_k \cdot \left|\sin\theta\right| d\theta$$

where f_{r1} and f_{r2} are the radial components of the tractions at the end cross section and r_1, r_2 and θ_1, θ_2 identify the fan position.

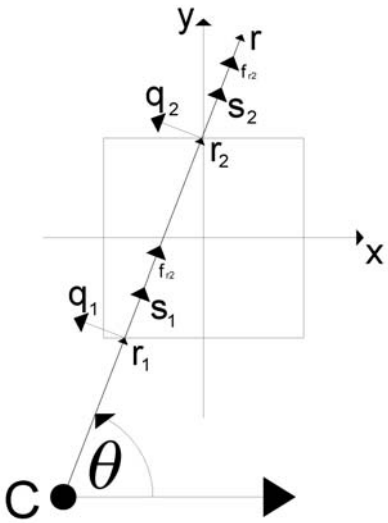

Fig. 4.4a System of Cartesian coordinates

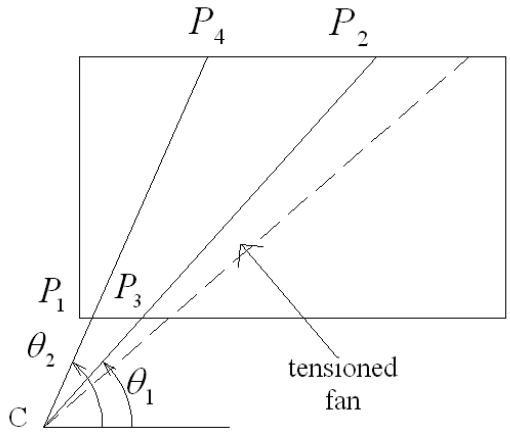

Fig. 4.4b System of Polar coordinates

The Total Complementary Energy (TCE) for a prescribed displacements at the end cross-sections is:

$$TCE = \frac{1}{2} t\int_{\theta_1}^{\theta_2}\int_{r_1}^{r_2} \frac{\sigma_r^2}{E} r \cdot dr d\theta - t\int_{\theta_1}^{\theta_2} \left(f_{r1} s_1 r_1 + f_{r2} s_2 r_2 \right) d\theta = -\frac{1}{2} t\int_{\theta_1}^{\theta_2} E r_0 (s_1 - s_2) d\theta \tag{4.7}$$

The values of the forces N_k, T_k, M_k and of the energy TCE are a function of the coordinates of the fan vertex. Therefore, their position can be obtained minimizing the TCE expression and the abscissas of the points of intersection P1, P2, P3, P4 of the lateral edge of the fan with the end cross sections of the panel, see Fig. 4.4.

It is observed here that the displacement field that minimizes the TCE is also a field that satisfies the kinematic equations.

This formulation is based on the hypothesis that the radial stresses converge to a single point (the panel resists by mean of only one strut inside the total length). If this assumption is removed, the equations described above are still working but the final minimization procedure will result a function of the abscissas of the $2(n_f + 1)$ points of intersection of the lateral edges of the elementary fans with the end cross sections of the panel. This element is called MultiFan according Braga and Liberatore 1996. n_f represents the number of fan used to describe the stress pattern within one element due to vertical and horizontal forces acting.

4.2.5 Parametric study

In the previous sections it is described the general formulation of the MultiFan element according previous studies of Braga and Dolce 1982 and Braga and Liberatore 1990_a. The major drawback of this procedure is the difficulty to obtain the stiffness matrix of the element in a reasonable computational time since it can be determined only using the Castigliano theorem deriving the force vector with respect to the displacement vector. These vectors are determined minimizing the total complementary energy (TCE) as described previously. Therefore it is very useful to obtain a closed form expression for the total energy, force vector and stiffness matrix of a masonry panel under vertical and horizontal forces that can account for shear, compression and flexural failure. The starting point for this achievement is the previous formulation of the MultiFan element and a parametric study allows determining a function of the slenderness and the deformation field within the panel able to approximate the energy function. Determining the analytical expression of the energy allows deriving directly the force vector and the stiffness matrix of the panel simplifying the description of his behavior and the implementation in a nonlinear finite element framework based on the displacement method as Opensees. This is also possible because the final expression of TCE is a function of the displacement vectors meaning that is a function of the displacement and rotations of the upper and bottom faces of the panel. The starting point is the displacement vector of the panel:

$$u = (u_1, v_1, \varphi_1, u_2, v_2, \varphi_2)^T \tag{4.8}$$

This vector can be determined by combination of three rigid displacements:

$$\begin{aligned} u &= (u_1 + u_2)/2 \\ v &= (v_1 + v_2)/2 \\ \varphi &= (\varphi_1 + \varphi_2)/2 \end{aligned} \tag{4.9}$$

and three deformation

$$\begin{aligned} \Delta u &= (u_2 - u_1) + \varphi\, h \\ \Delta v &= (v_2 - v_1) \\ \Delta \varphi &= (\varphi_2 - \varphi_1) \end{aligned} \tag{4.10}$$

To describe the force vector, stiffness matrix and energy of the panel the important terms are the ones that allow defining the strain vector:

$$\begin{aligned} \varepsilon_1 &= \Delta u / L \\ \varepsilon_2 &= \Delta v / L \\ \varepsilon_3 &= \Delta \varphi \end{aligned} \tag{4.11}$$

To the aim of the implementation, the deformation can be expressed in polar coordinates. The transformation equations to move from a Cartesian to a spherical coordinate system read as:

$$\begin{aligned} \rho &= \sqrt{\varepsilon_1^2 + \varepsilon_2^2 + \varepsilon_3^2} \\ \xi &= \arctan 2(\varepsilon_3, \varepsilon_1) \\ \eta &= \arcsin \frac{\varepsilon_2}{\sqrt{\varepsilon_1^2 + \varepsilon_2^2 + \varepsilon_3^2}} \end{aligned} \tag{4.12}$$

or the inverse:

$$\begin{aligned} \varepsilon_1 &= \rho \cos\eta \cos\xi \\ \varepsilon_2 &= \rho \sin\eta \\ \varepsilon_3 &= \rho \cos\eta \sin\xi \end{aligned} \tag{4.13}$$

Performing a parametric analysis in the polar coordinate system: the elastic potential energy of a panel can be expressed as the product of the slenderness μ , the thickness t, the elastic modulus E, the base and the self weight ρ of the panel multiplied for a function that define the behavior of the panel (moving from the elastic stage until the failure)

$$V = \mu \, \Pi_1 \tag{4.14}$$

$$\Pi = \frac{Etl^2}{\mu} \rho^2 \, V \tag{4.15}$$

$$V = \begin{cases} \frac{1}{48}(13 - 11\cos 2\chi) & \left(\chi \le -\arctan\frac{1}{2}\right) & -\textit{ Panel reacting totally} \\ \frac{1}{6\cos\chi}\left(\frac{1}{2}\cos\chi - \sin\chi\right)^3 & \left(-\arctan\frac{1}{2} < \chi < \arctan\frac{1}{2}\right) & -\textit{ Panel reacting partially} \\ 0 & \left(\chi \ge \arctan\frac{1}{2}\right) & -\textit{ Panel not reacting} \end{cases} \tag{4.16}$$

The force vector of the panel can now be determined as the derivative of the elastic potential energy versus the displacement vector according the general expression:

$$f = (T_1, N_1, M_1, T_2, N_2, M_2)^T \tag{4.17}$$

$$f_k = \frac{\partial \Pi}{\partial u_k} = \frac{\partial \Pi}{\partial \varepsilon_i} \frac{\partial \varepsilon_i}{\partial u_k} \qquad (i = 1, 2, 3 \,; \quad k = 1, \ldots\ldots, 6) \tag{4.18}$$

while, the tangent stiffness matrix of the panel can be determined as the derivative of the force vector versus the displacement vector according the general expression:

$$s_{hk} = \frac{\partial f_h}{\partial u_k} = \frac{\partial^2 \Pi}{\partial \varepsilon_i} \frac{\partial \varepsilon_i}{\partial u_k} \qquad (i = 1, 2, 3 \,; \quad k = 1, \ldots\ldots, 6) \tag{4.19}$$

According to this formulation the macro finite element is implemented in the finite element open source program Opensees. To allow a better understanding and check of the MultiFan behavior, a Matlab implementation is also developed and provided in appendix 2 as a standalone routine.

4.2.6 Improved monotonic formulation

After the monotonic version of the model is developed and validated, changes in the monotonic formulation are introduced to avoid drawback due to the assumption of elastic behavior in compression of the panel. This assumption leads in fact to results in terms of ductility (that is total drift before collapse) not reliable since the existing model could not represent failure due to compression. This problem can be easily solved introducing further failure modes of the panel according the Italian Standard. A schematic of the model implied by NTC2008 and Circ. 2009 for the 3D analysis of perforated URM walls is shown in Fig. 4.5.

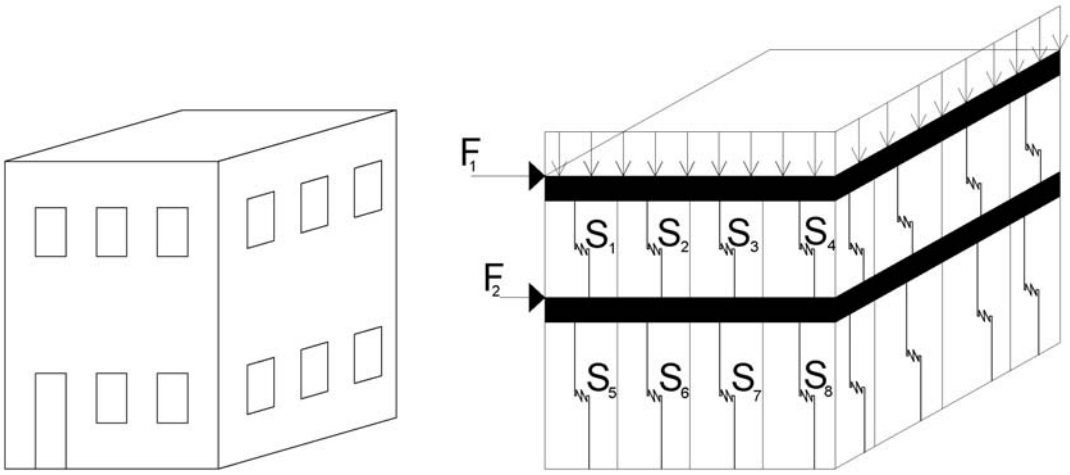

Fig. 4.5 Spring model for masonry buildings

As clear from Fig. 4.5, the model employs springs to capture the response of individual piers. The properties and constitutive laws of these springs are based largely on past component tests and are dependent on the gravity loads and dimensions of each pier, see Fig. 4.6. In addition, the spandrels of URM walls can be considered as further element of the structural model or simply to affect only the boundary conditions of the in-plane piers (i.e. fixed-fixed or cantilever). This is in particular allowed when buildings in historical centers are investigated if the assumption of good connection between orthogonal walls can be accepted, Circ. 2009. In this case, to calculate the story response of a wall, the displacements of each pier spring (within a story) are assumed to be equal at each step and the resistances of these springs are added together (i.e. springs in parallel). The response of the entire building is then determined by combining the responses of each story as springs in series. This approach is well known as POR approach since it was introduced from Tomazevic 1978 or PORFLEX when also bending failure is considered.

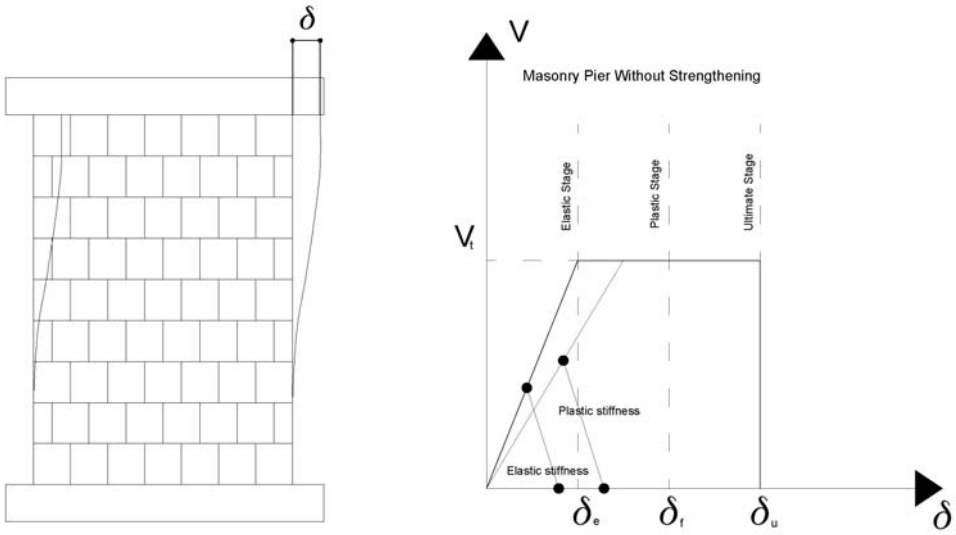

Fig. 4.6 Schematic of the constitutive law presented in NTC2008 for the analysis of URM walls

Such models can be used in conjunction with both the linear static method and nonlinear static (i.e. pushover) method of evaluation. In the case of the linear static method, each spring stiffness is taken as the elastic stiffness of the corresponding pier, see eq. 4.20 and Fig. 4.7.

$$K = \frac{GA}{1.2h}\frac{1}{1+\frac{1}{1.2}\frac{G}{E}\left(\frac{h}{b}\right)^2} \tag{4.20}$$

where it is:

$K = Elastic\ Stiffness\ of\ \ pier$
$G = Shear\ \mathrm{mod}ulus\ of\ \ masonry$
$E = Elastic\ \mathrm{mod}ulus\ of\ \ masonry$
$A_n = Cross\ \mathrm{sec}tion\ area\ of\ \ the\ \ pier$
$H = Height\ of\ \ the\ \ pier$
$b_m = Width\ of\ \ the\ \ pier$

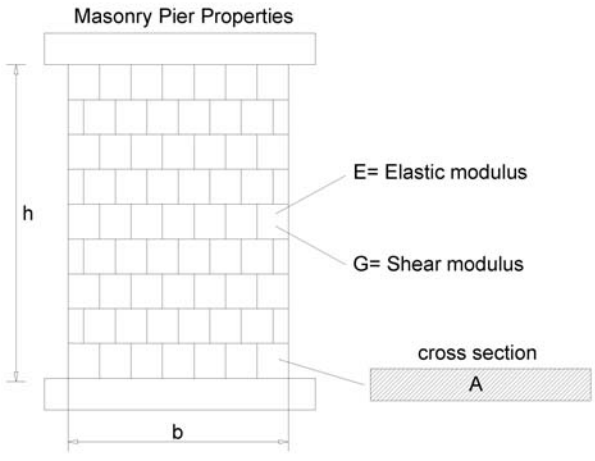

Fig. 4.7 Scheme of the masonry pier properties

In the case of the nonlinear static method, each possible failure mode according NTC 2008, namely: shear due to diagonal traction, shear due to bed joint sliding and rocking/toe

crushing has to be included in the constitutive law of the pier and the spandrel.

The updated MultiFan Element moves from similar considerations, but the behavior in the elastic stage is defined by the different fans distribution in the panel, while springs are required to add failure mechanisms in the constitutive law. The element still has four nodes where each node has two degrees of freedom because the node displacements of the springs are reduced using condensation techniques so if the nodes of the global MultiFan Element are nodes 1, 2, 3, 4, and the nodes of the sub-structure are nodes 5, 6, 7, 8 where each node has three degrees of freedom, the static condensation is done to get the stiffness matrix of the system as a function of only the nodes 1,2,3,4, see Fig. 4.8.

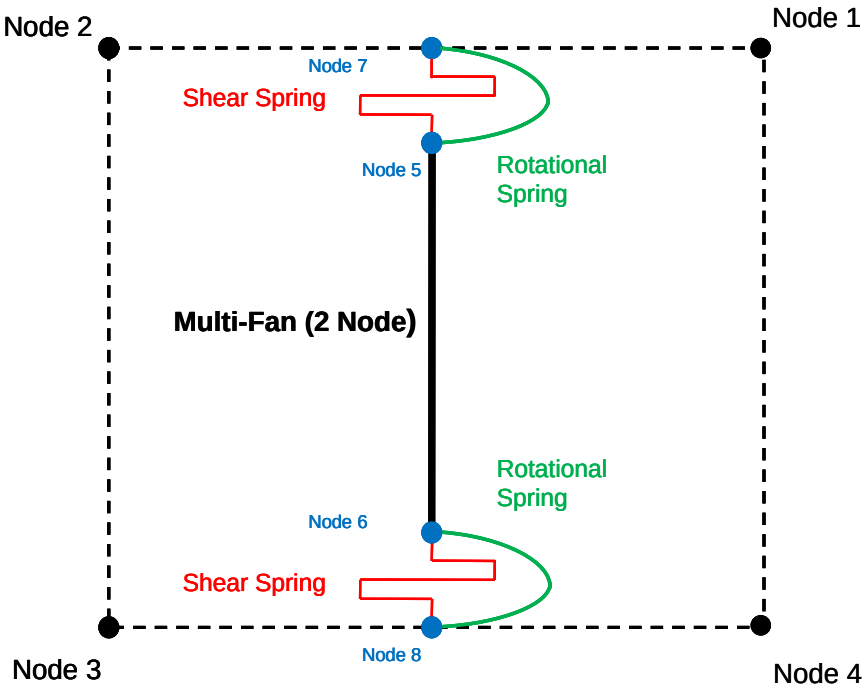

Fig. 4.8. Cyclic MultiFan element

The static condensation method is used to obtain the total stiffness matrix of the MultiFan element system and its application is very similar to application of boundary conditions to the resulting linear algebraic equations system obtained with the finite element discretization.

The condensation method results in fixing some values of unknown terms in the nodal displacement vector. The system of equations resulting from the static analysis for the MultiFan system is divided in two parts, the first contains the degrees of freedom

having the external displacement or force applied, and the second denotes the inner degree of freedom. This leads to:

$$\begin{Bmatrix} F \\ R \end{Bmatrix} = \begin{bmatrix} K_{11} & K_{12} \\ K_{12}^T & K_{22} \end{bmatrix} \begin{Bmatrix} v \\ x \end{Bmatrix} \tag{4.21}$$

where:

$\{F\}$ = Loads (Known forces) $\{v\}$= Outer degrees of freedom

$\{R\}$ = Zero $\{x\}$= Inner degrees of freedom

The previous formulation in matrix notation gives two partial equations:

$$(a) \quad \{F\} = [K_{11}]\{v\} + [K_{12}]\{x\} \tag{4.22}$$

$$(b) \quad \{R\} = [K_{12}^T]\{v\} + [K_{22}]\{x\} = 0$$

The second provides a static relationship between x and v:

$$x = -(k_{22})^{-1} k_{12}\, v \tag{4.23}$$

This leads to

$$k_{tt} v = F \tag{4.24}$$

where

$$k_{tt} = k_{11} - (k_{12})^T (k_{22})^{-1} (k_{12}) \tag{4.25}$$

is the total stiffness matrix of the MultiFan system

The updated MultiFan Element includes a zero-length (ZLH) spring in shear and in bending. According the general formulation of the plasticity theory discussed in chapter 2, the working process of the new MultiFan element can be described in few steps: first, check the yielding functions and conditions for each possible failure mode, if the ZLH Spring is in the elastic loading state, then the stiffness of the Zero-length spring has a value much bigger than the MultiFan element, so it act as a rigid bar and all the deformation happens only in the MultiFan element that will define the elastic part of the curve. If the ZLH Spring is in the yielding state, the stiffness of the Zero-length Spring assumes a very small value and will control the yielding displacement while the MultiFan element will not deform anymore. To better illustrate how the Zero-Length spring works, the MultiFan element system is simplified as in Fig. 4.9:

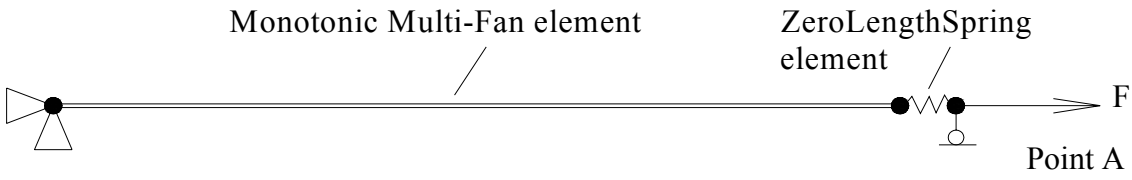

Fig. 4.9 Structural scheme of the coupled behaviour: ZLH spring and MultiFan element

It is a series system composed of the MF element and the ZLH. To model the spring mathematical behavior, classical rate-dependent plasticity can be used. The mechanical response of the one-dimensional frictional device illustrated in Fig. 4.10 can be expressed according local governing equations in chapter 3:

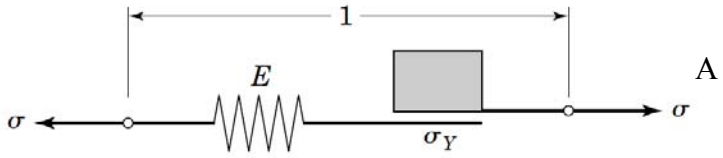

Fig. 4.10 The zero length spring model: elastic part and friction part

The elastic stress-strain relationship for the global MultiFan element is given by:

$$\sigma = D_{MultiFan}\left(\varepsilon - \varepsilon^{p}\right) \tag{4.26}$$

Where:

$$D_{MultiFan} = \frac{K_{Multifan} K_{spring}}{K_{Multifan} + K_{spring}} \tag{4.27}$$

and $K_{Multifan}$ is the stiffness of the MultiFan element and K_{spring} the stiffness of the Zero-length spring.

Flow rule and isotropic hardening law is written as:

$$\dot{\varepsilon}^{p} = \lambda \operatorname{sign}(\sigma) \qquad \dot{\kappa} = \dot{\lambda} \tag{4.28}$$

Yield condition is expressed in the form:

$$f(\sigma,\kappa) = |\sigma| - (\sigma_{Y} + h\,\kappa) \le 0 \tag{4.29}$$

Kuhn–Tucker complementarity conditions are:

$$\lambda \ge 0,\ f(\sigma,\kappa) \le 0,\ \lambda f(\sigma,\kappa) = 0 \tag{4.30}$$

Consistency condition is formulated as:

$$\lambda \dot{f}(\sigma,\kappa) = 0 \left(if \quad f(\sigma,\kappa) = 0 \right) \tag{4.31}$$

The horizontal displacement of point A is first due to the elongation of the MultiFan element, and second due to the deformation of the ZLH spring. The total displacement is therefore obtained adding the nonlinear elastic reversible part due to the MultiFan element to the plastic, irreversible part due to the ZLH spring:

$$\varepsilon = \varepsilon_e + \varepsilon_p \tag{4.32}$$

Moreover, the dependence of the stress vector with the elastic strain vector ε_e can be expressed as:

$$\sigma = D_{Multifan}\ \varepsilon_e \tag{4.33}$$

with $D_{MultiFan}$ the stiffness matrix of the global MultiFan element defined according the formulation in the precedent paragraph.

Combining eqs. 4.32 and 4.33 results in:

$$\sigma = D_{MultiFan} \left(\varepsilon - \varepsilon_p \right) \tag{4.34}$$

where the remaining part of the strain ε_p due to the ZLH is permanent, or plastic, and can be obtained by subtracting the MultiFan contribution from the total strain.

Moreover, the plastic strain vector is written as the product of a scalar $\dot{\lambda}$ defined as the plastic multiplier and a vector m (flow rule):

$$\dot{\varepsilon}_p = \dot{\lambda} m \tag{4.35}$$

The definition of the plastic flow direction *m* is assessed with the Drucker assumption that mathematically, it states that:

$$\dot{\sigma}^T \dot{\varepsilon}_p = 0 \tag{4.36}$$

Loading/unloading can be conveniently established in standard Kuhn-Tucker form by means of the conditions:

$$\dot{\lambda}_i \geq 0 \quad f_i \leq 0 \quad \dot{\lambda}_i f_i = 0 \tag{4.37}$$

where $\dot{\lambda}_i$ is the plastic multiplier rate.

In this case, the yield function is also dependent on a scalar measure of the plastic strain tensor:

$$f(\sigma,\kappa) = |\sigma| - (\sigma_Y + h\,\kappa) \le 0 \tag{4.38}$$

where the yield stress value is a function (hardening law) of the scalar κ, which is introduced as a measure for the amount of hardening or softening in the ZLH spring, therefore the Prager consistency condition in absence of hardening:

$$n^T \dot{\sigma} = 0 \tag{4.39}$$

where *n* is the gradient vector of the yield function:

$$n = \frac{\partial f}{\partial \sigma} \tag{4.40}$$

now in presence of hardening it gives:

$$f = 0 \text{ and } \dot{f} = \frac{\partial f(\sigma)}{\partial \sigma}\dot{\sigma} = n^T \dot{\sigma} = 0$$

and this yields

$$\dot{f} = \frac{\partial f(\sigma)}{\partial \sigma}\dot{\sigma} + \frac{\partial f(\kappa)}{\partial \kappa}\dot{\kappa} = n^T \dot{\sigma} - h\,\dot{\lambda} = 0 \tag{4.41}$$

With the position

$$n^T = \frac{\partial f(\sigma)}{\partial \sigma} \tag{4.42}$$

$$h = -\frac{\partial f(\kappa)}{\partial \kappa}\dot{\kappa}\left(\frac{1}{\dot{\lambda}}\right) \tag{4.43}$$

this leads to:

$$\dot{\lambda} = \frac{n^T \dot{\sigma}}{h} \tag{4.44}$$

with *h* the hardening modulus. If now we combine the time derivative of eq. 4.34, the flow rule eq. 4.35 with the consistency condition for hardening/softening plasticity eq. 4.41, this results in the following stress-strain relation:

$$\dot{\sigma} + \frac{D_{MultiFan}\, n^T \dot{\sigma}}{h} m = D_{MultiFan}\,\dot{\varepsilon} \tag{4.45}$$

That after mathematical manipulation it reads

$$\dot{\sigma}\left(\frac{1}{D_{MultiFan}}+\frac{n^T}{h}m\right)=\dot{\varepsilon} \tag{4.46}$$

And finally, it provides the relation between the stress rate and the strain rate

$$\dot{\sigma}=\left[D_{MultiFan}-\frac{D_{MultiFan}\,m\,n^T D_{MultiFan}}{h+n^T D_{MultiFan}\,m}\right]\dot{\varepsilon} \tag{4.47}$$

and the expression of the stiffness matrix:

$$\mathbf{D}^{ep}=\left.\frac{d\sigma_{n+1}}{d\varepsilon_{n+1}}\right|_{n+1}=\left[D_{MultiFan}-\frac{D_{MultiFan}\,m\,n^T D_{MultiFan}}{h+n^T D_{MultiFan}\,m}\right]; \tag{4.48}$$

The previous equation in pure uniaxial stressing condition reads:

$$\dot{\varepsilon}=\dot{\sigma}\left(\frac{1}{D_{MultiFan}}+\frac{1}{h}\right)\rightarrow\dot{\sigma}=\left(\frac{D_{MultiFan}\,h}{D_{MultiFan}+h}\right)\dot{\varepsilon} \tag{4.49}$$

Loading Branch

Loading happens when the following two conditions are met:

$$(\sigma-\sigma_{\max})\varepsilon>0 \tag{4.50}$$

$$f(\sigma,\kappa)=|\sigma|-(\sigma_Y+h\,\kappa)\le 0 \tag{4.51}$$

Take $\varepsilon>0$ as an example. From eq. 4.50, the current stress is bigger than the maximum stress recorded in the history, and from eq. 4.51 the current stress is smaller than the yield stress, so the system can only be in the loading branch. In the FEM program, a purely elastic trial step is defined by:

$$\begin{cases}\sigma_{n+1}^{trial}=\sigma_n+D_e\Delta\varepsilon_n^p\\ \Delta\varepsilon_{n+1}^{trial}=\Delta\varepsilon_n^p\\ \Delta\kappa_{n+1}^{trial}=\Delta\kappa_n\\ f_{n+1}^{trial}=\left|\sigma_{n+1}^{trial}\right|-(\sigma_Y+h\,\kappa_n)\end{cases} \tag{4.52}$$

If $f_{n+1}^{trial}\le 0$, then the trial state is admissible and there is an instantaneous elastic process, as a result:

$$\begin{cases} \varepsilon_{n+1}^{p} = \varepsilon_{n}^{p} \\ \kappa_{n+1} = \kappa_{n} \\ \sigma_{n+1} = \sigma_{n+1}^{trial} \end{cases} \tag{4.53}$$

The above solution satisfies the stress-strain relationship, the flow rule, the hardening law and the Kuhn-Tucker conditions, because $f_{n+1} = f_{n+1}^{trial} \le 0$ and $\Delta\lambda = 0$ are consistent with the Kuhn-Tucker conditions in incremental form. So this solution is unique and the trial state is the solution to the problem, see Fig. 4.11.

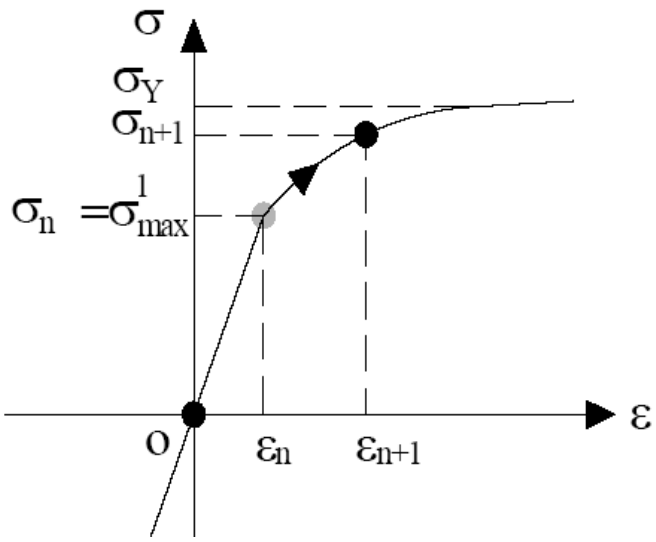

Fig. 4.11 Loading Branch of the cyclic MultiFan element

In the loading branch, the stiffness of the Zero-length Spring takes a much higher value than the MultiFan element, so the Zero-length Spring acts as a rigid bar and almost all the deformation happens only in the MultiFan element. In this series system, the total stiffness is obtained as

$$K_{Multifan} \ll K_{spring} \rightarrow D_{multifan} = \frac{K_{Multifan} K_{spring}}{K_{Multifan} + K_{spring}} \approx K_{Multifan} \tag{4.54}$$

which means in the loading branch, the behavior of the system is basically identical to the monotonic MultiFan element.

Yielding Branch

Yielding happens when the yielding function is equal to zero:

$$f(\sigma, \kappa) = |\sigma| - (\sigma_Y + h\,\kappa) = 0 \tag{4.55}$$

The trial state in the incremental form is calculated as:

$$f_{n+1}^{trial} = \left|\sigma_{n+1}^{trial}\right| - \left(\sigma_Y + h\,\kappa_n\right) > 0 \tag{4.56}$$

which is not allowed so only the following equations can be satisfied:

$$f(\sigma_{n+1}, \kappa_{n+1}) = 0 \tag{4.57}$$
$$\Delta\lambda > 0$$

Therefore the trial state is not equal to the actual state and the return mapping algorithm is performed, which is given by:

$$\Delta\lambda_{n+1} = \frac{f_{n+1}^{trial}}{D_e + h}$$

$$\begin{cases} \sigma_{n+1} = \sigma_{n+1}^{trial} - D_e \Delta\varepsilon_{n+1}^{p} \\ \varepsilon_{n+1}^{p} = \varepsilon_n^{p} + \Delta\lambda_{n+1} \\ \Delta\kappa_{n+1} = \Delta\kappa_n + \Delta\lambda_{n+1} \end{cases} \tag{4.58}$$

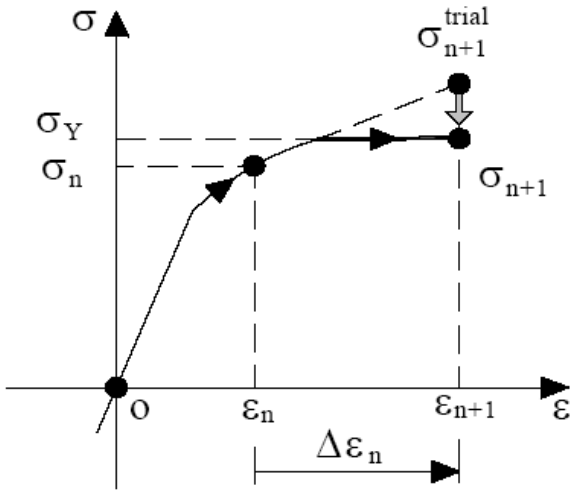

Fig. 4.12 Yielding branch of the cyclic MultiFan element

In the Yielding branch, the stiffness of the Zero-length Spring takes a very small value, and its resisting force goes into the plastic part, see Fig. 4.12. Therefore a large deformation under a small load increment is obtained while the MultiFan element will not deform in this state:

$$K_{Multifan} \gg K_{spring} \rightarrow D_{multifan} = \frac{K_{Multifan} K_{spring}}{K_{Multifan} + K_{spring}} \approx K_{spring} \tag{4.59}$$

meaning that all the deformation is happening in the Zero-length spring, that controls the plastic deformation of the system. The yielding value σ_Y takes into account the major failure modes, which leads:

$$\begin{aligned} &\sigma_Y = V_{bjs} && \text{for bed joint sliding} \\ &\sigma_Y = V_{dt} && \text{for diagonal cracking} \\ &\sigma_Y = V_r = \frac{2M_u}{H} && \text{for rocking / toe crushing} \end{aligned} \tag{4.60}$$

where using the NTC2008 formulation, the new failures modes are introduced according these formulas:

For bed joint sliding

$$V_{bjs} = (\tau_{0d} + \tan\phi \frac{P}{A_n})\ b_m\ t_m \tag{4.61}$$

for diagonal cracking

$$V_{dt} = \tau_d\ \ b_m\ t_m \tag{4.62}$$

for rocking / toe crushing

$$V_r = \frac{2M_u}{H} \tag{4.63}$$

$$M_u = \left(b_m^2\ t_m\ \frac{P}{A_n}\ \frac{1}{2} \right) \left(1 - \frac{P}{A_n} \frac{1}{0{,}85\, f_m^c} \right) \tag{4.64}$$

where:

$$\tau_d = \frac{1.5\tau_{0d}}{b_m / H} \sqrt{1 + \frac{\sigma_0}{1.5\ \tau_{0d}}} \tag{4.65}$$

H is the effective height of the pier, b_m is the width of the masonry pier, $\sigma_0 = \frac{P}{A_n}$

where P is the vertical compressive force above the pier and τ_d is the shear strength of the masonry and τ_{0d} is the shear strength of the masonry in absence of compression. Moreover: t_m is the thickness of the masonry pier, f_t^m is the tensile strength, f_c^m is the compressive strength of masonry and finally A_n is the net area of the pier.

4.3 Comparison between macro-modeling and micro–modeling results

The micro-modeling approach described in the previous chapter and employed to develop the analyses using a discrete element approach based on interface elements is used to assess the macro element results. In particular two cases studies were employed according to Lourenço 1996. The geometric configuration of the wall (with and without openings) and the load pattern is described in Fig. 4.13.

4.3.1 T.U Eindhoven shear walls – monotonic load

In this example, it is assessed the structural behavior of a masonry wall in shear. The assessment of this specimen has been published by Lourenço 1997 and is considered a good benchmark to validate the capabilities of the macro-modeling approach implemented in OpenSees. The shear walls have a width/height ratio of one with dimensions 990 × 1000 [mm^2], built up with 18 courses, from which 16 courses are active and 2 courses are clamped in steel beams, see Fig. 4.13. The walls are made of wire-cut solid clay bricks with dimensions 210 × 52 × 100 [mm^3] and 10 [mm] thick mortar, prepared with a volumetric cement:lime:sand ratio of 1: 2: 9. The material data are obtained from existent results on tension, compression and shear tests as reported in Lourenço 1996.

Different vertical precompression uniformly distributed forces *p* are applied to the walls, before a horizontal load is monotonically increased under top displacement control *d* in a confined way, i.e. keeping the bottom and top boundaries horizontal and precluding any vertical movement. To the aim of validate the macro-approach two walls are considered: the first without any opening and the second with a hole in the central part. Initial vertical loads *p* applied equals 0. 30 [N/mm^2] ≡ 30 [kN].

The strategy used in the micro modeling analysis is to represent separately the brick, the mortar joint and also the interface, in particular interface elements are created in the centre line of a brick to allow openings due to compression failure of the brick. For the numerical analyses units are represented by plane stress continuum elements (8-noded) while line interface elements (6-noded) adopted for the joints and for the potential vertical cracks in the middle of the unit. Each unit is modeled with 4 × 2 elements, see Fig. 4.14. For the joints and for the potential cracks in the units, the composite interface model presented in chapter 3 is adopted with exponential tensile and shear softening. The friction angle is assumed constant and equal to 0.75. The dilatancy angle is assumed to equal zero. Only eight and nine macro elements are considered using the MultiFan approach, see Fig. 4.15.

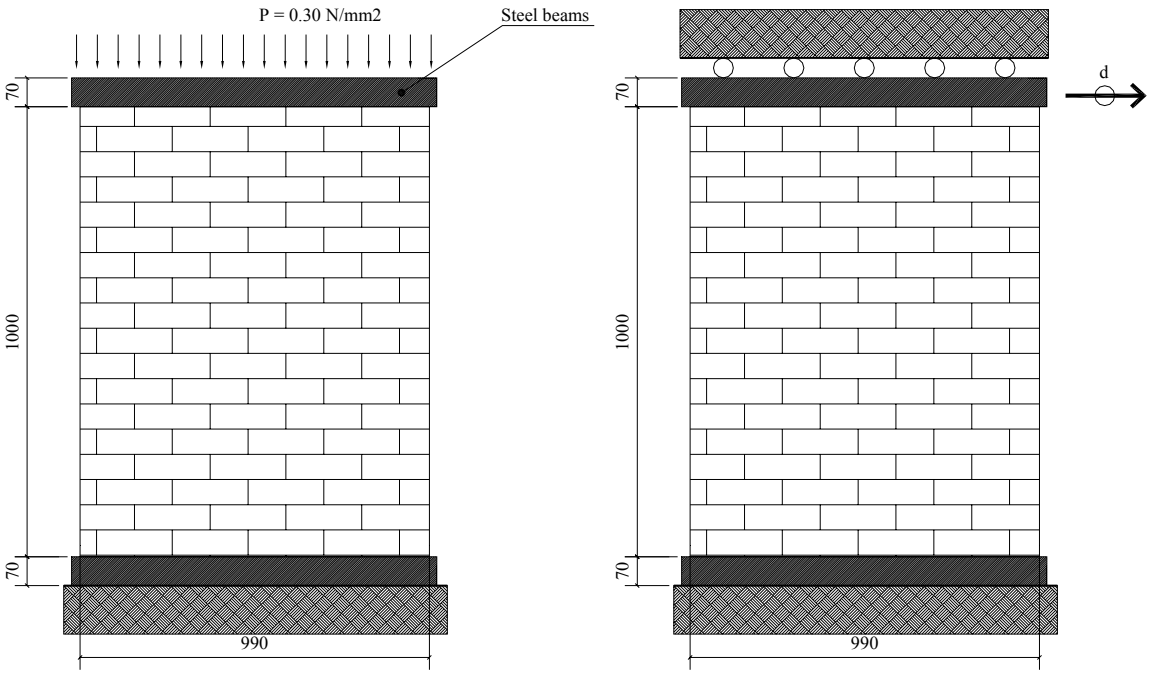

(a)

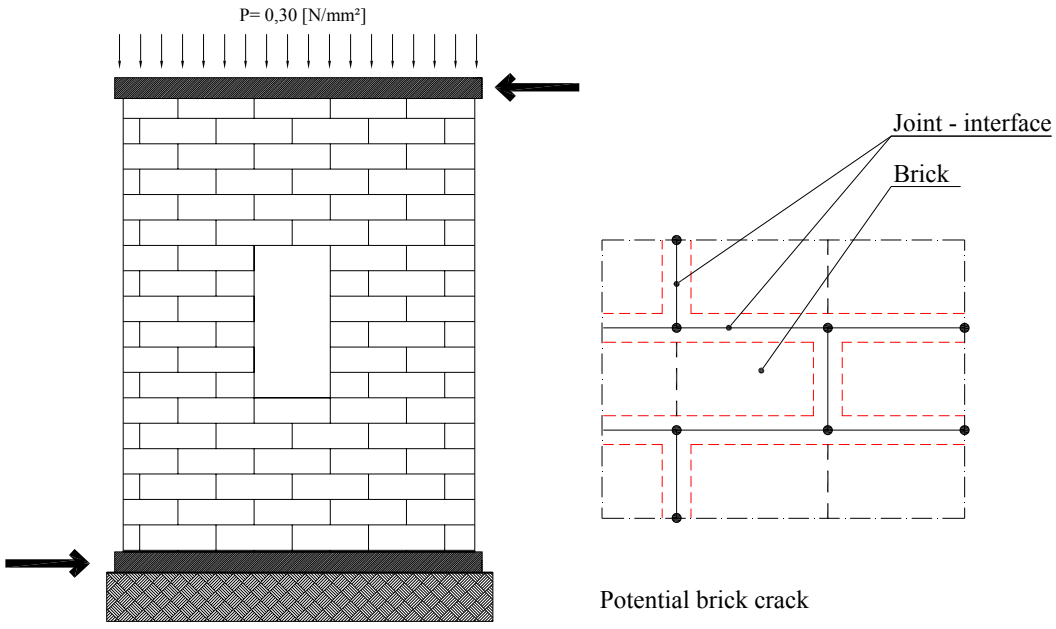

(b)

Fig. 4.13. Test setup, geometrical configuration and mesh strategy for: (a) solid wall; (b) wall with opening

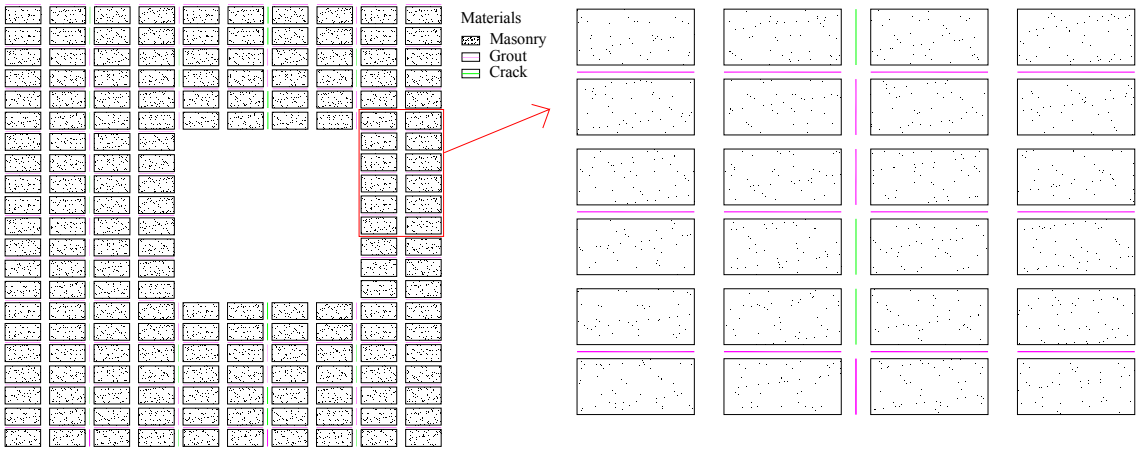

Fig. 4.14 Mesh strategy used in the finite element micro modeling approach

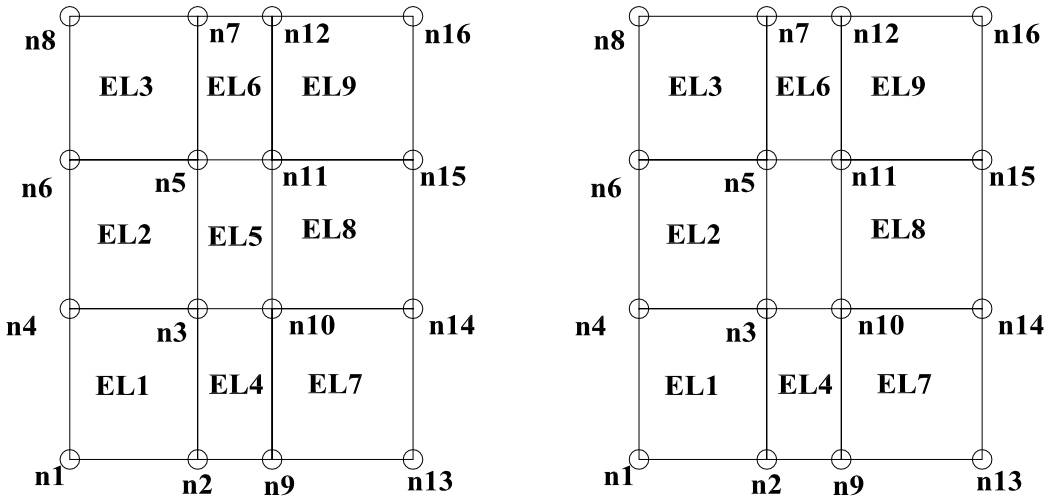

Fig. 4.15 Mesh configuration and number of elements used with the macro model

When micro modeling is used, the analyses are carried out with indirect displacement control, whereas the snap-backs and snap-through are traced with CMOD control over the most active interface. When macro modeling is used, the analyses are carried out with direct displacement control. In the following pictures, the results obtained with the different approaches are provided, see Fig. 4.16 and 4.17. It is clear that the micro modeling approach provides more accurate results (even if it requires a huge computational effort) in particular in terms of failure mechanism, see Fig. 4.18. At the same time the macro approach gives reasonable results and therefore can be used to assess the safety of big aggregates of masonry buildings.

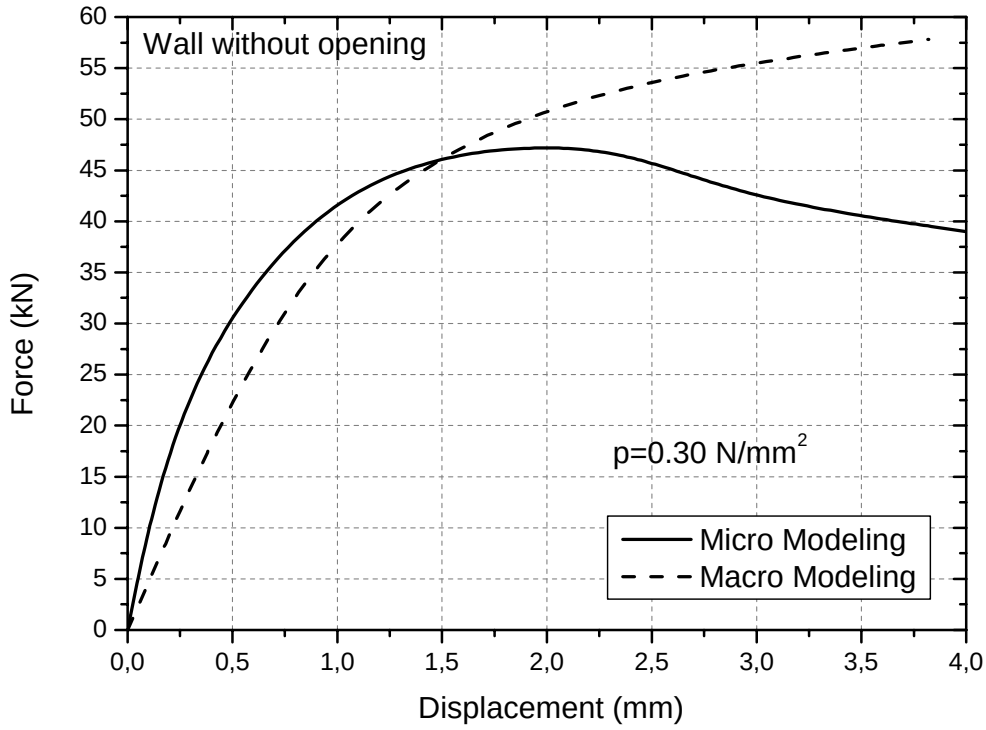

(a)

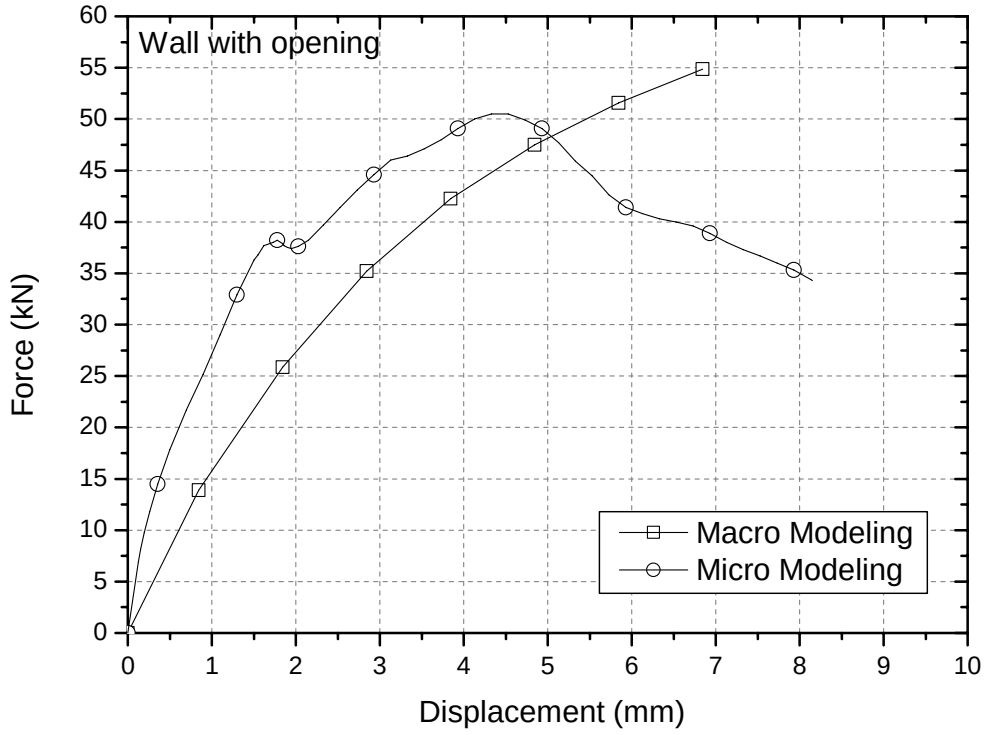

(b)

Fig. 4.16 Comparison of the results obtained with the micro modeling and macro modeling in terms of pushover curves: (a) solid wall; (b) wall with opening

In particular in the next two graphs, Fig. 4.17, the global behavior represented in Fig. 4.16 is analyzed considering the contribution of each element in the mesh. It is clear that the major contribution to the global strength is due to the shear strength in pier 7 at the bottom-right side of the walls. An important contribution is also due to pier 2 (at middle of the panel, left side) and pier 8 (middle of the panel, right side). Pier 1 (at the bottom of the panel, left side) is almost not taking shear force. The spandrel behavior (elements 4 and 6) is represented on the negative part of the graph but it is clear that these elements provide a low contribution to the total shear strength since they just provide a connection between the left and right side of the walls. Pier 5 at the center of the panel is present only in the solid wall and it is clear as in this case a fan can generate connecting piers 3 and 7 along the main diagonal of the panel, this results in the numerical analysis in higher values of the shear strength in element 7, while when an opening exist the stress and the fans move around the opening. Another difference is visible: the fan distribution in element 1 changes a little when the wall has an opening since the total shear value from positive becomes negative (even if in both cases almost zero) meaning that a rotation exist in the fan distribution within this pier.

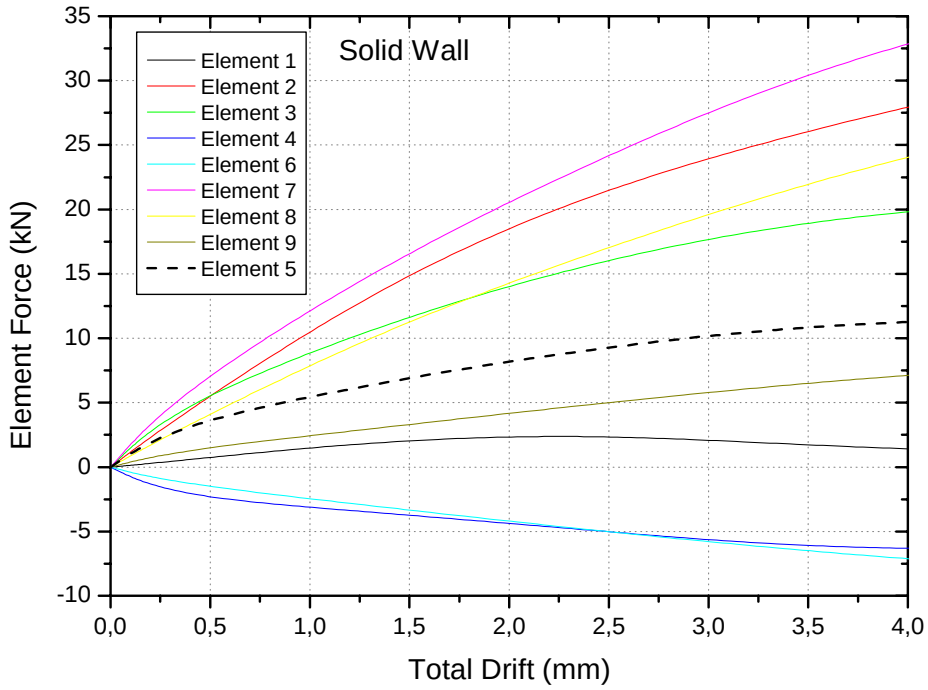

(a)

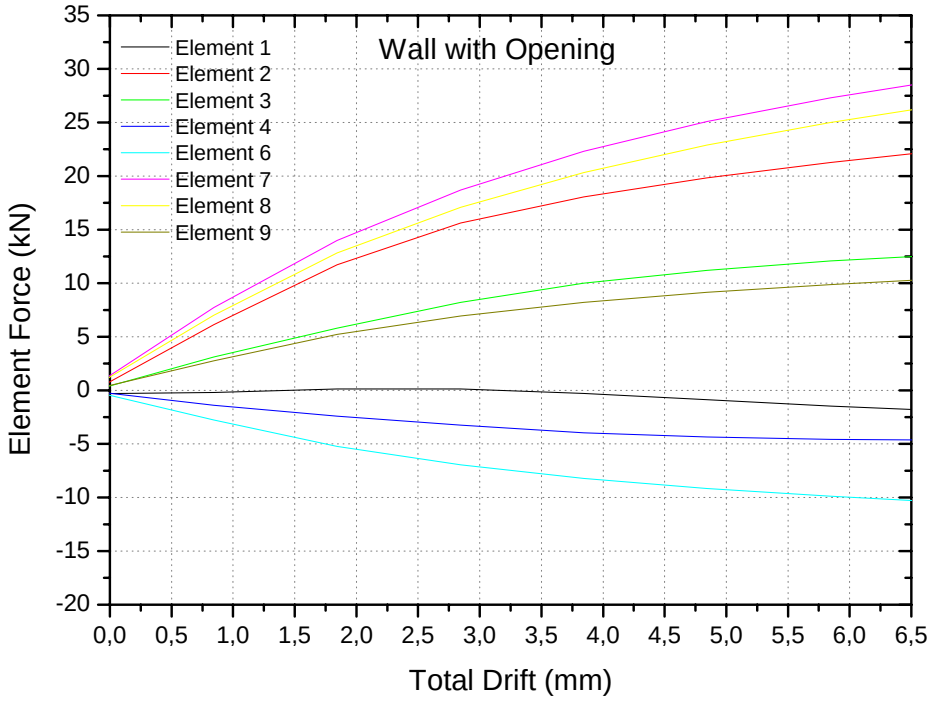

(b)

Fig. 4.17 Shear force distribution in each element versus the total drift at the top of the wall (MPa): (a) solid wall; (b) wall with opening

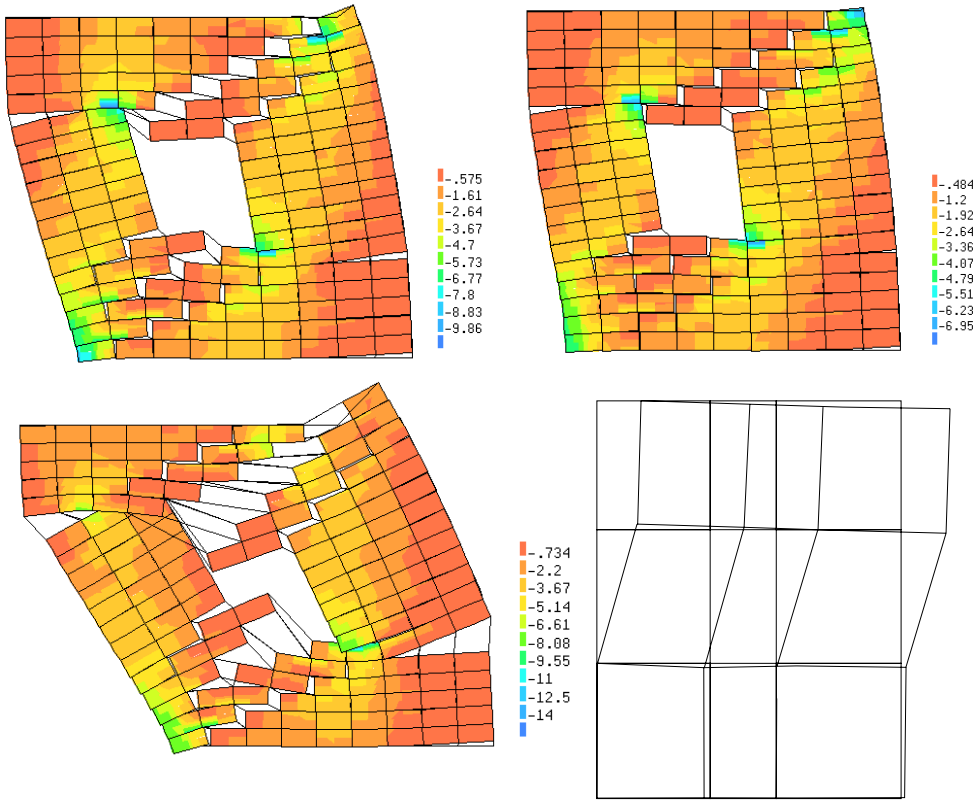

(a) (b)

Fig. 4.18 Failure mechanisms obtained using: (a) the micro modeling approach (MPa); (b) the macro modeling approach

4.3.2 Pavia prototype – monotonic load

The macro model developed and implemented is used also to simulate the experimental tests made in Pavia on a building according Calvi and Magenes 1997, see Fig. 4.19.

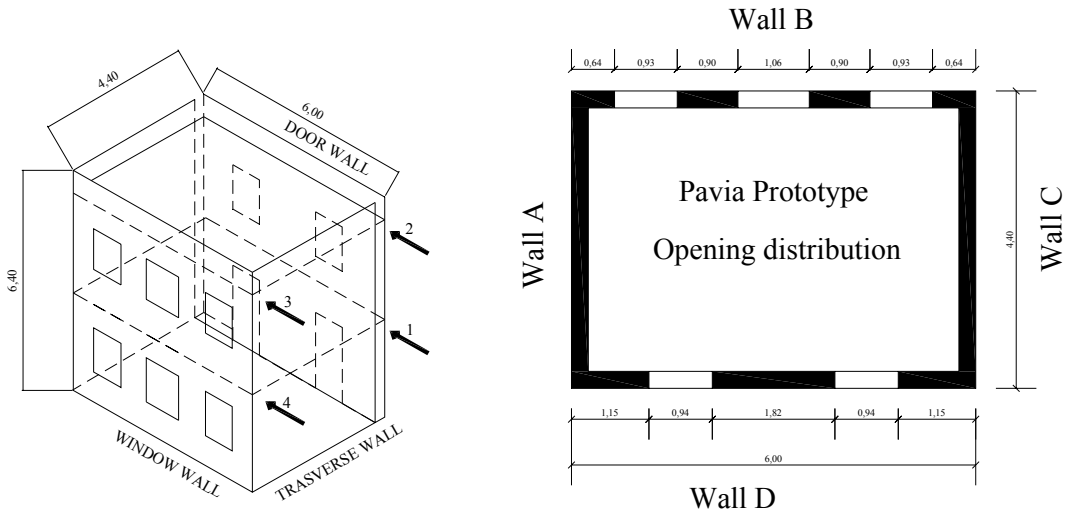

Fig. 4.19 Geometry of the prototype

First, linear analyses are performed to assess the stress distribution for a low load level, then the finite element mesh for wall B and D is created using a macro model approach, see Fig. 4.20.

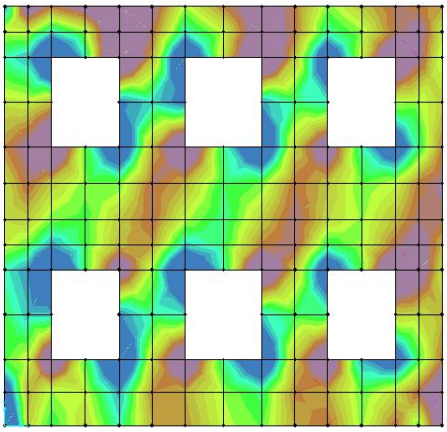

Wall B

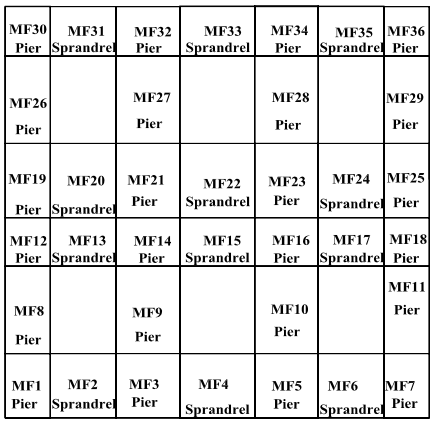

Wall B

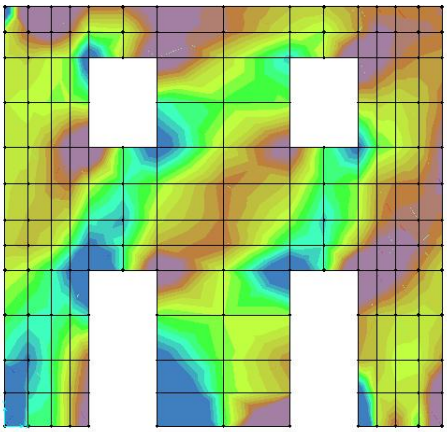

Wall D

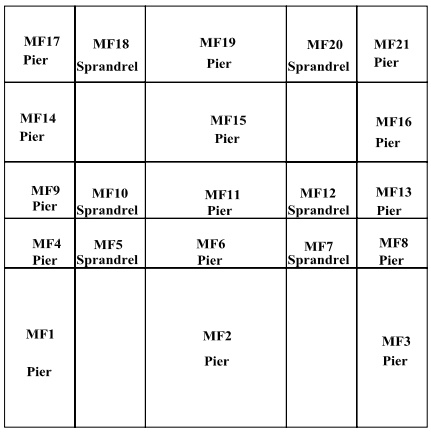

Wall D

Fig. 4.20 Finite element linear analysis results for a unit horizontal force applied at the top (principal stress distribution) and mesh used in the macro modeling approach

After the model is created in Opensees: the comparison between the experimental results (wall B and D) and the numerical results obtained with the approach presented are provided in Fig. 4.21 and 4.22. A good agreement can be observed. The structure is symmetric for both the wall A and B therefore the behavior is not depending from the direction of application of the load. The deformed shape and shear force distribution of Wall D and B in the maximum positive displacement are shown in the Fig. 4.21

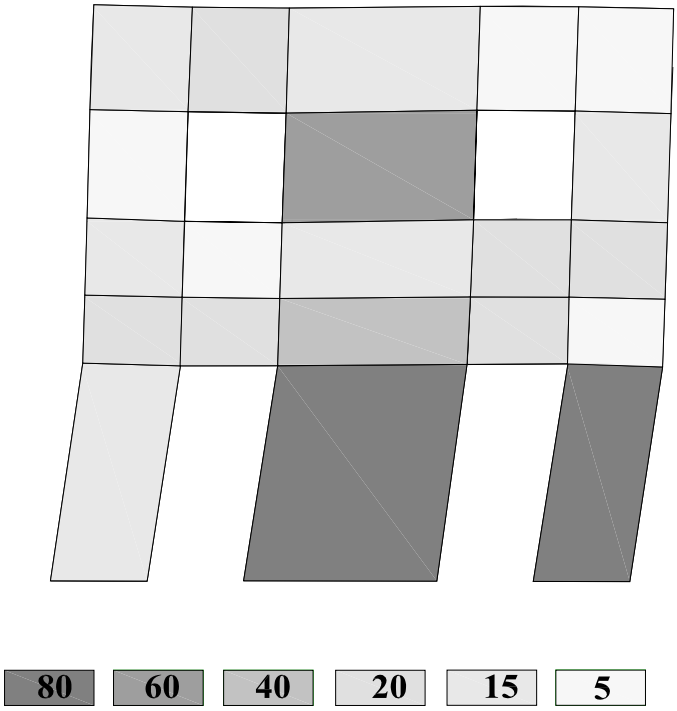

(a)

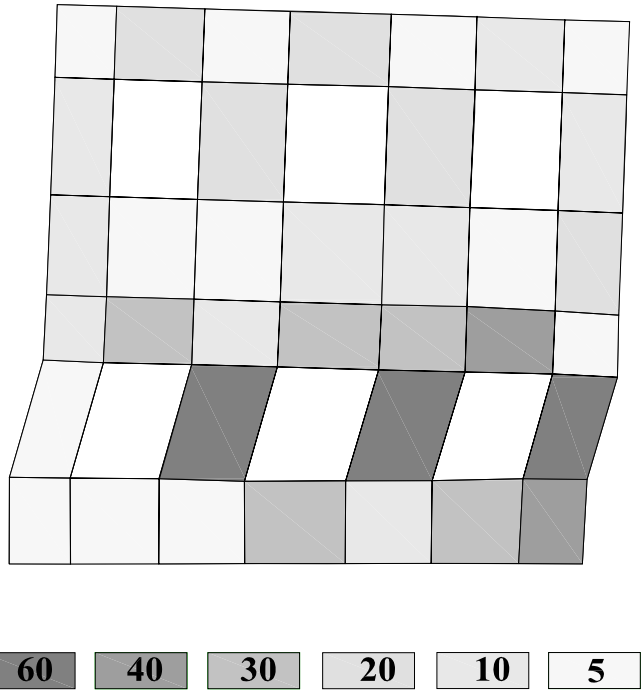

(b)

Fig. 4.21 Finite element results: shear force distribution in the piers for: (a) Wall D; (b) Wall B

When the Wall D is push to the maximum positive displacement, the right and central piers (Element 3 and 2) in the first storey have the highest shear force: respectively around 60 and 80 kN. In particular the central pier is taking a big percentage of the total shear force applied to the façade (180 kN) since it has a large cross section. The left pier (Element 1) at the opposite side has a lower shear force around 15 kN.

The deformation happens mainly in the first storey as it is clear looking the deformed mesh and in agreement with the experimental results. Similar to the behavior of Wall D, also in Wall B the majority of the deformation is in the first-story. When the Wall B attains the maximum positive displacement, the two central piers (Element 10 and Element 9) in the first storey have the highest shear force, which is around 60 kN. The shear force in the right pier (Element 11) is around 40 kN. Again the pier at the opposite side (Element 4) takes a relative low shear force, around 10 kN. The axial forces decrease from the compressive side (Element 11 and 10) to the tension side (Element 8). As a consequence, some elements on the left sides fail due to rocking being the shear strength of the elements on the right side improved by the higher compression load. This is coherent with the experimental results. Moreover, diagonal cracks developed above the exterior piers at the east side of the building during the experiment and this is described by the numerical model since the shear force in element 19 presents negative values meaning that there is an inversion of the fan distribution and that tensile stress are present in the direction opposite to the fan.

Wall B reached its maximum lateral strength of around 170 kN at a displacement of 22 mm while a drift of 28 mm was observed during the test, similarly the maximum shear strength of Wall D is 160 kN according numerical analysis while the test provided a value around 20 kN higher. The ultimate strength is reached in the numerical analysis for a displacement of 22 mm while again a slightly more ductility was found in the experimental analysis where the final drift was again around 28 mm, see Fig. 4.22.

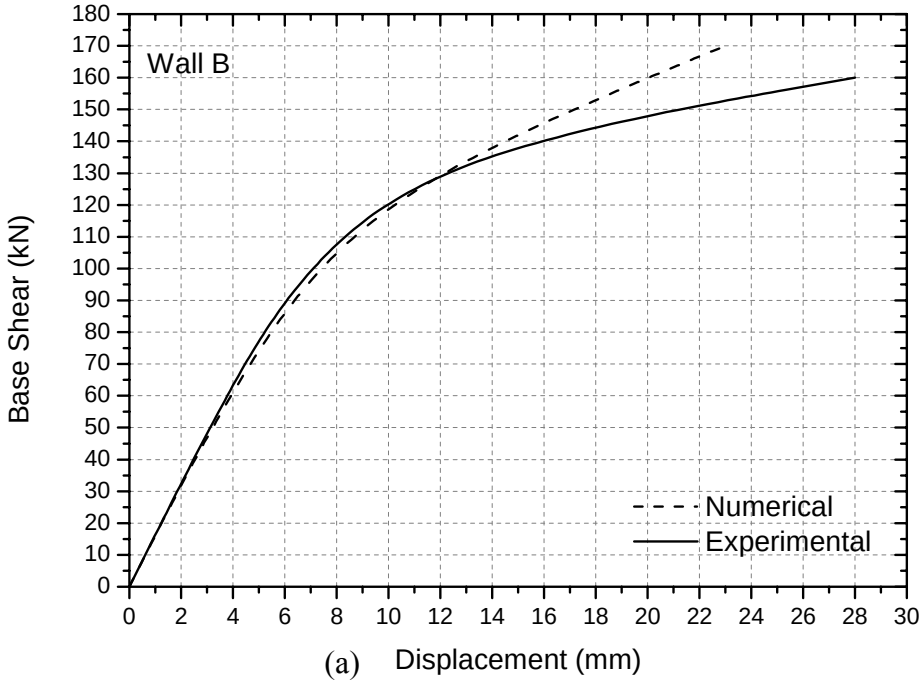

(a)

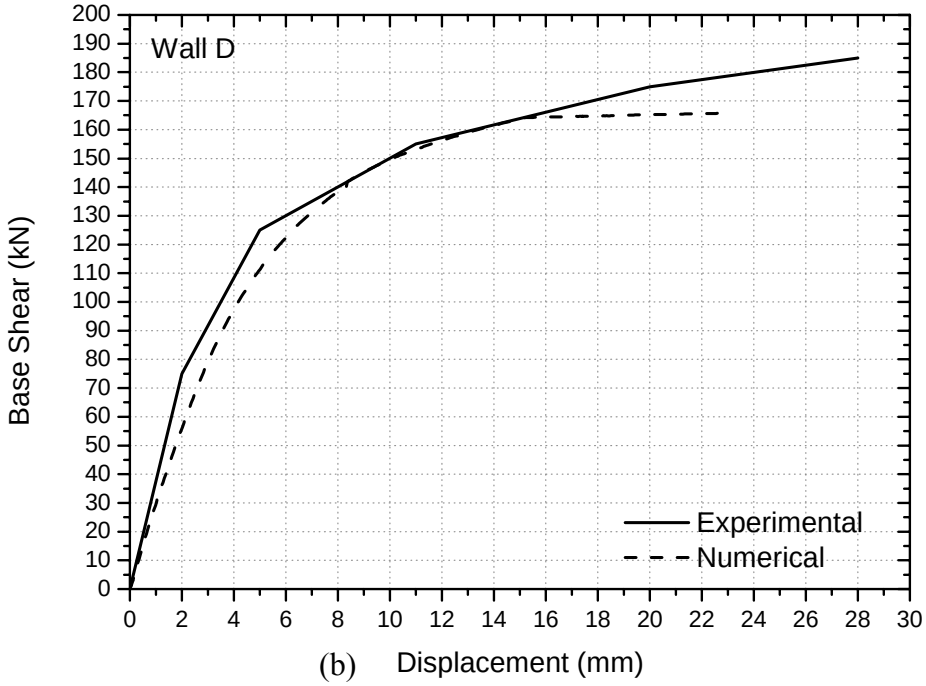

(b)

Fig.4.22 Comparison between experimental results and pushover curves obtained with the MultiFan element implemented in Opensees: (a) Wall B; (b) Wall D

4.4 Implementation of the model: Cyclic formulation

After the monotonic version of the model is developed and validated, some modifications are introduced to allow numerical modeling of the cyclic behavior of masonry buildings under horizontal seismic forces.

Unloading, reloading and friction Branch

When the Loading/Yielding condition is not satisfied, the system can be in the unloading, reloading or the friction branch. This situation happens when the following inequality holds:

$$\left(\sigma - \sigma_{\max}\right)\varepsilon < 0 \tag{4.66}$$

If $\varepsilon > 0$, eq. 4.66 means that if the σ is increasing, the system can only be in the reloading branch while if σ is decreasing, it can only be in the unloading branch or the friction branch, see Fig. 4.23. Because the force-displacement relationship is about the global series system, so in the equations ε is used to denote the total deformation of the series system. The admissible stress region is enclosed by the unloading, reloading and the friction branch and two additional yield functions are needed and defined as:

$$f_{RE} = |\sigma| - D_{RE}\,|\varepsilon| \le 0 \tag{4.67}$$
$$f_{FR} = -sign(\varepsilon)\,\sigma + D_{RE}\varepsilon + sign(\varepsilon)\,\sigma_{FR} < 0$$

where f_{RE} and f_{FR} are the yield functions for the reloading branch and friction branch respectively.

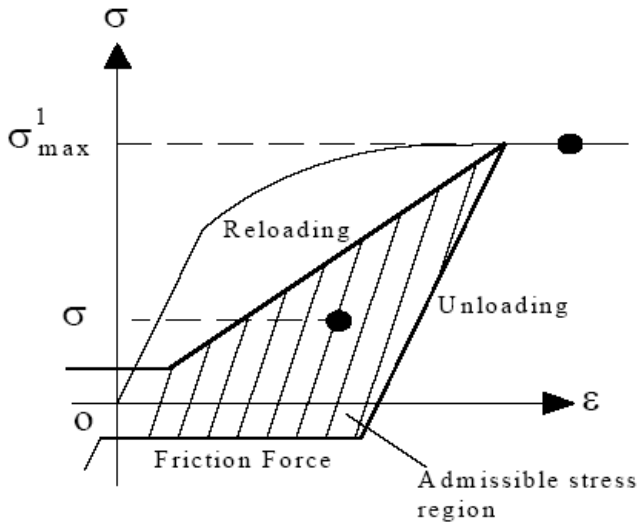

Fig. 4.23 Admissible stress region

Then a trail state is considered and this purely elastic (trail) step is defined by the formulas:

$$\begin{cases} \sigma_{n+1}^{trial} = \sigma_n + D_{UL}\Delta\varepsilon_n^p \\ \Delta\varepsilon_{n+1}^{trial} = \Delta\varepsilon_n^p \\ \Delta\kappa_{n+1}^{trial} = \Delta\kappa_n \end{cases} \tag{4.68}$$

in which D_{UL} is the unloading stiffness. When both the following conditions are satisfied:

$$\begin{aligned} f_{RE} &= \left|\sigma_{n+1}^{trial}\right| - D_{RE}\left|\varepsilon_{n+1}^{trial}\right| < 0 \\ f_{FR} &= -sign(\varepsilon_{n+1}^{trial})\,\sigma_{n+1}^{trial} + D_{RE}\varepsilon_{n+1}^{trial} + sign(\varepsilon_{n+1}^{trial})\,\sigma_{FR} < 0 \end{aligned} \tag{4.69}$$

the trial state is admissible and the system is in the unloading branch, see Fig. 4.24 and there is no plastic flow. This yields to:

$$\begin{cases} \sigma_{n+1} = \sigma_{n+1}^{trial} \\ \Delta\varepsilon_{n+1} = \Delta\varepsilon_n^p \\ \Delta\kappa_{n+1} = \Delta\kappa_n \end{cases} \tag{4.70}$$

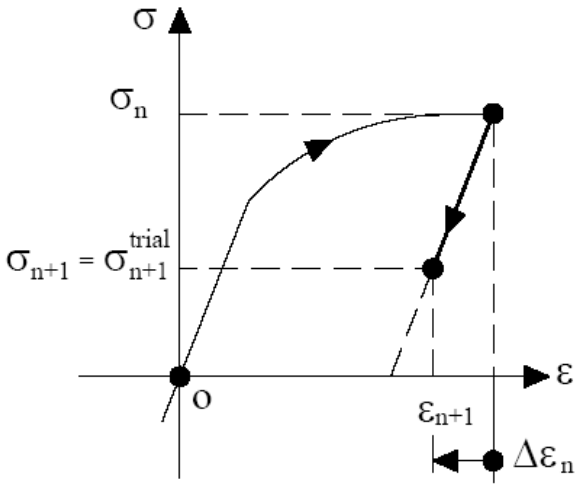

Fig. 4.24 Unloading Branch of the cyclic MultiFan element

The system is in the friction branch, see Fig. 4.25, when the following two inequalities are satisfied:

$$\begin{aligned} &\left(\sigma_{n+1}^{trial} - \sigma_{\max}\right)\varepsilon < 0 \\ &f_{FR}^{trial} = -sign(\varepsilon_{n+1}^{trial})\,\sigma_{n+1}^{trial} + D_{RE}\varepsilon_{n+1}^{trial} + sign(\varepsilon_{n+1}^{trial})\,\sigma_{FR} \geq 0 \end{aligned} \tag{4.71}$$

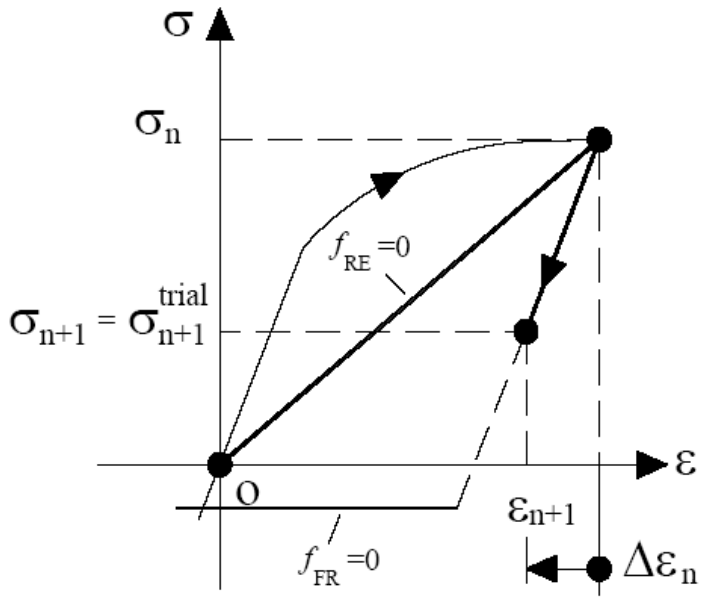

Fig. 4.25 Friction Force Branch of the cyclic MultiFan element

If $\varepsilon > 0$, the fist inequality eq. 4.71 can assure that the system is not in the loading branch or the yielding branch. The second inequality means that the stress already goes below the lower boundary defined by the friction branch which is used to model the small residual friction force of the masonry panel when the crack is closing. This branch is almost parallel to the ε axis and it has a very small tangent stiffness D_{FR} to avoid the numerical problem caused by the zero tangent stiffness. So when $f_{FR}^{trial} > 0$ the actual state is given by:

$$\Delta\lambda_{n+1} = 0 \tag{4.72}$$

$$\begin{cases} \sigma_{n+1} = D_{FR}\varepsilon + sign(\varepsilon)\sigma_{FR} \\ \varepsilon_{n+1}^{p} = \varepsilon_{n}^{p} \\ \Delta\kappa_{n+1} = \Delta\kappa_{n} \end{cases}$$

which means that no plastic flow happens and the stress is moving along the line defined by:

$$\sigma = D_{FR}\left|\varepsilon\right| + sign(\varepsilon)\,\sigma_{FR} \tag{4.73}$$

Finally, when the following two inequalities are satisfied, the system is in the reloading branch, see Fig. 4.26:

$$\left(\sigma_{n+1}^{trial} - \sigma_{\max}\right)\varepsilon < 0 \tag{4.74}$$

$$f_{RE}^{trial} = \left|\sigma_{n+1}^{trial}\right| - D_{RE}\left|\varepsilon\right| \geq 0$$

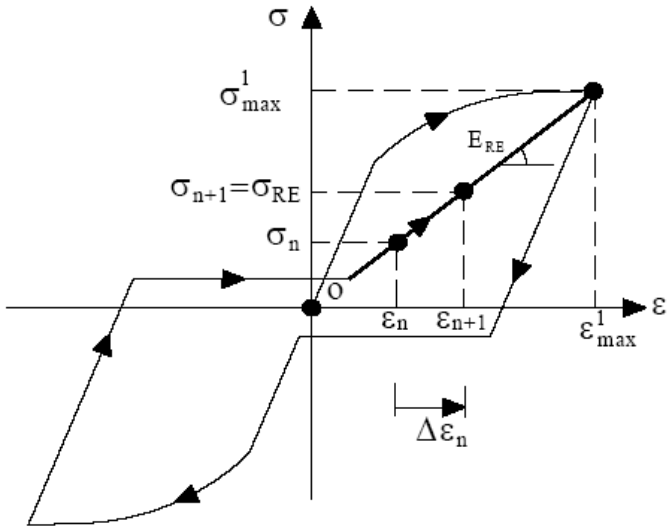

Fig. 4.26 Reloading Branch of the cyclic MultiFan element

The fist inequality eq. 4.74 can assure that the system is not in the loading branch or the yielding branch. The second inequality means that the stress already goes beyond the upper boundary defined by the reloading branch, which a straight line is always pointing towards the last unloading point in the yielding branch. The reloading stiffness is defined by:

$$D_{RE} = \frac{\sigma_{\max}}{\varepsilon_{\max}} \tag{4.75}$$

where $\sigma_{\max}$ and $\varepsilon_{\max}$ are the stress with the maximum magnitude and the corresponding strain, in the positive and negative direction respectively. So when $f_{RE}^{trial} > 0$, the actual state is given by:

$$\Delta\lambda_{n+1} = 0 \tag{4.76}$$

$$\begin{cases} \sigma_{n+1} = D_{RE}\left|\varepsilon\right| \\ \varepsilon_{n+1}^{p} = \varepsilon_{n}^{p} \\ \Delta\kappa_{n+1} = \Delta\kappa_{n} \end{cases}$$

which means the stress is moving along the line defined by $\sigma = D_{RE}\left|\varepsilon\right|$ and no plastic flow happens, until the system yields again and reaches the boundary defined by:

$$f\left(\sigma,\kappa\right) = \left|\sigma\right| - \left(\sigma_{Y} + h\,\kappa\right) = 0 \tag{4.77}$$

Application 1

According to this formulation, the cyclic behavior of only one MF element with ZLH inside presents the following characteristics, see Fig. 4.27 and 4.28:

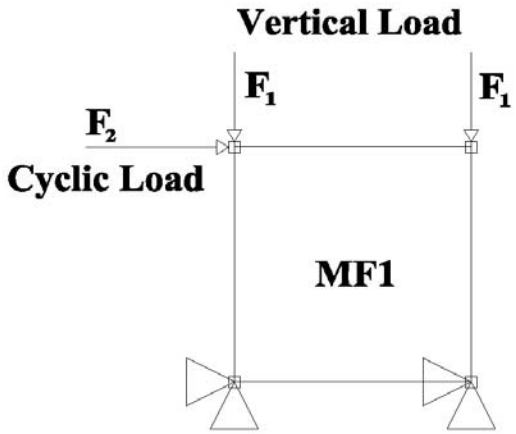

Fig. 4.27 Geometry and load condition of the model used in the analysis

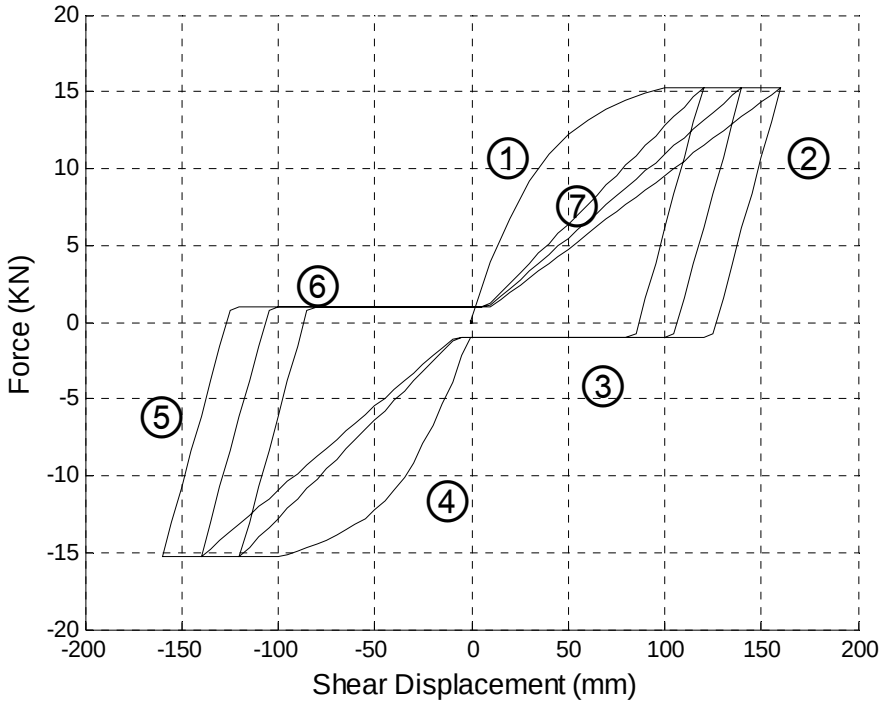

Fig. 4.28 Cyclic behavior of one element system

1. Loading branch, (including the yielding branch if it happens)
2. Unloading branch (unloading from the loading or yielding branch)
3. Friction Force branch (to model the closing of the crack)
4. Loading in another direction
5. Unloading in another direction
6. Zero-load branch in another direction
7. Reloading, which goes along a line point to the last point in the previous loading branch

Application 2

A simple structure with five elements is used here to check the global behavior of the developed finite element according geometrical and load configuration in Fig. 4.29.

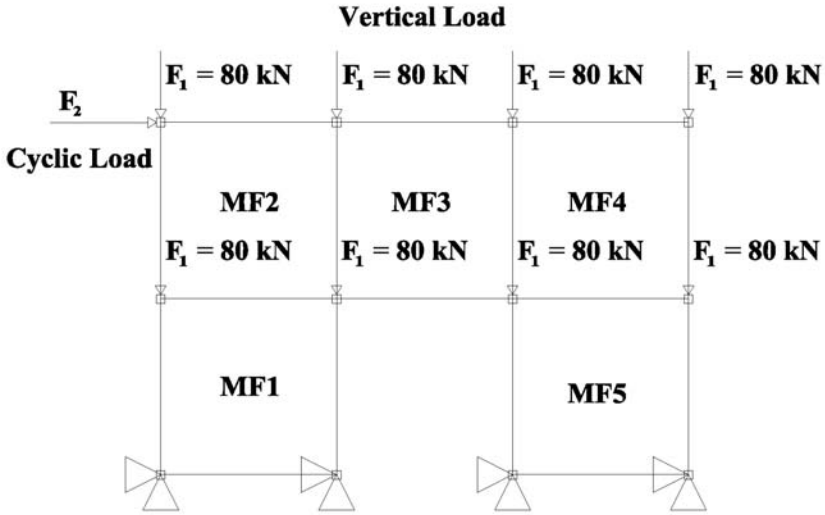

Fig. 4.29 Geometry and load condition of the model used in the analysis

The global curve representing the base-shear force versus the top displacement is plotted in Fig. 4.30, giving the full cyclic behavior of the analyzed structure. In Fig. 4.31 and 4.32 the local behavior of the bottom panels 1 and 5 is also provided. And finally in Fig. 4.33 the three curves are compared.

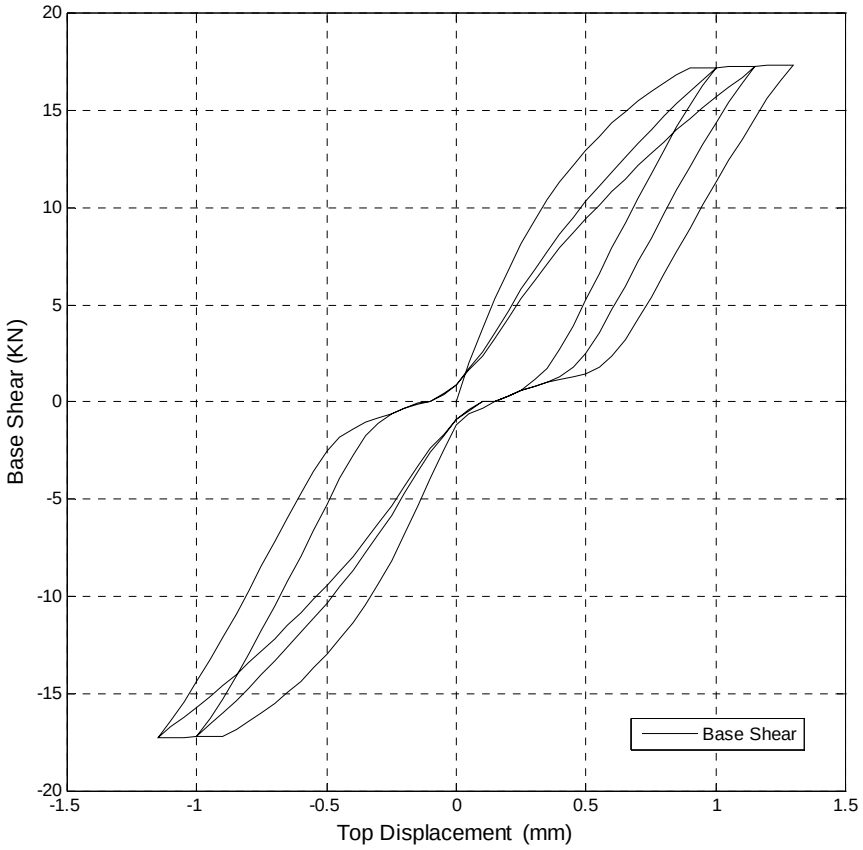

Fig. 4.30 Full cyclic behavior

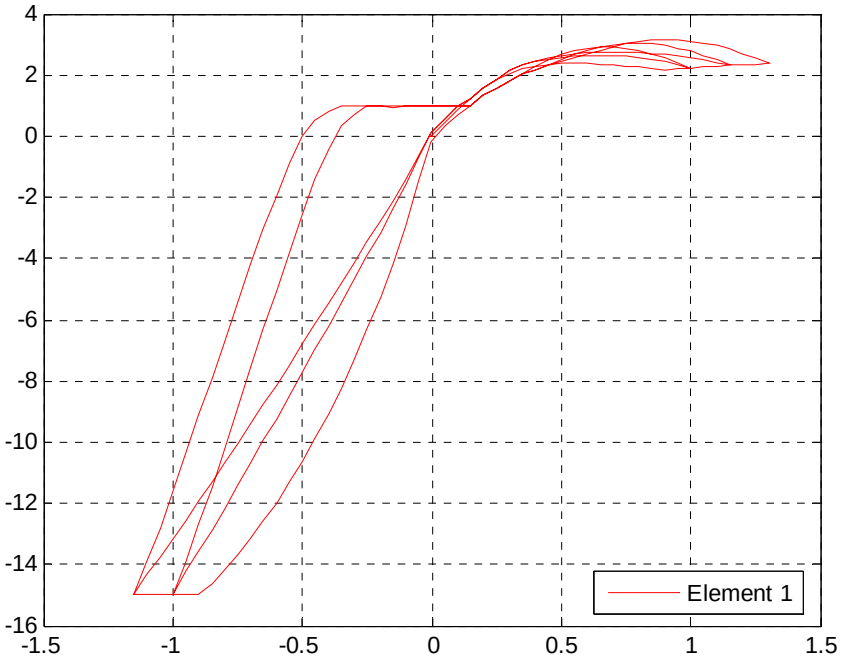

Fig. 4.31 Shear Force of Element 1 vs. Top Displacement

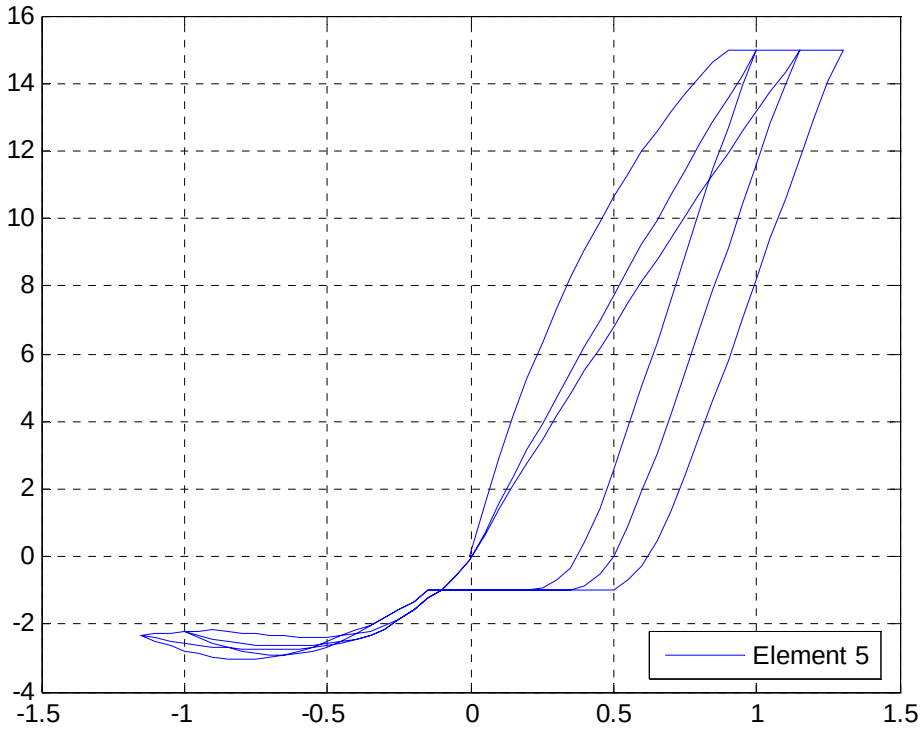

Fig. 4.32 Shear Force of Element 5 vs. Top Displacement

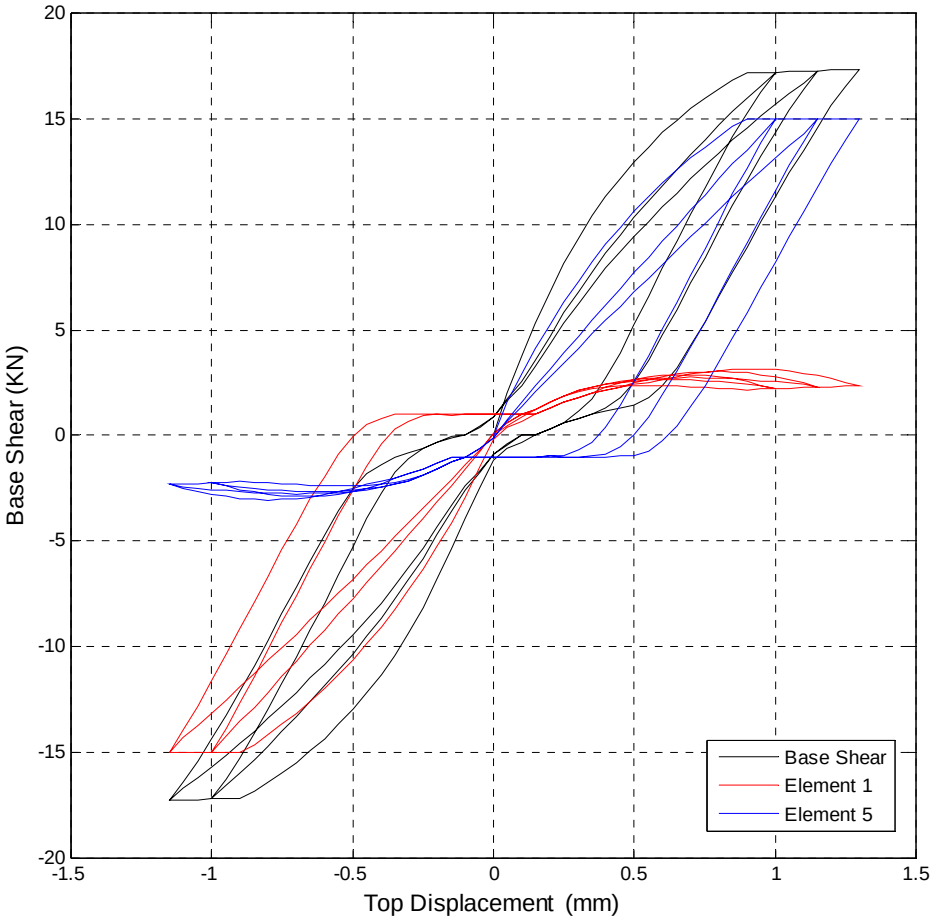

Fig. 4.33 Shear Force vs. Top Displacement

4.4.1 Application 3: Pavia shear walls – cyclic load

The micro-modeling approach is again used to provide a comparison to the macro element results according the formulation presented in the previous section. In particular, a change in the constitutive law is considered according to formulation in Oliveira 2004. In this section the finite element analyses with the micro approach are not performed but it is referred directly to the available results in the literature.

Two types of masonry walls were chosen as representatives of the building prototype tested at Pavia University within the framework of the research program promoted by CNR. The two walls were made of 250×120×55 mm^3 brick units and hydraulic lime mortar (the same materials as those used to construct the building prototype) arranged in two-wythes thickness English bond pattern with the same width of 1000 mm, the same thickness of 250 mm, the same joint thickness of 10 mm, but different heights, see Fig. 4.34 and Fig. 4.35. The higher wall (HW) presented a height/width ratio of 2.0 whereas the lower wall (LW) presented a ratio of 1.35. The tests were performed at the Joint Research Centre (JRC), Ispra, Italy (Anthoine et al. 1995). The experimental results have shown that the different height/width ratio implies quite important changes in the wall's overall behavior. These changes are most certainly related to the activation of different mechanisms of nonlinearity, namely cracking of the joints, frictional sliding along the joints, tensile and shear rupture of the units and compressive failure of masonry.

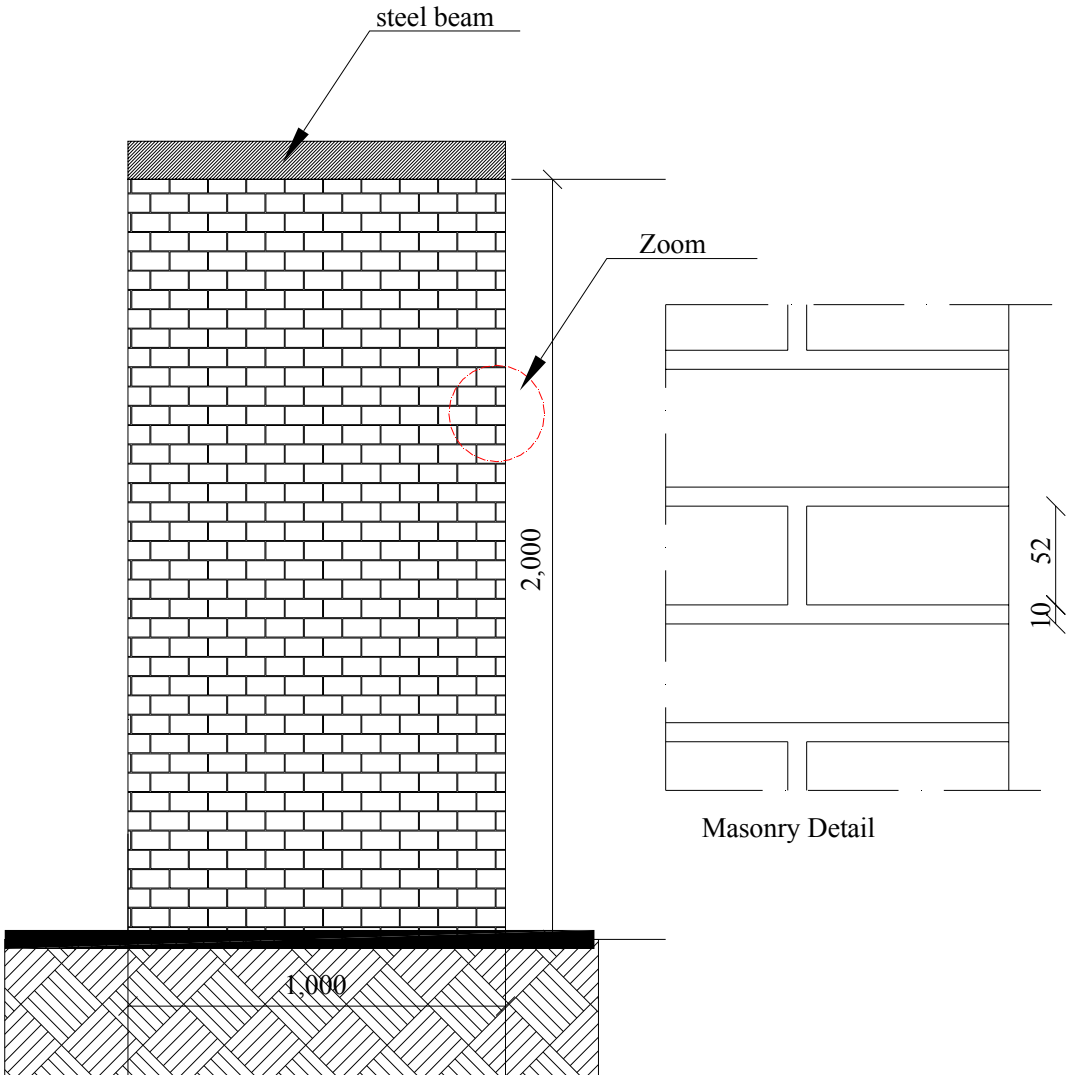

Fig. 4.34 Unreinforced masonry shear walls: high wall (HW)

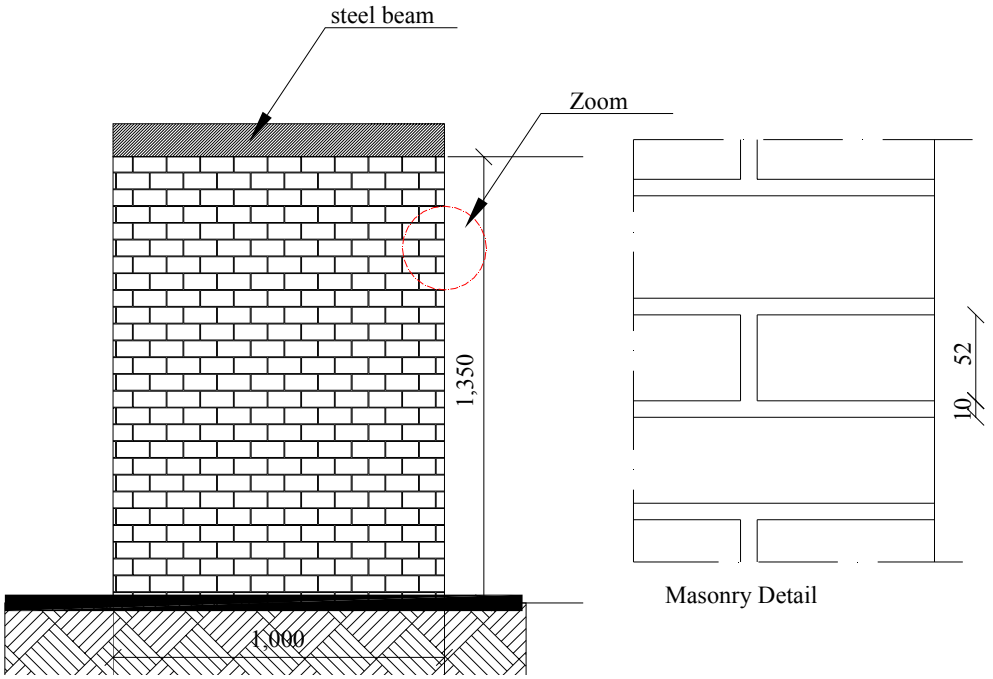

Fig. 4.35 Unreinforced masonry shear walls: low wall (LW)

Load and boundary conditions were chosen in order to reproduce the real conditions experienced by the walls during a seismic occurrence as well as possible. In this way, a uniform, vertical, compressive load was initially applied. Afterwards, a quasi-static cyclic horizontal displacement was imposed on the steel beam, at the top of the wall. The experimental set-up was such that the steel beam was prevented from rotating, thus allowing the same vertical and horizontal displacements at all points of the beam, see Anthoine et al. 1995. Both walls were initially subjected to a uniform vertical load of 150 kN, resulting in an average normal stress of 0.6 N/mm^2. Keeping this vertical load constant, increasing, alternated, in-plane horizontal displacements were imposed on each wall, as schematically illustrated in Fig. 4.36 (Oliveira 2004).

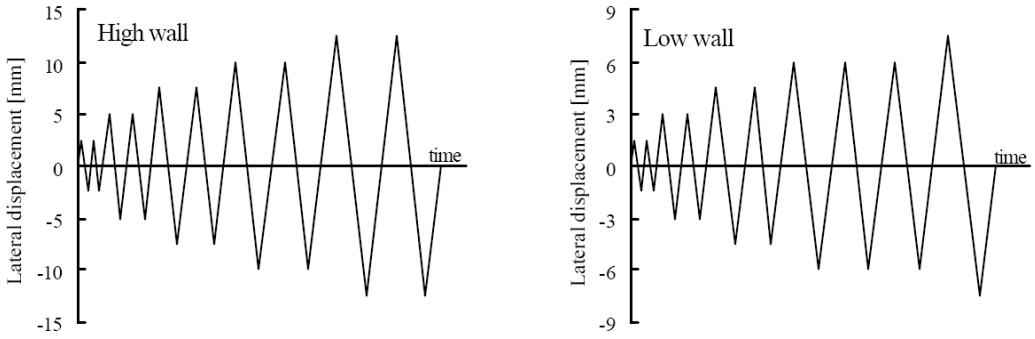

Fig. 4.36 Experimental imposed lateral displacements: (a) high wall; (b) low wall.

The performance of the developed constitutive model will be now investigated against two groups of masonry structures:

a) failure in shear

b) failure in bending

The final aim is to reproduce the main features that characterize cyclic behavior with the MultiFan element, while the main inelastic mechanisms such as cracking of the joints, frictional sliding along the joints and compressive failure of masonry involved can be described only by using a micro approach. In what follows, the structural response of the high and low wall is analyzed.

High wall

In order to understand the overall structural behavior, a cyclic analysis is carried out. The cyclic response of the high wall, in terms of the base shear versus the imposed displacement at the top of the wall, is plotted in Fig. 4.37, and 4.38. The comparison between experimental results, micro modeling results in literature and the macro approach proposed in this study: shows that the MultiFan element can capture the cyclic behavior of the masonry wall. The structural behavior is mainly characterized by the opening of the top and bottom bed joints, in close resemblance with a rigid body movement: rocking failure. It is stressed here the great importance of an accurate modeling of the boundary conditions and the difficulty of an appropriate definition of the model parameters due to the inexistence of available experimental data.

Low wall

Again in order to understand the overall structural behavior, a cyclic analysis is performed. The cyclic response of the low wall, in terms of the base shear versus the imposed displacement at the top of the wall, is plotted in Fig. 4.39, 4.40, and 4.41. The comparison between experimental results, micro modeling results in literature and the macro approach proposed in this study: shows that the MultiFan element can capture the cyclic behavior of the masonry wall. The structural behavior is now mainly characterized by shear failure and diagonal cracking.

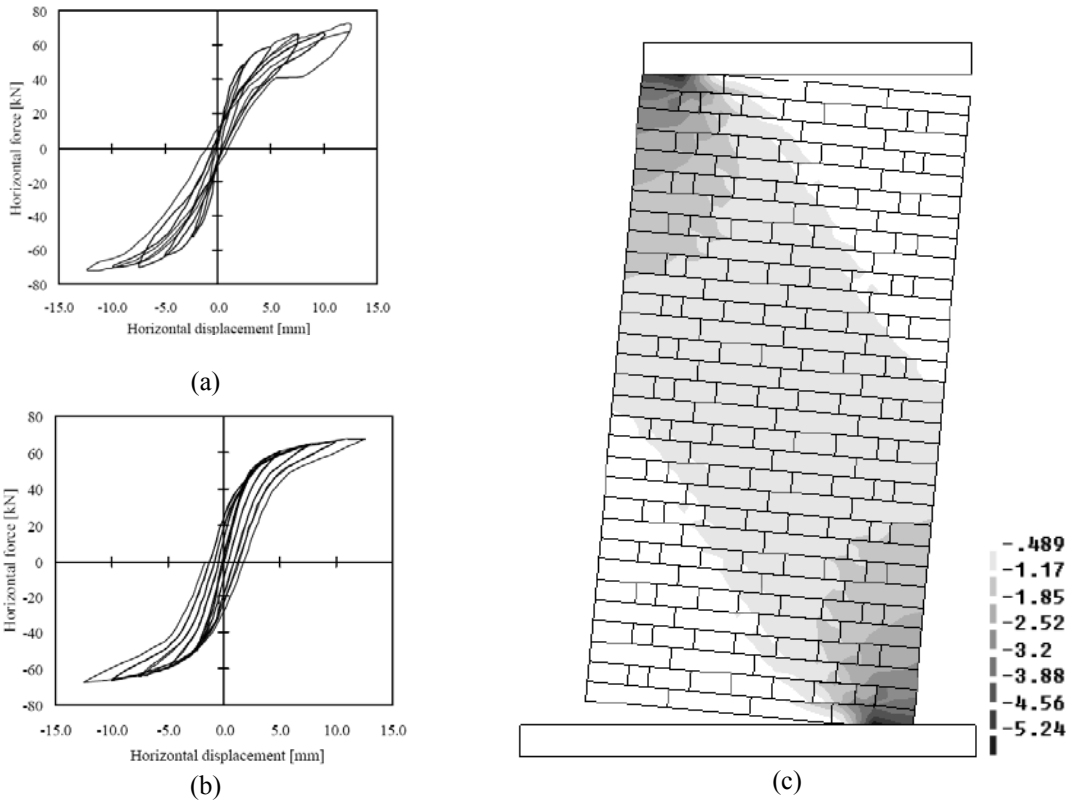

Fig. 4.37 High wall: cyclic results in terms of: (a) experimental results (Anthoine et al., 1995); (b) Numerical horizontal load-displacement diagram (micro-modeling); (c) Deformed mesh and contour level of stress (Oliveira 2004).

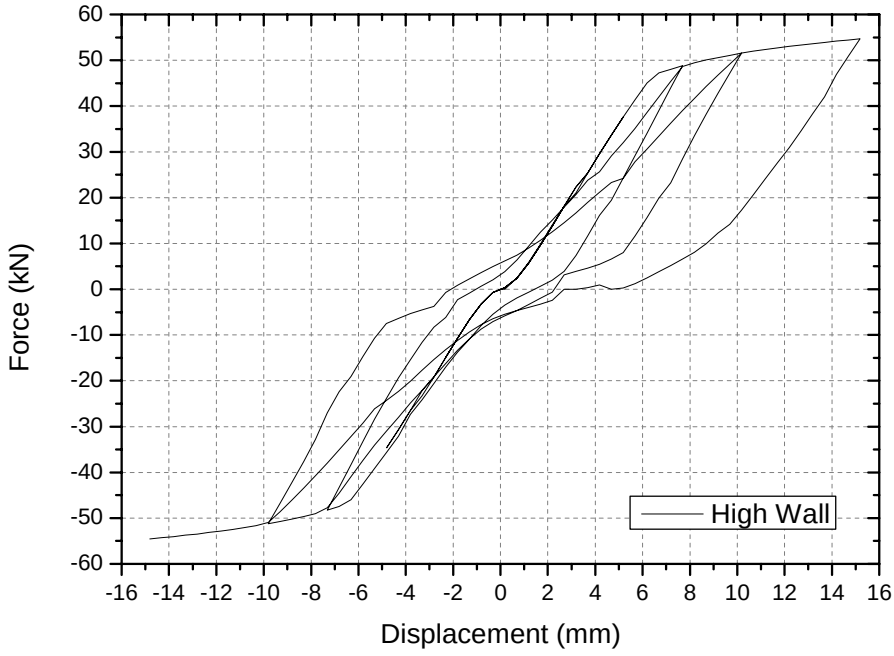

Fig. 4.38 High wall: cyclic numerical results in terms of horizontal load-displacement diagram with the MultiFan element

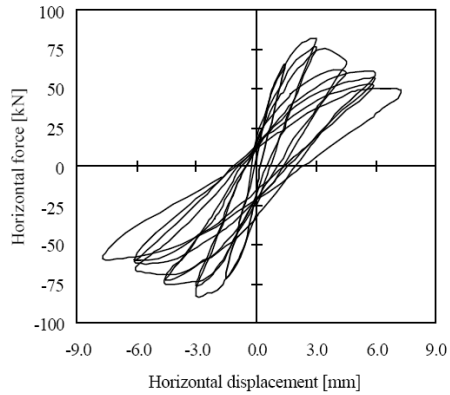

(a)

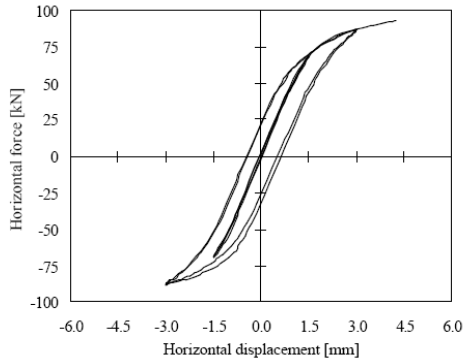

(b)

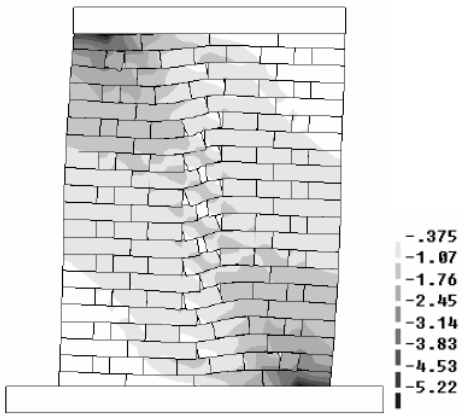

(c)

Fig. 4.39 Low wall: cyclic results in terms of: (a) experimental results (Anthoine et al., 1995); (b) Numerical horizontal load-displacement diagram (micro-modeling); (c) Deformed mesh and contour level of stress (Oliveira 2004).

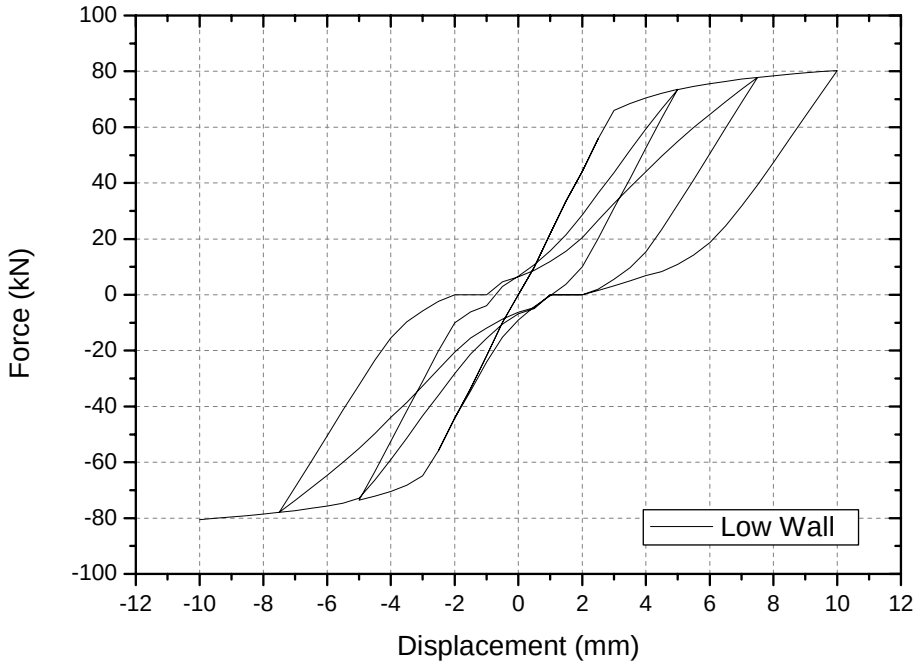

Fig. 4.40 Low wall: cyclic numerical results in terms of horizontal load-displacement diagram with the MultiFan element

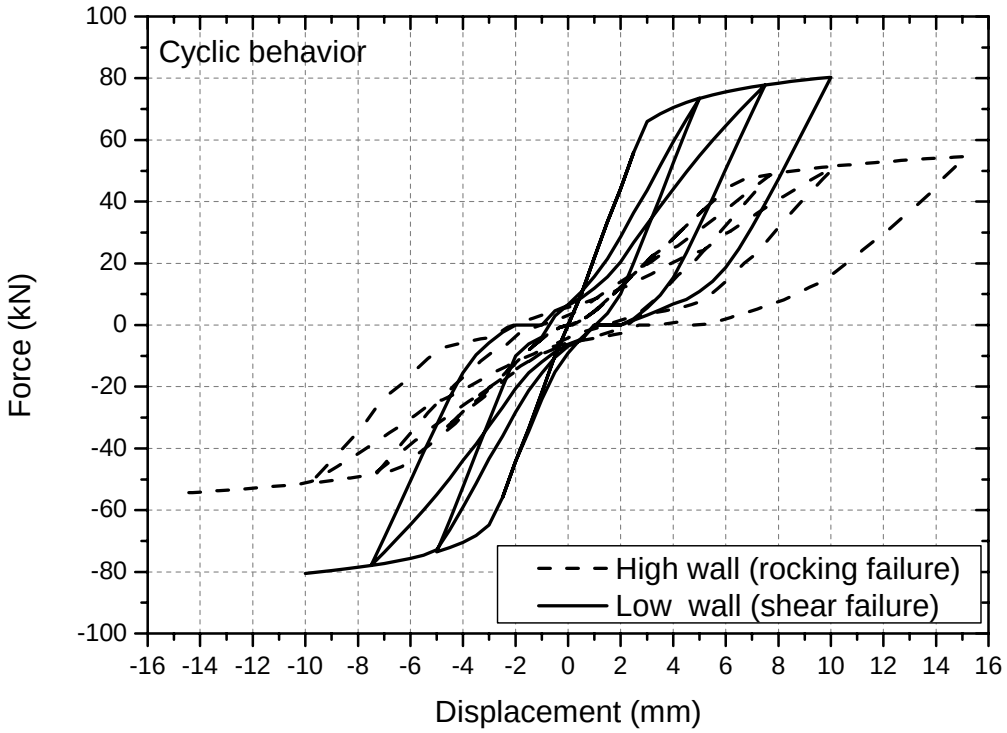

Fig. 4.41 Cyclic numerical results in terms of horizontal load-displacement diagram with the MultiFan element: comparison between high wall and low wall response

4.5 Constitutive model for reinforced FRP-masonry

The material properties of the FRP are well known in contrast to the material properties of masonry which are always a matter of debate. The FRP is usually classified on the basis of the geometrical properties, such as thickness and type of application to the surface, and on the mechanical properties, such as characteristic limit stress and elastic modulus. The material properties are defined on the basis of a standard tension test and the stress-strain diagram obtained from the test. The constitutive model of the FRP is described with an elastic-brittle behavior but in the framework of a macro-modeling description of a strengthened masonry panel it is necessary to define for the global system an elasto-plastic spring with hardening. The uniaxial elasto-plastic constitutive model can be again derived from the multi-axial constitutive model described in chapter 2. If an incremental formulation is used with strain decomposition according to:

$$\dot{\varepsilon} = \dot{\varepsilon}_e + \dot{\varepsilon}_p \tag{4.78}$$

the stress rate is given by

$$\dot{\sigma} = \rho_{FRP} E_{FRP} \dot{\varepsilon}_e \tag{4.79}$$

with ρ_{FRP} the reinforcement ratio. The uniaxial formulation of the plasticity model is given by:

$$f = \left[\sigma^2\right]^{1/2} - \bar{\sigma}(\kappa) \tag{4.80}$$

with the equivalent stress $\bar{\sigma}(\kappa)$ being the yield stress of the FRP defined as a function of the hardening parameter κ. The evolution of the plastic strain is given by the associated flow rule:

$$\dot{\varepsilon}_p = \dot{\lambda} m = \dot{\lambda}\ \mu\ n \tag{4.81}$$

where

$$n^T = \frac{\partial f(\sigma)}{\partial \sigma} \rightarrow \dot{\varepsilon}_p = \dot{\lambda}\frac{\partial f(\sigma)}{\partial \sigma} = \dot{\lambda}\frac{\sigma}{\bar{\sigma}} \tag{4.82}$$

with the assumption of work hardening the evolution of the internal variable is given by

$$\dot{\kappa} = \dot{\lambda} \tag{4.83}$$

The return-mapping algorithm is now given by the scalar equation which can be solved with a local Newton-Raphson procedure. The consistent tangent stiffness matrix is derived from the updated stress using a fully implicit Euler backward method:

$$\sigma_n = \sigma_0 + E_{FRP}\,\Delta\varepsilon - \Delta\lambda E_{FRP}\, m_n \tag{4.84}$$

with the derivative given by

$$\dot{\sigma} = E_{FRP}\ \dot{\varepsilon} - \dot{\lambda}\, E_{FRP}\, n - \Delta\lambda E_{FRP}\ \frac{\partial^2 f}{\partial \sigma^2}\dot{\sigma} \tag{4.85}$$

The consistency condition

$$\dot{f} = \frac{\partial f(\sigma)}{\partial \sigma}\dot{\sigma} + \frac{\partial f(\kappa)}{\partial \kappa}\dot{\kappa} = n^T\ \dot{\sigma} - h\,\dot{\lambda} = 0 \tag{4.86}$$

then results in the relation:

$$\dot{\lambda} = \frac{n^T\ \dot{\sigma}}{h} \tag{4.87}$$

with the hardening parameter h:

$$h = -\frac{\partial \sigma(\kappa)}{\partial \kappa} \dot{\kappa} \left(\frac{1}{\dot{\lambda}} \right) = \frac{\partial \sigma(\kappa)}{\partial \kappa} \tag{4.88}$$

Because the second derivative of the yield function with respect to the stress is equal to zero, the consistent tangent stiffness matrix is identical to the continuum tangent stiffness matrix:

$$\dot{\sigma} = \left[E_{FRP} - \frac{E_{FRP}\, m\, n^T E_{FRP}}{h + n^T E_{FRP}\, m} \right] \dot{\varepsilon} \tag{4.89}$$

4.6 FRP strengthening spring models

The primary objective of this paragraph is to define simplified models that could be used to perform seismic analysis on URM masonry building after retrofit with FRP. The approach taken allows to extend the existing model implied by the Norme tecniche per le costruzioni (NTC2008), that provide a very little guidance on the analysis of URM piers strengthened with FRP. The modifications here primarily consist of definition of appropriated spring models able to describe the behavior of strengthened piers.

When dealing with URM walls retrofitted with FRP under in-plane loads two main categories of failures mode can be identified: flexural type and shear type. Moreover, it is possible to distinguish between effective strain-based models (Triantafillou 1998; Triantafillou and Antonopoulos 2000) and truss analogy-based models (Nanni and Tumialan; Garbin, Galati et al. 2007). In particular, the FRP application is depending from the failure mode that has to be prevented. Only the FRP retrofit involving the use of strips is considered here, according investigation in chapter 3. In this frame, several experimental studies have been conducted in order to investigate the effectiveness of FRP overlays as a retrofitting method for in-plane URM piers.

Previous research, Moon 2004, has showed that two approaches are more suitable for the in-plane retrofit with FRP: the first employs sheets bonded over the entire area of the pier, the second only in specific locations. In particular, vertical and diagonal strips configuration are the most efficient configuration of FRP according these experimental results, as shown in Fig. 4.42.

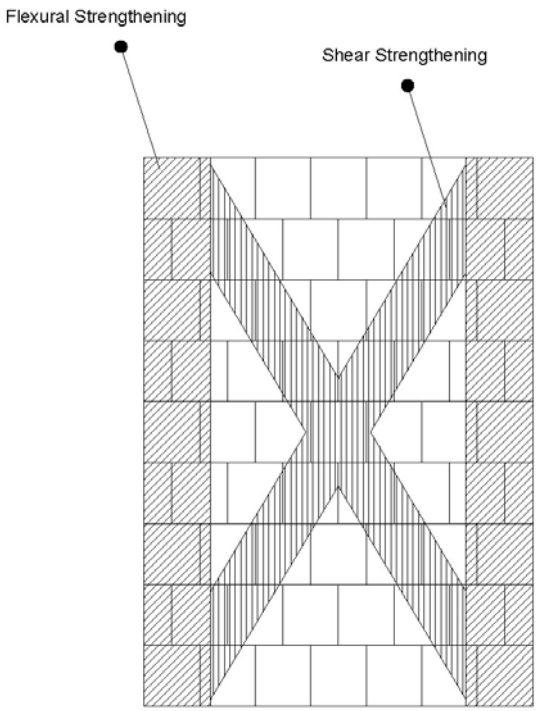

Fig. 4.42 URM retrofit with FRP strips

Moon 2004, starting from the recommendations for the pier model presented in FEMA 356 extended them to predict the response of URM piers following the application of FRP overlays. In his work several expression are derived to describe the strength and displacement response of strengthened URM pier for each of the failure modes experimentally observed, which are:

- Tension failure of flexural FRP
- Debonding of flexural FRP
- Compressive failure of masonry
- Shear failure of flexural FRP (bed-joint sliding)
- Tension failure of diagonal tension FRP
- Debonding of diagonal tension FRP

Now, briefly these constitutive laws are discussed with the aim to include in the numerical analysis the effects due to the FRP application, for a complete discussion the reader can refer to Moon 2004. It is observed here that the first branch in the next force-drift relationships is always elastic and to define the values V_{t1} and δ_e the FRP contribution can be neglected and therefore it is possible to use the values available for URM masonry piers, see eq. 4.20.

Tension failure of flexural FRP

The moment that cause the FRP strip failure can be expressed with the following equation:

$$M_{tf} = \frac{f_{fu} t_m (b_m/3)^2}{2\,n\left(b_m - \frac{w_f}{2} - \frac{b_m}{3}\right)}\left(\frac{b_m}{2} - \frac{b_m}{3} * \frac{1}{3}\right) + f_{fu}\; w_f t_f \left(b_m - \frac{w_f}{2} - \frac{b_m}{2}\right) \tag{4.90}$$

where:

w_f = width of the flexural FRP

t_f = thickness of the flexural FRP

f_{fu} = Tensile strength if the FRP

Similarly to URM masonry walls, the shear capacity associated with the tension failure of flexural FRP can be obtained by summing moments about the base of the pier according this expression:

$$V_{tf} = \frac{2M_{tf}}{H} = V_{t3} \tag{4.91}$$

Finally, for the displacement at tension failure of flexural FRP, this expression can be obtained:

$$\Delta_{tf} = \frac{f_{fu}\; H^2}{n\; E_m (d - c_{tf})}\left(\frac{1}{2} - \frac{1}{6\gamma}\right) = \delta_f \tag{4.92}$$

where:

E_m = elastic modulus of the masonry prism

$d = b_m - \frac{w_f}{2}$

$c_{tf} \approx$ the location of the neutral axis

while

$V_{t2} = V_R$ corresponding to the rocking residual strength

$\delta_u = \Delta_R$ corresponding to the rocking max displacement

The resulting force drift relationship is shown in Fig. 4.43. It is assumed that prior to reaching the rocking capacity of the URM pier, the pier behaves as if it were unreinforced. In addition, once the flexural FRP has failed, it is assumed that the force-drift relationship reverts to the force-drift curve associated with rocking/toe crushing of

a URM pier.

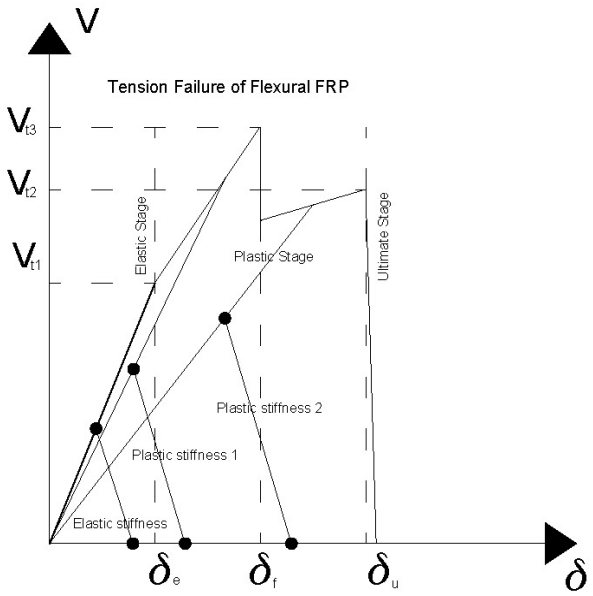

Fig. 4.43 Force-drift relationship associated with the tension failure of flexural FRP

Debonding of flexural FRP

At a first stage, the moment that cause the debonding of flexural FRP can be expressed with the following equation:

$$M_{db1} = \frac{f_{db} t_m c_{db}^{\,2}}{2\, n\,(d - c_{db})}\left(\frac{b_m}{2} - \frac{c_{db}}{3}\right) + f_{db}\; w_f t_f \left(d - \frac{b_m}{2}\right) \tag{4.93}$$

where:

$c_{db} \approx$ The location of the neutral axis

$f_{db} \approx$ Bond strength

The shear capacity associated with the debonding failure of flexural FRP can be obtained by summing moments about the base of the pier according this expression:

$$V_t = \frac{2\alpha M_{db}}{H} = V_{t2} \tag{4.94}$$

For the displacement at debonding of flexural FRP, this relation can be used:

$$\Delta_{db1} = \frac{f_{db}\, H^2}{E_f\,(d - c_{db})}\left(\frac{1}{2} - \frac{1}{6\gamma}\right) = \delta_f \tag{4.95}$$

A second stage exists where it results for the moment that cause the debonding of flexural FRP and the shear capacity associated with the debonding failure of flexural FRP

$$M_{db2} = f_{db}\ w_f t_f \left(d - \frac{b_m}{2} \right) + \left(0.8\ f_m^{'} t_m a_{db}\right)\left(\frac{b_m - a_{db}}{2} \right) \tag{4.96a}$$

$$V_{db2} = \frac{2\alpha M_{db2}}{H} = V_{t3} \tag{4.96b}$$

and the displacement as:

$$\Delta_{db2} = \left(\frac{0.0035\,(0.8)}{a_{db}} \right)(H)^2 \left(\frac{1}{2} - \frac{1}{6\gamma} \right) = \delta_u \tag{4.97}$$

where

$$a_{db} = \frac{P + f_{db} w_f t_f}{0.8\ f_m^{'} t_m} \tag{4.98}$$

Based on this analysis, the resulting force drift relationship for the debonding of flexural FRP is shown in Fig. 4.44.

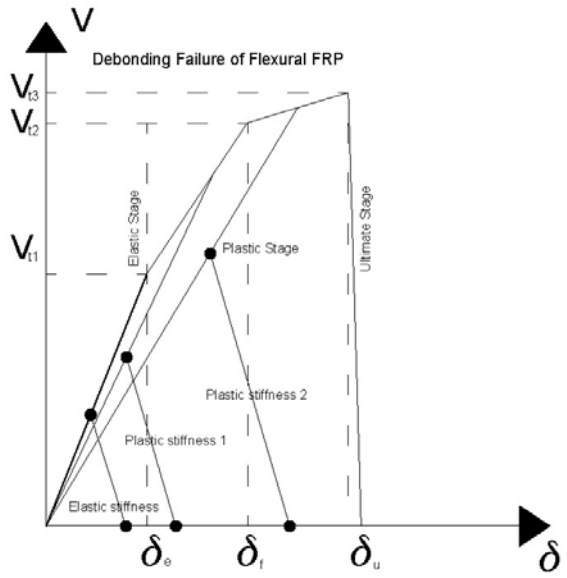

Fig. 4.44 Force-drift relationship associated with the debonding of flexural FRP

Shear failure of flexural FRP

The shear capacity due to the shear failure of flexural FRP can be obtained summing the resistance due to friction to the shear strength of the flexural FRP according the following:

$$V_{sf} = \mu P + \tau_f\ w_f\ t_t = V_{t3} \tag{4.99}$$

The displacement associated with this failure mode is quite difficult to approximate. Due to the complexity of this issue, the drift associated with this failure mode can be assumed to be 0.4%, which is the drift suggested by FEMA 356 for bed-joint sliding:

$$\delta_{f1} = 0.4\%\ H \tag{4.100a}$$

Two more stages can be determined to define the global force - drift relation:

$$\delta_{f2} = 0.8\% H \tag{4.100b}$$

and

$$\delta_u = 1.2\% H \tag{4.100c}$$

Moreover,

$$V_{t2} = V_{bjs}$$

it corresponds to the shear bed joint sliding residual strength. The resulting force-drift relationship is given in Fig. 4.45:

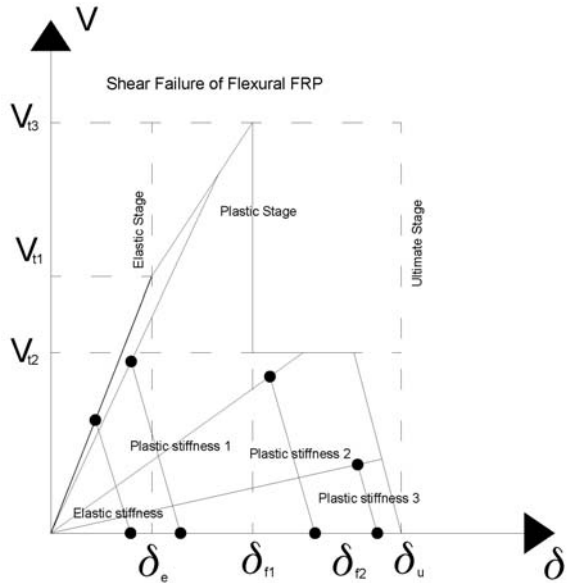

Fig. 4.45 Force-drift relationship associated with the shear failure of flexural FRP

Tension failure of Diagonal FRP

To obtain a force-drift relationship for the tension failure of the diagonal FRP, the contribution of the FRP is added to the diagonal tension capacity of the pier piers to obtain the following expression:

$$V_{dttf} = f_{dt}^{'}\ L\ t_m \left(\frac{L}{h}\right)\sqrt{1+\frac{P}{A_n f_{dt}^{'}}} + f_{fu}\ w_{dt}\ t_{dt}\ \cos\theta = V_t \tag{4.101}$$

The force-drift relationship can be assumed to be linear until reaching the maximum capacity and once the diagonal tension capacity of the pier is overcome, the lateral resistance decreases rapidly to zero, see Fig. 4.46.

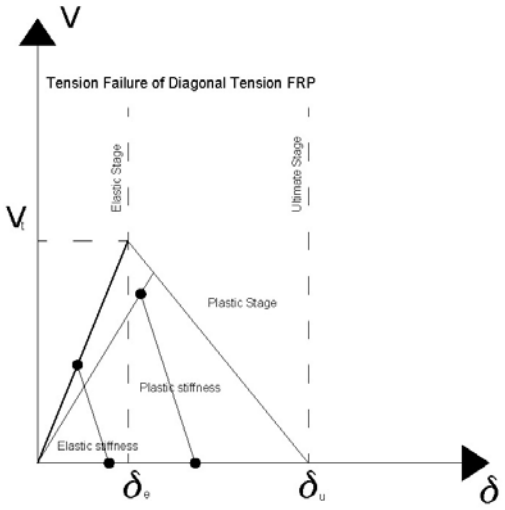

Fig. 4.46 Force-drift relationship associated with the tension failure of diagonal FRP

The displacement can be expressed as:

$$\Delta_u = 2\,\Delta_e = \frac{2V_{dttf}}{K_{el}} = \delta_u \tag{4.102}$$

Debonding of Diagonal Tension FRP

Finally, the shear capacity associated with the debonding of diagonal FRP reads:

$$V_{dtb1} = f_{dt}^{'}\; L\; t_m \left(\frac{L}{h}\right)\sqrt{1+\frac{P}{A_n f_{dt}^{'}}} + f_{db}\; w_{dt}\; t_{dt}\; \cos\theta = V_t \tag{4.103}$$

The total strength results from two contributions: the total resistance of the pier which is the shear capacity corresponding to the debonding of the diagonal FRP and the FRP contribution. The displacement associated with the complete debonding of the diagonal FRP can be calculated as:

$$\Delta_u = \frac{f_{db}}{E_f}\sqrt{L^2+h^2} = \delta_u \tag{4.104}$$

The first descending portion of the curve corresponds to a progressive debonding of the diagonal FRP. To simplify the numerical implementation, a bilinear curve can be used. The general force-drift relationship corresponding to debonding of diagonal FRP is shown in Fig. 4.47.

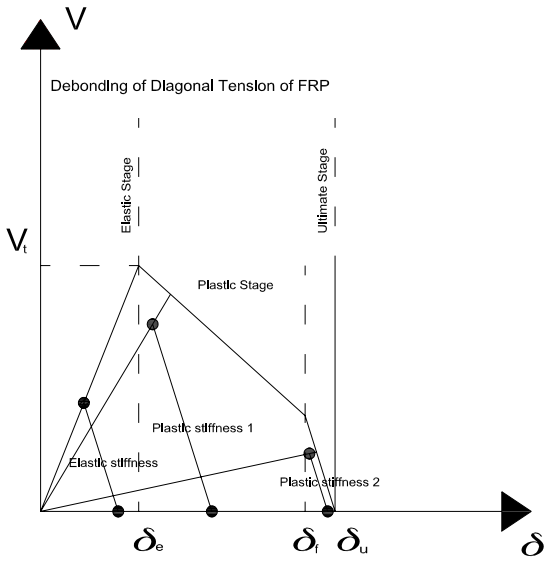

Fig. 4.47 Force-drift relationship associated with the debonding of diagonal tension FRP

4.6.1 Numerical implementation of a simplified pushover analysis

Starting from the general formulation and the constitutive laws presented above, furthermore, a simplified procedure can be implemented in a Matlab program, see appendix 3. The hypotheses required are provided here:

1) The constitutive law of each pier is multi-linear with elastic and plastic phases according to NTC 2008 and FEMA code

2) The maximum strength acting on each pier can be obtained according the unreinforced or strengthened formulation including different failure modes: shear and rocking for unreinforced walls and shear, flexural and debonding for strengthened walls

3) During the elastic stage, the elastic stiffness of each pier is determined directly according the general formulation, while during the plastic stage the stiffness can be assessed as the ratio between the current strength and displacement since are given the constitutive laws and the procedure is displacement controlled:

$$K_s = \frac{V_{ui}}{\delta_i} \tag{4.105}$$

4) The seismic force is determined according the elastic spectrum and behavior factor formulation in chapter 2

5) The walls are well connected: both in plane and out of plane

6) The seismic force is distributed to each floor of the building

7) The seismic force is considered applied into the center of mass of each floor

8) The seismic force at each floor is taken from each pier according his stiffness

9) Torsional forces due to eccentricity between the center of mass and stiffness are also applied to each pier

10) Once the elastic stage is reached, for each step of analysis is required to update the position of the center of stiffness.

The steps according the implementation are the following for the case of seismic force in the Y direction:

a) determine the elastic stiffness and the strength for each of the possible failure modes of each pier

b) determine the minimum floor ratio between strength at the elastic limit and elastic stiffness of each pier.

$$\delta_{ei} = \frac{V_{ei}}{K_{ei}} \tag{4.106}$$

This ratio identifies the first pier that will reach the limit of the elastic stage:

$$\delta_{ei} = \delta_{e0i} \tag{4.107}$$

At this given displacement δ_{e0i} is determined the reacting force induced on each pier as:

$$V_i = K_{ei}\delta_{e0i} \tag{4.108}$$

c) Each pier will move according the formula:

$$\delta_i = \frac{\sum_i V_i}{\sum_i K_{ei}} \tag{4.109}$$

d) In presence of eccentricity between center of mass and stiffness, a torsional moment will exist equal to $\sum_i V_i \left(X_r - X_c\right)$ that will generate a rotation and a correction in the displacement of each pier. To include this correction during the analysis it is necessary to determine the minimum ratio:

$$a_{i_{\min}} = \left(\frac{\delta_{e0i}}{\delta_i}\right)_{\min} = \delta_R \tag{4.110}$$

that represents the displacement of the center of stiffness. Consequently, it is possible to determine the corrected displacement of each pier from geometrical considerations as

$$\delta_i = \delta_R \; q_i \tag{4.111}$$

e) Once the elastic limit is reached from one pier at least, the plastic stage starts. The procedure increments of 5% the displacement of the center of stiffness as

$$\delta_R^i = (1 + 0.05)\,\delta_R \tag{4.112}$$

f) Again the displacement and the reacting force of each pier are determined as $\delta_i^{'} = \delta_R^i\, q_i$ and $V_i^{'} = K_{ei}\delta_i^{'}$ for the pier still in the elastic stage and $V_i^{'} = K_{si}\,\delta_i^{'}$ for the pier in the post elastic stage.

g) It is calculated again the total stiffness of the floor as

$$\sum_i K_{ei} + \sum_i K_{si}$$

h) It is known the update total reacting force:

$$\sum_i V_i^i$$

i) Each pier will move according the formula:

$$\delta_i^{''} = \frac{\sum_i V_i^{'}}{\sum_i K_{ei} + \sum_i K_{si}}$$

j) The procedure return to step (e) and restart each operation until step (j) and until convergence can be found.

An application of this simplified procedure to a strengthened masonry building will be provided in the next chapter.

4.7 Summary

In this chapter, a finite element is proposed for the analysis of the response of masonry buildings under seismic actions. Only one element is needed to model an individua1 masonry pane1 in the structure, so that the global system has a relatively few degree of freedom. Numerica1 comparisons with the 2D cracking/shearing/crushing/ finite element of DIANA, and experimental comparisons with the response of panels loaded by axial force, shear and bending moment show a good level of accuracy in the stress range of interest for design and retrofitting purposes. The micro-modeling strategy detailed in chapter 3 is first used to validate the macro-modeling approach and both the results are compared referring to the experimental tests of shear walls performed in the past at the University of Eindhoven. The no tension MultiFan

approach has been implemented in the object-oriented nonlinear dynamic analysis program Opensees. Then a zero-length spring has been added to the MultiFan element system to model shear and bending failure and the cyclic behavior. Again the cyclic results are compared with experimental results performed at the University of Pavia and results obtained in the past using an advanced micro-modeling material model developed at the University of Minho to describe cyclic behavior of masonry panels. Finally, a simplified procedure is also presented to include FRP effects in the model. The MultiFan element developed here will be used in the next chapter to analyze the structural behavior of two building prototypes experimented at the University of Pavia and at the Georgia Institute of Technology to show as a satisfactory degree of accuracy at the global level, while keeping a reasonable computational time for the analyses, can be achieved when complex assemblages in 3D are analyzed even in the case of cyclic loads or when strengthening techniques are considered. However, further development of the concepts discussed should be based on significant additional experimental evidence combined with systematic numerical simulation. In particular, detailed micro-modeling is regarded as the most promising means to progress in the development of a very consistent technique of analysis based on simple equilibrium models (struts and tie).

5 Applications

In this chapter, the MultiFan element implementation is applied to simulate two previous experimental tests on full-scale unreinforced and strengthened masonry structures under cyclic loading. The aim of this chapter is to provide further evidence to support strut and tie models as an effective approach for nonlinear analysis of masonry buildings in the finite element framework. This is obtained showing how experimental cyclic envelopes and failure mechanisms are effectively predicted.

5.1 Pavia University Prototype

5.1.1 General consideration

A strut and tie analysis on a two story unreinforced masonry building experimentally tested by Magenes et al. 1995, is considered. The structure, see Fig. 5.1, reproduces some structural characteristics of typically existing URM buildings in the historical center of Italy regions. The Cyclic MultiFan element is here used for the simulation of some of the brick masonry walls of the building prototypes experimented at the department of structural engineering in Pavia under cyclic load conditions. This test has been chosen by several researchers as a benchmark for the numerical modeling of masonry structures using finite element methods.

5.1.2 Structural model

The model of the masonry prototype is shown in Fig. 5.2. The MultiFan element is used not only for the panel, that is the parts between the openings, but for all the rectangular parts in which the wall is decomposed. The elements whose free edges are vertical will be denoted hereafter as "piers" (their rigid edges are horizontal) and those whose free edges are horizontal as "spandrels" (their rigid edges are vertical). Using elements which assume that two edges are free is correct only for the vertical panels between openings. However, since the displacement field and the base shear are mainly determined by these elements, the model can be regarded as acceptable, if only the overall response is looked for.

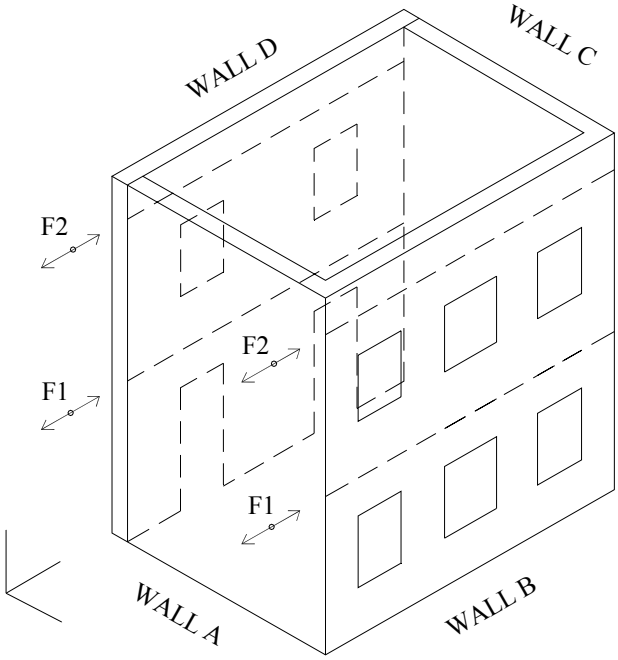

Fig. 5.1 3D view of the prototype: wall A-B-C-D

Wall B presents additional problems due to the interaction with the orthogonal walls A and C. Despite it is not easy to foresee the influence of the connections with orthogonal walls during the load application, wall B was analyzed alone. The main features of the model are summarized in Fig. 5.2.

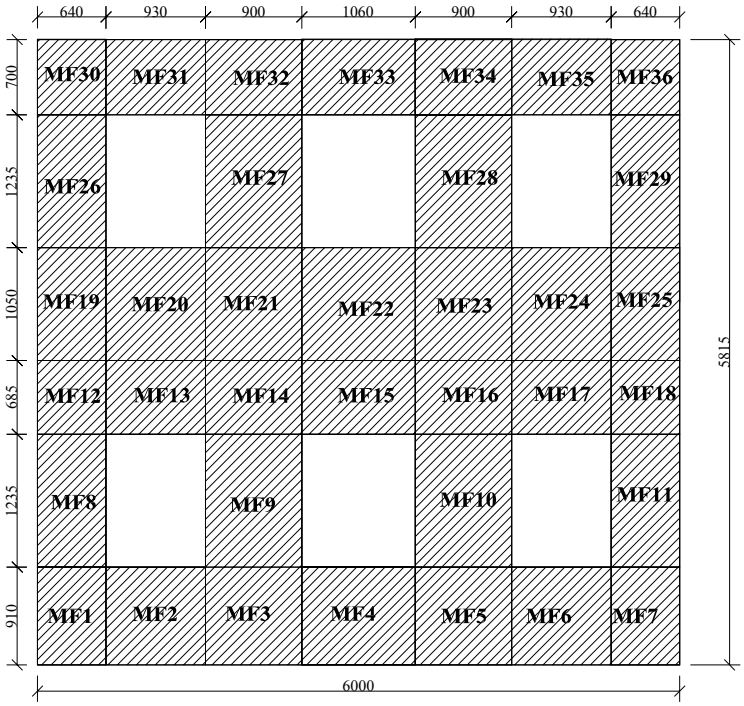

Fig. 5.2. Geometric description (mm) of wall B

5.1.3 Characterization of the material

The material properties used for numerical simulation are given in Tab. 5.1. The modulus of elasticity was estimated from the cyclic experimental results using the method proposed by Magenes and Calvi 1997 for walls showing a diagonal shear cracking response. Specifically, the value of 1410 MPa provides a base shear versus top displacement response that intersects the cyclic envelope at 75% of the maximum base shear. The value of 1410 MPa compares well with the lower anisotropic stiffness value used in simulations of the same wall by Gambarotta and Lagomarsino 1997. The tensile strength was estimated from experimental results as an average of the mortar tensile strength (0.05 MPa) and the mortar shear strength (0.18 MPa) because both shear and tensile failure are expected to concentrate in the weak mortar. The compressive strength is equal to 4 MPa.

Tab. 5.1 Material properties of the masonry

Masonry					
E_m	ν	f_c	f_t	ρ	$\tan\phi$
1410 $[\mathrm{N/mm^2}]$	0,15	4 $[\mathrm{N/mm^2}]$	0,1 $[\mathrm{N/mm^2}]$	1800 kg/m^3	0,3

5.1.4 Load conditions

The building geometry and loading conditions are shown in Fig. 5.3. The floor and roof, both realized by a series of isolated steel beams, had negligible diaphragm stiffness so only the walls were modeled. Total vertical loads equal to 248.4 kN and 236.8 kN were distributed along walls B and D at the height of the first and second floor, respectively. During the test, horizontal cyclic loads were applied to simulate seismic forces at the locations indicated in Fig. 5.3.

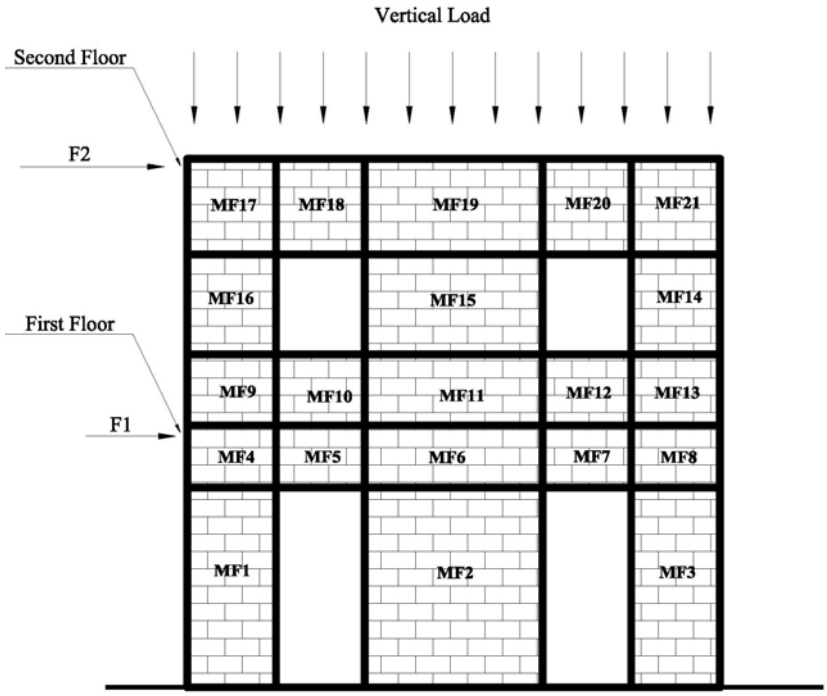

Fig. 5.3. MultiFan element model and load condition of wall D

5.1.5 Numerical analysis and discussion of the results of Wall B

The finite element model is made up of 56 nodes and 36 elements. Each panel in the structure is modeled through a single MF element. The displacement history is performed by imposing the horizontal displacement w_1 and w_2 to the nodes at the floor levels of floor 1 and floor 2 (with free vertical displacements). The cyclic response of the window wall B2, in terms of the base shear versus the imposed second floor displacement w_2, is plotted in Fig. 5.4. The comparison between experimental results and the numerical simulation shows that the MultiFan element can capture the cyclic behavior of the masonry structure.

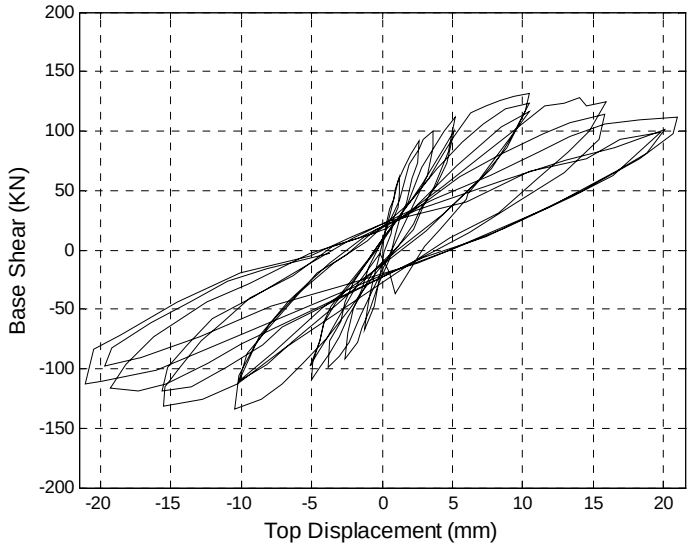

(a)

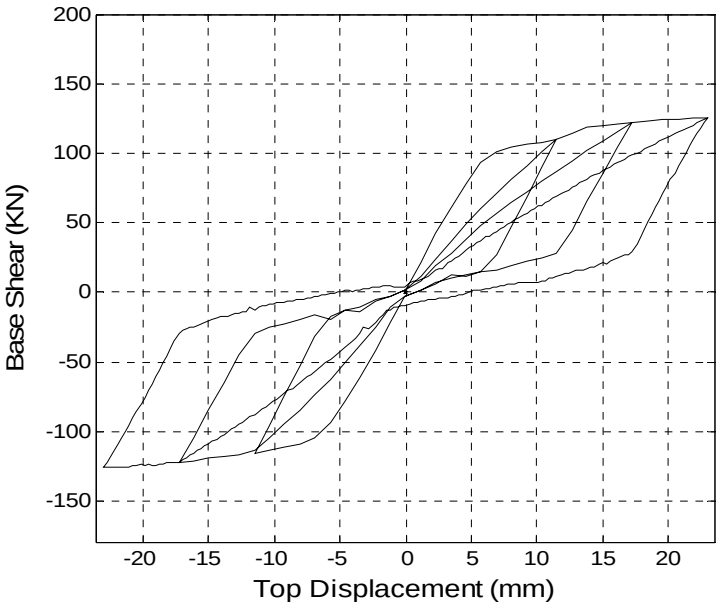

(b)

Fig. 5.4 Cyclic response of door wall B2: a) experimental; b) MF numerical simulation

The simulation slightly underestimates the shear strength, possibly due to the assumption of cyclic loading, or the material properties which are difficult to estimate accurately. Note that the simulated response is the same in both directions, as Wall B is symmetric. At a roof displacement of 5 mm, the behavior is already nonlinear since, in the test, cracking was already concentrated around the lintels, with shear failure above

the doors, and some rocking failure was present in the piers. At the ultimate displacement, the slight shearing of the outer piers at the first floor and the shear failure of the first floor center pier are also in good agreement with numerical results. At the same time, the slight rocking failure of the second story outer piers and the cracking above the second floor windows are not observed in the numerical analysis.

5.1.6 Numerical analysis and discussion of the results of Wall D

The same approach used to discretize wall B and the same assumptions about material properties, finite element model and load applications are applied to perform the pushover analysis of wall D. The geometry of the wall is illustrated in Fig. 5.5.

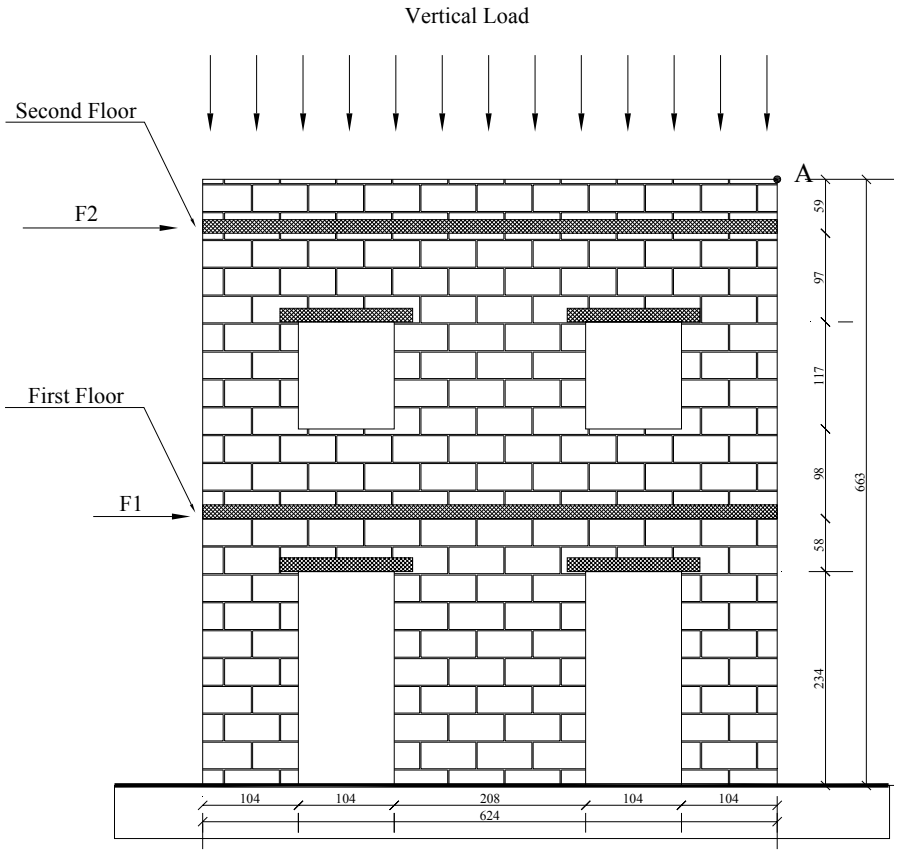

Fig. 5.5 Geometric description (cm) of wall D

Again the results in terms of the base shear versus the imposed second floor displacement are plotted in Fig. 5.6 a, b, c, d where the comparison is given between experimental results from Magenes and Calvi 1997 and recent numerical approaches based on finite element analysis, see Gambarotta and Lagomarsino 1997 or Brasile 2007.

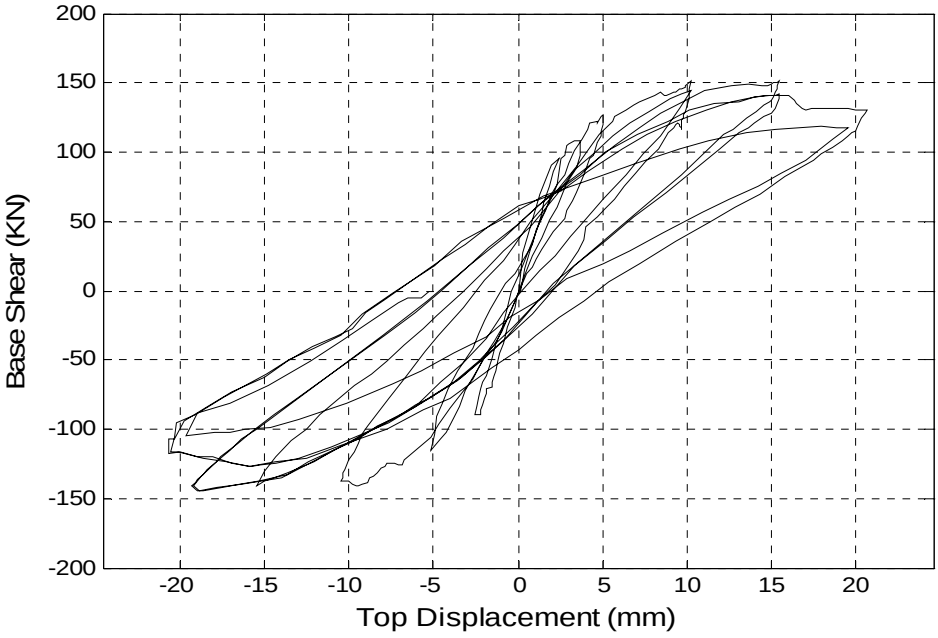

a) Cyclic response according Magenes and Calvi 1997

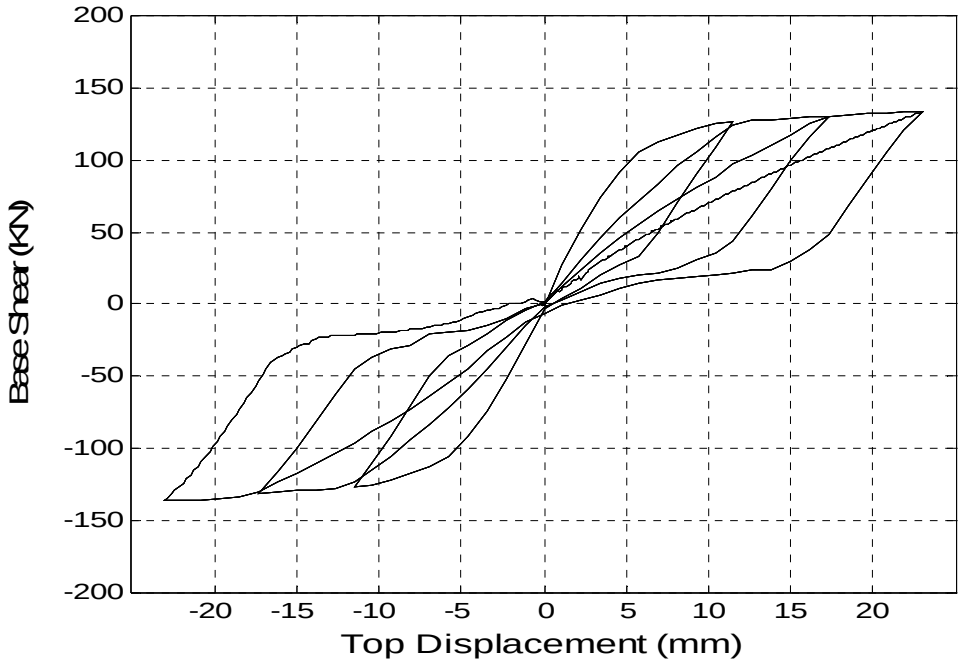

b) Cyclic response according MultiFan numerical simulation

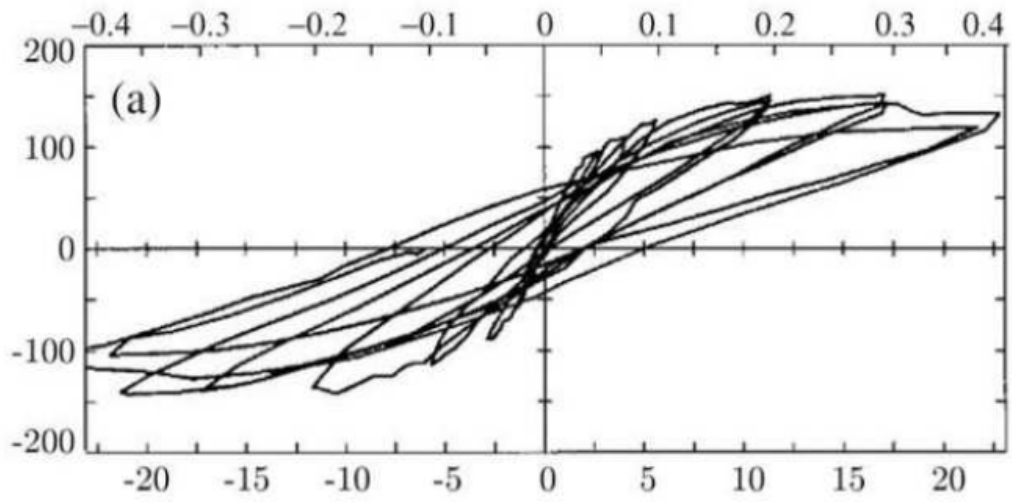

c) Cyclic response according Brasile, Casciaro et al. 2007

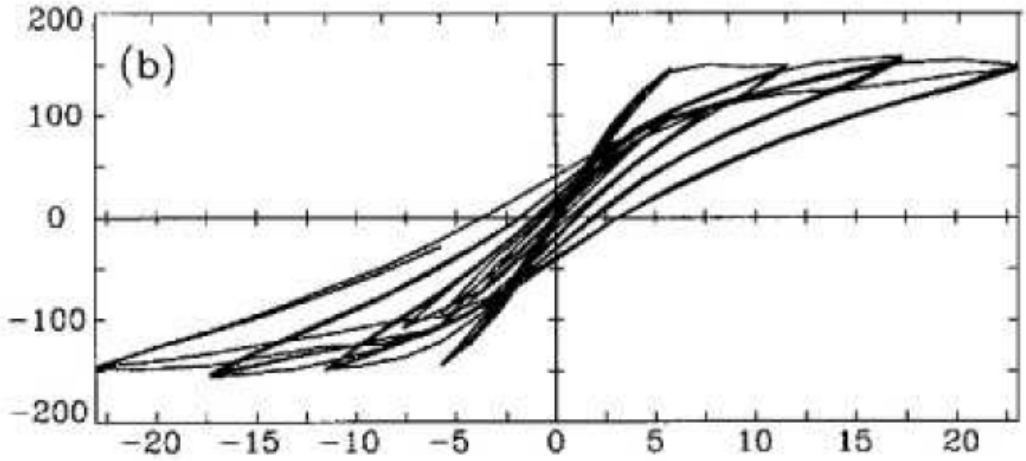

d) Cyclic response according Gambarotta and Lagomarsino 1997

Fig. 5.6 Cyclic response of door wall B2: (a) experimental; (b) MF numerical simulation; (c) Brasile and Casciaro 2007 numerical simulation; (d) Gambarotta and Lagomarsino 2007 numerical simulation

5.2 Georgia Tech Prototype

5.2.1 General consideration

A strut and tie analysis on a two story unreinforced and strengthened masonry building experimentally tested by Moon et al. 2004, is considered. The structure, see Fig. 5.7, reproduces some structural characteristics of typically existing URM buildings in the mid-America area. The Cyclic MultiFan element is here used for the simulation of some of the brick masonry walls of the building prototypes experimented at the Georgia Institute of Technology.

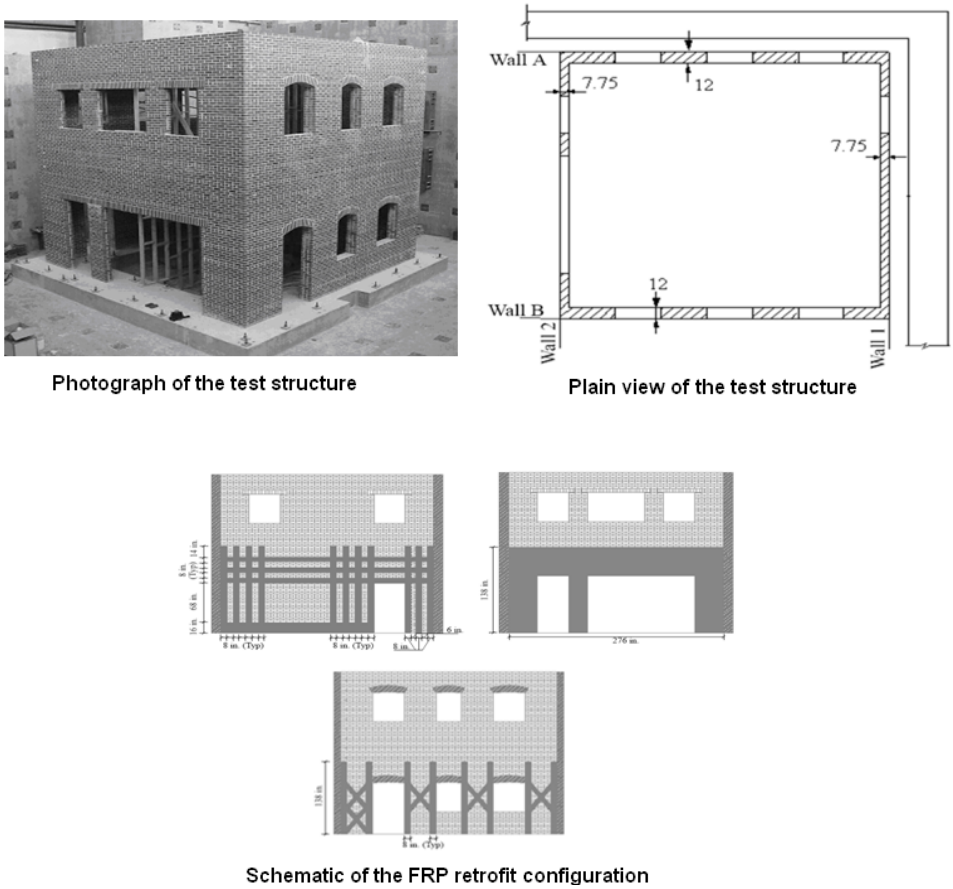

Fig. 5.7 Geometry of the building prototype with indication of strengthened parts (Moon 2004)

5.2.2 Structural model

The dimensions of the structure are 7.32×7.32 m in plan, with story heights of 3.6 m for the first story and 3.54 m for the second story. The structure is constituted by four

masonry walls labeled walls A, B, 1, and 2, respectively, see Fig. 5.8.

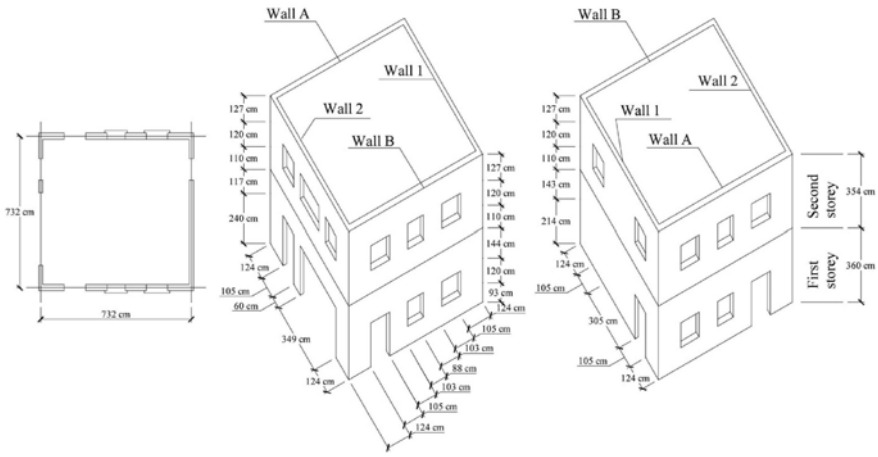

Fig. 5.8 Building geometry (Tiani Yi 2004)

The walls have different thicknesses and opening ratios. Walls 1 and 2 are composed of brick masonry with thickness 20 cm. Wall 1 has relatively small openings, whereas wall 2 contains a large door opening and larger window openings. Therefore, the large difference in stiffness between walls 1 and 2 allows the torsional behavior of the URM building to be investigated. Walls A and B are identical, and with a nominal thickness equal to 30 cm. The moderate opening ratios in these two walls are representative of many existing masonry buildings. The aspect ratios of piers range from 0.4 to 4.0. The four masonry walls are considered perfectly connected at the corners, a feature not always reproduced in the past URM tests. This allows investigating also the contribution of the transverse walls to the strength of the overall building. For walls A and B, Moon et al. 2004, employed masonry arch lintels, whereas for walls 1 and 2, steel lintels were used. A wood diaphragm and a timber roof are present in correspondence of the floors. A preliminary linear analysis is performed to understand possible crack distribution and identify piers and spandrel elements to be used in the macro modeling, Fig. 5.9.

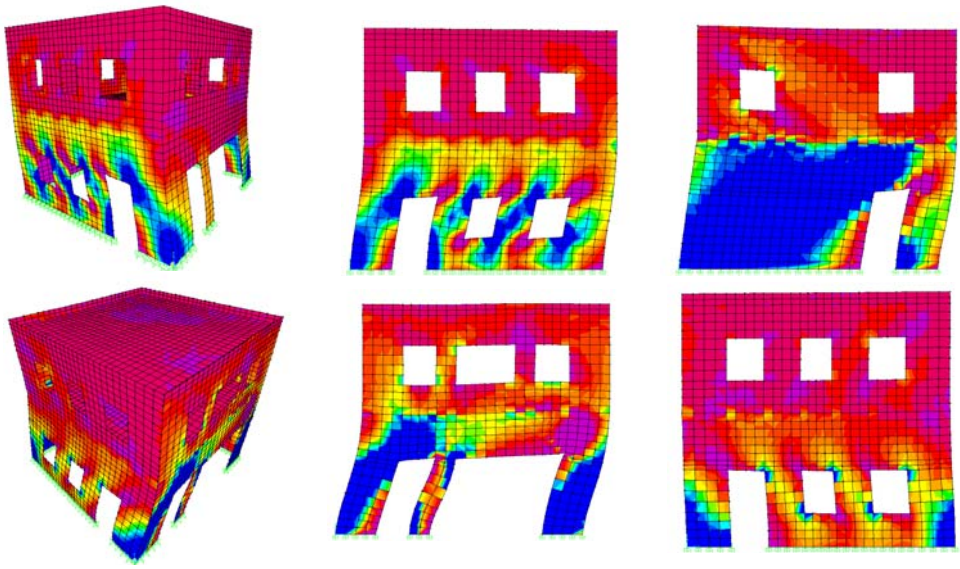

Fig. 5.9 Principal stress distribution

Chen 2011, developed a complete analysis of the prototype using the macro approach and showing the different behavior of the four walls in the model (A, B, 1 and 2). In particular, a comparison between experimental and numerical results is provided in terms of base shear – total drift curves (during a cyclic application of the load), see Fig. 5.10a,b.

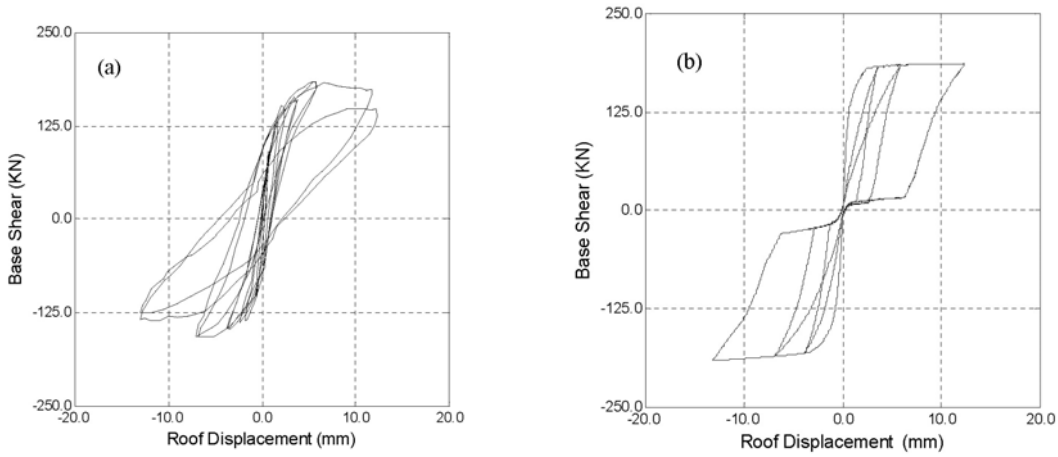

(a) Experimental results (b) Numerical results

Fig. 5.10 Base shear versus roof displacement response of Wall B: (a) Experimental results; (b) Numerical results

In particular, in Chen 2011, a program is also developed for the post processing of the finite element results. As an example, the results obtained for wall B are provided in Fig. 5.11a, b for the maximum positive displacement in terms of shear force and normal force distribution in the piers.

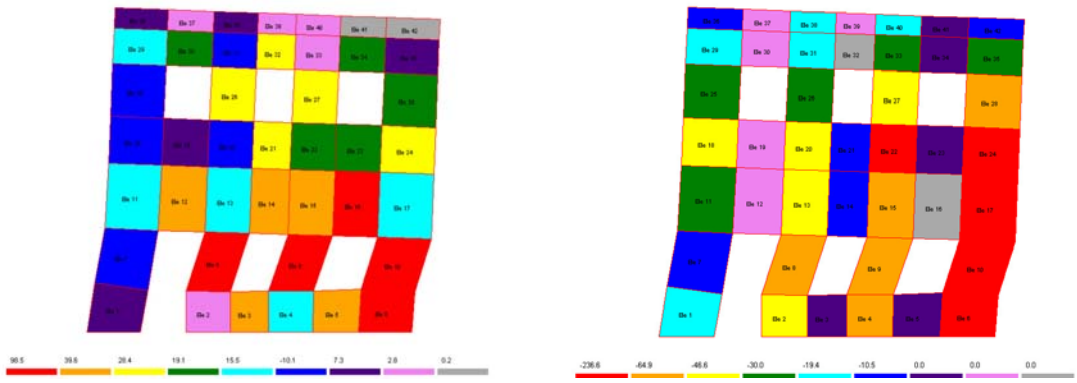

(a) (b)

Fig. 5.11 Shear force (a) and normal force (b) contour levels for the maximum positive displacement

In this work, instead, the focus is the numerical analysis of the wall B prior and after strengthening.

5.2.3 Characterization of the material

Both solid bricks and hollow cored bricks are employed in the structure. The nominal dimensions of both types of bricks are 200 × 89 mm (length × width). The cored bricks contain a longitudinal hole through the center with a diameter of 22 mm. Solid bricks are used for the lower 54 courses in the first story of the test structure to approximately the 3.8 m level, whereas cored bricks are used for the remaining parts of the structure. The mechanical properties of the bricks and mortar are reported in Tab. 5.2. Such characteristics are found to be in agreement both with experimental data collected and the pushover analyses presented in Moon et al. 2004.

Tab. 5.2 Material properties of the masonry

Masonry					
E_m	ν	f_c	f_t	ρ	$\tan\phi$
1500 $[\mathrm{N/mm^2}]$	0,15	10 - solid brick 4 - hollow brick $[\mathrm{N/mm^2}]$	0,1 $[\mathrm{N/mm^2}]$	2219 kg/m^3	0,3

5.2.4 Load conditions

Vertical loading is constituted only by the wall's self weight, and the permanent loads of the first floor and of the roof. In order to numerically reproduce the actual experimental set-up, horizontal loads, depending on the displacement controller, are applied in correspondence to the first and second floor levels of wall B. The masonry self weight, which corresponds to a large percentage of the total gravity load, is supposed for the sake of simplicity, to be concentrated in correspondence to the first and second floors.

5.2.5 Numerical analysis and discussion of the results

The finite element model is made up of 56 nodes and 36 elements. Each panel in the structure is modeled through a single MF element. The results obtained with the MultiFan element model (i.e. failure shear at the base and failure mechanism) are compared with the experimental force–displacement diagrams in Fig. 5.12, where the total shears at the base of walls B are reported. The analysis gives a base shear of 150 and 180 kN for wall B (equal to A in the experimental case), in excellent agreement with the results obtained experimentally for the URM building before and after strengthening, see Moon 2004. The comparison between the results at collapse obtained with the model proposed when strengthening is included in the analysis is also provided in Fig. 5.12 a, b, and Fig. 5.13. In particular, Fig. 5.13 shows the comparison in terms of experimental and numerical results for the 4 cases: masonry modeled as a no tension material with infinite and finite compression strength prior to retrofit and after strengthening. The final aim to get a good estimation of the experimental behavior is achieved.

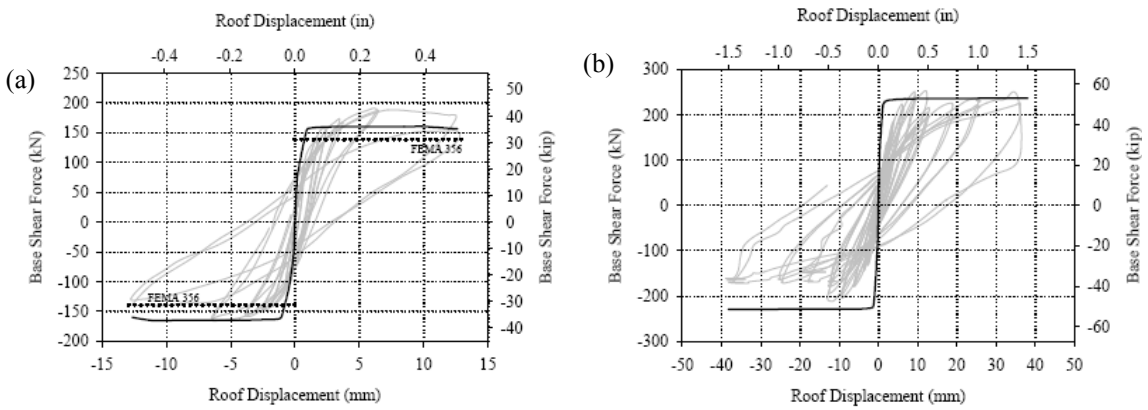

Fig. 5.12a, b Experimental base shear versus roof displacement response of wall B prior (a) and after to retrofit (b)

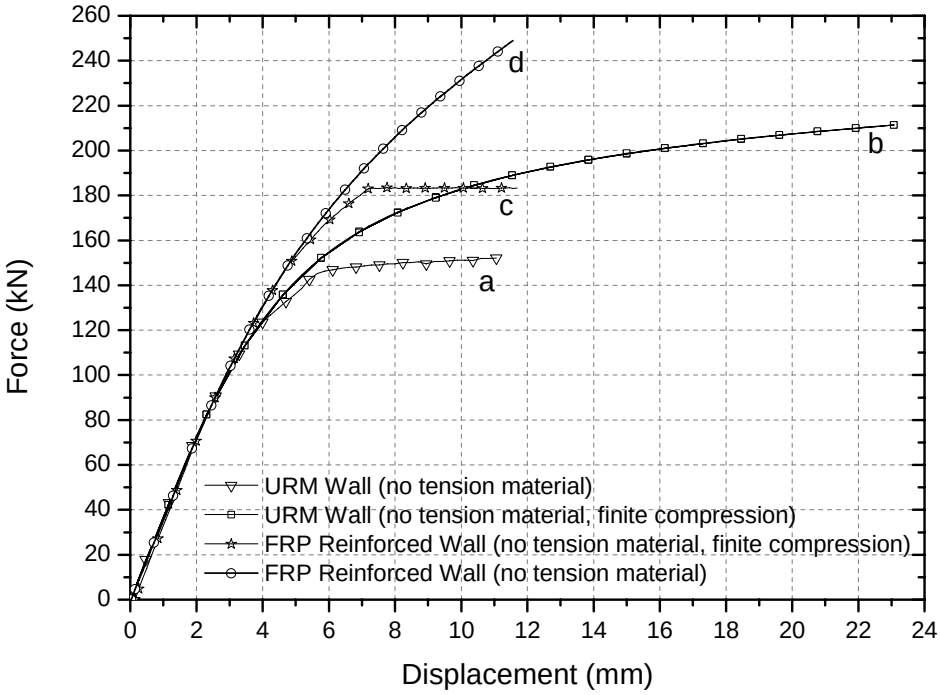

Fig. 5.13 Numerical base shear versus roof displacement response of Wall B prior and after to retrofit

5.2.6 Simplified Pushover analysis

Utilizing the approach in chapter 4, nonlinear pushover analysis of URM perforated walls is also carried out. The program was employed to analyze each wall of the test structure before and after retrofit. Comparisons between the simplified model predictions and the experimental results are provided here. The analysis is carried out to determine the demand on each pier due to the equivalent lateral load. These forces are compared with predetermined values to assess the performance level of each pier and, then, of the facades

and finally of the building. In the case of the nonlinear static method, each spring is defined by a nonlinear force-displacement curve based on the governing failure mode. The analysis is performed by imposing increasing lateral displacements.

The pushover analysis is performed considering 13 elements, where wall 1 to 5 react in the Y direction and wall 6 to 13 react in the X direction. The results in terms of building strength capacity are provided in Tab. 5.3 (global behavior) while the resistance of each pier during the loading process is also provided. It is clear that the simplified approach allows determining the building load capacity due to seismic forces and the increment due to the FRP application. In particular the final strength is 158 kN for the URM building and around 191 kN after FRP retrofit. The numerical results provide a reasonable description of the structural behavior when compared with the experimental results. After the strengthening, the walls can perform an extra contribution due to the influence of the FRP. The collapse is obtained after the failure of two walls (6 and 10) after reaching the load value that cause debonding at the masonry FRP interface. Each wall in any case shows an extra resistance and in particular, the shear response has an important increase due to the FRP application.

Tab. 5.3 Pushover analysis: seismic resistance of FRP piers and URM/strengthened building

	Elastic Limit (kN)		**Cracking Limit (kN)**		**Ultimate Limit (kN)**	
	Before strengthening	After Strengthening	Before strengthening	After Strengthening	Before strengthening	After Strengthening
Local Behavior						
Wall 1	0,42	0,513	0,51	1,07	0,62	1,18
Wall 2	0,21	0,25	0,25	0,52	0,3	0,573
Wall 3	0,43	0,519	0,52	1,08	In 0,63	1,19
Wall 4	1,47	1,78	1,79	3,71	2,17	4,09
Wall 5	0,43	0,519	0,52	1,08	0,63	1,19
Wall 6	23,56	23,5	23,86	0	23,86	0
Wall 7	14,43	15,2	17,52	31,6	20,2	34,9
Wall 8	8,55	9,38	10,39	19,5	12,61	21,5
Wall 9	14,43	15,2	17,52	31,6	20,2	34,9
Wall 10	23,86	23,9	23,86	0	23,86	0
Wall 11	14,62	15,4	17,79	31,9	20,2	35,2
Wall 12	8,66	9,51	10,54	19,7	12,83	21,8
Wall 13	14,62	15,4	17,79	31,9	20,2	35,2
Global Behavior	**125,69**	**131,07**	**142,86**	**173,66**	**158,31**	**191,72**
Displacement (mm)	6		7		8	

The displacements are also in the range described in the experimental analysis available, in particular the elastic stage presents a 6mm drift and at the collapse the global displacement is equal to 8 mm.

5.3 Summary

Numerical modeling of historical masonry constructions is a particularly difficult task, mainly due to lack of knowledge related to the mechanical properties of materials, which renders very difficult the use of advanced nonlinear constitutive models unless an experimental program is carried out.

In this chapter, the MultiFan element developed is used to analyze the structural behavior of two building prototypes experimented at the University of Pavia and at the Georgia Institute of Technology. It is shown that a satisfactory accuracy at the global level is obtained, while keeping a reasonable computational effort for the analyses. This can be achieved when complex assemblages in 3D are analyzed even in the case of cyclic loads or when strengthening techniques are considered.

6 Concluding remarks and future work

The focus of this study was on the seismic retrofit of URM structures using FRP materials as strengthening solution. To the knowledge of the author, there are no specific standard procedures available for this purpose even in the recent Italian Code DM2008. Moreover, the Aquila Earthquake has drastically shown the high vulnerability of masonry construction in the Mid and South Italy region where most of the historical centre have a configuration similar to the Paganica case study illustrated in chapter 2. Nowadays it is clear that the behaviour of a single building cannot be deeply understood without extending the analysis to the entire cluster around.

In this framework a primary issue before performing seismic assessment is the availability of sophisticated numerical tools that allow accurate material model of each component keeping at the same time a reasonable computational time for the structural analysis. Therefore, the primary contributions of this thesis can be synthesized in the development of a material model for the analysis of the FRP-masonry interface and of a suitable finite element for analysis of masonry buildings under seismic actions. In particular, the identification of local effects at the FRP-masonry interface with a micro-modelling approach (currently not addressed in the standard for FRP-masonry substrates) greatly improves the understanding of FRP strengthened structures. The results allow the consolidated knowledge of URM component behaviour, both before and after retrofit, to be utilized more effectively: in fact a model capable of accurately predicting the debonding of FRP from masonry is very useful to develop springs models capable of accurately predicting the response of URM piers or spandrels following retrofit with FRP strips. A summary of the main results of this research is presented in this chapter. Finally, a brief description of areas where future research is recommended is given.

Micro modeling

A first attempt of this study was to fill the lack in the literature of reliable debonding models for the FRP and masonry. Since results in this area are scarce, research efforts are needed. In chapter 3, an approach based on the incremental theory of multi-surface plasticity is presented. Zero-thickness interface elements are used to capture the development and propagation of debonding in the masonry layer adjacent to the adhesive layer. The monotonic constitutive model of the interface is defined by a

convex composite yield criterion, composed by three individual yield functions, where softening behaviour has been considered for all modes (tension, shear and compression). The model is able to assess the influence of several parameters on the FRP-masonry interfacial behaviour, showing that the cohesion and the shear fracture energy of the interface are the most important. Comparisons between the predictions of this model and selected test results have shown that the ultimate load (around to 4kN) and the effective bond length (around 150mm) can be assessed through the numerical analysis. Once the model was validated, the influence of various FRP properties on the effectiveness of URM arch or pier retrofit was investigated, in particular allowing exploring the highly nonlinear pseudo-ductile response associated with progressive debonding. The accuracy of the advanced model developed for the analysis of the FRP-masonry interface was assessed through comparisons with past component tests. A simplified bilinear bond-slip model and an analytical solution were calibrated. Comparing together, experimental, numerical and analytical results, it was possible to conclude that also for FRP-masonry joints, four states are successively found (see chapter 3) but in this case, the softening-debonding stage is very small because the phenomenon of stress propagation along the bond length interests large regions of the adherent and adherend materials even for low load levels.

Furthermore, aiming to improve the existing interface model, a new multi-linear hardening law was proposed for shear and tension modes of failure and implemented in the finite element program Diana as a user subroutine. Coupled behaviour for tension and shear mode was considered for the masonry-FRP interface only in terms of strength but not damage, that is a possible step for future research. This new multi-linear hardening/softening law can be used to describe in a more general way, the behaviour of the FRP-masonry joint, allowing defining the softening due to debonding at the interface as a function of 10 parameters (including the cohesion and the fracture energy of the interface) that can easily be determined based on experimental results. This is very important during the numerical analysis to exploit the ductility of the strengthened system. The updated constitutive law was again used to simulate and predict the stress distribution on curved FRP masonry interfaces for different bond lengths (100, 150, 200 mm) aiming to assess the level of normal and shear stresses in the substrate. Again reasonable good results were obtained if compared with the experimental. These

numerical results are important because scarce FRP masonry related studies are found in the literature, probably due to difficulties on finding an experimental setup able to capture adequate key parameters and overcome the low tensile strength of the masonry when curved joints are analyzed. The big advantage to have a suitable material model for the finite element analysis, despite also some analytical formulation exist to solve simple case studies, is the possibility to analyze complex structures after retrofit. In particular masonry arch bridges or vaults are the structural elements most suitable for this purpose. Therefore, a plane stress finite element model of semi-circular masonry arches strengthened with composite materials was created aiming to reproduce experimental results available in literature. With this numerical model, it was possible to obtain similar peak loads and mechanisms of failure when compared with experiments, in particular, the change of the four hinge failure mechanism for unstrengthened arch to only the three hinge mechanism plus a further release (FRP debonding or shear failure) for the arches strengthened continuously at the intrados or the extrados.

Macro modeling

Based on a strut and tie description of the masonry panel an advanced constitutive model is established able to describe the cyclic behaviour introducing a very simple yield condition. Zero-Length springs have been added to the MultiFan element system to model shear and bending failure modes, the cyclic and the strengthening effects. Experimental data in the literature are used both for the validation of the existing constitutive model and for his extension to describe characteristic features associated with the structural behaviour under cyclic loading. Moreover the micro-modelling strategy is also used to validate the macro-modelling approach. In particular, the MultiFan element proposed has been implemented in the Object-Oriented Nonlinear Dynamic Analysis program Opensees and it is extremely effective for the seismic analysis of masonry buildings. The unloading and re-loading behaviour is described in a nonlinear fashion, adopting suitable laws based on a phenomenological extension of experimental results. The performance of the developed constitutive model is assessed by comparisons against experimental results available in literature, both at the component level (masonry walls) and at the global level (masonry buildings and facades). Comparison between experimental and numerical results showed that the most

relevant features observed such as bending or shear failure, stiffness degradation and energy dissipation are captured by the model, which enables its use for the analysis and study of cluster of masonry structures under cyclic loading. It was observed that the failure patterns were correlated with the amount of compressive loading. For lower confining stress levels, failure occurred by rotation and crushing of part of the wall whereas for higher vertical loads shear failure was activated. Initially, the horizontal load displacement diagrams of the walls exhibited large stiffness and elastic behaviour afterwards continuous stiffness degradation occurred under increasing horizontal deformation. As a benchmark of the new finite element, the building prototypes experimented at the Department of Structural Mechanics of the University of Pavia and at the Georgia Institute of Technology were chosen. In terms of the effectiveness of the retrofit systems investigated, the following conclusions are drawn: FRP reinforcement has the ability to increase base shear capacity of URM buildings, the goal of the FRP techniques is to localize failures close to the base of the building and the numerical model proposed can describe the increase of strengthening due to FRP application. The analytical portion of this study aimed to investigate the ability of simplified models based on springs to predict overall structure response. The model supplied by DM2008 and FEMA356 was modified to include the effect of FRP strips application on the pier response. Based on the results of this analytical study, **s**implified approaches like the pushover springs models presented in chapter 4, can provide good predictions of the response of low-rise URM structures both before and after retrofit providing a suitable tool to estimate the base shear versus top displacement curves.

Recommendations and future work

Nonlinear finite element analysis is a very useful tool to describe the main features characterizing the application of FRP as a reinforcement of arched structures, masonry panels and masonry buildings. Advanced numerical model based on a micro-modelling approach is recommended to predict the bond phenomenon at local level up to failure, identifying the strain and slip distribution, the local bond stress peak and its migration along the bond length at different load levels, while bilinear bond slip model can still be used to provide a simplified description of the debonding process and an estimation of the bond strength necessary to characterize the structural behaviour of a pier after shear or bending strengthening. The constitutive law proposed can be very useful to

understand the failure process even close to collapse, since debonding at the FRP-masonry interface and shear failure of the masonry joints were clearly described with the numerical analysis. Moreover the numerical analyses show that full length GFRP reinforcement placed at the intrados is recommended to increase the strength of the system since present higher peak load values, while full length GFRP reinforcement placed at the extrados is more suitable when the concern is the increase of the ductility. The MultiFan approach is also recommended as a suitable tool to seismic assessment of masonry buildings, since the macro-approach allows a reduction of the computational efforts due to the nonlinear analysis. Moreover from the results, it is clear that in-plane wall retrofits should employ both vertical and horizontal FRP reinforcement to prevent the progressive opening of cracks during cyclic loading due to shear and bending. The effective height of piers should be defined as the height over which a compression strut is likely to form, not the height of adjacent openings and therefore the knowledge of the bending moment at the bottom and top face of the MultiFan element is suitable for this purpose. Future work in several areas uncovered here has to be developed. Further investigations with a structure subjected to dynamic loading are suggested as well as full-scale dynamic tests of similar buildings are recommended to assess influence of these effects on the behaviour of individual piers. A more accurate method of determining the shear strength of URM piers is required. Such a model should include a method to separate diagonal tension failures that occur through units with those that occur in the bed joints. Another improvement is to introduce suitable degradation law for the stiffness and the global energy during the cyclic processes. This is possible by introducing a dependence of these quantities from the drift of a single MultiFan element but it has the drawback of drastically reducing the convergence of the numerical algorithm implemented. On the other hand, for the element itself, it is still necessary to improve convergence at reversals, perform further parametric studies and validation studies, and introduce the out of plane behaviour. Flange participation also affects the structural behaviour when sufficient connection between orthogonal walls is present but was not investigated here. Finally, the macro model developed in the Opensees framework could be developed in a manner suitable for parallel computing making possible the structural analysis of large clusters of masonry buildings in historical centre aiming to assess and mitigate their earthquake risk.

7 References

Addessi, D., S. Marfia and E. Sacco (2002). "A plastic nonlocal damage model." Computer Methods in Applied Mechanics and Engineering **191**(13-14): 1291-1310.

Addessi, D., E. Sacco and A. Paolone (2010). "Cosserat model for periodic masonry deduced by nonlinear homogenization." European Journal of Mechanics a-Solids **29**(4): 724-737.

Aiello, M. A., F. Micelli and L. Valente (2007). "Structural upgrading of masonry columns by using composite reinforcements." Journal of Composites for Construction **11**(6): 650-658.

Aiello, M. A., F. Micelli and Valente (2009). "FRP Confinement of Square Masonry Columns." Journal of Composites for Construction **13**(2): 148-158.

Aiello, M. A. and S. M. Sciolti (2006). "Bond analysis of masonry structures strengthened with CFRP sheets." Construction and Building Materials **20**(1-2): 90-100.

Alfano, G. and E. Sacco (2006). "Combining interface damage and friction in a cohesive-zone model." International Journal For Numerical Methods In Engineering **68**(5): 542-582.

Anthoine, A. (1992). "In-plane behavior of masonry: A literature review." Report EUR 13840 EN, Commission of the European Communities, JRC - Institute for Safety Technology, Ispra, Italy.

Anthoine, A., G. Magonette and G. Magenes (1995). " Shear-compression testing and analysis of brick masonry walls." G. Duma (ed.): Proc. 10th European Conference on Earthquake Engineering, 3, pp. 1657-1662.

Barros, J. A. O., J. T. Oliveira, E. Bonaldo and P. B. Lourenço (2006). "Flexural behavior of reinforced masonry panels." Aci Structural Journal **103**(3): 418-426.

Basílio, I. (2008). "Strengthening of arched masonry structures with composite materials; Reforço de estruturas de alvenaria em arco com materiais compósitos."

Bathe, K.-J. (1996). Finite element procedures. Englewood Cliffs, N.J., Prentice Hall.

Block, P. (2005). " Equilibrium systems : studies in masonry structure." Massachusetts Institute of Technology. Dept.

Block, P. (2009). " Trust Network Analysis : exploring three-dimensional equilibrium." Massachusetts Institute of Technology. Dept.

Braga, F. and M. Dolce (1982). "A method for the analysis of seismic-safe multi-storey buildings." Proc. 6th I.B.Ma.C., Rome: 1088-1099.

Braga, F. and D. Liberatore (1990). "A Finite Element for the Analysis of the Response of Masonry Buildings under Seismic Actions." 5th North American Masonry Conference, Urbana, U.S.A., pp 201-212.

Braga, F. and D. Liberatore (1990). "Elastic Potential Energy, Force Vector and Stiffness of a No-Tension Panel." Atti dell'Istituto di Scienza e Tecnica delle Costruzioni, n. 18, Potenza, Italy.

Braga, F., D. Liberatore and E. Mancinelli (1996). "Numerical Simulation of the Experimental Behavior of Masonry Panels and Walls under Horizontal Loads." 11th World Conference on Earthquake Engineering, Acapulco, Mexico.

Braga, F., D. Liberatore and G. Spera (1998). "A Computer Program for the Seismic Analysis of Complex Masonry Buildings." Computer methods in structural masonry **4**: 309-316.

Brasile, S., R. Casciaro and G. Formica (2007). "Finite element formulation for nonlinear analysis of masonry walls." Computer & Structures, Volume 88, Issue 3-4: 135-143.

Brencich, A. and L. Gambarotta (2005). "Mechanical response of solid clay brickwork under eccentric loading. Part II: CFRP reinforced masonry." Materials And Structures **38**(276): 267-273.

Brencich, A. and S. Lagomarsino (1997). "A Macro-Element dynamic model for masonry shear walls" In G.N. Pande & J. Middleton (ed.s), Computer methods in structural masonry - 4; Proc. Intern. Symp., Pratolino (FI), 3-5 september 1997. Swansea: Books a& Journals International.

Cancelliere, I., M. Imbimbo and E. Sacco (2010). "Experimental tests and numerical modeling of reinforced masonry arches." Engineering Structures **32**(3): 776-792.

Cavicchi, A. and L. Gambarotta (2005). "Collapse analysis of masonry bridges taking into account arch-fill interaction." Engineering Structures **27**(4): 605-615.

Cavicchi, A. and L. Gambarotta (2006). "Two-dimensional finite element upper bound limit analysis of masonry bridges." Computers & Structures **84**(31-32): 2316-2328.

Cavicchi, A. and L. Gambarotta (2007). "Lower bound limit analysis of masonry bridges including arch-fill interaction." Engineering Structures **29**(11): 3002-3014.

Chen, W.-F. and D. J. Han (1988). Plasticity for structural engineers. New York, Springer-Verlag.

Chen, Z. X. (2011). "Non linear multi-fan finite element for analysis of masonry buildings under seismic action." PhD dissertation, University of Rome

Chen, Z. X., C. Maruccio, D. Liberatore and G. Monti (2010). "Nonlinear multifan finite element for analysis of Masonry Buildings under Seismic Action". 14th World Conference on Earthquake Engineering, Greece.

CNR-DT (2004). "Istruzioni per la progettazione, esecuzione e il controllo di interventi di consolidamento statico mediante l'utilizzo di compositi Fibro Rinforzati."

Comite Euro-International du Beton (1990). "Bulletin d'information 195/196, CEB-FIP Model Code." Lusanne, Switzerland.

Croci, G. (1998). "The Basilica of St. Francis of Assisi after the September 1997 Earthquake." Structural engineering international **8**(1): 56-58.

Croci, G. (2001). "Strengthening the Basilica of St. Francis of Assisi after the September 1997 Earthquake." Structural engineering international **11**: 207-211.

D'Asdia, P. and A. Viskovic (1994). "L'analisi sismica degli edifici in muratura. " Ingegneria Sismica, Anno XI, N.1, 1994, pp. 32-42.

Dai, J., T. Ueda and Y. Sato (2005). "Development of the Nonlinear Bond Stress-Slip Model of Fiber Reinforced Plastics Sheet-Concrete Interfaces with a Simple Method." Journal of composites for construction. **9**(1): 52.

De Borst R. (1991). "Computational methods in non-linear solid mechanics: part I1, Material non-linearity and solution techniques." TNO-IBBC and TU-Delft Report nr. 25-2-90-5-04, TNO Building and construction research, Delft, the Netherlands

De Lorenzis, L., J. G. Teng and L. Zhang (2006). "Interfacial stresses in curved members bonded with a thin plate." International Journal Of Solids And Structures **43**(25-26): 7501-7517.

De Lorenzis, L., R. Dimitri and A. La Tegola (2007). "Reduction of the lateral thrust of masonry arches and vaults with FRP composites." Construction and Building Materials **21**(7): 1415-1430.

De Lorenzis, L. and G. Zavarise (2008). "Modeling of mixed-mode debonding in the peel test applied to superficial reinforcements." International Journal Of Solids And Structures **45**(20): 5419-5436.

De Jong, M. J., L. De Lorenzis, S. Adams and J. A. Ochsendorf (2008). "Rocking Stability of Masonry Arches in Seismic Regions." Earthquake Spectra **24**(4): 847-865.

Dunne, F. and N. Petrinic (2006). "Introduction to computational plasticity." Oxford Univ. Press

Feenstra, P. H. (1993). Computational aspects of biaxial stress in plain and reinforced concrete. Delft, Netherlands, Delft University Press.

FIB Bulletin No.14. (2001). "Externally bonded FRP reinforcement for RC structures." Lusanne, Switzerland.

Foraboschi, P. (2004). "Strengthening of Masonry Arches with Fiber-Reinforced Polymer Strips." Journal of composites for construction. **8**(3): 191.

Gambarotta, L. and S. Lagomarsino (1997). "Damage models for the seismic response of brick masonry shear walls .1. The mortar joint model and its applications." Earthquake Engineering & Structural Dynamics **26**(4): 423-439.

Gambarotta, L. and S. Lagomarsino (1997). "Damage models for the seismic response of brick masonry shear walls .2. The continuum model and its applications." Earthquake Engineering & Structural Dynamics **26**(4): 441-462.

Ganz, H. R. and B. Thurlimann (1983). "Strength of brick walls under normal force and shear." Proceedings of the 8th international symposium on load bearing brickwork, London, UK.

Garbin, E., N. Galati, A. Nanni and C. Modena (2007). "Provisional design guidelines for the strengthening of masonry structures subject to in-plane loading." 10th NAMC. St.Louis, Missouri, USA, 13 pp. - CD-ROM.

Gilbert, M. (2005). "Ring: Theory and modelling guide. Computational limit analysis and design unit." University of Sheffield, UK.

Gilbert, M., C. Casapulla and H. M. Ahmed (2006). "Limit analysis of masonry block structures with non-associative frictional joints using linear programming." Computers & Structures **84**(13-14): 873-887.

Gilbert, M. and C. Melbourne (1994). "Rigid-block analysis of masonry structures." Structural engineer **72**(21): 356.

Grande, E., M. Imbimbo and E. Sacco (2011). "Bond behaviour of CFRP laminates glued on clay bricks: Experimental and numerical study." Composites Part B-Engineering **42**(2): 330-340.

Grande, E., G. Milani and E. Sacco (2008). "Modelling and analysis of FRP-strengthened masonry panels." Engineering Structures **30**(7): 1842-1860.

Heyman, J. (1982). The masonry arch. Chichester; New York, E. Horwood ; Halsted Press.

Heyman, J. (1995). The stone skeleton : structural engineering of masonry architecture. Cambridge; New York, Cambridge University Press.

Heyman, J. (2007). Structural Analysis : A Historical Approach. Cambridge, Cambridge University Press.

Hill, R. (1950). The Mathematical theory of plasticity, by R. Hill. Oxford, the Clarendon press.

Hill, R. (1998). The mathematical theory of plasticity. Oxford, Clarendon Press.

Huerta Fernández, S. (2001). "Mechanics of masonry vaults: The equilibrium approach."

Koiter, W. T. (1953). "Stress-strain relations, uniqueness and variational theorems for elasticplastic materials with a singular yield surface." Q. Appl. Math., 11(3), pp. 350-354.

Icomos (2001). "Recommendations for the analysis, conservation and structural restoration of architectural heritage."

Lourenço, P. B., J. G. Rots and P. H. Feenstra (1995). "A tensile Rankine type orthotropic model for masonry." Computer methods in structural masonry, 3, eds.

Lourenço, P. B. (1996). "Computational strategies for masonry structures." PhD dissertation; Delft, the Netherlands.

Lourenco, P. B. and J. G. Rots (1997). "Multisurface interface model for analysis of masonry structures." Journal Of Engineering Mechanics-Asce **123**(7): 660-668.

Lourenco, P. B., R. De Borst and J. G. Rots (1997). "A plane stress softening plasticity model for orthotropic materials." International Journal For Numerical Methods In Engineering **40**(21): 4033-4057.

Lourenco, P. B., J. G. Rots and J. Blaauwendraad (1998). "Continuum model for masonry: Parameter estimation and validation." Journal Of Structural Engineering-Asce **124**(6): 642-652.

Lourenco, P. B. (2000). "Anisotropic softening model for masonry plates and shells." Journal Of Structural Engineering-Asce **126**(9): 1008-1016.

Lourenço, P. B. (2001). "Analysis of historical constructions: From thrust-lines to advanced simulations." Historical constructions, University of Minho, Guimaraes, Portugal.

Lourenço, P. B. (2002). "Computations of historical masonry constructions." Progress in structural engineering and materials

Lourenço, P. B. (2004). "Analysis and restoration of ancient masonry structures: Guidelines and Examples." Innovative materials and technologies for restoration, University of Lecce, Italy.

Lourenco, P. B. (2006). "Recommendations for restoration of ancient buildings and the survival of a masonry chimney." Construction and Building Materials **20**(4): 239-251.

Lourenco, P. B. (2006). "Structural masonry and earthquakes." Construction and Building Materials **20**(4): 199-199.

Lourenço, P. B. (2007). "Structural behavior of civil engineering structures : highlight in historical and masonry structures."

Lourenço, P. B. (2007). "Structural restoration of monuments : recommendations and advances in research and practice."

Lourenco, P. B., D. V. Oliveira, P. Roca and A. Orduna (2005). "Dry joint stone masonry walls subjected to in-plane combined loading." Journal Of Structural Engineering-Asce **131**(11): 1665-1673.

Lu, X. Z., J. G. Teng, L. P. Ye and J. J. Jiang (2005). "Bond-slip models for FRP sheets/plates bonded to concrete." Engineering Structures **27**(6): 920-937.

Lu, X. Z., L. P. Ye, J. G. Teng and J. J. Jiang (2005). "Meso-scale finite element model for FRP sheets/plates bonded to concrete." Engineering Structures **27**(4): 564-575.

Lu, X. Z., J. J. Jiang, J. G. Teng and L. P. Ye (2006). "Finite element simulation of debonding in FRP-to-concrete bonded joints." Construction and Building Materials **20**(6): 412-424.

Luciano, R. and E. Sacco (1997). "Homogenization technique and damage model for old masonry material." International Journal Of Solids And Structures **34**(24): 3191-3208.

Luciano, R. and E. Sacco (1998). "A damage model for masonry structures." European Journal of Mechanics a-Solids **17**(2): 285-303.

Luciano, R. and E. Sacco (1998). "Damage of masonry panels reinforced by FRP sheets." International Journal Of Solids And Structures **35**(15): 1723-1741.

Magenes, G. and G. M. Calvi (1996). "Perspectives for the calibration of simplified methods for the seismic analysis of masonry walls." L. Gambarotta (ed.), Masonry Mechanics between theory and practice, Proc. Nat. Conf. , Messina, 18-20 september: 503-512.

Magenes, G. (2000). "A method for pushover analysis in seismic assessment of masonry building." 12th World Conference on Earthquake Engineering, Auckland, New Zeland, January 30-February 4, (CD-ROM)

Magenes, G. and G. M. Calvi (1997). "In-plane seismic response of brick masonry walls." Earthquake Engineering & Structural Dynamics **26**(11): 1091-1112.

Magenes, G., G. R. Kingsley and G. M. Calvi (1995). "Seismic testing of a full-scale, two-story masonry building: test procedure and measured experimental response." Consiglio nazionale delle ricerche, Gruppo nazionale per la Difesa dai terremoti, Pavia, Italy.

Maravegias, S. and T. C. Triantafillou (1996). "Numerical study of anchors for composite prestressing straps." Composite Structures **35**(3): 323-330.

Marfia, S., M. Ricamato and E. Sacco (2008). "Stress Analysis of Reinforced Masonry Arches." International Journal for Computational Methods in Engineering Science and Mechanics **9**(2): 77-90.

Marfia, S. and E. Sacco (2001). "Modeling of reinforced masonry elements." International Journal Of Solids And Structures **38**(24-25): 4177-4198.

Maruccio, C., I. Basilio, D. V. Oliveira and P. B. Lourenço (2009). "Nonlinear finite element analysis of FRP strengthened masonry arches". 3º Convegno Nazionale Meccanica delle Strutture in Muratura Rinforzate con Compositi, Venice (Italia).

Maruccio, C., Z. X. Chen, D. V. Oliveira, G. Monti and P. B. Lourenço (2010). "Nonlinear Finite Element Analysis of Strengthened Masonry Buildings subject to Seismic Action". Tenth International Conference on Computational Structures Technology, Valencia (Spain), Civil-Comp Proceedings.

Maruccio, C., D. V. Oliveira and P. B. Oliveira (2008). "Development of a constitutive model for the masonry - FRP interface behaviour". 8th World congress on computational mechanics, Venice (Italy).

Maruccio, C., D. V. Oliveira and P. B. Lourenço (2009). "An advanced constitutive model for the FRP - masonry interfacial behaviour". Congreso de Métodos Numéricos en Ingeniería, Universidade Politécnica da Catalunha, Barcelona (Spain).

Maruccio, C., D. V. Oliveira and P. B. Lourenço (2009). "Analisi numerica del comportamento strutturale di un ponte in muratura". XIII Convegno di Ingegneria Sismica, Bologna (Italia).

Maruccio, C., D. V. Oliveira, G. Monti and P. B. Lourenço (2010). "Nonlinear analysis of masonry structures: comparison between micro-modeling and macro-modeling approaches". 4th European conference on computational mechanics, Paris (France).

Massart, T. J., R. H. J. Peerlings and M. G. D. Geers (2007). "Structural Damage Analysis of Masonry Walls using Computational Homogenization." International Journal of Damage Mechanics **16**(2): 199-226.

Milani, G., P. B. Lourenco and A. Tralli (2006). "Homogenised limit analysis of masonry walls, Part I: Failure surfaces." Computers & Structures **84**(3-4): 166-180.

Milani, G., P. B. Lourenco and A. Tralli (2006). "Homogenised limit analysis of masonry walls, Part II: Structural examples." Computers & Structures **84**(3-4): 181-195.

Monti, G., C. Maruccio and A. Lucchini (2009). "Structural analysis of a strategic building." Proc.
of the Sustainable Infrastructure Strategies Conference, Rome (Italy)

Moon, F. L. (2004). "Seismic strengthening of low-rise unreinforced masonry structures with flexible diaphragms." PhD Dissertaion; Georgia Institute of Technology, Atlanta, GA.

Nanni, A. and G. Tumialan (2003). "Fiber Reinforced Composites for the Strengthening of Masonry Structures. " Structural Engineering International, IABSE, Zurich, Switzerland, SEI Vol. 13, No. 4, pp. 271-278.

Ochsendorf J. (2002). "Collapse of Masonry Structure: stability and safety of masonry arches, vaults, and buttresses under static and dynamic loading, based on limit analysis." PhD Dissertation, Cambridge University.

Oliveira, D. V. and P. B. Lourenco (2004). "Implementation and validation of a constitutive model for the cyclic behaviour of interface elements." Computers & Structures **82**(17-19): 1451-1461.

Oliveira, D. V., P. B. Lourenco and P. Roca (2006). "Cyclic behaviour of stone and brick masonry under uniaxial compressive loading." Materials And Structures **39**(2): 247-257.

Oliveira, D. V., I. Basilio and P. B. Lourenço (2010). "Experimental Behavior of FRP Strengthened Masonry Arches." Journal of Composites for Construction **14**(3): 312-322.

Oliveira, D. V., I. Basilio and P. B. Lourenço (2011). "Experimental Bond Behavior of FRP Sheets Glued on Brick Masonry." Journal of Composites for Construction **15**(1): 32-41.

Oliveira, D. V., C. Maruccio and P. B. Lourenço (2007). "Numerical modelling of a load test on a masonry arch bridge". Arch Bridges '07 Conference, Funchal, Madeira (Portugal).

Orduña, A. (2003). "Seismic assessment of ancient masonry structures by rigid blocks limit analysis." PhD Dissertation, Universidade do Minho, Guimarães, Portugal.

Orduna, A. and P. B. Lourenco (2003). "Cap model for limit analysis and strengthening of masonry structures." Journal Of Structural Engineering-Asce **129**(10): 1367-1375.

Orduna, A. and P. B. Lourenco (2005). "Three-dimensional limit analysis of rigid blocks assemblages. Part II: Load-path following solution procedure and validation." International Journal Of Solids And Structures **42**(18-19): 5161-5180.

Pena, F., P. B. Lourenco, N. Mendes and D. V. Oliveira (2010). "Numerical models for the seismic assessment of an old masonry tower." Engineering Structures **32**(5): 1466-1478.

Piet (1970). "Prescripciones del Instituto Eduardo Torroja: Obras de Fábrica." Madrid, Spain

Pina-Henriques, J. and P. B. Lourenco (2006). "Masonry compression: a numerical investigation at the meso-level." Engineering Computations **23**(3-4): 382-407.

Roca, P. (2006). "Assessment of masonry shear-walls by simple equilibrium models." Construction and Building Materials **20**(4): 229-238.

Romano, A. and J. Ochsendorf (2010). "The Mechanics of Gothic Masonry Arches." International Journal of Architectural Heritage **4**(1): 59-82.

RSA (1983). "Regulamento de segurança e acções para estruturas de edifícios e pontes. Decreto-Lei N.º235/83." Imprensa Nacional, Casa da Moeda, Lisboa, Portugal.

Sacco, E. (2009). "A nonlinear homogenization procedure for periodic masonry." European Journal of Mechanics a-Solids **28**(2): 209-222.

Sacco, E. and J. Toti (2010). "Interface Elements for the Analysis of Masonry Structures." International Journal for Computational Methods in Engineering Science and Mechanics **11**(6): 354-373.

Schellekens, J. and R. De Borst (1993). "On the numerical integration of interface elements." Int. J. Num. Meth. Engrg., 36, pp. 43-66.

Senthivel, R. and P. B. Lourenco (2009). "Finite element modelling of deformation characteristics of historical stone masonry shear walls." Engineering Structures **31**(9): 1930-1943.

Tianyi Yi. (2004). "Experimental Investigation and Numerical Simulation of an Unreinforced Masonry Structure with Flexible Diaphragms." PhD Dissertation, Georgia Institute of Technology

TNO Building and Construction Research (1999). "Diana User's Manual Release 8.2." Delft, The Netherlands

Tomazevic, M. (1978). "The computer program POR." Ljubljana, Institute for Testing and Research in Materials and Structures-ZRMK

Triantafillou, T. C. (1998). "Composites: a new possibility for the shear strengthening of concrete, masonry and wood." Composites Science and Technology **58**(8): 1285-1295.

Triantafillou, T. (1998). "Strengthening of Masonry Structures Using Epoxy-Bonded FRP Laminates." Journal of composites for construction **2**(2): 96-104.

Triantafillou, T. and C. Antonopoulos (2000). "Design of concrete flexural members strengthened in shear with FRP." J. Comp. for Constr., ASCE, **4**(4): 198-205.

Trovalusci, P. and R. Masiani (2003). "Non-linear micropolar and classical continua for anisotropic discontinuous materials." International Journal of Solids and Structures **40**(5): 1281-1297.

Trovalusci, P. and R. Masiani (2005). "A multifield model for blocky materials based on multiscale description." International Journal of Solids and Structures **42**(21-22): 5778-5794.

Tumialan, G. (2001). "Strengthening of masonry structures with FRP composites." PhD Dissertation; University of Missouri – Rolla, Usa.

Turco, V., S. Secondin, A. Morbin, M. R. Valluzzi and C. Modena (2006). "Flexural and shear strengthening of un-reinforced masonry with FRP bars." Composites Science And Technology **66**(2): 289-296.

Valluzzi, M. R., M. Valdemarca and C. Modena (2001). "Behavior of brick masonry vaults strengthened by FRP laminates." Journal of Composites for Construction **5**(3): 163-169.

Valluzzi, M. R., D. Tinazzi and C. Modena (2002). "Shear behavior of masonry panels strengthened by FRP laminates." Construction and Building Materials **16**(7): 409-416.

Valluzzi, M. R., L. Binda and C. Modena (2002). "Experimental and analytical studies for the choice of repair techniques applied to historic buildings." Materials And Structures **35**(249): 285-292.

Valluzzi, M. R., L. Binda and C. Modena (2005). "Mechanical behaviour of historic masonry structures strengthened by bed joints structural repointing." Construction and Building Materials **19**(1): 63-73.

Valluzzi, M. R., D. Tinazzi and C. Modena (2005). "Strengthening of masonry structures under compressive loads by FRP strips: Local-global mechanical behaviour." Science and Engineering of Composite Materials **12**(3): 203-218.

Valluzzi, M. R. (2007). "On the vulnerability of historical masonry structures: analysis and mitigation." Materials And Structures **40**(7): 723-743.

Yuan, H., J. G. Teng, R. Seracino, Z. S. Wu and J. Yao (2004). "Full-range behavior of FRP-to-concrete bonded joints." Engineering Structures **26**(5): 553-565.

Yuan, H., J. F. Chen, J. G. Teng and X. Z. Lu (2007). "Interfacial stress analysis of a thin plate bonded to a rigid substrate and subjected to inclined loading." International Journal of Solids and Structures **44**(16): 5247-5271.

Zienkiewicz, O. C., R. L. Taylor and Knovel (2005). "The finite element method for solid and structural mechanics."

Zienkiewicz, O. C., R. L. Taylor and J. Z. Zhu (2005). "The finite element method its basis and fundamentals."

Zucchini, A. and P. B. Lourenco (2002). "A micro-mechanical model for the homogenisation of masonry." International Journal Of Solids And Structures **39**(12): 3233-3255.

Zucchini, A. and P. B. Lourenco (2004). "A coupled homogenisation-damage model for masonry cracking." Computers & Structures **82**(11-12): 917-929.

Zucchini, A. and P. B. Lourenco (2009). "A micro-mechanical homogenisation model for masonry: Application to shear walls." International Journal Of Solids And Structures **46**(3-4): 871-886.

Appendix 1: FRP-masonry interface material model (Fortran implementation)

```
subroutine usrifc(u0, du, nt, age0, dtime, temp0, dtemp, elemen,
     $                 intpt, coord, se, iter, usrmod, usrval, nuv,
     $                 usrsta, nus, usrind, nui, tra, stiff )
c
      character*6      usrmod
      integer          nt, nuv, nus, nui, elemen, intpt, iter
      double precision u0(nt),du(nt), age0, dtime, temp0, dtemp,
     $                 coord(3), se(nt,nt), usrval(nuv), usrsta(nus),
     $                 tra(nt), stiff(nt,nt)
      integer          usrind(nui)
C
C.....................................................
C...  DIANA/NL/XQ31/IFCLIB/IFMAS1
C...
C...   Composite 2d interface plasticity model for masonry (strain
hardening):
c...       - straight tension cut-off
c...       - Coulomb friction law
c...       - elliptical cap
c...
c...  Softening in tension
c...       - Exponentional law
c...       - Multilinear law
c...  Softening in shear
c...       - Exponentional law
c...       - Multilinear law
c...  Hardening/Softening in compression
C...       - Parabolic hardening
c...       - Parabolic/Exponential softening
c...
c...  Return mapping
c...       - Newton-Raphson Method
c...
c...  Tangent operator
c...       - Consistent
c...
c...  Local contol parameters
c...       - MITER = 30     , Maximum number of local iterations
c...       - EPS0  = 1.D-5  , Tolerance in the return mapping
C...
C...  called from: DIANA/NL/XQ31/ELMYN/YNIF
C...
C.....................................................................
..
C
      double precision eps0
      integer          mtr
      parameter        ( eps0 = 1.d-5, mtr=2 )
C
      DOUBLE PRECISION UV
C
      INTEGER          LIN, LOUT
      COMMON /INOUT /  LIN, LOUT
C
```

```
      LOGICAL          SW
      COMMON /SWITCH/  SW(6)
C
      DOUBLE PRECISION TRAT(MTR), U(MTR), DTRA(MTR), EPS, f, f1, f2,
f3,
     $                    upeq, dl1, dl2, dl3, ft, dyiedk, c, tanphi,
gfi,
     $                        gfii, ft0, c0, tanph0, fc0, capval(2),
frcval(3),
     $                hs(10),
     $                p(mtr,mtr), ptra(mtr), fc, alfa, usrst1(3),
     $                mocval(2)
      INTEGER          ISPLSV, idum, modul
      LOGICAL          SWSV(6), tensil, shear, cap
      character*8      mode
c
      CALL LMOVE( SW, SWSV, 6 )
c      IF ( elemen.EQ.1 .AND. intpt.EQ.1 ) CALL LSET( .TRUE., SW(1), 6
)
c
c...     Preliminary Checks
      if ( nt .ne. 2 ) THEN
         print *, 'SUBROUTINE VALID ONLY FOR PLANE STRESS'
         print *, 'PLEASE UPDATE CODE'
         call prgerr ( 'USRIFC', 1)
      end if
c
      if ( usrmod .eq. 'MASINT' ) THEN
      goto 5000
cm
      else
      if ( usrmod .eq. 'FRPINT' ) THEN
      goto 2000
cm
      end if

 5000 continue
      end if
c
c
c      print *, 'PLEASE PROVIDE APPROPRIATE usrifc.f'
c      call prgerr ( 'USRIFC', 1)

c
      if ( nuv .ne. 10 ) THEN
         print *, 'WRONG NUMBER OF MATERIAL PARAMETERS <> 10'
         print *, 'PLEASE PROVIDE AS INPUT:'
         print *,
     $     'ft  GfI  c  tanphi  tanpsi  GfII  fm  Css Gfc eps_peak'
         call prgerr ( 'USRIFC', 1)
      end if
c
      if ( nus .ne. 3 ) THEN
         print *, 'WRONG NUMBER OF STATE VARIABLES <> 3'
         print *, 'PLEASE PROVIDE AS INPUT: 0.0  0.0  0.0'
         call prgerr ( 'USRIFC', 1)
      end if
c
      if ( nui .ne. 1 ) THEN
```

```
         print *, 'WRONG NUMBER OF INTEGER INDICATORS <> 1'
         print *, 'PLEASE PROVIDE AS INPUT: 0'
         call prgerr ( 'USRIFC', 1)
      end if
c
c...     Material Parameters
c...     Tension mode
      ft        = usrval(1)
      gfi       = usrval(2)
      frcval(1) = usrval(3)
      frcval(2) = usrval(4)
      frcval(3) = usrval(5)
      gfii      = usrval(6)
      capval(1) = usrval(7)
      capval(2) = usrval(8)
      c         = frcval(1)
      alfa      = gfi / gfii * c / ft
      isplsv    = usrind(1)
      mocval(1) = usrval(9)
      mocval(2) = usrval(10)
c
c...     Initialize
      usrind(1) = 0
      tanphi    = 0.D0
      fc        = 0.D0
      tensil    = .false.
      shear     = .false.
      cap       = .false.
      dl1       = 0.d0
      dl2       = 0.d0
      dl3       = 0.d0
      CALL RSET( 0.D0, p, nt*nt )
      p(1,1) = 2.D0
      p(2,2) = 2.D0 * capval(2)
      call rmove ( usrsta, usrst1, nus )
C
C...     PREDICTOR
      CALL UVPW( u0, DU, nt, U )
      CALL RAB( se, nt, nt, DU, 1, DTRA )
      CALL UVPW( TRA, DTRA, nt, TRAT )
      IF ( SW(2) ) THEN
         CALL PRIVEC( u0, nt, 'U-0   ' )
         CALL PRIVEC( DU, nt, 'DU-0  ' )
         CALL PRIVEC( U, nt, 'U-NEW ' )
         CALL PRIVEC( TRA, nt, 'TRA-0 ' )
         CALL PRIVEC( DTRA, nt, 'DTRA-0' )
         CALL PRIVEC( TRAT, nt, 'TRAT-0' )
      END IF
c
c...     Shear stress is assumed positive
c...     In the end if the return mapping follows a correction
      modul = 0
      if ( trat(2) .ne. 0.d0 ) modul = trat(2) / abs( trat(2) )
      trat(2) = abs( trat(2) )
c
c...     yield properties at test stress
      upeq = usrsta(1) + alfa * usrsta(2)
      call cutoha( ft, upeq, dyiedk, usrval(1), gfi )
```

```
      upeq = usrsta(1) / alfa + usrsta(2)
      call coulha( c, tanphi, upeq, dyiedk, frcval, gfii )
      call caphar2( fc, usrsta(3), dyiedk, capval, mocval )
      ft0    = ft
      c0     = c
      tanph0 = tanphi
      fc0    = fc
C
C...     YIELD FUNCTION AT TEST STRESS
c...
c...     f1 = trat(1) - ft
c...
c...     f2= trat(2) + trat(1)*tanphi - c
c...
c...                        T                2
c...     F3 = 1/2 * [TRAT] *[P]*[TRAT] - fc
      f1 = trat(1) - ft
      f2 = trat(2) + trat(1) * tanphi - c
      call rab( p, nt, nt, trat, 1, ptra )
      f3 = .5D0 * uv( trat, ptra, nt ) - fc * fc
c
c...       Tolerance is the squared average of possible active yield
functions
      f = .5D0 * sqrt( ( f1 + abs( f1 ) ) ** 2 +
     $    ( f2 + abs( f2 ) ) ** 2 + ( f3 + abs( f3 ) ) ** 2 )
      if ( se(1,1) .lt. 1.D5 ) then
         EPS = max( EPS0 * ABS( F ), 1.D-14 )
      else
c
c...        Correction for dummy stifness
         EPS = max( EPS0 * EPS0 * ABS( F ), 1.D-14 )
      endif
      IF ( SW(2) ) THEN
         CALL PRIVAL( F1, 'F1-0' )
         CALL PRIVAL( F2, 'F2-0' )
         CALL PRIVAL( F3, 'F3-0' )
      END IF
C
      if ( f1 .gt. eps ) tensil = .true.
      if ( f2 .gt. eps ) shear = .true.
      if ( f3 .gt. eps ) cap = .true.
c
c...     Return mapping
      IF ( ( tensil ) .or. ( shear ) .or. ( cap ) ) then
c
c...        Start with single modes
         if ( tensil ) then
            upeq = usrsta(1) + alfa * usrsta(2)
            call rmcuto( nt, se, tra, trat, eps, upeq,
     $                   stiff, dl1, idum, modul, f1, usrval )
            usrsta(1) = upeq - alfa * usrsta(2)
c
c...           Check other modes
            f2 = abs( tra(2) ) + tra(1) * tanph0 - c0
            call rab( p, nt, nt, tra, 1, ptra )
            f3 = .5D0 * uv( tra, ptra, nt ) - fc0 * fc0
            if ( f2 .lt. eps .and. f3 .lt. eps ) then
               f = f1
               mode = 'TENSION '
```

```
               goto 1000
            end if
         end if
c
         if ( shear ) then
            call rmove ( usrst1, usrsta, nus )
            upeq = usrsta(1) / alfa + usrsta(2)
            call rmcoula( nt, se, tra, trat, eps, upeq, stiff, dl2,
     $                    idum, modul, f2, usrval )
            usrsta(2) = upeq - usrsta(1) / alfa
c
c...           Check other modes
            f1 = tra(1) - ft0
            call rab( p, nt, nt, tra, 1, ptra )
            f3 = .5D0 * uv( tra, ptra, nt ) - fc0 * fc0
            if ( f1 .lt. eps .and. f3 .lt. eps ) then
               f = f2
               mode = 'SHEAR   '
               goto 1000
            end if
         end if
c
         if ( cap ) then
            call rmove ( usrst1, usrsta, nus )
            call rmacap( nt, se, tra, trat, eps, usrsta(3),
     $                  stiff, dl3, idum, modul, f3, usrval )
c
c...           Check other modes
            f1 = tra(1) - ft0
            f2 = abs( tra(2) ) + tra(1) * tanph0 - c0
            if ( f1 .lt. eps .and. f2 .lt. eps ) then
               f = f3
               mode = 'CAP     '
               goto 1000
            end if
         endif
c
c...        Now the corners
c...        Corner 12
         if ( tensil .or. shear ) then
            call rmove ( usrst1, usrsta, nus )
            call  rmco12a(  nt,  se,  tra,  trat,  eps,  usrsta(1),
usrsta(2),
     $                    stiff, dl1, dl2, alfa, idum, modul, f1, f2,
     $                    usrval )
            call rab( p, nt, nt, tra, 1, ptra )
            f3 = .5D0 * uv( tra, ptra, nt ) - fc0 * fc0
            if ( f3 .lt. eps .and. dl1 .gt. 0.d0 .and. dl2 .gt. 0.d0 )
     $         then
               f = max( abs( f1) , abs( f2 ) )
               mode = 'CORNER12'
               goto 1000
            end if
         end if
c
c...        Corner 23
         if ( shear .or. cap ) then
            call rmove ( usrst1, usrsta, nus )
```

```
            upeq = usrsta(1) / alfa + usrsta(2)
            call rmco23a( nt, se, tra, trat, eps, upeq, usrsta(3),
     $         stiff, dl2, dl3, idum, modul, f2, f3, usrval )
            usrsta(2) = upeq - usrsta(1) / alfa
            f1 = tra(1) - ft0
            if ( f1 .lt. eps .and. dl2 .gt. 0.d0 .and. dl3 .gt. 0.d0 )
     $         then
               f = max( abs( f2) , abs( f3 ) )
               mode = 'CORNER23'
               goto 1000
            end if
         end if
c
c...        Return mapping was not successful
         call errmsg( 'NLXQ31', 5, elemen, intpt, 9.999d0, eps,
     $                'MASINT:::IFMAS1' )
 1000       continue
c
         usrind(1) = +1
C
      ELSE
C
c...        Elastic
         IF ( ISPLSV .EQ. +1 ) usrind(1) = -1
         CALL RMOVE( se, stiff, nt*nt )
         CALL UVPW( TRA, DTRA, nt, TRA )
      END IF
C
      IF ( SW(2) ) THEN
         CALL PRIVEC( TRA, nt, 'TRAn+1' )
         CALL PRIMAT( stiff, nt, nt, 'stiff..' )
      END IF
C
      IF ( ( usrind(1) .EQ. 1 ) .AND. ( ISPLSV .NE. 1 ) ) THEN
         WRITE ( LOUT, 6 ) elemen, intpt, mode, F
      END IF
C
      CALL LMOVE( SWSV, SW, 6 )
C
    6 FORMAT ( ' ELEMENT:', I4, '   IP:', I4, ' BECOMES PLASTIC IN ',
     $         A8, ' : ACCURACY  F=', 1P, E11.3 )
c      end if
c
      goto 8000
c
c     if ( usrmod .eq. 'FRPINT' ) THEN
c     goto 2000
cm
 2000 continue
c     end if
c      if ( usrmod .ne. 'FRPINT' ) THEN
c         print *, 'YIELD CRITERIA <MASINT> NOT USED'
c        print *, 'YIELD CRITERIA <FRPINT> NOT USED'
c         print *, 'PLEASE PROVIDE APPROPRIATE usrifc.f'
c         call prgerr ( 'USRIFC', 1)
c      end if
c
      if ( nuv .ne. 19 ) THEN
         print *, 'WRONG NUMBER OF MATERIAL PARAMETERS <> 19'
```

```
         print *, 'PLEASE PROVIDE AS INPUT:'
         print *,
     $     'ft  GfI  c  tanphi  tanpsi  GfII  fm  Css Gfc eps_peak
     $      hs1 hs2 hs3 hs4 hs5 hs6 hs7 hs8 hs9 '
         call prgerr ( 'USRIFC', 1)
       end if
c
       if ( nus .ne. 3 ) THEN
         print *, 'WRONG NUMBER OF STATE VARIABLES <> 3'
         print *, 'PLEASE PROVIDE AS INPUT: 0.0  0.0  0.0'
         call prgerr ( 'USRIFC', 1)
       end if
c
       if ( nui .ne. 1 ) THEN
         print *, 'WRONG NUMBER OF INTEGER INDICATORS <> 1'
         print *, 'PLEASE PROVIDE AS INPUT: 0'
         call prgerr ( 'USRIFC', 1)
       end if
c
c...     Material Parameters
c...     Tension mode
       ft        = usrval(1)
       gfi       = usrval(2)
       frcval(1) = usrval(3)
       frcval(2) = usrval(4)
       frcval(3) = usrval(5)
       gfii      = usrval(6)
       capval(1) = usrval(7)
       capval(2) = usrval(8)
       c         = frcval(1)
       alfa      = gfi / gfii * c / ft
       isplsv    = usrind(1)
       mocval(1) = usrval(9)
       mocval(2) = usrval(10)
       hs(1) = usrval(11)
       hs(2) = usrval(12)
       hs(3) = usrval(13)
       hs(4) = usrval(14)
       hs(5) = usrval(15)
       hs(6) = usrval(16)
       hs(7) = usrval(17)
       hs(8) = usrval(18)
       hs(9) = usrval(19)
       hs(10) = -( -gfii + c * hs(7) - c * hs(6) - hs(2) * hs(6) +
     $          hs(2) * hs(8) - hs(3) * hs(7) + hs(3) * hs(9) -
     $          hs(4) * hs(8) - hs(9) * hs(5) ) / ( hs(5) + hs(4) )

c
c...     Initialize
       usrind(1) = 0
       tanphi    = 0.D0
       fc        = 0.D0
       tensil    = .false.
       shear     = .false.
       cap       = .false.
       dl1       = 0.d0
       dl2       = 0.d0
       dl3       = 0.d0
```

```
      CALL RSET( 0.D0, p, nt*nt )
      p(1,1) = 2.D0
      p(2,2) = 2.D0 * capval(2)
      call rmove ( usrsta, usrst1, nus )
C
C...     PREDICTOR
      CALL UVPW( u0, DU, nt, U )
      CALL RAB( se, nt, nt, DU, 1, DTRA )
      CALL UVPW( TRA, DTRA, nt, TRAT )
      IF ( SW(2) ) THEN
         CALL PRIVEC( u0, nt, 'U-0   ' )
         CALL PRIVEC( DU, nt, 'DU-0  ' )
         CALL PRIVEC( U, nt, 'U-NEW ' )
         CALL PRIVEC( TRA, nt, 'TRA-0 ' )
         CALL PRIVEC( DTRA, nt, 'DTRA-0' )
         CALL PRIVEC( TRAT, nt, 'TRAT-0' )
      END IF
c
c...     Shear stress is assumed positive
c...     In the end if the return mapping follows a correction
      modul = 0
      if ( trat(2) .ne. 0.d0 ) modul = trat(2) / abs( trat(2) )
      trat(2) = abs( trat(2) )
c
c...     yield properties at test stress
      upeq = usrsta(1) + alfa * usrsta(2)
      call cutoha( ft, upeq, dyiedk, usrval(1), gfi )
      upeq = usrsta(1) / alfa + usrsta(2)
C
==================ENTRY============================================


C        write (LOUT, * ) 'Main part input'
C        WRITE ( LOUT, 34 ) elemen, intpt, hs(1), hs(10)


C
==================ENTRY============================================
      call coulhaB( c, tanphi, upeq, dyiedk, frcval, gfii, hs )
      call caphar2( fc, usrsta(3), dyiedk, capval, mocval )
      ft0    = ft
      c0     = c
      tanph0 = tanphi
      fc0    = fc
C
==================ENTRY============================================

C        OPEN  ( 34,FILE='ft')
C        WRITE ( 34, * ) ft
C        CLOSE (34)
C
C        OPEN  ( 35,FILE='c')
C        WRITE ( 35, * ) c
C        CLOSE (35)


         WRITE (LOUT, 34 ) ft, c
   34    format ( ' ft:', E11.3, ' c:', E11.3 )
```

```
C
==================ENTRY=============================================

C
C...     YIELD FUNCTION AT TEST STRESS
c...
c...     f1 = trat(1) - ft
c...
c...     f2= trat(2) + trat(1)*tanphi - c
c...
c...                        T                2
c...     F3 = 1/2 * [TRAT] *[P]*[TRAT] - fc
      f1 = trat(1) - ft
      f2 = trat(2) + trat(1) * tanphi - c
      call rab( p, nt, nt, trat, 1, ptra )
      f3 = .5D0 * uv( trat, ptra, nt ) - fc * fc
c
c...       Tolerance is the squared average of possible active yield
functions
      f = .5D0 * sqrt( ( f1 + abs( f1 ) ) ** 2 +
     $    ( f2 + abs( f2 ) ) ** 2 + ( f3 + abs( f3 ) ) ** 2 )
      if ( se(1,1) .lt. 1.D5 ) then
         EPS = max( EPS0 * ABS( F ), 1.D-14 )
      else
c
c...        Correction for dummy stifness
         EPS = max( EPS0 * EPS0 * ABS( F ), 1.D-14 )
      endif
      IF ( SW(2) ) THEN
         CALL PRIVAL( F1, 'F1-0' )
         CALL PRIVAL( F2, 'F2-0' )
         CALL PRIVAL( F3, 'F3-0' )
      END IF
C
      if ( f1 .gt. eps ) tensil = .true.
      if ( f2 .gt. eps ) shear = .true.
      if ( f3 .gt. eps ) cap = .true.
c
c...     Return mapping
      IF ( ( tensil ) .or. ( shear ) .or. ( cap ) ) then
c
c...        Start with single modes
         if ( tensil ) then
            upeq = usrsta(1) + alfa * usrsta(2)
            call rmcuto( nt, se, tra, trat, eps, upeq,
     $                   stiff, dl1, idum, modul, f1, usrval )
            usrsta(1) = upeq - alfa * usrsta(2)
c
c...           Check other modes
            f2 = abs( tra(2) ) + tra(1) * tanph0 - c0
            call rab( p, nt, nt, tra, 1, ptra )
            f3 = .5D0 * uv( tra, ptra, nt ) - fc0 * fc0
            if ( f2 .lt. eps .and. f3 .lt. eps ) then
               f = f1
               mode = 'TENSION '
               goto 3000
            end if
```

```
         end if
c
         if ( shear ) then
            call rmove ( usrst1, usrsta, nus )
            upeq = usrsta(1) / alfa + usrsta(2)
            call rmcoulb( nt, se, tra, trat, eps, upeq, stiff, dl2,
     $                    idum, modul, f2, usrval, hs )
            usrsta(2) = upeq - usrsta(1) / alfa
c
c...           Check other modes
            f1 = tra(1) - ft0
            call rab( p, nt, nt, tra, 1, ptra )
            f3 = .5D0 * uv( tra, ptra, nt ) - fc0 * fc0
            if ( f1 .lt. eps .and. f3 .lt. eps ) then
               f = f2
               mode = 'SHEAR   '
               goto 3000
            end if
         end if
c
         if ( cap ) then
            call rmove ( usrst1, usrsta, nus )
            call rmacap( nt, se, tra, trat, eps, usrsta(3),
     $                   stiff, dl3, idum, modul, f3, usrval )
c
c...           Check other modes
            f1 = tra(1) - ft0
            f2 = abs( tra(2) ) + tra(1) * tanph0 - c0
            if ( f1 .lt. eps .and. f2 .lt. eps ) then
               f = f3
               mode = 'CAP     '
               goto 3000
            end if
         endif
c
c...        Now the corners
c...        Corner 12
         if ( tensil .or. shear ) then
            call rmove ( usrst1, usrsta, nus )
            call  rmco12b(  nt,  se,  tra,  trat,  eps,  usrsta(1),
usrsta(2),
     $                    stiff, dl1, dl2, alfa, idum, modul, f1, f2,
     $                    usrval, hs )
            call rab( p, nt, nt, tra, 1, ptra )
            f3 = .5D0 * uv( tra, ptra, nt ) - fc0 * fc0
            if ( f3 .lt. eps .and. dl1 .gt. 0.d0 .and. dl2 .gt. 0.d0 )
     $         then
               f = max( abs( f1) , abs( f2 ) )
               mode = 'CORNER12'
               goto 3000
            end if
         end if
c
c...        Corner 23
         if ( shear .or. cap ) then
            call rmove ( usrst1, usrsta, nus )
            upeq = usrsta(1) / alfa + usrsta(2)
            call rmco23b( nt, se, tra, trat, eps, upeq, usrsta(3),
     $         stiff, dl2, dl3, idum, modul, f2, f3, usrval, hs )
```

```
            usrsta(2) = upeq - usrsta(1) / alfa
            f1 = tra(1) - ft0
            if ( f1 .lt. eps .and. dl2 .gt. 0.d0 .and. dl3 .gt. 0.d0 )
     $         then
               f = max( abs( f2) , abs( f3 ) )
               mode = 'CORNER23'
               goto 3000
            end if

         end if
c
c...        Return mapping was not successful
          call errmsg( 'NLXQ31', 5, elemen, intpt, 9.999d0, eps,
     $                'FRPINT:::IFMAS1' )
 3000 continue
c
         usrind(1) = +1
C
      ELSE
C
c...        Elastic
         IF ( ISPLSV .EQ. +1 ) usrind(1) = -1
         CALL RMOVE( se, stiff, nt*nt )
         CALL UVPW( TRA, DTRA, nt, TRA )
      END IF
C
      IF ( SW(2) ) THEN
         CALL PRIVEC( TRA, nt, 'TRAn+1' )
         CALL PRIMAT( stiff, nt, nt, 'stiff..' )
      END IF
C
      IF ( ( usrind(1) .EQ. 1 ) .AND. ( ISPLSV .NE. 1 ) ) THEN
         WRITE ( LOUT, 6 ) elemen, intpt, mode, F
      END IF
C
      CALL LMOVE( SWSV, SW, 6 )
C
c
c
 8000 continue
c
c
      END

c
      subroutine caphar2( yield, upeq, dyiedk, capval, mocval )
C
C.....................................................COPYRIGHT  (C)  TNO-
IBBC
C...  DIANA/NL/XQ31/IFCLIB/ELLIHA
C...
C...  Calculates hardening modulus and yield value for elliptical cap
C...
C.....................................................................
..
C
      logical          sw
      common /switch/  sw(6)
```

```
c
      double precision dyiedk, yield, upeq, gfc, kpeak,
     $                 capval(2), mocval(2)
c
      dyiedk = 0.D0
c
      yield = capval(1)
      gfc   = mocval(1)
      kpeak = mocval(2)
c
c...     3-Curves inelastic law
      call funch3( upeq, gfc, kpeak, yield, dyiedk, 0.d0 )
c
      if ( sw(2) ) then
         call prival( yield,  'FC    ' )
         call prival( dyiedk, 'DYIEDK' )
      end if
c
      end
      subroutine coulha( yield, tanphi, upeq, dyiedk, frcval, gfii )
C
C.....................................................COPYRIGHT  (C)  TNO-
IBBC
C...  DIANA/NL/XQ31/IFCLIB/CUTOHA
C...
C...   Calculates  hardening  modulus  and  yield  values  for  Coulomb
friction
C...
C.....................................................................
..
C
c
      logical          sw
      common /switch/  sw(6)
c
      double precision frcval(3)
c
      double precision dyiedk, yield, upeq, c, rdum, gfii,
     $                 tanfi0, tanfiu, tanphi
C
      c = frcval(1)
      tanfi0 = frcval(2)
      tanfiu = tanfi0
      rdum = exp( - ( c / gfii ) *  upeq  )
      yield  = c * rdum
      tanphi = tanfi0 + ( tanfiu - tanfi0 ) * ( c - yield ) / c
c...     Tangent at yield value-equiv. plastic strain diagram
      dyiedk = - ( c * c / gfii ) * rdum
c
      if ( sw(2) ) then
         call prival( yield,  'COHESI' )
         call prival( tanphi, 'TANPHI' )
         call prival( dyiedk, 'DYIEDK' )
      end if
c
      end
      subroutine cutoha( yield, upeq, dyiedk, ft, gfi )
C
```

```
C.....................................................COPYRIGHT  (C)  TNO-
IBBC
C...  DIANA/NL/XQ31/IFCLIB/CUTOHA
C...
C...   Calculates  hardening  modulus  and  yield  value  for  a  straight
tension
C...  cut-off
C...
C.....................................................................
..
C
      logical          sw
      common /switch/  sw(6)
C
      double precision dyiedk, yield, upeq, ft, rdum, gfi
C
      rdum = exp( - ( ft / gfi ) *  upeq  )
      yield = ft * rdum
C...     Tangent at fct-equiv. plastic strain diagram
      dyiedk = - ( ft * ft / gfi ) * rdum
C
      if ( sw(2) ) then
         call prival( yield,  'FT    ' )
         call prival( dyiedk, 'DYIEDK' )
      end if
C
      end
      subroutine funch3( epeq, gf, epeq1, yield, dyiedk, e )
C
C.....................................................COPYRIGHT  (C)  TNO-
IBBC
C...
C...  Calculate yield value and tangent to yield_value - kappa diagram
c...                            for  parabolic  hardening  followed  by
parabolic/exponential
c...            softening
c...
c...  input:
c...     arg.list:  epeq   - equivalent plastic strain
C...
c...  output:
c...     arg.list:  yield  - current yield value
c...                dyiedk - tangent to sigma_eq.-eq._plastic_strain
C...
C.....................................................................
..
C
      logical          sw
      common /switch/  sw(6)
c
      double precision dyiedk, f00, f0, fc, yield, fu,
     $                 m, epeq1, sepeq1, epeq2, epeq, gf, e
c
  100 continue
c
      f0 = 0.3333333d0 * yield
cc    f0 = 0.1666667d0 * yield
```

```
      fc = 1.0d0 * yield

CC    f00 = 0.5d0 * yield
      f00 = 0.7d0 * yield

CC    fu = 0.1d0 * yield
      fu = 0.01d0 * yield

      sepeq1 = epeq1 * epeq1

      epeq2 = 75.d0 / 67.d0 * gf / yield + epeq1
CC    epeq2 = 0.30d0 * (75.d0 / 67.d0 * gf / yield) + epeq1
c
c...        Define the derivative in the origin
      if ( epeq .eq. 0.D0 ) epeq = 1.d-12
c
c...      check if a local snap-back in the stress-strain diagram is
found
c...     If so, reduce yield strength accordingly
      if ( e .ne. 0 ) then
         if ( epeq2 .lt. ( yield / e + epeq1 ) ) then
            yield = ( -.87524278d0 * epeq1 + sqrt( .76604992d0 *
     $              sepeq1 + 3.6585365d0 / e * gf ) ) / 2.d0 * e
            goto 100
         end if
      end if
c
      if ( epeq .le. epeq2 ) then
         if ( epeq .le. epeq1 ) then
            m = sqrt( abs( ( 2.D0 * epeq / epeq1 -
     $                epeq * epeq / sepeq1 ) ) )
            yield = f0 + ( fc - f0 ) * m
         else
            yield = ( f00 - fc ) / ( epeq2 - epeq1 ) ** 2 *
     $              ( epeq - epeq1 ) ** 2 + fc
         end if
      else
         m = 2.D0 * ( f00 - fc ) / ( epeq2 - epeq1 )
         yield = f00 + ( fu - f00 ) * ( 1.D0 -
     $           exp( m / ( f00 - fu ) * ( epeq - epeq2 ) ) )
      end if
c
C...     TANGENT AT sigma_equivalent-KAPPA DIAGRAM (KAPPA = UT-PL)
      if ( epeq .le. epeq2 ) then
         if ( epeq .le. epeq1 ) then
            dyiedk = ( fc - f0 ) * ( 2.D0 / epeq1 - 2.D0 *
     $               epeq / sepeq1) / 2.D0 / m
         else
            dyiedk = 2.D0 * ( f00 - fc ) / ( epeq2 - epeq1 )
     $               ** 2 * ( epeq - epeq1 )
         end if
      else
         dyiedk = m * exp( m / ( f00 - fu ) * ( epeq - epeq2 ) )
      end if
C
      return
c
      END
      subroutine rmacap( ntr, tule, tra, trat, eps, upeq, tunl, dl,
```

```
     $                   nuinac, modul, f, usrval )
C
C.............................................COPYRIGHT  (C)  TNO-
IBBC
C...  DIANA/NL/XQ31/IFCLIB/RMACAP
C...
C...  Return mapping and consistent tangent for elliptical cap
c...
C...  miter=30
C...
C...  Called from: DIANA/NL/XQ31/IFCLIB/IFMAS1
C...
C.....................................................................
..
C
      integer          mtr, miter
      parameter        ( mtr=2, miter=30 )
c
      double precision uv
c
      double precision tule(*), tra(*), usrval(*)
      integer          ntr
c
      double precision relp
      integer          ielp, il, ip
      logical          lelp
      common /nlxqel/  relp(10), ielp(10), lelp(10)
      equivalence      ( il    , ielp(1) ), ( ip    , ielp(2) )
c
      integer          lin, lout
      common /inout /  lin, lout
c
      logical          sw
      common /switch/  sw(6)
c
      double precision trat(mtr), dgradg(mtr), gradf(mtr), h(mtr*mtr),
     $                 gradg(mtr), dgradf(mtr), dgdft(mtr*mtr),
     $                 tunl(mtr*mtr), yt(mtr*mtr), capval(2),
     $                 a(mtr*mtr), invd(mtr*mtr), p(mtr,mtr),
     $                 dkdsig(mtr), dsigdl(mtr), uela(mtr)
      double precision dl, yield, f, dyiedk, dupeq, rdum, dkdl,
     $                 upeq, dfdl, dfdk, eps, beta
      integer          iter, nuinac, modul
c
c...     Initialize
      capval(2) = usrval(8)
      call rset( 0.D0, p, ntr*ntr )
      p(1,1) = 2.D0
      p(2,2) = 2.D0 * capval(2)
c
      dyiedk = 0.D0
      dl     = 0.d0
c
      if ( sw(2) ) then
         print*, 'INELASTIC BEHAVIOUR FOR CAP MODE'
         call prival( eps,  'TOLCHK' )
         call privec( trat, ntr,  'TRAT  ' )
      end if
```

```
c
c...                    -1
c...     [invd] = [tule]
      call rmove( tule, invd, ntr*ntr )
      call invsym( invd, ntr )
      call filma( 1, invd, ntr )
c
c                         -1
c...     [uela] = [tule]  *[trat]
      call rab( invd, ntr, ntr, trat, 1, uela )
c
      do 100, iter = 1, miter
c
         if ( sw(2) ) then
            call priivl( iter, 'ITER  ' )
         end if
c
c...                       -1           -1
c...        [tra] = { [tule]  + dl*[p] }   * [uela]
         call uvpws( invd, p, ntr*ntr, dl, a )
         call invsym( a, ntr )
         call filma( 1, a, ntr )
         call rab( a, ntr, ntr, uela, 1, tra )
c
c...         Calculate equivalent plastic strain
         call rab( p, ntr, ntr, tra, 1, gradf )
         dupeq = dl * sqrt( uv( gradf, gradf, ntr ) )
         rdum = upeq + dupeq
         call caphar2( yield, rdum, dyiedk, usrval(7), usrval(9) )
         f = 0.5d0 * uv( tra, gradf, ntr ) - yield * yield
c
         if ( sw(2) ) then
            call prival( f,            'F-CHK ' )
            call prival( dl,           'DL    ' )
            call prival( upeq + dupeq, 'UPEQ  ' )
            call privec( tra, ntr,     'TRA   ' )
            call privec( gradf, ntr,   'GRADF' )
         end if
c
         if ( abs( f ) .lt. eps ) goto 200
c
c...           Newton-Method
c...                                              T
c...          dfdl = { [gradf] + [dfdk]*[dkdsig] } * [dsigdl] + dfdk *
dkdl
c
         dfdk = -2.d0 * yield * dyiedk
c
         rdum = sqrt( uv( gradf, gradf, ntr ) )
         call rab( p, ntr, ntr, gradf, 1, dkdsig )
         call uvs( dkdsig, ntr, dl / rdum, dkdsig )
c
         call rab( a, ntr, ntr, gradf, 1, dsigdl )
         call uvs( dsigdl, ntr, -1.d0, dsigdl )
c
         dkdl = rdum
c
         dfdl = uv( gradf, dsigdl, ntr ) +
     $          dfdk * uv( dkdsig, dsigdl, ntr ) + dfdk * dkdl
```

```
         dl = dl - ( f / dfdl )
c
  100 continue
      write( lout, 1 ) il, ip, f
      nuinac = nuinac + 1
C
  200 continue
      upeq = upeq + dupeq
      tra(2) = tra(2) * modul
c
c...     Consistent tangent
      call rab( p, ntr, ntr, tra, 1, gradf )
      dkdl = sqrt( uv( gradf, gradf, ntr ) )
      call rab( p, ntr, ntr, gradf, 1, dkdsig )
      call uvs( dkdsig, ntr, dl / dkdl, dkdsig )
      dfdk = -2.d0 * yield * dyiedk
c
c...     correct [d]
      call uvpws( invd, p, ntr*ntr, dl, h )
      call invsym( h, ntr )
      call filma( 1, h, ntr )
c
c...     make gradg
      call rmove( gradf, gradg, ntr )
c
c...     correct gradf
      call uvpws( gradf, dkdsig, ntr, dfdk, gradf )
c
      if ( sw(2) ) then
         call primat( h, ntr, ntr, 'h.....' )
      end if
c...                 T
c...     beta = gradf  [tule]  gradg
      call rab( h, ntr, ntr, gradg, 1, dgradg )
      beta = uv( gradf, dgradg, ntr )
c                     T
c...     dgradf = [ h ] * gradf
      call ratb( h, ntr, ntr, gradf, 1, dgradf )
c...     dgradg = [ tule ] * gradg
      call rab( h, ntr, ntr, gradg, 1, dgradg )
c                                          T             T
c...     dgdft = [ h ] * { gradg } * ( [ h ] * { gradf } )
      call rabt( dgradg, ntr, 1, dgradf, ntr, dgdft )
      call uvs( dgdft, ntr*ntr, -1.d0 / ( beta - dfdk * dkdl ), yt )
      call uvpw( h, yt, ntr*ntr, tunl )
C
      return
c
    1 format ( ' ELEMENT:', I4, '   IP:', I4,
     $         ' CAP INACCURATE  F=',1P, E11.3  )
      end
      subroutine rmco12a( ntr, tule, tra, trat, eps, upeq1, upeq2,
     $                    tunl, dl1, dl2, alfa, nuinac, modul, f1, f2,
     $                    usrval )
C
C.....................................................COPYRIGHT  (C)  TNO-
IBBC
C...  DIANA/NL/XQ31/IFCLIB/RMCO12
```

```
C...
C...  Return Mapping and Consistent Tangent for Corner of Coulomb
c...         Friction with Tension Cut-Off
c...
C...  miter=30
C...
C...  Called from: DIANA/NL/XQ31/IFCLIB/IFMAS1
C...
C.....................................................................
..
C
      integer          mtr, miter
      parameter        ( mtr=2, miter=30 )
c
      double precision tule(*), tra(*), usrval(*)
      integer          ntr
c
      double precision relp
      integer          ielp, il, ip
      logical          lelp
      common /nlxqel/  relp(10), ielp(10), lelp(10)
      equivalence      ( il    , ielp(1) ), ( ip    , ielp(2) )
c
      integer          lin, lout
      common /inout /  lin, lout
c
      logical          sw
      common /switch/  sw(6)
c
      double precision tunl(mtr*mtr), trat(mtr), gradf1(mtr),
     $                 gradf2(mtr), gradg1(mtr), gradg2(mtr),
     $                 jacob(2,2), x(2), s(2), func(2), u(mtr,mtr),
     $                 v(mtr,mtr), e(mtr,mtr), invmat(mtr*mtr),
     $                 mdum(mtr,mtr), vtd(mtr,mtr), du(mtr,mtr)
      double precision c, tanphi, tanpsi, c0, tanfi0, tanps0, tanfiu,
     $                 tanpsu, dyi1dk, dyi2dk, alfa, f1, f2, dl1, dl2,
     $                 dk1, dk2, upeq1, upeq2, f, rdum1, rdum2, eps,
     $                 rdum, dk1dl1, dk1dl2, dk2dl1, dk2dl2, phidk2,
     $                 psidk2, sigdl1, sigdl2, taudl2, ft
      integer          iter, nuinac, modul
C
c...     Initialize
      c0 = usrval(3)
      tanfi0 = usrval(4)
      tanps0 = usrval(5)
      tanfiu = tanfi0
      tanpsu = tanps0
c
      dyi1dk = 0.D0
      dyi2dk = 0.D0
      call rset(0.d0, x, 2 )
c
      if ( sw(2) ) then
         print*, 'INELASTIC BEHAVIOUR FOR CORNER 12'
         call prival( eps,  'TOLCHK' )
         call privec( trat, ntr,  'TRAT  ' )
      end if
c
      do 100, iter = 1, miter
```

```
c
         if ( sw(2) ) then
            call priivl( iter, 'ITER  ' )
         end if
c
         dl1 = x(1)
         dl2 = x(2)
c
         dk1 = sqrt( dl1 * dl1 + dl2 * dl2 * alfa * alfa )
         dk2 = sqrt( dl1 * dl1 / alfa / alfa + dl2 * dl2 )
         rdum1 = upeq1 + alfa * upeq2 + dk1
         rdum2 = upeq1 / alfa + upeq2 + dk2
         call cutoha( ft, rdum1, dyi1dk, usrval(1), usrval(2) )
         call coulha( c, tanphi, rdum2, dyi2dk, usrval(3), usrval(6) )
         tanpsi = tanps0 + ( tanpsu - tanps0 ) * ( c0 - c ) / c0
c
         tra(1) = trat(1) - dl1 * tule(1) - dl2 * tule(1) * tanpsi
         tra(2) = trat(2) - dl2 * tule(4)
         f1     = tra(1) - ft
         f2     = tra(2) + tra(1) * tanphi - c
c
         if ( sw(2) ) then
            call prival( f1,       'F1-CHK' )
            call prival( f2,       'F2-CHK' )
            call prival( dl1,      'DL1   ' )
            call prival( dl2,      'DL2   ' )
            call prival( rdum1,    'UPEQ1 ' )
            call prival( rdum2,    'UPEQ2 ' )
            call privec( tra, ntr, 'TRA   ' )
         end if
         f = sqrt( f1 * f1 + f2 * f2 )
         if ( abs( f ) .lt. eps ) goto 200
         func(1) = f1
         func(2) = f2
c
c...
c...           Newton Method
         if ( dk1 .gt. 1.d-14 ) then
            dk1dl1 = dl1 / dk1
            dk1dl2 = alfa * alfa * dl2 / dk1
         else
            dk1dl1 = 1.d0
            dk1dl2 = 0.d0
         end if
         if ( dk2 .gt. 1.d-14 ) then
            dk2dl1 = dl1 / alfa / alfa / dk2
            dk2dl2 = dl2 / dk2
         else
            dk2dl1 = 0.d0
            dk2dl2 = 1.d0
         end if
         psidk2 = - ( tanpsu - tanps0 ) / c0 * dyi2dk
         phidk2 = - ( tanfiu - tanfi0 ) / c0 * dyi2dk
         sigdl1 = - tule(1) - dl2 * tule(1) * psidk2 * dk2dl1
         sigdl2 = - tule(1) * tanpsi - dl2 * tule(1) * psidk2 * dk2dl2
         taudl2 = - tule(4)
c
         jacob(1,1) = sigdl1 - dyi1dk * dk1dl1
```

```
         jacob(1,2) = sigdl2 - dyi1dk * dk1dl2
         jacob(2,1) =          sigdl1 * tanphi +
     $                tra(1) * phidk2 * dk2dl1 - dyi2dk * dk2dl1
         jacob(2,2) = taudl2 + sigdl2 * tanphi +
     $                tra(1) * phidk2 * dk2dl2 - dyi2dk * dk2dl2
         if ( sw(2) ) then
            call primat( jacob, 2, 2, 'JACOB' )
         end if
c
         call inv2( jacob, invmat, rdum )
         call rab( invmat, 2, 2, func, 1, s )
         call uvs( s, 2, -1.D0, s )
         call uvpw( x, s, 2, x )
c
  100 continue
      write( lout, 1 ) il, ip, f
      nuinac = nuinac + 1
c
  200 continue
c
c...      Do  not  add  the  entire  dk1  and  dk2.  A  division  directly
proportional
c...    to dl1  and dl2 is assumed
      upeq1 = upeq1 + dk1 * dl1 / ( dl1 + dl2 )
      upeq2 = upeq2 + dk2 * dl2 / ( dl1 + dl2 )
      tra(2) = tra(2) * modul
c
c...     Consistent Tangent
      rdum    = ( 1.d0 + tra(1) * ( tanfiu - tanfi0 ) / c0 ) * dyi2dk
      gradf1(1) = 1.D0
      gradf1(2) = 0.D0
      gradg1(1) = 1.D0
      gradg1(2) = 0.D0
      gradf2(1) = tanphi
      gradf2(2) = modul
      gradg2(1) = tanpsi
      gradg2(2) = modul
      if ( dk1 .gt. 1.d-14 ) then
         dk1dl1 = dl1 / dk1
         dk1dl2 = alfa * alfa * dl2 / dk1
      else
         dk1dl1 = 1.d0
         dk1dl2 = 0.d0
      end if
      if ( dk2 .gt. 1.d-14 ) then
         dk2dl1 = dl1 / alfa / alfa / dk2
         dk2dl2 = dl2 / dk2
      else
         dk2dl1 = 0.d0
         dk2dl2 = 1.d0
      end if
c
c...     correct gradg
      gradg1(1) = gradg1(1) - dl2 * ( tanpsu-tanps0 ) / c0 * dyi2dk
     $            * dk2dl1
      gradg2(1) = gradg2(1) - dl2 * ( tanpsu-tanps0 ) / c0 * dyi2dk
     $            * dk2dl2
c
c...     fill matrices [u], [v], [e]
```

```
      u(1,1) = gradg1(1)
      u(2,1) = gradg1(2)
      u(1,2) = gradg2(1)
      u(2,2) = gradg2(2)
c
      v(1,1) = gradf1(1)
      v(2,1) = gradf1(2)
      v(1,2) = gradf2(1)
      v(2,2) = gradf2(2)
c
      e(1,1) = - dyi1dk * dk1dl1
      e(1,2) = - dyi1dk * dk1dl2
      e(2,1) = - rdum * dk2dl1
      e(2,2) = - rdum * dk2dl2
c
c...                                  T                -1    T
c...     [tunl] = [d] - [d] [u] { [v]  [d] [u] - [e] }   [v]  [d]
      call ratb( v, ntr, ntr, tule, ntr, vtd )
      call rab( vtd, ntr, ntr, u, ntr, mdum )
      call uvpws( mdum, e, ntr*ntr, -1.d0, mdum )
      call inv2( mdum, invmat, rdum )
      call rab( invmat, ntr, ntr, vtd, ntr, mdum )
      call rab( tule, ntr, ntr, u, ntr, du )
      call rab( du, ntr, ntr, mdum, ntr, tunl )
      call uvpws( tule, tunl, ntr*ntr, -1.d0, tunl )
c
      return
c
    1 format ( ' ELEMENT:', I4, '   IP:', I4,
     $         ' CORNER12 INACCURATE  F=',1P, E11.3  )
      end
      subroutine  rmco23a(  ntr,  tule,  tra,  trat,  eps,  upeq2,  upeq3,
tunl,
     $                dl2, dl3, nuinac, modul, f2, f3, usrval)
C
C.............................................COPYRIGHT  (C)  TNO-
IBBC
C...  DIANA/NL/XQ31/IFCLIB/RMCO23
C...
C...  Return Mapping and Consistent Tangent for Corner of Coulomb
c...         Friction with Elliptical Cap
c...
C...  miter=30
C...
C...  Called from: DIANA/NL/XQ31/IFCLIB/IFMAS1
C...
C.....................................................................
..
C
      integer          mtr, miter
      parameter        ( mtr=2, miter=30 )
c
      double precision uv
c
      double precision tule(*), tra(*), usrval(*)
      integer          ntr
c
      double precision relp
```

```
      integer          ielp, il, ip
      logical          lelp
      common /nlxqel/  relp(10), ielp(10), lelp(10)
      equivalence      ( il    , ielp(1) ), ( ip    , ielp(2) )
c
      integer          lin, lout
      common /inout /  lin, lout
c
      logical          sw
      common /switch/  sw(6)
c
      double precision tunl(mtr*mtr), trat(mtr), gradf2(mtr),
     $                 gradf3(mtr), gradg2(mtr), gradg3(mtr),
     $                 jacob(2,2), x(2), s(2), func(2), h(mtr*mtr),
     $                 u(mtr,mtr), v(mtr,mtr), e(mtr,mtr),
     $                 invmat(mtr*mtr), mdum(mtr,mtr), vtd(mtr,mtr),
     $                 du(mtr,mtr), dk3dsg(mtr)
      double precision capval(2), p(mtr,mtr)
      double precision c, tanphi, tanpsi, c0, tanfi0, tanps0, tanfiu,
     $                 tanpsu, unconf, yield, dyi2dk, dyi3dk, f2, f3,
     $                      dl2, dl3, eps, upeq2, upeq3, rdum, rdum1,
rdum2,
     $                 rdum3, f, df3dk3, tanps1, sigma2, taudl2,
     $                 sigdl2, phidk2, psidk2, taudl3, sigdl3,
     $                 k3dtau, k3dsig, dk3dl3
      integer          iter, nuinac, modul
c
c...     Initialize
      c0 = usrval(3)
      tanfi0 = usrval(4)
      tanps0 = usrval(5)
      tanfiu = tanfi0
      tanpsu = tanps0
      unconf = -1.d+20 * usrval(3)
c
      call rset( 0.D0, p, ntr*ntr )
      capval(2) = usrval(8)
      p(1,1) = 2.D0
      p(2,2) = 2.D0 * capval(2)
c
      call rset(0.d0, x, 2 )
      dyi2dk = 0.D0
      dyi3dk = 0.D0
c
      if ( sw(2) ) then
         print*, 'INELASTIC BEHAVIOUR FOR CORNER 23'
         call prival( eps,  'TOLCHK' )
         call privec( trat, ntr,  'TRAT  ' )
      end if
c
      do 100, iter = 1, miter
c
         if ( sw(2) ) then
            call priivl( iter, 'ITER  ' )
         end if
c
         dl2 = x(1)
         dl3 = x(2)
         if ( dl3 .lt. 0.d0 ) dl3 = 0.d0
```

```
          rdum2 = upeq2 + dl2
          call coulha( c, tanphi, rdum2, dyi2dk, usrval(3), usrval(6) )
          tanps1 = tanps0 + ( tanpsu - tanps0 ) * ( c0 - c ) / c0
          rdum   = 1.d0 / ( 1.d0 - dl2 * tule(1) * tanps1 / unconf +
     $             2.d0 * dl3 * tule(1) )
          rdum1  = 1.d0 / ( 1.d0 + 2.d0 * capval(2) * dl3 * tule(4) )
          tra(1) = rdum * ( trat(1) - dl2 * tule(1) * tanps1 )
c
c...          Adjust the dilatancy angle to zero for tra(1) higher than
unconf
          if ( tra(1) .le. unconf ) then
             tanps0 = 0.d0
             tanpsu = 0.d0
             tanps1 = 0.d0
             rdum   = 1.d0 / ( 2.d0 * dl3 * tule(1) )
             tra(1) = rdum * trat(1)
          end if
          tra(2) = rdum1 * ( trat(2) - dl2 * tule(4) )
c
c...          Calculate equivalent plastic strain for cap
          call rab( p, ntr, ntr, tra, 1, gradf3 )
          rdum3 = upeq3 + dl3 * sqrt( uv( gradf3, gradf3, ntr ) )
          call caphar2( yield, rdum3, dyi3dk, usrval(7), usrval(9) )
          f2     = tra(2) + tra(1) * tanphi - c
          f3     = 0.5d0 * uv( tra, gradf3, ntr ) - yield * yield
c
          if ( sw(2) ) then
             call prival( f2,       'F2-CHK' )
             call prival( f3,       'F3-CHK' )
             call prival( dl2,      'DL2   ' )
             call prival( dl3,      'DL3   ' )
             call prival( rdum2,    'UPEQ2 ' )
             call prival( rdum3,    'UPEQ3 ' )
             call privec( tra, ntr, 'TRA   ' )
          end if
          f = sqrt( f2 * f2 + f3 * f3 )
          if ( abs( f ) .lt. eps ) goto 200
          func(1) = f2
          func(2) = f3
c
c...
c...           Newton Method
          sigma2 = sqrt( tra(1) * tra(1) + ( capval(2) * tra(2) ) ** 2
)
          taudl2 = - tule(4) * rdum1
          psidk2 = - ( tanpsu - tanps0 ) / c0 * dyi2dk
          sigdl2 = tule(1) * (  dl2 * psidk2
     $             + tanps1 ) * ( tra(1) / unconf - 1.d0 ) * rdum
          phidk2 = - ( tanfiu - tanfi0 ) / c0 * dyi2dk
          taudl3 = -2.d0 * capval(2) * tule(4) * tra(2) * rdum1
          sigdl3 = -2.d0 * tule(1) * tra(1) * rdum
          k3dsig = 2.d0 * dl3 * tra(1) / sigma2
          k3dtau = 2.d0 * dl3 * tra(2) * capval(2) * capval(2) / sigma2
          dk3dl3 = 2.d0 * sigma2
c
          jacob(1,1) = taudl2 + sigdl2 * tanphi + tra(1) * phidk2 -
     $                 dyi2dk
          jacob(1,2) = taudl3 + sigdl3 * tanphi
```

```
         jacob(2,1) = 2.d0 * tra(1) * sigdl2 + 2.d0 * capval(2) *
     $                tra(2) * taudl2 - 2.d0 * yield * dyi3dk *
     $                ( k3dsig * sigdl2 + k3dtau * taudl2 )
         jacob(2,2) = 2.d0 * tra(1) * sigdl3 + 2.d0 * capval(2) *
     $                tra(2) * taudl3 - 2.d0 * yield * dyi3dk *
     $                ( dk3dl3 + k3dsig * sigdl3 + k3dtau * taudl3 )
         if ( sw(2) ) then
            call primat( jacob, 2, 2, 'JACOB' )
         end if
c
         call inv2( jacob, invmat, rdum )
         call rab( invmat, 2, 2, func, 1, s )
         call uvmw( x, s, 2, x )
         if ( x(2) .le. 0.d0 ) then
            x(2) = 0.d0
            x(1) = dl2 - f2 / jacob(1,1)
         end if
c         call lnsear( func, x, s, 2, tule, trat,
c     $                   upeq2, tanpsu, tanps0, c0, unconf, capval,
c     $                   p, ntr, upeq3 )
c
  100 continue
      write( lout, 1 ) il, ip, f
      nuinac = nuinac + 1
c
  200 continue
      upeq2 = rdum2
      upeq3 = rdum3
      tra(2) = tra(2) * modul
c
c...       Consistent Tangent
c
c...         Adjust the dilatancy angle to zero for tra(1) higher than
unconf
      if ( tra(1) .le. unconf ) then
         tanps0 = 0.d0
         tanpsu = 0.d0
      end if
      tanps1 = tanps0 + ( tanpsu - tanps0 ) * ( c0 - c ) / c0
      tanpsi = tanps1 * ( 1.d0 - tra(1) / unconf )
      gradf2(1) = tanphi
      gradf2(2) = modul
      gradg2(1) = tanpsi
      gradg2(2) = modul
      call rab( p, ntr, ntr, tra, 1, gradf3 )
      call rmove( gradf3, gradg3, ntr )
c
c...     correct gradg2
      gradg2(1) = gradg2(1) - dl2 * ( tanpsu-tanps0 ) / c0 * dyi2dk
     $            * ( 1.d0 - tra(1) / unconf )
c
c...     correct gradf3
      df3dk3 = -2.d0 * yield * dyi3dk
      dk3dl3 = sqrt( uv( gradf3, gradf3, ntr ) )
      call uvs( gradf3, ntr, dl3 / dk3dl3, dk3dsg )
      call uvpws( gradf3, dk3dsg, ntr, df3dk3, gradf3 )
c
c...     correct [d] for [h]
      call rmove( tule, h, ntr*ntr )
```

```
      h(1) = 1.d0 / ( 1.d0 / tule(1) + dl2 * tanps1 / unconf +
     $                dl3 * p(1,1) )
      h(4) = 1.d0 / ( 1.d0 / tule(4) + dl3 * p(1,1) )
c
c...     fill matrices [u], [v], [e]
      u(1,1) = gradg2(1)
      u(2,1) = gradg2(2)
      u(1,2) = gradg3(1)
      u(2,2) = gradg3(2)
c
      v(1,1) = gradf2(1)
      v(2,1) = gradf2(2)
      v(1,2) = gradf3(1)
      v(2,2) = gradf3(2)
c
      e(1,1) = - ( 1.d0 + tra(1) * ( tanfiu - tanfi0 ) / c0 ) * dyi2dk
      e(1,2) = 0.d0
      e(2,1) = 0.d0
      e(2,2) = df3dk3 * dk3dl3
c
c...                                    T                -1    T
c...     [tunl] = [h] - [h] [u] { [v]  [h] [u] - [e] }   [v]  [h]
      call ratb( v, ntr, ntr, h, ntr, vtd )
      call rab( vtd, ntr, ntr, u, ntr, mdum )
      call uvpws( mdum, e, ntr*ntr, -1.d0, mdum )
      call inv2( mdum, invmat, rdum )
      call rab( invmat, ntr, ntr, vtd, ntr, mdum )
      call rab( h, ntr, ntr, u, ntr, du )
      call rab( du, ntr, ntr, mdum, ntr, tunl )
      call uvpws( h, tunl, ntr*ntr, -1.d0, tunl )
c
      return
c
    1 format ( ' ELEMENT:', I4, '   IP:', I4,
     $         ' CORNER23 INACCURATE  F=',1P, E11.3  )
c
      end
      subroutine rmcoula( ntr, tule, tra, trat, eps, upeq, tunl, dl,
     $                    nuinac, modul, f, usrval )
C
C.....................................................COPYRIGHT  (C)  TNO-
IBBC
C...  DIANA/NL/XQ31/IFCLIB/RMCUTO
C...
C...  Return mapping and consistent tangent for Coulomb friction law
c...
C...  miter=30
C...
C...  Called from: DIANA/NL/XQ31/IFCLIB/IFMAS1
C...
C.....................................................................
..
C
      integer          mtr, miter
      parameter        ( mtr=2, miter=30 )
c
      double precision uv
c
```

```
      double precision tule(*), tra(*), usrval(*)
      integer          ntr
c
      double precision relp
      integer          ielp, il, ip
      logical          lelp
      common /nlxqel/  relp(10), ielp(10), lelp(10)
      equivalence      ( il    , ielp(1) ), ( ip    , ielp(2) )
c
      integer          lin, lout
      common /inout /  lin, lout
c
      logical          sw
      common /switch/  sw(6)
c
      double precision tunl(mtr*mtr), trat(mtr), gradg(mtr),
     $                 dgradg(mtr), dl, gradf(mtr), dgradf(mtr),
     $                 dgdft(mtr*mtr), f, eps, beta, h(mtr*mtr)
      double precision c, tanphi, tanpsi, c0,
     $                 tanfi0, tanps0, tanfiu, tanpsu, unconf, tanps1
      integer          iter, nuinac, modul
      double precision upeq, dyiedk, dfdl, rdum
c
c...     Initialize
      c0 = usrval(3)
      tanfi0 = usrval(4)
      tanps0 = usrval(5)
      tanfiu = tanfi0
      tanpsu = tanps0
      unconf = -1.d+20 * usrval(3)
c
      dyiedk = 0.D0
      dl     = 0.d0
c
      if ( sw(2) ) then
         print*, 'INELASTIC BEHAVIOUR FOR SHEAR MODE'
         call prival( eps,  'TOLCHK' )
         call privec( trat, ntr,  'TRAT  ' )
      end if
c
      do 100, iter = 1, miter
c
         if ( sw(2) ) then
            call priivl( iter, 'ITER  ' )
         end if
c
         call coulha( c, tanphi, upeq+dl, dyiedk, usrval(3), usrval(6)
)
c
         tanps1 = tanps0 + ( tanpsu - tanps0 ) * ( c0 - c ) / c0
         rdum   = 1.d0 / ( 1.d0 - dl * tule(1) * tanps1 / unconf )
         tra(1) = rdum * ( trat(1) - dl * tule(1) * tanps1 )
c
c...         Adjust the dilatancy angle to zero for tra(1) higher than
unconf
         if ( tra(1) .le. unconf ) then
            rdum   = 0.d0
            tra(1) = trat(1)
         end if
```

```
         tra(2) = trat(2) - dl * tule(4)
         f      = tra(2) + tra(1) * tanphi - c
c
         if ( sw(2) ) then
            call prival( f,         'F-CHK ' )
            call prival( dl,        'DL    ' )
            call prival( upeq + dl, 'UPEQ  ' )
            call privec( tra, ntr,  'TRA   ' )
         end if
         if ( abs( f ) .lt. eps ) goto 200
c...
c...        Newton Method
         dfdl = - tule(4) + ( tra(1) / unconf - 1.d0 ) *
     $          tule(1) * ( tanps1 - dl * ( tanpsu - tanps0 ) / c0 *
     $          dyiedk ) * rdum * tanphi -
     $          tra(1) * ( tanfiu - tanfi0 ) / c0 * dyiedk - dyiedk
         dl = dl - ( f / dfdl )
         if ( sw(2) ) then
            call prival( dfdl, 'DFDL  ' )
         end if
c
  100 continue
      write( lout, 1 ) il, ip, f
      nuinac = nuinac + 1
c
  200 continue
      upeq = upeq + dl
      tra(2) = tra(2) * modul
c
c...       Consistent Tangent
      rdum    = ( 1.d0 + tra(1) * ( tanfiu - tanfi0 ) / c0 ) * dyiedk
c
c...         Adjust the dilatancy angle to zero for tra(1) higher than
unconf
      if ( tra(1) .le. unconf ) then
         tanps0 = 0.d0
         tanpsu = 0.d0
      end if
      tanps1 = tanps0 + ( tanpsu - tanps0 ) * ( c0 - c ) / c0
      tanpsi = tanps1 * ( 1.d0 - tra(1) / unconf )
      gradf(1) = tanphi
      gradf(2) = modul
      gradg(1) = tanpsi
      gradg(2) = modul
c
c...     correct gradg
      gradg(1) = gradg(1) - dl * ( tanpsu-tanps0 ) / c0 * dyiedk
     $           * ( 1.d0 - tra(1) / unconf )
c
c...     correct [d]
      call rmove( tule, h, ntr*ntr )
      h(1) = 1.d0 / ( 1.d0 / tule(1) + dl * tanps1 / unconf )
c...                  T
c...     beta = gradf  [h]  gradg
      call rab( h, ntr, ntr, gradg, 1, dgradg )
      beta = uv( gradf, dgradg, ntr )
c...                   T
c...     dgradf = [ h ] * gradf
```

```
      call ratb( h, ntr, ntr, gradf, 1, dgradf )
c                                                T             T
c...     dgdft = [ h ] * { gradg } * ( [ h ] * { gradf } )
      call rabt( dgradg, ntr, 1, dgradf, ntr, dgdft )
      call uvpws( h, dgdft, ntr*ntr, -1.d0 / (beta+rdum), tunl )
c
      return
c
    1 format ( ' ELEMENT:', I4, '   IP:', I4,
     $         ' SHEAR INACCURATE  F=',1P, E11.3  )
      end
      subroutine rmcuto( ntr, tule, tra, trat, eps, upeq,
     $                   tunl, dl, nuinac, modul, f, usrval )
C
C.....................................................COPYRIGHT  (C)  TNO-
IBBC
C...  DIANA/NL/XQ31/IFCLIB/RMCUTO
C...
C...  Return mapping and consistent tangent for straight tension cut-
off
c...
C...  miter=30
C...
C...  Called from: DIANA/NL/XQ31/IFCLIB/IFMAS1
C...
C.....................................................................
..
C
      integer          mtr, miter
      parameter        ( mtr=2, miter=30 )
c
      double precision tule(*), tra(*), usrval(*)
      integer          ntr
c
      double precision relp
      integer          ielp, il, ip
      logical          lelp
      common /nlxqel/  relp(10), ielp(10), lelp(10)
      equivalence      ( il    , ielp(1) ), ( ip    , ielp(2) )
c
      integer          lin, lout
      common /inout /  lin, lout
c
      logical          sw
      common /switch/  sw(6)
c
      double precision tunl(mtr*mtr), trat(mtr), dl,
     $                 f, eps, ft, upeq, dyiedk, dfdl
      integer          iter, nuinac, modul
c
c...     Initialize
      dyiedk = 0.D0
      dl     = 0.d0
c...     Shear component ( constant )
      tra(2) = trat(2)
c
      if ( sw(2) ) then
         print*, 'INELASTIC BEHAVIOUR FOR TENSION MODE'
         call prival( eps,  'TOLCHK' )
```

```
         call privec( trat, ntr,  'TRAT  ' )
      end if
c
      do 100, iter = 1, miter
c
         if ( sw(2) ) then
            call priivl( iter, 'ITER  ' )
         end if
c
         call cutoha( ft, upeq + dl, dyiedk, usrval(1), usrval(2) )
         tra(1) = trat(1) - dl * tule(1)
         f = tra(1) - ft
c
         if ( sw(2) ) then
            call prival( f,         'F-CHK ' )
            call prival( dl,        'DL    ' )
            call prival( upeq + dl, 'UPEQ  ' )
            call privec( tra, ntr,  'TRA   ' )
         end if
         if ( abs( f ) .lt. eps ) goto 200
c...
c...           Newton Method
         dfdl = - tule(1) - dyiedk
         dl = dl - ( f / dfdl )
         if ( sw(2) ) then
            call prival( dfdl, 'DFDL  ' )
         end if
c
  100 continue
      write( lout, 1 ) il, ip, f
      nuinac = nuinac + 1
c
  200 continue
      upeq = upeq + dl
      tra(2) = tra(2) * modul
c
c...       Consistent Tangent
      call rset( 0.d0, tunl, ntr*ntr)
      tunl(1) = dyiedk * tule(1) / ( dyiedk + tule(1) )
      tunl(4) = tule(4)
c
      return
c
    1 format ( ' ELEMENT:', I4, '   IP:', I4,
     $         ' TENSION INACCURATE  F=',1P, E11.3  )
      end
c
c

      subroutine coulhaB( yield, tanphi, upeq, dyiedk, frcval, gfii,
     $             hs )
C
C.....................................................COPYRIGHT  (C)  TNO-
IBBC
C...  DIANA/NL/XQ31/IFCLIB/CUTOHA
C...
C...   Calculates  hardening  modulus  and  yield  values  for  Coulomb
friction
```

```
C...
C.....................................................................
..
C
c
      logical          sw
      common /switch/  sw(6)
c
      INTEGER          LIN, LOUT
      COMMON /INOUT /  LIN, LOUT

      double precision frcval(3)
      double precision hs(10)
c
      double precision dyiedk, yield, upeq, c, rdum, gfii,
     $                 tanfi0, tanfiu, tanphi
C
      c = frcval(1)
      tanfi0 = frcval(2)
      tanfiu = tanfi0
      tanphi = tanfi0 + ( tanfiu - tanfi0 ) * ( c - yield ) / c
      hs1 =hs(1)
      hs2 =hs(2)
      hs3 =hs(3)
      hs4 =hs(4)
      hs5 =hs(5)
      hs6 =hs(6)
      hs7 =hs(7)
      hs8 =hs(8)
      hs9 =hs(9)
      hs10=hs(10)

C          write (LOUT, * ) 'Main part inside'
C        WRITE  (LOUT, 34 ) hs(1), hs(10)
C   34    format ( ' hs1:', E11.3 , ' hs10:', E11.3 )


C                                                  ==================CM
ENTRY=============================================
C.... Evaluation of the yield value
C.... Tangent at yield value-equiv. plastic strain diagram

      if ( upeq .le. hs10 ) then
         if ( upeq .le. hs9 ) then
          if ( upeq .le. hs8 ) then
           if ( upeq .le. hs7 ) then
            if ( upeq .le. hs6 ) then
               yield  = ( c - hs1 ) / hs6 * upeq  + hs1
             dyiedk = ( c - hs1 ) / hs6
              else
            yield  = ( hs2 - c ) / ( - hs6 + hs7 ) * upeq +
     $                ( hs7 * c - hs2 * hs6 ) / ( - hs6 + hs7 )

            dyiedk = ( hs2 - c ) / ( - hs6 + hs7 )
            end if
           else
             yield  = ( hs3 - hs2 ) / ( - hs7 + hs8 ) * upeq +
     $                 ( hs8 * hs2 - hs3 * hs7 ) / ( - hs7 + hs8 )
```

```
               dyiedk = ( hs3 - hs2 ) / ( - hs7 + hs8 )
            end if
           else
              yield  = ( hs4 - hs3 ) / ( - hs8 + hs9 ) * upeq +
     $                  ( hs9 * hs3 - hs4 * hs8 ) / ( - hs8 + hs9 )

              dyiedk = ( hs4 - hs3 ) / ( - hs8 + hs9 )
         end if
        else
              yield  = ( hs5 - hs4 ) / ( - hs9 + hs10 ) * upeq +
     $                  ( hs10 * hs4 - hs5 * hs9 ) / ( - hs9 + hs10 )

              dyiedk = ( hs5 - hs4 ) / ( - hs9 + hs10 )
        end if
         else
              yield  = hs5
              dyiedk = 1.d-12
       end if
C                                                    ==================CM
ENTRY============================================

       if ( sw(2) ) then
          call prival( yield,  'COHESI' )
          call prival( tanphi, 'TANPHI' )
          call prival( dyiedk, 'DYIEDK' )
       end if
c
       end
c
c
       subroutine rmcoulb( ntr, tule, tra, trat, eps, upeq, tunl, dl,
     $                   nuinac, modul, f, usrval, hs )
C
C.....................................................COPYRIGHT  (C)  TNO-
IBBC
C...  DIANA/NL/XQ31/IFCLIB/RMCUTO
C...
C...  Return mapping and consistent tangent for Coulomb friction law
c...
C...  miter=30
C...
C...  Called from: DIANA/NL/XQ31/IFCLIB/IFMAS1
C...
C.....................................................................
..
C
       integer          mtr, miter
       parameter        ( mtr=2, miter=30 )
c
       double precision uv
c
       double precision tule(*), tra(*), usrval(*), hs(10)
       integer          ntr
c
       double precision relp
       integer          ielp, il, ip
       logical          lelp
       common /nlxqel/  relp(10), ielp(10), lelp(10)
```

```
      equivalence      ( il    , ielp(1) ), ( ip    , ielp(2) )
c
      integer          lin, lout
      common /inout /  lin, lout
c
      logical          sw
      common /switch/  sw(6)
c
      double precision tunl(mtr*mtr), trat(mtr), gradg(mtr),
     $                 dgradg(mtr), dl, gradf(mtr), dgradf(mtr),
     $                 dgdft(mtr*mtr), f, eps, beta, h(mtr*mtr)
      double precision c, tanphi, tanpsi, c0,
     $                 tanfi0, tanps0, tanfiu, tanpsu, unconf, tanps1
      integer          iter, nuinac, modul
      double precision upeq, dyiedk, dfdl, rdum
c
c...     Initialize
      c0 = usrval(3)
      tanfi0 = usrval(4)
      tanps0 = usrval(5)
      tanfiu = tanfi0
      tanpsu = tanps0
      unconf = -1.d+20 * usrval(3)
      hs1 =hs(1)
      hs2 =hs(2)
      hs3 =hs(3)
      hs4 =hs(4)
      hs5 =hs(5)
      hs6 =hs(6)
      hs7 =hs(7)
      hs8 =hs(8)
      hs9 =hs(9)
      hs10=hs(10)

c
      dyiedk = 0.D0
      dl     = 0.d0
c
      if ( sw(2) ) then
         print*, 'INELASTIC BEHAVIOUR FOR SHEAR MODE'
         call prival( eps,  'TOLCHK' )
         call privec( trat, ntr,  'TRAT  ' )
      end if
c
      do 100, iter = 1, miter
c
         if ( sw(2) ) then
            call priivl( iter, 'ITER  ' )
         end if
c
         call  coulhaB(  c,  tanphi,  upeq+dl,  dyiedk,  usrval(3),
usrval(6),
     $                 hs )
c
         tanps1 = tanps0 + ( tanpsu - tanps0 ) * ( c0 - c ) / c0
         rdum   = 1.d0 / ( 1.d0 - dl * tule(1) * tanps1 / unconf )
         tra(1) = rdum * ( trat(1) - dl * tule(1) * tanps1 )
c
```

```
c...         Adjust the dilatancy angle to zero for tra(1) higher than
unconf
         if ( tra(1) .le. unconf ) then
            rdum   = 0.d0
            tra(1) = trat(1)
         end if
         tra(2) = trat(2) - dl * tule(4)
         f      = tra(2) + tra(1) * tanphi - c
c
         if ( sw(2) ) then
            call prival( f,         'F-CHK ' )
            call prival( dl,        'DL    ' )
            call prival( upeq + dl, 'UPEQ  ' )
            call privec( tra, ntr,  'TRA   ' )
         end if
         if ( abs( f ) .lt. eps ) goto 200
c...
c...        Newton Method
         dfdl = - tule(4) + ( tra(1) / unconf - 1.d0 ) *
     $          tule(1) * ( tanps1 - dl * ( tanpsu - tanps0 ) / c0 *
     $          dyiedk ) * rdum * tanphi -
     $          tra(1) * ( tanfiu - tanfi0 ) / c0 * dyiedk - dyiedk
         dl = dl - ( f / dfdl )
         if ( sw(2) ) then
            call prival( dfdl, 'DFDL  ' )
         end if
c
  100 continue
      write( lout, 1 ) il, ip, f
      nuinac = nuinac + 1
c
  200 continue
      upeq = upeq + dl
      tra(2) = tra(2) * modul
c
c...       Consistent Tangent
      rdum    = ( 1.d0 + tra(1) * ( tanfiu - tanfi0 ) / c0 ) * dyiedk
c
c...         Adjust the dilatancy angle to zero for tra(1) higher than
unconf
      if ( tra(1) .le. unconf ) then
         tanps0 = 0.d0
         tanpsu = 0.d0
      end if
      tanps1 = tanps0 + ( tanpsu - tanps0 ) * ( c0 - c ) / c0
      tanpsi = tanps1 * ( 1.d0 - tra(1) / unconf )
      gradf(1) = tanphi
      gradf(2) = modul
      gradg(1) = tanpsi
      gradg(2) = modul
c
c...     correct gradg
      gradg(1) = gradg(1) - dl * ( tanpsu-tanps0 ) / c0 * dyiedk
     $           * ( 1.d0 - tra(1) / unconf )
c
c...     correct [d]
      call rmove( tule, h, ntr*ntr )
      h(1) = 1.d0 / ( 1.d0 / tule(1) + dl * tanps1 / unconf )
```

```
c...                 T
c...     beta = gradf  [h]  gradg
      call rab( h, ntr, ntr, gradg, 1, dgradg )
      beta = uv( gradf, dgradg, ntr )
c...                  T
c...     dgradf = [ h ] * gradf
      call ratb( h, ntr, ntr, gradf, 1, dgradf )
c                                          T             T
c...     dgdft = [ h ] * { gradg } * ( [ h ] * { gradf } )
      call rabt( dgradg, ntr, 1, dgradf, ntr, dgdft )
      call uvpws( h, dgdft, ntr*ntr, -1.d0 / (beta+rdum), tunl )
c
      return
c
    1 format ( ' ELEMENT:', I4, '   IP:', I4,
     $         ' SHEAR INACCURATE  F=',1P, E11.3  )
      end
c
c
      subroutine rmco12b( ntr, tule, tra, trat, eps, upeq1, upeq2,
     $                    tunl, dl1, dl2, alfa, nuinac, modul, f1, f2,
     $                    usrval, hs )
C
C.....................................................COPYRIGHT  (C)  TNO-
IBBC
C...  DIANA/NL/XQ31/IFCLIB/RMCO12
C...
C...  Return Mapping and Consistent Tangent for Corner of Coulomb
c...         Friction with Tension Cut-Off
c...
C...  miter=30
C...
C...  Called from: DIANA/NL/XQ31/IFCLIB/IFMAS1
C...
C.....................................................................
..
C
      integer          mtr, miter
      parameter        ( mtr=2, miter=30 )
c
      double precision tule(*), tra(*), usrval(*) , hs(10)
      integer          ntr
c
      double precision relp
      integer          ielp, il, ip
      logical          lelp
      common /nlxqel/  relp(10), ielp(10), lelp(10)
      equivalence      ( il    , ielp(1) ), ( ip    , ielp(2) )
c
      integer          lin, lout
      common /inout /  lin, lout
c
      logical          sw
      common /switch/  sw(6)
c
      double precision tunl(mtr*mtr), trat(mtr), gradf1(mtr),
     $                 gradf2(mtr), gradg1(mtr), gradg2(mtr),
     $                 jacob(2,2), x(2), s(2), func(2), u(mtr,mtr),
     $                 v(mtr,mtr), e(mtr,mtr), invmat(mtr*mtr),
```

```
     $                mdum(mtr,mtr), vtd(mtr,mtr), du(mtr,mtr)
      double precision c, tanphi, tanpsi, c0, tanfi0, tanps0, tanfiu,
     $                 tanpsu, dyi1dk, dyi2dk, alfa, f1, f2, dl1, dl2,
     $                 dk1, dk2, upeq1, upeq2, f, rdum1, rdum2, eps,
     $                 rdum, dk1dl1, dk1dl2, dk2dl1, dk2dl2, phidk2,
     $                 psidk2, sigdl1, sigdl2, taudl2, ft
      integer          iter, nuinac, modul
C
c...     Initialize
      c0 = usrval(3)
      tanfi0 = usrval(4)
      tanps0 = usrval(5)
      tanfiu = tanfi0
      tanpsu = tanps0
      hs1 =hs(1)
      hs2 =hs(2)
      hs3 =hs(3)
      hs4 =hs(4)
      hs5 =hs(5)
      hs6 =hs(6)
      hs7 =hs(7)
      hs8 =hs(8)
      hs9 =hs(9)
      hs10=hs(10)

c
      dyi1dk = 0.D0
      dyi2dk = 0.D0
      call rset(0.d0, x, 2 )
c
      if ( sw(2) ) then
         print*, 'INELASTIC BEHAVIOUR FOR CORNER 12'
         call prival( eps,  'TOLCHK' )
         call privec( trat, ntr,  'TRAT  ' )
      end if
c
      do 100, iter = 1, miter
c
         if ( sw(2) ) then
            call priivl( iter, 'ITER  ' )
         end if
c
         dl1 = x(1)
         dl2 = x(2)
c
         dk1 = sqrt( dl1 * dl1 + dl2 * dl2 * alfa * alfa )
         dk2 = sqrt( dl1 * dl1 / alfa / alfa + dl2 * dl2 )
         rdum1 = upeq1 + alfa * upeq2 + dk1
         rdum2 = upeq1 / alfa + upeq2 + dk2
         call cutoha( ft, rdum1, dyi1dk, usrval(1), usrval(2) )
         call coulhaB( c, tanphi, rdum2, dyi2dk, usrval(3), usrval(6),
     $                  hs )
         tanpsi = tanps0 + ( tanpsu - tanps0 ) * ( c0 - c ) / c0
c
         tra(1) = trat(1) - dl1 * tule(1) - dl2 * tule(1) * tanpsi
         tra(2) = trat(2) - dl2 * tule(4)
         f1     = tra(1) - ft
         f2     = tra(2) + tra(1) * tanphi - c
```

```
c
         if ( sw(2) ) then
            call prival( f1,       'F1-CHK' )
            call prival( f2,       'F2-CHK' )
            call prival( dl1,      'DL1   ' )
            call prival( dl2,      'DL2   ' )
            call prival( rdum1,    'UPEQ1 ' )
            call prival( rdum2,    'UPEQ2 ' )
            call privec( tra, ntr, 'TRA   ' )
         end if
         f = sqrt( f1 * f1 + f2 * f2 )
         if ( abs( f ) .lt. eps ) goto 200
         func(1) = f1
         func(2) = f2
c
c...
c...           Newton Method
         if ( dk1 .gt. 1.d-14 ) then
            dk1dl1 = dl1 / dk1
            dk1dl2 = alfa * alfa * dl2 / dk1
         else
            dk1dl1 = 1.d0
            dk1dl2 = 0.d0
         end if
         if ( dk2 .gt. 1.d-14 ) then
            dk2dl1 = dl1 / alfa / alfa / dk2
            dk2dl2 = dl2 / dk2
         else
            dk2dl1 = 0.d0
            dk2dl2 = 1.d0
         end if
         psidk2 = - ( tanpsu - tanps0 ) / c0 * dyi2dk
         phidk2 = - ( tanfiu - tanfi0 ) / c0 * dyi2dk
         sigdl1 = - tule(1) - dl2 * tule(1) * psidk2 * dk2dl1
         sigdl2 = - tule(1) * tanpsi - dl2 * tule(1) * psidk2 * dk2dl2
         taudl2 = - tule(4)
c
         jacob(1,1) = sigdl1 - dyi1dk * dk1dl1
         jacob(1,2) = sigdl2 - dyi1dk * dk1dl2
         jacob(2,1) =          sigdl1 * tanphi +
     $                tra(1) * phidk2 * dk2dl1 - dyi2dk * dk2dl1
         jacob(2,2) = taudl2 + sigdl2 * tanphi +
     $                tra(1) * phidk2 * dk2dl2 - dyi2dk * dk2dl2
         if ( sw(2) ) then
            call primat( jacob, 2, 2, 'JACOB' )
         end if
c
         call inv2( jacob, invmat, rdum )
         call rab( invmat, 2, 2, func, 1, s )
         call uvs( s, 2, -1.D0, s )
         call uvpw( x, s, 2, x )
c
  100 continue
      write( lout, 1 ) il, ip, f
      nuinac = nuinac + 1
c
  200 continue
c
```

```
c...      Do not add the entire dk1 and dk2. A division directly
proportional
c...    to dl1  and dl2 is assumed
      upeq1 = upeq1 + dk1 * dl1 / ( dl1 + dl2 )
      upeq2 = upeq2 + dk2 * dl2 / ( dl1 + dl2 )
      tra(2) = tra(2) * modul
c
c...     Consistent Tangent
      rdum    = ( 1.d0 + tra(1) * ( tanfiu - tanfi0 ) / c0 ) * dyi2dk
      gradf1(1) = 1.D0
      gradf1(2) = 0.D0
      gradg1(1) = 1.D0
      gradg1(2) = 0.D0
      gradf2(1) = tanphi
      gradf2(2) = modul
      gradg2(1) = tanpsi
      gradg2(2) = modul
      if ( dk1 .gt. 1.d-14 ) then
         dk1dl1 = dl1 / dk1
         dk1dl2 = alfa * alfa * dl2 / dk1
      else
         dk1dl1 = 1.d0
         dk1dl2 = 0.d0
      end if
      if ( dk2 .gt. 1.d-14 ) then
         dk2dl1 = dl1 / alfa / alfa / dk2
         dk2dl2 = dl2 / dk2
      else
         dk2dl1 = 0.d0
         dk2dl2 = 1.d0
      end if
c
c...     correct gradg
      gradg1(1) = gradg1(1) - dl2 * ( tanpsu-tanps0 ) / c0 * dyi2dk
     $           * dk2dl1
      gradg2(1) = gradg2(1) - dl2 * ( tanpsu-tanps0 ) / c0 * dyi2dk
     $           * dk2dl2
c
c...     fill matrices [u], [v], [e]
      u(1,1) = gradg1(1)
      u(2,1) = gradg1(2)
      u(1,2) = gradg2(1)
      u(2,2) = gradg2(2)
c
      v(1,1) = gradf1(1)
      v(2,1) = gradf1(2)
      v(1,2) = gradf2(1)
      v(2,2) = gradf2(2)
c
      e(1,1) = - dyi1dk * dk1dl1
      e(1,2) = - dyi1dk * dk1dl2
      e(2,1) = - rdum * dk2dl1
      e(2,2) = - rdum * dk2dl2
c
c...                                    T                -1    T
c...     [tunl] = [d] - [d] [u] { [v]  [d] [u] - [e] }   [v]  [d]
      call ratb( v, ntr, ntr, tule, ntr, vtd )
      call rab( vtd, ntr, ntr, u, ntr, mdum )
```

```
      call uvpws( mdum, e, ntr*ntr, -1.d0, mdum )
      call inv2( mdum, invmat, rdum )
      call rab( invmat, ntr, ntr, vtd, ntr, mdum )
      call rab( tule, ntr, ntr, u, ntr, du )
      call rab( du, ntr, ntr, mdum, ntr, tunl )
      call uvpws( tule, tunl, ntr*ntr, -1.d0, tunl )
c
      return
c
    1 format ( ' ELEMENT:', I4, '   IP:', I4,
     $         ' CORNER12 INACCURATE  F=',1P, E11.3  )
      end
      subroutine rmco23b( ntr, tule, tra, trat, eps, upeq2, upeq3,
tunl,
     $                dl2, dl3, nuinac, modul, f2, f3, usrval, hs)
C
C.............................................COPYRIGHT  (C)  TNO-
IBBC
C...  DIANA/NL/XQ31/IFCLIB/RMCO23
C...
C...  Return Mapping and Consistent Tangent for Corner of Coulomb
c...         Friction with Elliptical Cap
c...
C...  miter=30
C...
C...  Called from: DIANA/NL/XQ31/IFCLIB/IFMAS1
C...
C.....................................................................
..
C
      integer          mtr, miter
      parameter        ( mtr=2, miter=30 )
c
      double precision uv
c
      double precision tule(*), tra(*), usrval(*) , hs(10)
      integer          ntr
c
      double precision relp
      integer          ielp, il, ip
      logical          lelp
      common /nlxqel/  relp(10), ielp(10), lelp(10)
      equivalence      ( il    , ielp(1) ), ( ip    , ielp(2) )
c
      integer          lin, lout
      common /inout /  lin, lout
c
      logical          sw
      common /switch/  sw(6)
c
      double precision tunl(mtr*mtr), trat(mtr), gradf2(mtr),
     $                 gradf3(mtr), gradg2(mtr), gradg3(mtr),
     $                 jacob(2,2), x(2), s(2), func(2), h(mtr*mtr),
     $                 u(mtr,mtr), v(mtr,mtr), e(mtr,mtr),
     $                 invmat(mtr*mtr), mdum(mtr,mtr), vtd(mtr,mtr),
     $                 du(mtr,mtr), dk3dsg(mtr)
      double precision capval(2), p(mtr,mtr)
      double precision c, tanphi, tanpsi, c0, tanfi0, tanps0, tanfiu,
     $                 tanpsu, unconf, yield, dyi2dk, dyi3dk, f2, f3,
```

```
     $                     dl2, dl3, eps, upeq2, upeq3, rdum, rdum1,
rdum2,
     $                rdum3, f, df3dk3, tanps1, sigma2, taudl2,
     $                sigdl2, phidk2, psidk2, taudl3, sigdl3,
     $                k3dtau, k3dsig, dk3dl3
      integer         iter, nuinac, modul
c
c...     Initialize
      c0 = usrval(3)
      tanfi0 = usrval(4)
      tanps0 = usrval(5)
      tanfiu = tanfi0
      tanpsu = tanps0
      unconf = -1.d+20 * usrval(3)
      hs1 =hs(1)
      hs2 =hs(2)
      hs3 =hs(3)
      hs4 =hs(4)
      hs5 =hs(5)
      hs6 =hs(6)
      hs7 =hs(7)
      hs8 =hs(8)
      hs9 =hs(9)
      hs10=hs(10)

c
      call rset( 0.D0, p, ntr*ntr )
      capval(2) = usrval(8)
      p(1,1) = 2.D0
      p(2,2) = 2.D0 * capval(2)
c
      call rset(0.d0, x, 2 )
      dyi2dk = 0.D0
      dyi3dk = 0.D0
c
      if ( sw(2) ) then
         print*, 'INELASTIC BEHAVIOUR FOR CORNER 23'
         call prival( eps,  'TOLCHK' )
         call privec( trat, ntr,  'TRAT  ' )
      end if
c
      do 100, iter = 1, miter
c
         if ( sw(2) ) then
            call priivl( iter, 'ITER  ' )
         end if
c
         dl2 = x(1)
         dl3 = x(2)
         if ( dl3 .lt. 0.d0 ) dl3 = 0.d0
         rdum2 = upeq2 + dl2
         call coulhaB( c, tanphi, rdum2, dyi2dk, usrval(3), usrval(6),
     $                 hs )
         tanps1 = tanps0 + ( tanpsu - tanps0 ) * ( c0 - c ) / c0
         rdum   = 1.d0 / ( 1.d0 - dl2 * tule(1) * tanps1 / unconf +
     $            2.d0 * dl3 * tule(1) )
         rdum1  = 1.d0 / ( 1.d0 + 2.d0 * capval(2) * dl3 * tule(4) )
         tra(1) = rdum * ( trat(1) - dl2 * tule(1) * tanps1 )
```

```
c
c...         Adjust the dilatancy angle to zero for tra(1) higher than
unconf
         if ( tra(1) .le. unconf ) then
            tanps0 = 0.d0
            tanpsu = 0.d0
            tanps1 = 0.d0
            rdum   = 1.d0 / ( 2.d0 * dl3 * tule(1) )
            tra(1) = rdum * trat(1)
         end if
         tra(2) = rdum1 * ( trat(2) - dl2 * tule(4) )
c
c...         Calculate equivalent plastic strain for cap
         call rab( p, ntr, ntr, tra, 1, gradf3 )
         rdum3 = upeq3 + dl3 * sqrt( uv( gradf3, gradf3, ntr ) )
         call caphar2( yield, rdum3, dyi3dk, usrval(7), usrval(9) )
         f2     = tra(2) + tra(1) * tanphi - c
         f3     = 0.5d0 * uv( tra, gradf3, ntr ) - yield * yield
c
         if ( sw(2) ) then
            call prival( f2,       'F2-CHK' )
            call prival( f3,       'F3-CHK' )
            call prival( dl2,      'DL2   ' )
            call prival( dl3,      'DL3   ' )
            call prival( rdum2,    'UPEQ2 ' )
            call prival( rdum3,    'UPEQ3 ' )
            call privec( tra, ntr, 'TRA   ' )
         end if
         f = sqrt( f2 * f2 + f3 * f3 )
         if ( abs( f ) .lt. eps ) goto 200
         func(1) = f2
         func(2) = f3
c
c...
c...           Newton Method
         sigma2 = sqrt( tra(1) * tra(1) + ( capval(2) * tra(2) ) ** 2
)
         taudl2 = - tule(4) * rdum1
         psidk2 = - ( tanpsu - tanps0 ) / c0 * dyi2dk
         sigdl2 = tule(1) * (  dl2 * psidk2
     $             + tanps1 ) * ( tra(1) / unconf - 1.d0 ) * rdum
         phidk2 = - ( tanfiu - tanfi0 ) / c0 * dyi2dk
         taudl3 = -2.d0 * capval(2) * tule(4) * tra(2) * rdum1
         sigdl3 = -2.d0 * tule(1) * tra(1) * rdum
         k3dsig = 2.d0 * dl3 * tra(1) / sigma2
         k3dtau = 2.d0 * dl3 * tra(2) * capval(2) * capval(2) / sigma2
         dk3dl3 = 2.d0 * sigma2
c
         jacob(1,1) = taudl2 + sigdl2 * tanphi + tra(1) * phidk2 -
     $                dyi2dk
         jacob(1,2) = taudl3 + sigdl3 * tanphi
         jacob(2,1) = 2.d0 * tra(1) * sigdl2 + 2.d0 * capval(2) *
     $                tra(2) * taudl2 - 2.d0 * yield * dyi3dk *
     $                ( k3dsig * sigdl2 + k3dtau * taudl2 )
         jacob(2,2) = 2.d0 * tra(1) * sigdl3 + 2.d0 * capval(2) *
     $                tra(2) * taudl3 - 2.d0 * yield * dyi3dk *
     $                ( dk3dl3 + k3dsig * sigdl3 + k3dtau * taudl3 )
         if ( sw(2) ) then
            call primat( jacob, 2, 2, 'JACOB' )
```

```
         end if
c
         call inv2( jacob, invmat, rdum )
         call rab( invmat, 2, 2, func, 1, s )
         call uvmw( x, s, 2, x )
         if ( x(2) .le. 0.d0 ) then
            x(2) = 0.d0
            x(1) = dl2 - f2 / jacob(1,1)
         end if
c         call lnsear( func, x, s, 2, tule, trat,
c     $                   upeq2, tanpsu, tanps0, c0, unconf, capval,
c     $                   p, ntr, upeq3 )
c
  100 continue
      write( lout, 1 ) il, ip, f
      nuinac = nuinac + 1
c
  200 continue
      upeq2 = rdum2
      upeq3 = rdum3
      tra(2) = tra(2) * modul
c
c...       Consistent Tangent
c
c...         Adjust the dilatancy angle to zero for tra(1) higher than
unconf
      if ( tra(1) .le. unconf ) then
         tanps0 = 0.d0
         tanpsu = 0.d0
      end if
      tanps1 = tanps0 + ( tanpsu - tanps0 ) * ( c0 - c ) / c0
      tanpsi = tanps1 * ( 1.d0 - tra(1) / unconf )
      gradf2(1) = tanphi
      gradf2(2) = modul
      gradg2(1) = tanpsi
      gradg2(2) = modul
      call rab( p, ntr, ntr, tra, 1, gradf3 )
      call rmove( gradf3, gradg3, ntr )
c
c...     correct gradg2
      gradg2(1) = gradg2(1) - dl2 * ( tanpsu-tanps0 ) / c0 * dyi2dk
     $            * ( 1.d0 - tra(1) / unconf )
c
c...     correct gradf3
      df3dk3 = -2.d0 * yield * dyi3dk
      dk3dl3 = sqrt( uv( gradf3, gradf3, ntr ) )
      call uvs( gradf3, ntr, dl3 / dk3dl3, dk3dsg )
      call uvpws( gradf3, dk3dsg, ntr, df3dk3, gradf3 )
c
c...     correct [d] for [h]
      call rmove( tule, h, ntr*ntr )
      h(1) = 1.d0 / ( 1.d0 / tule(1) + dl2 * tanps1 / unconf +
     $                dl3 * p(1,1) )
      h(4) = 1.d0 / ( 1.d0 / tule(4) + dl3 * p(1,1) )
c
c...     fill matrices [u], [v], [e]
      u(1,1) = gradg2(1)
      u(2,1) = gradg2(2)
```

```
      u(1,2) = gradg3(1)
      u(2,2) = gradg3(2)
c
      v(1,1) = gradf2(1)
      v(2,1) = gradf2(2)
      v(1,2) = gradf3(1)
      v(2,2) = gradf3(2)
c
      e(1,1) = - ( 1.d0 + tra(1) * ( tanfiu - tanfi0 ) / c0 ) * dyi2dk
      e(1,2) = 0.d0
      e(2,1) = 0.d0
      e(2,2) = df3dk3 * dk3dl3
c
c...                                    T                -1    T
c...     [tunl] = [h] - [h] [u] { [v]  [h] [u] - [e] }   [v]  [h]
      call ratb( v, ntr, ntr, h, ntr, vtd )
      call rab( vtd, ntr, ntr, u, ntr, mdum )
      call uvpws( mdum, e, ntr*ntr, -1.d0, mdum )
      call inv2( mdum, invmat, rdum )
      call rab( invmat, ntr, ntr, vtd, ntr, mdum )
      call rab( h, ntr, ntr, u, ntr, du )
      call rab( du, ntr, ntr, mdum, ntr, tunl )
      call uvpws( h, tunl, ntr*ntr, -1.d0, tunl )
c
      return
c
    1 format ( ' ELEMENT:', I4, '   IP:', I4,
     $         ' CORNER23 INACCURATE  F=',1P, E11.3  )
c
      end
```

Appendix 2: MultiFan model (Matlab implementation)

```
function FAN_ml(varargin)
clear global; clear functions;

persistent as disp1 re ;
e=[];wt=[];rh=[];rl=[];
if isempty(disp1), disp1=zeros(1,8); end;
if isempty(re), re=zeros(1,8); end;
if isempty(as), as=zeros(8,8); end;
disp1(:)=[1d-00,-1d-00,1.0d+00,-
1.0d+00,0.0d+00,0.0d+00,0.0d+00,0.0d+00];
e=1.0d+00;
wt=2.0d+00;
rh=1.0d+00;
rl=1.0d+00;
[e,wt,rh,rl,disp1,re,as]=fan(e,wt,rh,rl,disp1,re,as);
end %program multifan
function [e,wt,rh,rl,dispmlv,re,as]=fan(e,wt,rh,rl,dispmlv,re,as);
persistent d2chi dchi dedu delta eps epsr f r sd stif u u1 u2 u3 uu v1
v2 v3 wm1 wm2 wv ww www z1 z2 z3 ;

as_orig=as;as_shape=[8,8];as=reshape([as_orig(1:min(prod(as_shape),num
el(as_orig))),zeros(1,max(0,prod(as_shape)-
numel(as_orig)))],as_shape);
if isempty(u), u=zeros(1,6); end;
if isempty(eps), eps=zeros(1,3); end;
if isempty(epsr), epsr=zeros(1,3); end;
if isempty(r), r=zeros(1,3); end;
if isempty(dedu), dedu=zeros(3,6); end;
if isempty(dchi), dchi=zeros(1,3); end;
if isempty(d2chi), d2chi=zeros(3,2); end;
if isempty(f), f=zeros(1,6); end;
```

```
if isempty(stif), stif=zeros(6,6); end;
if isempty(wv), wv=zeros(1,3); end;
if isempty(wm1), wm1=zeros(3,3); end;
if isempty(wm2), wm2=zeros(3,6); end;
if isempty(ww), ww=zeros(1,6); end;
if isempty(www), www=zeros(6,6); end;
if isempty(u1), u1=0; end;
if isempty(u2), u2=0; end;
if isempty(u3), u3=0; end;
if isempty(v1), v1=0; end;
if isempty(v2), v2=0; end;
if isempty(v3), v3=0; end;
if isempty(delta), delta=0; end;
if isempty(sd), sd=0; end;
if isempty(uu), uu=0; end;
if isempty(z1), z1=0; end;
if isempty(z2), z2=0; end;
if isempty(z3), z3=0; end;
rh=abs(rh);
rl=abs(rl);
pi     = acos(-1.0d+00);
pi2    = pi./2.0d+00;
atan05 = atan(0.5d+00);
%     inizializzazioni e trasformazioni
for  i=1:6;
 f(i)=0.0d+00;
 for  j=1:6;
  stif(i,j)=0.0d+00;
 end;  j=6+1;
end;  i=6+1;
%     initial valeues
et=e.*wt;
rmu=rh./rl;
writef(1,['%s %0.15g \n'], 'e=',(e));
writef(1,['%s %0.15g \n'], 'wt_Fortran=',(wt));
writef(1,['%s %0.15g \n'], 'rh=',(rh));
writef(1,['%s %0.15g \n'], 'rl=',(rl));
disp(['pausa:  premi  ENTER  per  continuare  ...',' --  Hit  Return  to
continue']);
pause ;
for    i=(1):(8),    writef(1,['%s    %0.15g    \n'],    'disp_fortran
=',dispmlv(i)); end;
writef(1,['%s \n'], 'inizio di stfpnl');
u(1) =(   dispmlv(5) + dispmlv(7)) ./ 2.0d+00;
u(2) =(   dispmlv(6) + dispmlv(8)) ./ 2.0d+00;
u(3) =( - dispmlv(6) + dispmlv(8)) ./ rl;
u(4) =(   dispmlv(1) + dispmlv(3)) ./ 2.0d+00;
u(5) =(   dispmlv(2) + dispmlv(4)) ./ 2.0d+00;
u(6) =(   dispmlv(2) - dispmlv(4)) ./ rl;
for i=(1):(6), writef(1,['%s %0.15g \n'], 'u =',u(i)); end;
disp(['pausa:  premi  ENTER  per  continuare  ...',' --  Hit  Return  to
continue']);
pause ;
%     calcolo vettore di deformazione in coordinate cartesiane
phi    =(u(3) + u(6)) ./ 2.0d+00;
eps(1) =(u(4) - u(1) + phi.*rh) ./ rl;
eps(2) =(u(5) - u(2))          ./ rl;
eps(3) =  u(6) - u(3);
%     calcolo vettore di deformazione in coordinate sferiche
```

```
r(1) = sqrt(eps(1).^2 + eps(2).^2 + eps(3).^2);
if(eps(1) ~= 0. || eps(3) ~= 0.)
 r(2) = atan2(eps(3),eps(1));
else;
 r(2) = 0.;
end;
if(r(1) > 0.)
 r(3) = asin(eps(2) ./ r(1));
else;
 r(3) = 0.;
end;
%     calcolo costanti, lambda e chi
cos2   = cos(r(2));
sin2   = sin(r(2));
cos22  = cos2.^2;
sin22  = sin2.^2;
dxi    = 2.0d+00 .* r(2);
cosd2  = cos(dxi);
sind2  = sin(dxi);
etapi2 = r(3) + pi2;
%     Formulazione mista di lambda (14/1/94).
for  il=1:2;
 eta2  =atan(max(abs(cos2)./rmu,abs(sin2)./2.0d+00));
 et2pi2=eta2 + pi2;
 if(il == 1)
  rlam     =     0.90587893d+00     +     0.23389918d+00./pi2     .*
atan(1.03936518d+00.*log(rmu./1.26606774d+00));
  rmult=(eta2-r(3))./et2pi2;
 else;
  rlam =(pi2+atan(0.5d+00))./(pi2+eta2);
  rmult=(r(3)+pi2) ./et2pi2;
 end;
 rlam2  = rlam.^2;
 psi    = sqrt(rlam2.*cos22 + sin22);
 rlam3  = 0.5d+00 .*(1.0d+00 - rlam2) ./ psi;
 psi1   = rlam3 .* sind2;
 psi2   = rlam3 .*(- psi1 .* sind2 ./ psi + 2.0d+00 .* cosd2);
 chi    = psi .* etapi2 - pi2;
 %     pannello non reagente
 if(r(3) >= eta2)
  tpe=0.;
  for  k=1:6;
   f(k)=0.;
   for  l=1:6;
    stif(k,l)=0.;
   end;  l=6+1;
  end;  k=6+1;
  continue;
 end;
 %     calcolo derivate di eps rispetto a u
 for  i=1:3;
  for  k=1:6;
   dedu(i,k) = 0.;
  end;  k=6+1;
 end;  i=3+1;
 rli = 1.0d+00 ./ rl;
 xl2l= rh ./(2.0d+00.*rl);
 dedu(1,1) = -rli;
```

```
 dedu(2,2) = -rli;
 dedu(1,3) =  xl2l;
 dedu(3,3) = -1.0d+00;
 dedu(1,4) =  rli;
 dedu(2,5) =  rli;
 dedu(1,6) =  xl2l;
 dedu(3,6) =  1.0d+00;
 for j=(1):(6), for i=(1):(3), writef(1,['%s %0.15g \n'], 'dedu( , )
=',dedu(i,j)); end; end;
 disp(['pausa: premi ENTER per continuare ...',' -- Hit Return to
continue']);
 pause ;
 %     calcolo costanti e funzioni trigonometriche
 etl2mu = et .* rl.^2 ./ rmu;
 rho    = r(1);
 rho2   = rho.^2;
 cos3   = cos(r(3));
 sin3   = sin(r(3));
 c2s3   = cos2 .* sin3;
 s2s3   = sin2 .* sin3;
 cos32  = cos3.^2;
 cosc   = cos(chi);
 sinc   = sin(chi);
 tanc   = tan(chi);
 t2c    = 1.0d+00 - 2.0d+00.*tanc;
 cosc2  = cosc.^2;
 sinc2  = sinc.^2;
 cosdc  = cosc2 - sinc2;
 sindc  = 2.0d+00.*sinc.*cosc;
 %     calcolo vettore di deformazione in coordinate cartesiane diviso
rho
 epsr(1) = cos2 .* cos3;
 epsr(2) =        sin3;
 epsr(3) = sin2 .* cos3;
 %     calcolo v e sue derivate prima e seconda rispetto a chi
 v=0;
 dvchi =0;
 d2vchi=0;
 if(chi <= -atan05)
  v      =(sinc2 + cosc2./1.2d+01) ./ 2.;
  dvchi  =(1.1d+01./2.4d+01) .* sindc;
  d2vchi =(1.1d+01./1.2d+01) .* cosdc;
 else;
  v      =(cosc./2.0d+00 - sinc).^3 ./(6.0d+00.*cosc);
  dvchi    =  -(1.0d+00./4.8d+01)  .*  t2c.^2  .*(2.0d+00  +  sindc  +
4.0d+00.*cosc2);
  d2vchi  =(1.0d+00./2.4d+01)  .*  t2c  .*(8.0d+00  +  4.0d+00  .*(tanc  +
1.0d+00./cosc2)+ t2c .*(2.0d+00.*sindc - cosdc));
 end;
 %     risoluzione forma indeterminata (eta+pi/2)/cos(eta)
 if(cos3 > 1.0d-08)
  ri1 = etapi2 ./ cos3;
 else;
  ri1 = 1.0d+00;
 end;
 %     calcolo derivate di chi rispetto a eps moltiplicate per rho
 p1r1 = psi1 .* ri1;
 ps3  = psi  .* sin3;
 dchi(1) = - p1r1.*sin2 - ps3.*cos2;
```

```
 dchi(2) =               psi.*cos3;
 dchi(3) =   p1r1.*cos2 - ps3.*sin2;
 %     risoluzione forma indeterminata dvchi/cos(eta)
 if(cos3 > 1.0d-08)
  ri2 = dvchi ./ cos3;
 else;
  ri2 = -(1.1d+01./1.2d+01) .* psi;
 end;
 %     calcolo derivate seconde di chi rispetto a xi ed eps
 p11r = psi1 .*(1.0d+00 + ri1.*sin3);
 pc32 = psi  .* cos32;
 d2chi(1,1) =(- psi2.*sin2 - psi1.*cos2) .* ri1 +(- psi1.*cos2 + psi
.*sin2) .* sin3;
 d2chi(2,1) =                          psi1 .* cos3;
 d2chi(3,1) =(   psi2.*cos2 - psi1.*sin2) .* ri1 +(- psi1.*sin2 - psi
.*cos2) .* sin3;
 d2chi(1,2) = - p11r.*sin2 - pc32.*cos2;
 d2chi(2,2) = - psi.*sin3.*cos3;
 d2chi(3,2) =   p11r.*cos2 - pc32.*sin2;
 %     calcolo energia potenziale totale
 tpe  = etl2mu .* rho2 .* v;
 %     calcolo vettore forze f
 for  i=1:3;
  wv(i)  =  etl2mu  .*(2.0d+00  .*  eps(i)  .*  v   +  rho  .*  dvchi  .*
dchi(i));
 end;  i=3+1;
 [dedu,wv,ww]=atb(dedu,wv,ww,6,3);
 %c     moltiplicazione coefficienti formulazione mista
 for  i=1:6;
  f(i) = f(i) + rmult .* ww(i);
 end;  i=6+1;
 %c      il calcolo della matrice di rigidezza tangente viene skippato
in quanto non affidabile;
 for  i=1:3;
  for  j=1:i;
   wm1(i,j)   =         2.0d+00   .*   dvchi   .*(epsr(i).*dchi(j)   +
epsr(j).*dchi(i)) + d2vchi .* dchi(i) .* dchi(j);
   if(i == j)
    wm1(i,i) = wm1(i,i) + 2.0d+00 .* v;
   end;
  end;  j=i+1;
 end;  i=3+1;
 for  i=1:3;
  for  j=1:i;
   wm1(i,j) = wm1(i,j) - dvchi .* dchi(i) .* epsr(j);
  end;  j=i+1;
 end;  i=3+1;
 for  i=1:3;
  wm1(i,1)    =((wm1(i,1).*1.0d+20    +(    -    d2chi(i,1).*sin2    -
d2chi(i,2).*c2s3) .* ri2.*1.0d+20))./1.0d+20;
 end;  i=3+1;
 for  i=2:3;
  wm1(i,2) = wm1(i,2)                           + d2chi(i,2).*cos3  .*
ri2;
 end;  i=3+1;
 wm1(3,3) = wm1(3,3) +(   d2chi(3,1).*cos2 - d2chi(3,2).*s2s3) .* ri2;
 for  i=1:3;
  for  j=1:i;
```

```
   wm1(i,j) = etl2mu .* wm1(i,j);
  end;  j=i+1;
 end;  i=3+1;
 for  i=1:2;
  for  j=i+1:3;
   wm1(i,j) = wm1(j,i);
  end;  j=3+1;
 end;  i=2+1;
 %c     Il calcolo degli invaruanti viene skippato
 %!! GO TO 225
 if(false)
  %c     calcolo invarianti
  rinv1 = wm1(1,1) + wm1(2,2) + wm1(3,3);
  rinv2 = wm1(1,1).*wm1(2,2)+ wm1(2,2).*wm1(3,3)+ wm1(3,3).*wm1(1,1) -
wm1(1,2).^2 - wm1(2,3).^2 - wm1(3,1).^2;
  rinv3  =  wm1(1,1).*wm1(2,2).*wm1(3,3)+  wm1(1,2).*wm1(2,3).*wm1(3,1)+
wm1(1,3).*wm1(2,1).*wm1(3,2)     -     wm1(3,1).*wm1(2,2).*wm1(1,3)     -
wm1(3,2).*wm1(2,3).*wm1(1,1) - wm1(3,3).*wm1(2,1).*wm1(1,2);
  %c     calcolo coefficienti equazione cubica
  b1 =-rinv1;
  b2 = rinv2;
  b3 =-rinv3;
  %c    soluzione equazione cubica
  pp=-b1.^2./3.0d+00 + b2;
  qq=b1.^3./1.35d+01 - b1.*b2./3.0d+00 + b3;
  qm=qq./2.0d+00;
  delta=qq.^2./4.0d+00 + pp.^3./2.7d+01;
  sd=sqrt(delta);
  u1=-qm+sd;
  r1=u1;
  absu1=abs(u1).^(1.0d+00./3.0d+00);
  argu1=atan2(imag(u1),r1)./3.0d+00;
  u1=absu1.*complex(cos(argu1),sin(argu1));
  uu=complex(0.0d+00,2.0d+00.*pi./3.0d+00);
  u2=u1.*exp( uu);
  u3=u1.*exp(-uu);
  v1=-pp./(3.0d+00.*u1);
  v2=-pp./(3.0d+00.*u2);
  v3=-pp./(3.0d+00.*u3);
  z1=u1+v1 - b1./3.0d+00;
  z2=u2+v2 - b1./3.0d+00;
  z3=u3+v3 - b1./3.0d+00;
  x1=z1;
  x2=z2;
  x3=z3;
  x1=min([x1,x2,x3]);
  %c        se  l'autovalore  piu'  piccolo  x1  e'  inferiore  a  1.0d-
02*etl2mu, si somma alla diagonale
  %c      principale la quantita' 1.0d-02*etl2mu - x1 !c   x11=1.0d-
02*etl2mu - x1
  x11=1.0d+00-x1;
  if(x11 <= 0.0d+00)
   go to 240;
  end;
  writef(1,['%s \n'], 'autovalore negativo o nullo');
  disp(['pausa:  premi  ENTER  per  continuare  ...',' --  Hit  Return  to
continue']);
  pause ;
 end;
```

```
 for  i=1:3;
  wm1(i,i)=wm1(i,i);
 end;  i=3+1;
 [wm1 ,dedu,wm2 ]=mab(wm1 ,dedu,wm2 ,3,3,6);
 [dedu,wm2 ,www ]=matb(dedu,wm2 ,www ,3,6,6);
 for  i=1:6;
  for  j=1:6;
   stif(i,j) = stif(i,j) + rmult .* www(i,j);
  end;  j=6+1;
 end;  i=6+1;
 for  j=(1):(6),  for  i=(1):(6  ),  writef(1,['%s  %0.15g  \n'],
'stif()=',stif(i,j)); end; end;
 disp(['pausa:  premi  ENTER  per  continuare  ...',' --  Hit  Return  to
continue']);
 pause ;
end;  il=2+1;
for i = 1 : 6;
 for j = 1: 6;
  writef(1,['%s %0.15g \n'], 'i =',i);
  writef(1,['%s %0.15g \n'], 'j =',j);
  writef(1,['%s %0.15g \n'], 'stif =',stif(i,j));
  disp(['pausa:  premi  ENTER  per  continuare  ...',' --  Hit  Return  to
continue']);
  pause ;
 end; j = 6+1;
end; i = 6+1;
disp(['pausa:  premi  ENTER  per  continuare  ...',' --  Hit  Return  to
continue']);
pause ;
for i=(1):(6), writef(1,['%s %0.15g \n'], 'f =',f(i)); end;
disp(['pausa:  premi  ENTER  per  continuare  ...',' --  Hit  Return  to
continue']);
pause ;
re(1) = f(4) ./ 2.0d+00;
re(2) = f(5) ./ 2.0d+00 + f(6) ./ rl;
re(3) = f(4) ./ 2.0d+00;
re(4) = f(5) ./ 2.0d+00 - f(6) ./ rl;
re(5) = f(1) ./ 2.0d+00;
re(6) = f(2) ./ 2.0d+00 - f(3) ./ rl;
re(7) = f(1) ./ 2.0d+00;
re(8) = f(2) ./ 2.0d+00 + f(3) ./ rl;
writef(1,['%s \n'], 'fine di stfpnl');
disp(['pausa:  premi  ENTER  per  continuare  ...',' --  Hit  Return  to
continue']);
pause ;
for i=(1):(8), writef(1,['%s %0.15g \n'], '       re =',re(i)); end;
disp(['pausa:  premi  ENTER  per  continuare  ...',' --  Hit  Return  to
continue']);
pause ;
for  i=1:6;
 as(i,1) = stif(i,4) ./ 2.0d+00;
 as(i,2) = stif(i,5) ./ 2.0d+00 + stif(i,6) ./ rl;
 as(i,3) = stif(i,4) ./ 2.0d+00;
 as(i,4) = stif(i,5) ./ 2.0d+00 - stif(i,6) ./ rl;
 as(i,5) = stif(i,1) ./ 2.0d+00;
 as(i,6) = stif(i,2) ./ 2.0d+00 - stif(i,3) ./ rl;
 as(i,7) = stif(i,1) ./ 2.0d+00;
 as(i,8) = stif(i,2) ./ 2.0d+00 + stif(i,3) ./ rl;
```

```
end;  i=6+1;
for  j=1:8;
 a1 = as(4,j) ./ 2.0d+00;
 a2 = as(5,j) ./ 2.0d+00 + as(6,j) ./ rl;
 a3 = as(5,j) ./ 2.0d+00 - as(6,j) ./ rl;
 a4 = as(1,j) ./ 2.0d+00;
 a5 = as(2,j) ./ 2.0d+00 - as(3,j) ./ rl;
 a6 = as(2,j) ./ 2.0d+00 + as(3,j) ./ rl;
 as(1,j) = a1;
 as(2,j) = a2;
 as(3,j) = a1;
 as(4,j) = a3;
 as(5,j) = a4;
 as(6,j) = a5;
 as(7,j) = a4;
 as(8,j) = a6;
end;  j=8+1;
for  i=(1):(8),  writef(1,['%s  %0.15g  \n'],  'dispmlv  =',dispmlv(i));
end;
for i=(1):(8), writef(1,['%s %0.15g \n'], ' re =',re(i)); end;
for   j=(1):(8),   for   i=(1):(8   ),   writef(1,['%s   %0.15g   \n'],
'as_fortran()=',as(i,j)); end; end;
writef(1,['%s %0.15g \n'], 'tpe =',(tpe));
disp(['pausa:  premi  ENTER  per  continuare  ...',' --  Hit  Return  to
continue']);
pause ;
for i = 1 : 8;
 for j = 1: 8;
  writef(1,['%s %0.15g \n'], 'i =',i);
  writef(1,['%s %0.15g \n'], 'j =',j);
  writef(1,['%s %0.15g \n'], 'as =',as(i,j));
  disp(['pausa:  premi  ENTER  per  continuare  ...',' --  Hit  Return  to
continue']);
  pause ;
 end; j = 8+1;
end; i = 8+1;
disp(['Multifan Fine!',' -- Hit Return to continue']);
pause ;
as_orig(1:prod(as_shape))=as;as=as_orig;
end %subroutine  fan
    % . . . . . .
. .
    %c     c = aT b
    %c     a(n,m), b(n), c(m)
function [a,b,c,m,n]=atb(a,b,c,m,n);

a_orig=a;a_shape=[n,m];a=reshape([a_orig(1:min(prod(a_shape),numel(a_o
rig))),zeros(1,max(0,prod(a_shape)-numel(a_orig)))],a_shape);
for  i=1:m;
 c(i) = 0.;
 for  j=1:n;
  c(i) = c(i) + a(j,i).*b(j);
 end;  j=n+1;
end;  i=m+1;
a_orig(1:prod(a_shape))=a;a=a_orig;
return;
end %subroutine atb
    % . . . . . .
. .
```

```
function [a,b,c,l,m,n]=mab(a,b,c,l,m,n);

a_orig=a;a_shape=[m,l];a=reshape([a_orig(1:min(prod(a_shape),numel(a_o
rig))),zeros(1,max(0,prod(a_shape)-numel(a_orig)))],a_shape);
b_orig=b;b_shape=[l,n];b=reshape([b_orig(1:min(prod(b_shape),numel(b_o
rig))),zeros(1,max(0,prod(b_shape)-numel(b_orig)))],b_shape);
c_orig=c;c_shape=[m,n];c=reshape([c_orig(1:min(prod(c_shape),numel(c_o
rig))),zeros(1,max(0,prod(c_shape)-numel(c_orig)))],c_shape);
for  i=1:m;
 for  j=1:n;
  c(i,j) = 0.;
  for  k=1:l;
   c(i,j) = c(i,j) + a(i,k).*b(k,j);
  end;  k=l+1;
 end;  j=n+1;
end;  i=m+1;
a_orig(1:prod(a_shape))=a;a=a_orig;
b_orig(1:prod(b_shape))=b;b=b_orig;
c_orig(1:prod(c_shape))=c;c=c_orig;
return;
end %subroutine mab
    % . . . . . . . . . . . . . . . . . . . . . . . . . . . . . . . . . .
. .
function [a,b,c,l,m,n]=matb(a,b,c,l,m,n);

a_orig=a;a_shape=[l,m];a=reshape([a_orig(1:min(prod(a_shape),numel(a_o
rig))),zeros(1,max(0,prod(a_shape)-numel(a_orig)))],a_shape);
b_orig=b;b_shape=[l,n];b=reshape([b_orig(1:min(prod(b_shape),numel(b_o
rig))),zeros(1,max(0,prod(b_shape)-numel(b_orig)))],b_shape);
c_orig=c;c_shape=[m,n];c=reshape([c_orig(1:min(prod(c_shape),numel(c_o
rig))),zeros(1,max(0,prod(c_shape)-numel(c_orig)))],c_shape);
for  i=1:m;
 for  j=1:n;
  c(i,j) = 0.;
  for  k=1:l;
   c(i,j) = c(i,j) + a(k,i).*b(k,j);
  end;  k=l+1;
 end;  j=n+1;
end;  i=m+1;
a_orig(1:prod(a_shape))=a;a=a_orig;
b_orig(1:prod(b_shape))=b;b=b_orig;
c_orig(1:prod(c_shape))=c;c=c_orig;
return;
end %subroutine matb

function out=writef(fid,varargin)
% function out=writef(fid,varargin)
%  Catches fortran stdout (6) and reroutes in to Matlab's stdout (1)
%  Catches fortran stderr (0) and reroutes in to Matlab's stderr (2)
if isnumeric(fid)
 if fid==6,      out=fprintf(1,varargin{:});
 elseif fid==0,  out=fprintf(2,varargin{:});
 elseif isempty(fid) %% treat empty array like a string array [sethg
2008-03-03]
  out=sprintf(varargin{:});
  if nargin>2 %set the calling var to out
   if ~isempty(inputname(1)), assignin('caller',inputname(1),out); end
  end
```

```
 else,           out=fprintf(fid,varargin{:});
 end
elseif ischar(fid)
 out=sprintf(varargin{:});
 if nargin>2 %set the calling var to out
  if ~isempty(inputname(1)), assignin('caller',inputname(1),out); end
 end
else,            out=fprintf(fid,varargin{:});
end
end
```

Appendix 3: Simplified pushover analysis (Matlab implementation)

```
function FRPushover_ml(varargin)
clear global; clear functions;

persistent a ort eldispa crtdsp crtdspm dctlt dx dy esce qratio
fileimp fileout qratiom firstCall gt shrmd shrmdz h hm V1 hend lvfu
lvfur nmbr pz rnmbr spx spy tk tkm wght wghtr Stffsz Stffszz shrstr
Title hght x y stiffnesszx stiffnesszy strght FRPstrengthening fdt ffu
wdt tdt costeta fdb Ef ddebonding FRPhu1 FRPhu2 eldipla3 crtdisp3
eldipla1 eldipla2 crtdisp1 crtdisp2 dshear stiffnesszx2  ; if
isempty(firstCall),firstCall=1;end;
nz=[];stiffnessex=[];stiffnessey=[];tx=[];ty=[];spxm=[];spym=[];vmx=[]
;vmy=[];xp=[];yp=[];Erst=[];tke=[];dcs=[];qratioma=[];nmc=[];
if isempty(dx), dx=zeros(1,500); end;
if isempty(dy), dy=zeros(1,500); end;
if isempty(x), x=zeros(1,500); end;
if isempty(y), y=zeros(1,500); end;
if isempty(wght), wght=zeros(1,500); end;
if isempty(hght), hght=zeros(1,500); end;
if isempty(shrmd), shrmd=zeros(1,500); end;
if isempty(shrstr), shrstr=zeros(1,500); end;
if isempty(ort), ort=zeros(1,500); end;
if isempty(Stffsz), Stffsz=zeros(1,500); end;
if isempty(pz), pz=zeros(1,500); end;
if isempty(dctlt), dctlt=zeros(1,500); end;
if isempty(nmbr), nmbr=zeros(1,500); end;
if isempty(shrmdz), shrmdz=zeros(1,500); end;
if isempty(Stffszz), Stffszz=zeros(1,500); end;
if isempty(rnmbr), rnmbr=zeros(1,500); end;
if isempty(wghtr), wghtr=zeros(1,500); end;
if isempty(Title), Title=zeros(1,18); end;
```

```
if isempty(strght), strght=zeros(1,500); end;
if isempty(FRPstrengthening), FRPstrengthening=zeros(1,500); end;
if isempty(fdt), fdt=zeros(1,500); end;
if isempty(ffu), ffu=zeros(1,500); end;
if isempty(wdt),  wdt=zeros(1,500); end;
if isempty(tdt), tdt=zeros(1,500); end;
if isempty(costeta), costeta=zeros(1,500); end;
if isempty(fdb), fdb=zeros(1,500); end;
if isempty(Ef), Ef=zeros(1,500); end;
if isempty(ddebonding), ddebonding=zeros(1,500); end;
if isempty(FRPhu1), FRPhu1=zeros(1,500); end;
if isempty(FRPhu2), FRPhu2=zeros(1,500); end;
if isempty(eldipla3), eldipla3=zeros(1,500); end;
if isempty(crtdisp3), crtdisp3=zeros(1,500); end;
if isempty(eldipla1), eldipla1=zeros(1,500); end;
if isempty(eldipla2), eldipla2=zeros(1,500); end;
if isempty(crtdisp1), crtdisp1=zeros(1,500); end;
if isempty(crtdisp2), crtdisp2=zeros(1,500); end;
if isempty(dshear), dshear=zeros(1,500); end;
if isempty(stiffnesszx2), stiffnesszx2=zeros(1,500); end;

if isempty(stiffnesszx), stiffnesszx=zeros(1,500); end;
if isempty(stiffnesszy), stiffnesszy=zeros(1,500); end;
if isempty(eldispa), eldispa=zeros(1,500); end;
if isempty(crtdsp), crtdsp=zeros(1,500); end;
if isempty(h), h=zeros(1,500); end;
if isempty(V1), V1=zeros(1,500); end;
if isempty(tk), tk=zeros(1,500); end;
if isempty(qratio), qratio=zeros(1,500); end;
if isempty(spx), spx=zeros(1,500); end;
if isempty(spy), spy=zeros(1,500); end;
if isempty(hend), hend=zeros(1,500); end;
if isempty(hm), hm=zeros(1,500); end;
if isempty(crtdspm), crtdspm=zeros(1,500); end;
if isempty(tkm), tkm=zeros(1,500); end;
if isempty(qratiom), qratiom=zeros(1,500); end;
if isempty(lvfu), lvfu=zeros(1,500); end;
if isempty(lvfur), lvfur=zeros(1,500); end;
if isempty(fileimp), fileimp=repmat(' ',1,12); end;
if isempty(fileout), fileout=repmat(' ',1,12); end;
if isempty(esce), esce=false; end;
if isempty(a), a=cell(1,2); end;
if isempty(gt), gt=zeros(1,5); end;
if firstCall,   a{1} =['X'];  end;
if firstCall,  a{2}=['Y'];  end;
firstCall=0;
gt(:)=0;
fileimp = 'MB.IN';
fileout = 'MB.OUT';
fid_5=fopen(fileimp,'r');
if fid_5==-1
 error('Provide input file');
end
fid_6=fopen(fileout,'w');
if fid_6==-1
 error('Provide output file');
end
ndim = 500;
```

```
coscsy = 1000.;
coscg = 1000.;
[ Title]=fgetl(fid_5);
%   Format
ge=0;
rnz =fscanf(fid_5,'%g',1);
ve =fscanf(fid_5,'%g',1);
ge =fscanf(fid_5,'%g',1);
shrstre =fscanf(fid_5,'%g',1);
Stffse =fscanf(fid_5,'%g',1);
pae =fscanf(fid_5,'%g',1);
wghtttl=fscanf(fid_5,'%g',1);
nz = fix(rnz);
nmct = fix(nz./3);
ge = ge.*coscg;
Stffse = Stffse.*coscsy;
for i = 1 : nz;
 rnmbr(i) =fscanf(fid_5,'%g',size( rnmbr(i) ));
 dx(i) =fscanf(fid_5,'%g',size( dx(i) ));
 dy(i) =fscanf(fid_5,'%g',size( dy(i) ));
 x(i) =fscanf(fid_5,'%g',size( x(i) ));
 y(i) =fscanf(fid_5,'%g',size( y(i) ));
 wght(i) =fscanf(fid_5,'%g',size( wght(i) ));
 wghtr(i) =fscanf(fid_5,'%g',size(wghtr(i) ));
 hght(i) =fscanf(fid_5,'%g',size( hght(i) ));
 shrmd(i) =fscanf(fid_5,'%g',size( shrmd(i) ));
 shrstr(i) =fscanf(fid_5,'%g',size( shrstr(i) ));
 ort(i) =fscanf(fid_5,'%g',size( ort(i) ));
 pz(i)=fscanf(fid_5,'%g',size( pz(i)));
 dctlt(i)=fscanf(fid_5,'%g',size( dctlt(i)));
%
 strght(i)=fscanf(fid_5,'%g',size( strght(i)));
 fdt(i)=fscanf(fid_5,'%g',size( fdt(i)));
 ffu(i)=fscanf(fid_5,'%g',size( ffu(i)));
 wdt(i)=fscanf(fid_5,'%g',size( wdt(i)));
 tdt(i)=fscanf(fid_5,'%g',size( tdt(i)));
 costeta(i)=fscanf(fid_5,'%g',size( costeta(i)));
 fdb(i)=fscanf(fid_5,'%g',size( fdb(i)));
 Ef(i)=fscanf(fid_5,'%g',size( Ef(i)));
%
 garbage=fscanf(fid_5,'%g',1);
 rnmbrs = rnmbr(i);
 nmbr(i) = fix(fix(rnmbrs));
 shrmd(i) = shrmd(i).*coscg;
 if( hght(i)<=0 )
  hght(i) = ve;
 end;
 if( shrmd(i)<=0 )
  shrmd(i) = ge;
 end;
 if( shrstr(i)<=0 )
  shrstr(i) = shrstre;
 end;
 Stffsz(i) = Stffse;
 if( pz(i)<=0 )
  pz(i) = pae;
 end;
 if( pz(i)==99 )
  pz(i) = 0;
```

```
 end;
 if((dctlt(i)<=0 && pz(i)<=0) )
  dctlt(i) = 1.5;
 end;
 if((dctlt(i)<=0 && pz(i)>0) )
  dctlt(i) = 2.0;
 end;
end; i = nz+1;
writef(fid_6,[ '\n ' , '\n ' ,repmat(' ',1,3),repmat('%4c',1,18) '
\n'], Title);
writef(fid_6,[ '\n ' , '\n ' , '\n ' ,repmat(' ',1,34),'Pier
Properties', '\n ' , '\n ' ,repmat(' ',1,6),'DX',repmat('
',1,6),'DY',repmat(' ',1,6),'X',repmat(' ',1,7),'Y',repmat('
',1,7),'wght',repmat(' ',1,7),'wghtr',repmat(' ',1,9),'V',repmat('
',1,9),'G',repmat(' ',1,7),'Shear strength',repmat('
',1,4),'Angle',repmat(' ',1,6),'Stffs',repmat(' ',1,8),'PA',repmat('
',1,2),'DU/eldispa', '\n ' ,repmat(' ',1,5),'(M)',repmat('
',1,5),'(M)',repmat(' ',1,5),'(M)',repmat(' ',1,5),'(M)',repmat('
',1,4),'(T/M2)',repmat(' ',1,3),'(T/M2)',repmat('
',1,7),'(M)',repmat(' ',1,3),'(T/M2)/1000',repmat('
',1,1),'(T/M2)',repmat(' ',1,3),'(degrees)',repmat('
',1,1),'(T/M2)/1000',repmat(' ',1,1),'(0/00)' ' \n']);
for i = 1 : nz;
 shrmdz(i) = shrmd(i)./1000.;
 Stffszz(i) = Stffsz(i)./1000.;
 Strngthnng = pz(i);
 %  Strngthnng > 0 ==> Strengthening
 if( Strngthnng<=0 )
  writef(fid_6,['%3i',repmat(['%7.3f',repmat(' ',1,1)]
,1,4),'%7.3f',repmat(' ',1,2),'%7.3f',repmat(' ',1,5),'%7.3f',repmat('
',1,2),'%8.3f',repmat(' ',1,2),'%7.3f',repmat('
',1,2),repmat(['%7.3f',repmat(' ',1,3)] ,1,3),'%3.1f' ' \n'], nmbr(i)
, dx(i) , dy(i) , x(i) , y(i) ,wght(i) , wghtr(i) , hght(i) ,
shrmdz(i) , shrstr(i) ,ort(i) , pz(i) , pz(i) , dctlt(i), strght(i) ,
fdt(i) , ffu(i) , wdt(i) , tdt(i) , costeta(i) , fdb(i) , Ef(i));
 else;
  writef(fid_6,['%3i',repmat(['%7.3f',repmat(' ',1,1)]
,1,4),'%7.3f',repmat(' ',1,2),'%7.3f',repmat(' ',1,5),'%7.3f',repmat('
',1,2),'%8.3f',repmat(' ',1,2),'%7.3f',repmat('
',1,2),repmat(['%7.3f',repmat(' ',1,3)] ,1,3),'%3.1f' ' \n'], nmbr(i)
, dx(i) , dy(i) , x(i) , y(i) ,wght(i) , wghtr(i) , hght(i) ,
shrmdz(i) , shrstr(i) ,ort(i) , Stffszz(i) , pz(i) , dctlt(i),
strght(i) , fdt(i) , ffu(i) , wdt(i) , tdt(i) , costeta(i) , fdb(i) ,
Ef(i));
 end;
end; i = nz+1;
ssf = 0.;
sfx = 0.;
sfy = 0.;
for i = 1 : nz;
 ort(i) = ort(i).*3.141593./180.;
end; i = nz+1;
for i = 1 : nz;
 sf = wght(i).*dx(i).*dy(i);
 ssf = ssf + sf;
 sfx = sfx + sf.*x(i);
 sfy = sfy + sf.*y(i);
end; i = nz+1;
```

```
tx = sfx./ssf;
ty = sfy./ssf;
stiffnessex = 0.;
stiffnessey = 0.;
for i = 1 : nz;
 stiffnesszx(i)
=(shrmd(i).*dx(i).*dy(i))./(1.2.*hght(i).*(1.+1.33.*(hght(i)./dx(i)).^
2));
 stiffnesszy(i)
=(shrmd(i).*dx(i).*dy(i))./(1.2.*hght(i).*(1.+1.33.*(hght(i)./dy(i)).^
2));
 az = stiffnesszx(i);
 bz = stiffnesszy(i);
 stiffnesszx(i) = az.*cos(ort(i)).^2 + bz.*sin(ort(i)).^2;
 stiffnesszy(i) = bz.*cos(ort(i)).^2 + az.*sin(ort(i)).^2;
 stiffnessex = stiffnessex + stiffnesszx(i);
 stiffnessey = stiffnessey + stiffnesszy(i);
end; i = nz+1;
[nz,stiffnesszx,stiffnesszy,stiffnessex,stiffnessey,x,y,tx,ty,spx,spy,
spxm,spym,vmx,vmy,xp,yp]=sub1(nz,stiffnesszx,stiffnesszy,stiffnessex,s
tiffnessey,x,y,tx,ty,spx,spy,spxm,spym,vmx,vmy,xp,yp);
writef(fid_6,[ '\n ' , '\n ' , '\n ' ,repmat(' ',1,30),'Definitions',
'\n ' , '\n ' ,repmat(' ',1,30),'   V1  Force at ultimate state', '\n
' ,repmat(' ',1,30),'   eldispa  Displacement Allowed', '\n '
,repmat(' ',1,30),'DU/eldispa  Ductility', '\n ' ,repmat(' ',1,30),'
K   stiffness', '\n ' ,repmat(' ',1,30),'   H   Reaction Force', '\n '
,repmat(' ',1,30),'   D   displacement', '\n ' ,repmat(' ',1,30),'
qratio  Ratio q', '\n ' ,repmat(' ',1,30),'Weight 1
=','%10.3f',repmat(' ',1,1),'T', '\n ' ,repmat(' ',1,30),'Weight
2=','%10.3f',repmat(' ',1,1),'T', '\n ' ,repmat(' ',1,30),'     X
Y  ', '\n ' ,repmat(' ',1,30),repmat(' ',1,2),'%7.3f',repmat('
',1,2),'%7.3f',repmat(' ',1,10),'Center of Mass', '\n ' ,repmat('
',1,30),repmat(' ',1,2),'%7.3f',repmat(' ',1,2),'%7.3f',repmat('
',1,10),'Center of Stiffness' ' \n'], wghtttl , ssf , tx , ty , xp ,
yp);

kd = 1;
%  Calculation in X-Y direction
while (1);
 gt(:)=0;
 esce = false;
 for i = 1 : nz;
  hend(i) = 0;
  V1(i) =
dx(i).*dy(i).*shrstr(i).*sqrt(1.+(wght(i)+wghtr(i))./(1.5.*shrstr(i))+
(wght(i).*wghtr(i))./(2.25.*shrstr(i).^2));
  V1(i) = V1(i).*0.9;
  %
  eldispa3(i) = V1(i)./stiffnesszx(i);
  crtdsp(i) = eldispa3(i)./spx(i);

  FRPhu1(i) = V1(i)*1.1 +ffu(i)*wdt(i)*tdt(i)*costeta(i)
  FRPhu1(i) = FRPhu1(i)*0.9
  eldispa1(i) = FRPhu1(i)/stiffnesszx(i)
  crtdsp1(i) = eldispa1(i)/spx(i)
  dshear(i)=2*eldispa1(i)

  FRPhu2(i) = V1(i)*1.1+fdb(i)*wdt(i)*tdt(i)*costeta(i)
```

```
  FRPhu2(i) = FRPhu2(i)*0.9
  eldispa2(i) = FRPhu2(i)/stiffnesszx(i)
  crtdsp2(i) = eldispa2(i)/spx(i)
  ddebonding(i)=
(fdb(i)/Ef(i))*costeta(i)*sqrt(dx(i)*dx(i)+hght(i)*hght(i))
  eldispa(i) = eldispa3(i)
  crtdsp(i) = crtdsp(i)/spx(i)
  if (FRPhu1(i)>FRPhu2(i))   mxdsp(i)=ddebonding(i)
  if (FRPhu1(i)<FRPhu2(i))   mxdsp(i)=dshear(i)
  % Cla
  %



  if( i==1 )
   dmin = crtdsp(1);
  end;
  if( i~=1 )
   if((abs(crtdsp(i))-abs(dmin))<0. )
    dmin = crtdsp(i);
   end;
  end;
 end; i = nz+1;
 writef(fid_6,[ '\n ' , '\n ' , '\n ' ,repmat(' ',1,30),'Wall
Properties ','%1s' ' \n'], a{kd});
 writef(fid_6,[repmat(' ',1,37),'V1',repmat('
',1,8),'eldispa',repmat(' ',1,9),'K', '\n ' ,repmat('
',1,37),'(T)',repmat(' ',1,7),'(M)',repmat(' ',1,6),'(T/M)' ' \n']);
  for i=(1):(nz), writef(fid_6,[repmat('
',1,29),'%3i',repmat('%10.3f',1,3) '
\n'],nmbr(i),V1(i),eldispa(i),stiffnesszx(i)); end;
  dcme = dmin.*spxm;
 Erst = 0.;
 for i = 1 : nz;
  crtdsp(i) = dmin.*spx(i);
  h(i) = crtdsp(i).*stiffnesszx(i);
  Erst = Erst + h(i);
  qratio(i) = crtdsp(i)./eldispa(i);
 end; i = nz+1;
 vke = Erst./ssf;
 if( wghtttl>0. )
  vke = Erst./wghtttl;
 end;
 writef(fid_6,[ '\n ' , '\n ' , '\n ' ,repmat(' ',1,30),'Floor
Properties ','%1s' ' \n'], a{kd});
 writef(fid_6,[ '\n ' , '\n ' ,repmat(' ',1,27),'Floor Elastic Limit'
' \n']);
  writef(fid_6,[ '\n ' ,repmat(' ',1,35),'Reaction Force','%10.3f','
T', '\n ' ,repmat(' ',1,35),'displacement   ','%10.3f',' M', '\n '
,repmat(' ',1,35),'stiffness     ','%10.3f',' T/M', '\n ' ,repmat('
',1,35),'VK            ','%10.3f' ' \n'], Erst , dcme , stiffnessex ,
vke);
 writef(fid_6,[ '\n ' , '\n ' ,repmat(' ',1,22),'Piers Elastic Limit'
' \n']);
  writef(fid_6,[ '\n ' ,repmat(' ',1,38),'H',repmat('
',1,9),'D',repmat(' ',1,9),'K',repmat(' ',1,8),'qratio', '\n '
,repmat(' ',1,37),'(T)',repmat(' ',1,7),'(M)',repmat(' ',1,6),'(T/M)'
' \n']);
```

```
 for i=(1):(nz), writef(fid_6,[repmat('
',1,29),'%3i',repmat('%10.3f',1,4) '
\n'],nmbr(i),h(i),crtdsp(i),stiffnesszx(i),qratio(i)); end;
 qratioma = 0.;
 nmc = 0;
 nmcu = 0;
 dcs = dmin;
  %   Cracking state
  while (1);
  dcs = 1.05.*dcs;

[nz,Erst,tke,dcs,qratioma,nmc,stiffnesszx,eldispa,spx,crtdsp,V1,h,tk,q
ratio,pz,dctlt,hend,lvfu]=sub2(nz,Erst,tke,dcs,qratioma,nmc,stiffnessz
x,eldispa,spx,crtdsp,V1,h,tk,qratio,pz,dctlt,hend,lvfu);
  if( qratioma>1.2 )
   dcme = dcs.*spxm;
   vke = Erst./ssf;
   if( wghtttl>0. )
    vke = Erst./wghtttl;
   end;
   writef(fid_6,[ '\n ' , '\n ' ,repmat(' ',1,24),'Cracking Floor
Behavioun' ' \n']);
   writef(fid_6,[ '\n ' ,repmat(' ',1,35),'Reaction Force','%10.3f','
T', '\n ' ,repmat(' ',1,35),'displacement   ','%10.3f',' M', '\n '
,repmat(' ',1,35),'stiffness     ','%10.3f',' T/M', '\n ' ,repmat('
',1,35),'VK            ','%10.3f' ' \n'], Erst , dcme , tke , vke);
   writef(fid_6,[ '\n ' , '\n ' ,repmat(' ',1,19),'Cracking Pier
Behaviour' ' \n']);
   writef(fid_6,[ '\n ' ,repmat(' ',1,38),'H',repmat('
',1,9),'D',repmat(' ',1,9),'K',repmat(' ',1,8),'qratio', '\n '
,repmat(' ',1,37),'(T)',repmat(' ',1,7),'(M)',repmat(' ',1,6),'(T/M)'
' \n']);
   for i=(1):(nz), writef(fid_6,[repmat('
',1,29),'%3i',repmat('%10.3f',1,4) '
\n'],nmbr(i),h(i),crtdsp(i),tk(i),qratio(i)); end;
   kc = 0;
   V1e = Erst;
   dcmem = dcme;
   dcmep = dcme;
   tkem = tke;
  else;
   [nz,tk,tke,y,ty,spx,spxm,vmy]=sub3(nz,tk,tke,y,ty,spx,spxm,vmy);
   continue;
  end;
  break;
 end;
 %   Plastic state
  while (1);
  gt(2)=0;

[nz,Erst,tke,dcs,qratioma,nmc,stiffnesszx,eldispa,spx,crtdsp,V1,h,tk,q
ratio,pz,dctlt,hend,lvfu,FRPhu1,FRPhu2,mxdsp,zkzx2,strght,eldispla1,el
displa2,
eldispla3]=sub2(nz,Erst,tke,dcs,qratioma,nmc,stiffnesszx,eldispa,spx,c
rtdsp,V1,h,tk,qratio,pz,dctlt,hend,lvfu,FRPhu1,FRPhu2,mxdsp,zkzx2,strg
ht,eldispla1,eldispla2, eldispla3);
  if( nmc>0 )
   for i = 1 : nmc;
    kmur = lvfu(i);
```

```
    lvfur(i) = fix(nmbr(kmur));
   end; i = nmc+1;
  end;
  if( ~(~(nmc>0) || esce ||(V1e>Erst)) )
   vke = V1e./ssf;
   if( wghtttl>0. )
    vke = V1e./wghtttl;
   end;
   writef(fid_6,[ '\n ' , '\n ' , '\n ' ,repmat(' ',1,27),'Wall
Collapse N=','%3i' ' \n'], lvfur(1));
   writef(fid_6,[ '\n ' ,repmat(' ',1,35),'Reaction Force','%10.3f','
T', '\n ' ,repmat(' ',1,35),'displacement   ','%10.3f',' M', '\n '
,repmat(' ',1,35),'stiffness     ','%10.3f',' T/M', '\n ' ,repmat('
',1,35),'VK            ','%10.3f' ' \n'], V1e , dcmem , tkem , vke);
   writef(fid_6,[ '\n ' , '\n ' ,repmat(' ',1,20),'Ultimate state
Piers' ' \n']);
   writef(fid_6,[ '\n ' ,repmat(' ',1,38),'H',repmat('
',1,9),'D',repmat(' ',1,9),'K',repmat(' ',1,8),'qratio', '\n '
,repmat(' ',1,37),'(T)',repmat(' ',1,7),'(M)',repmat(' ',1,6),'(T/M)'
' \n']);
   for i=(1):(nz), writef(fid_6,[repmat('
',1,29),'%3i',repmat('%10.3f',1,4) '
\n'],nmbr(i),hm(i),crtdspm(i),tkm(i),qratiom(i)); end;
   esce = true;
  end;
  if( Erst>V1e )
   V1e = Erst;
   kc = 0;
   nmcu = nmc;
   for i = 1 : nz;
    hm(i) = h(i);
    crtdspm(i) = crtdsp(i);
    tkm(i) = tk(i);
    qratiom(i) = qratio(i);
   end; i = nz+1;
   dcmem = dcme;
   tkem = tke;
  else;
   kc = kc + 1;
  end;
  if( kc<20 )
   if( nmc<nmct )
    [nz,tk,tke,y,ty,spx,spxm,vmy]=sub3(nz,tk,tke,y,ty,spx,spxm,vmy);
    dcs = 1.05.*dcs;
    dcme = dcs.*spxm;
    f = dcme./dcmep;
    if( abs(f)>1.5 )
     vke = V1e./ssf;
     if( wghtttl>0. )
      vke = V1e./wghtttl;
     end;
     if( nmcu==0 )
      writef(fid_6,[ '\n ' , '\n ' ,repmat(' ',1,24),'Limit state
floor behavior' ' \n']);
      writef(fid_6,[ '\n ' ,repmat(' ',1,35),'Reaction
Force','%10.3f',' T', '\n ' ,repmat(' ',1,35),'displacement
','%10.3f',' M', '\n ' ,repmat(' ',1,35),'stiffness     ','%10.3f','
```

```
T/M', '\n ' ,repmat(' ',1,35),'VK            ','%10.3f' ' \n'], V1e ,
dcmem , tkem , vke);
      writef(fid_6,[ '\n ' , '\n ' ,repmat(' ',1,20),'Ultimate state
Piers' ' \n']);
      writef(fid_6,[ '\n ' ,repmat(' ',1,38),'H',repmat('
',1,9),'D',repmat(' ',1,9),'K',repmat(' ',1,8),'qratio', '\n '
,repmat(' ',1,37),'(T)',repmat(' ',1,7),'(M)',repmat(' ',1,6),'(T/M)'
' \n']);
      for i=(1):(nz), writef(fid_6,[repmat('
',1,29),'%3i',repmat('%10.3f',1,4) '
\n'],nmbr(i),hm(i),crtdspm(i),tkm(i),qratiom(i)); end;
      gt(3)=1;
      break;
     end;
     writef(fid_6,[ '\n ' , '\n ' ,repmat(' ',1,40),'Torsional
failure' ' \n']);
      if( nmcu==0 )
      writef(fid_6,[ '\n ' , '\n ' ,repmat(' ',1,24),'Floor Ultimate
state properties' ' \n']);
      writef(fid_6,[ '\n ' ,repmat(' ',1,35),'Reaction
Force','%10.3f',' T', '\n ' ,repmat(' ',1,35),'displacement
','%10.3f',' M', '\n ' ,repmat(' ',1,35),'stiffness     ','%10.3f','
T/M', '\n ' ,repmat(' ',1,35),'VK            ','%10.3f' ' \n'], V1e ,
dcmem , tkem , vke);
      writef(fid_6,[ '\n ' , '\n ' ,repmat(' ',1,20),'Ultimate state
Piers' ' \n']);
     else;
      writef(fid_6,[ '\n ' , '\n ' ,repmat(' ',1,22),'Displacement
increments', '\n ' ,repmat(' ',1,22),'Walls collapsed ' ' \n']);
      for i=(1):(nmcu), writef(fid_6,[repmat('
',1,21),repmat('%6i',1,8) ' \n'],lvfur(i)); end;
      writef(fid_6,[ '\n ' ,repmat(' ',1,35),'Reaction
Force','%10.3f',' T', '\n ' ,repmat(' ',1,35),'displacement
','%10.3f',' M', '\n ' ,repmat(' ',1,35),'stiffness     ','%10.3f','
T/M', '\n ' ,repmat(' ',1,35),'VK            ','%10.3f' ' \n'], V1e ,
dcmem , tkem , vke);
      writef(fid_6,[ '\n ' ,repmat(' ',1,32),'Wall Behavior' ' \n']);
     end;
     writef(fid_6,[ '\n ' ,repmat(' ',1,38),'H',repmat('
',1,9),'D',repmat(' ',1,9),'K',repmat(' ',1,8),'qratio', '\n '
,repmat(' ',1,37),'(T)',repmat(' ',1,7),'(M)',repmat(' ',1,6),'(T/M)'
' \n']);
     for i=(1):(nz), writef(fid_6,[repmat('
',1,29),'%3i',repmat('%10.3f',1,4) '
\n'],nmbr(i),hm(i),crtdspm(i),tkm(i),qratiom(i)); end;
     gt(3)=1;
     break;
    else;
     dcmep = dcme;
     gt(2)=1;
    end;
   end;
  end;
  if(gt(2)==0)
   break;
  end;
 end;

 if(gt(3)==0)
```

```
  vke = V1e./ssf;
  if( wghtttl>0. )
   vke = V1e./wghtttl;
  end;
  if( nmcu~=0 )
   writef(fid_6,[ '\n ' , '\n ' ,repmat(' ',1,22),'Displacement
increments', '\n ' ,repmat(' ',1,22),'Walls collapsed ' ' \n']);
   for i=(1):(nmcu), writef(fid_6,[repmat(' ',1,21),repmat('%6i',1,8)
' \n'],lvfur(i)); end;
   writef(fid_6,[ '\n ' ,repmat(' ',1,35),'Reaction Force','%10.3f','
T', '\n ' ,repmat(' ',1,35),'displacement   ','%10.3f',' M', '\n '
,repmat(' ',1,35),'stiffness     ','%10.3f',' T/M', '\n ' ,repmat('
',1,35),'VK            ','%10.3f' ' \n'], V1e , dcmem , tkem , vke);
   writef(fid_6,[ '\n ' ,repmat(' ',1,32),'Wall Behavior' ' \n']);
   writef(fid_6,[ '\n ' ,repmat(' ',1,38),'H',repmat('
',1,9),'D',repmat(' ',1,9),'K',repmat(' ',1,8),'qratio', '\n '
,repmat(' ',1,37),'(T)',repmat(' ',1,7),'(M)',repmat(' ',1,6),'(T/M)'
' \n']);
   for i=(1):(nz), writef(fid_6,[repmat('
',1,29),'%3i',repmat('%10.3f',1,4) '
\n'],nmbr(i),hm(i),crtdspm(i),tkm(i),qratiom(i)); end;
  end;
  writef(fid_6,[ '\n ' , '\n ' ,repmat(' ',1,24),'Floor Ultimate state
properties' ' \n']);
  writef(fid_6,[ '\n ' ,repmat(' ',1,35),'Reaction Force','%10.3f','
T', '\n ' ,repmat(' ',1,35),'displacement   ','%10.3f',' M', '\n '
,repmat(' ',1,35),'stiffness     ','%10.3f',' T/M', '\n ' ,repmat('
',1,35),'VK            ','%10.3f' ' \n'], V1e , dcmem , tkem , vke);
  writef(fid_6,[ '\n ' , '\n ' ,repmat(' ',1,20),'Ultimate state
Piers' ' \n']);
  writef(fid_6,[ '\n ' ,repmat(' ',1,38),'H',repmat('
',1,9),'D',repmat(' ',1,9),'K',repmat(' ',1,8),'qratio', '\n '
,repmat(' ',1,37),'(T)',repmat(' ',1,7),'(M)',repmat(' ',1,6),'(T/M)'
' \n']);
  for i=(1):(nz), writef(fid_6,[repmat('
',1,29),'%3i',repmat('%10.3f',1,4) '
\n'],nmbr(i),hm(i),crtdspm(i),tkm(i),qratiom(i)); end;
 end;
 if( kd<2 )
  kd = 2;
  for i = 1 : nz;
   b = x(i);
   x(i) = y(i);
   y(i) = b;
   b = dx(i);
   dx(i) = dy(i);
   dy(i) = b;
   stiffnesszx(i) = stiffnesszy(i);
   spx(i) = spy(i);
  end; i = nz+1;
  stiffnessex = stiffnessey;
  spxm = spym;
  ty = tx;
  vmy = vmx;
  gt(1)=1;
 end;
 if(gt(1)==0)
  break;
```

```
 end;
end;
%
end %program Pushover
    %
function
[nz,stiffnesszx,stiffnesszy,stiffnessex,stiffnessey,x,y,tx,ty,spx,spy,
spxm,spym,vmx,vmy,xp,yp]=sub1(nz,stiffnesszx,stiffnesszy,stiffnessex,s
tiffnessey,x,y,tx,ty,spx,spy,spxm,spym,vmx,vmy,xp,yp);

xp = 0.;
yp = 0.;
for i = 1 : nz;
 xp = xp + stiffnesszy(i).*x(i)./stiffnessey;
 yp = yp + stiffnesszx(i).*y(i)./stiffnessex;
end; i = nz+1;
ex = tx - xp;
ey = ty - yp;
xp1 = 0.;
yp1 = 0.;
for i = 1 : nz;
 xp1 = xp1 + stiffnesszx(i).*y(i).*y(i);
 yp1 = yp1 + stiffnesszy(i).*x(i).*x(i);
end; i = nz+1;
vmx = xp1 - stiffnessex.*yp.*yp;
vmy = yp1 - stiffnessey.*xp.*xp;
pm = vmx + vmy;
for i = 1 : nz;
 spx(i) = 1. + ey.*stiffnessex.*(y(i)-yp)./pm;
 spy(i) = 1. + ex.*stiffnessey.*(x(i)-xp)./pm;
end; i = nz+1;
spxm = 1. + ey.*ey.*stiffnessex./pm;
spym = 1. + ex.*ex.*stiffnessey./pm;
end % Sub1
    %
function
[nz,Erst,tke,dcs,qratioma,nmc,stiffnesszx,eldispa,spx,crtdsp,V1,h,tk,q
ratio,pz,dctlt,hend,lvfu,FRPhu1,FRPhu2,mxdsp,zkzx2,strght,eldispla1,el
displa2,
eldispla3]=sub2(nz,Erst,tke,dcs,qratioma,nmc,stiffnesszx,eldispa,spx,c
rtdsp,V1,h,tk,qratio,pz,dctlt,hend,lvfu,FRPhu1,FRPhu2,mxdsp,zkzx2,strg
ht,eldispla1,eldispla2, eldispla3);

Erst = 0;
tke = 0;
for i = 1 : nz;
 if( strght(i)<= 0) )
 crtdsp(i) = dcs.*spx(i);
 if( crtdsp(i)<=eldispa(i) )
  h(i) = crtdsp(i).*stiffnesszx(i);
  tk(i) = stiffnesszx(i);
 elseif( crtdsp(i)>dctlt(i).*eldispa(i) ) ;
  if( hend(i)==0 )
   hend(i) = 1;
   nmc = nmc + 1;
   lvfu(nmc) = fix(i);
  end;
  h(i) = 0;
```

```
  tk(i) = 0;
 else;
  h(i) = V1(i);
  tk(i) = V1(i)./crtdsp(i);
 end;
 Erst = Erst + h(i);
 tke = tke + tk(i);
 qratio(i) = crtdsp(i)./eldispa(i);
 if( qratioma<=qratio(i) )
  qratioma = qratio(i);
  %
 else;
 crtdsp(i) = dcs.*spx(i);
 eldispa(i) = max( eldispa1(i), eldispa2(i), eldispa3(i) )
  if( crtdsp(i)<=eldispa(i) )
  h(i) = crtdsp(i).*stiffnesszx(i);
  tk(i) = stiffnesszx(i);
 elseif( crtdsp(i)>dctlt(i).*eldispa(i) ) ;
  if( hend(i)==0 )
   hend(i) = 1;
   nmc = nmc + 1;
   lvfu(nmc) = fix(i);
  end;
  h(i) = 0;
  tk(i) = 0;
 else;
 %
 stiffnesszx2(i)=max(FRPhu1(i)/(mxdsp(i) - eldispla(i)),
FRPhu2(i)/(mxdsp(i) - eldispla(i)))
 V1(i)= max(FRPhu1(i), FRPhu2(i))
 h(i) = V1(i)-(crtdsp(i)-eldispla(i)).*stiffnesszx2(i);
 tk(i) = h(i)/crtdsp(i);
 %
 end;
 Erst = Erst + h(i);
 tke = tke + tk(i);
 qratio(i) = crtdsp(i)./eldispa(i);
 if( qratioma<=qratio(i) )
  qratioma = qratio(i);

 end;
end; i = nz+1;
end % Sub2
    %
function
[nz,tk,tke,y,ty,spx,spxm,vmy]=sub3(nz,tk,tke,y,ty,spx,spxm,vmy);

yp = 0.;
xp1 = 0.;
for i = 1 : nz;
 yp = yp + tk(i).*y(i)./tke;
 xp1 = xp1 + tk(i).*y(i).*y(i);
end; i = nz+1;
ey = ty - yp;
vmx = xp1 - tke.*yp.*yp;
pm = vmx + vmy;
for i = 1 : nz;
 spx(i) = 1. + ey.*tke.*(y(i)-yp)./pm;
```

```
end; i = nz+1;
spxm = 1. + ey.*ey.*tke./pm;
end % Sub3

function out=writef(fid,varargin)
if isnumeric(fid)
 if fid==6,      out=fprintf(1,varargin{:});
 elseif fid==0,  out=fprintf(2,varargin{:});
 elseif isempty(fid) %% treat empty array like a string array [sethg
2008-03-03]
  out=sprintf(varargin{:});
  if nargin>2 %set the calling var to out
   if ~isempty(inputname(1)), assignin('caller',inputname(1),out); end
  end
 else,           out=fprintf(fid,varargin{:});
 end
elseif ischar(fid)
 out=sprintf(varargin{:});
 if nargin>2 %set the calling var to out
  if ~isempty(inputname(1)), assignin('caller',inputname(1),out); end
 end
else,            out=fprintf(fid,varargin{:});
end
end


function varargout=readf(fid,fmtStr,n)
% function varargout=readf(fid,varargin),  Catches string fid's
if isnumeric(fid)
 if n==1
  [varargout]=textscan(fid,fmtStr);
 else
  [varargout{1:n}]=textscan(fid,fmtStr);
 end
elseif ischar(fid)
 [varargout{1:n}]=strread(fid,fmtStr);
end
end
```